KATHOLIEKE UNIVERSITEIT LEUVEN
Faculteit Ingenieurswetenschappen
Departement Werktuigkunde
Afdeling Biomechanica en Grafisch Ontwerpen
Celestijnenlaan 300C - B-3001 Leuven, Belgium

MATHEMATICAL MODELLING OF BONE REGENERATION DURING FRACTURE HEALING AND IMPLANT OSSEOINTEGRATION

Promotoren :
Prof. Dr. Ir. J. Vander Sloten
Prof. Dr. Ir. H. Van Oosterwyck

Proefschrift voorgedragen
tot het behalen van het
doctoraat in de
Ingenieurswetenschappen

door

Liesbet GERIS

Mei 2007

KATHOLIEKE UNIVERSITEIT LEUVEN
Faculteit Ingenieurswetenschappen
Departement Werktuigkunde
Afdeling Biomechanica en Grafisch Ontwerpen
Celestijnenlaan 300C - B-3001 Leuven, Belgium

MATHEMATICAL MODELLING OF BONE REGENERATION DURING FRACTURE HEALING AND IMPLANT OSSEOINTEGRATION

Examencommissie:
Prof. Dr. Ir. A. Haegemans,voorzitter
Prof. Dr. Ir. J. Vander Sloten, promotor
Prof. Dr. Ir. H. Van Oosterwyck, promotor
Prof. Dr. Dent. I. Naert
Prof. Dr. Ir. G. Van der Perre
Prof. Dr. Ir. G. De Roeck
Prof. Dr. Ir. Y. Moreau
Prof. Dr. Ir. R. Huiskes
(Technische Universiteit Eindhoven)
Prof. Dr. Ir. P. Prendergast
(Trinity College Dublin)

Proefschrift voorgedragen
tot het behalen van het
doctoraat in de
Ingenieurswetenschappen

door

Liesbet GERIS

UDC 681.3∗I6, 681.3∗J3 Mei 2007

© Katholieke Universiteit Leuven
Faculteit Ingenieurswetenschappen
Arenbergkasteel, B-3001 Heverlee (Leuven), Belgium

Alle rechten voorbehouden. Niets uit deze uitgave mag worden verveelvoudigd en/of openbaar gemaakt worden door middel van druk, fotokopie, microfilm, elektronisch of op welke andere wijze ook zonder voorafgaandelijke schriftelijke toestemming van de uitgever.

All rights reserved. No part of this publication may be reproduced in any form, by print, photoprint, microfilm or any other means without written permission from the publisher.

D/2007/7515/57
ISBN 978-90-5682-823-3
UDC 681.3∗I6, 681.3∗J3

het weten heft het geheim niet op maar verdiept het

Dietrich Bonhoeffer

Dankwoord

"Botregeneratie is een geheel van complexe fysiologische processen, waarbij de acties en interacties van vele celtypes betrokken zijn, gestuurd door een veelheid aan biochemische en mechanische factoren" (sectie 1.3, pagina 4). Eigenlijk lijkt dat behoorlijk sterk op een doctoraat, een doctoraat is immers een geheel van complexe wetenschappelijke processen, waarbij de acties en interacties van vele helpende handen betrokken zijn, gestuurd door een veelheid aan kansen en aanmoedigingen. Zonder cellen en groeifactoren geen botregeneratie en zonder helpende handen geen doctoraat. Het is dan ook met veel plezier dat ik op de eerste pagina's van mijn doctoraat deze helpende handen mag bedanken.

Vooreerst wil ik mijn promotor prof. Vander Sloten, hoofd van de afdeling Biomechanica en Grafisch Ontwerpen, bedanken. Hij gaf mij de kans om mijn twee lievelingsonderwerpen, biologie en modellering, te combineren in één doctoraat. Zijn brede visie op onderzoek en de vrijheid die ik kreeg om mijn eigen weg te zoeken, hebben in belangrijke mate bijgedragen tot dit werk en tot mijn eigen ontwikkeling als onderzoeker. Mijn dagelijkse begeleider en tevens promotor prof. Van Oosterwyck wil ik bedanken voor zijn hulp in alle onderdelen van dit doctoraat. Zijn grote expertise op het gebied van botregeneratie en zijn constructief kritische houding ten opzichte van modelleren zijn heel belangrijk geweest voor dit werk.

Prof. Van der Perre, voormalig hoofd van de afdeling, wil ik bedanken voor de kans die ik kreeg om onderzoek te doen in het fascinerende domein dat Biomechanica is. Prof. Naert wil ik bedanken voor zijn betrokkenheid bij dit onderzoek en voor het houden van de vinger aan de klinische pols. Prof. De Roeck wil ik bedanken voor de interesse waarmee hij dit onderzoek heeft opgevolgd. Verder wil ik prof. Moreau bedanken om op het laatste nippertje nog tijd te willen vrijmaken om deel uit te maken van deze examencommissie. I would like to thank prof. Huiskes and prof. Prendergast for their interest in my work. It is a great honour for me that they both accepted to be part of this examination committee. Prof. Haegemans wil ik tenslotte bedanken om, *ad interim* en voor de eerste keer in het nieuwe systeem, de eindfase van dit

doctoraat in goede banen te hebben geleid.

Het Fonds voor Wetenschappelijk Onderzoek Vlaanderen (FWO Vlaanderen) wil ik bedanken voor het aspirantenmandaat dat mij gedurende de afgelopen vier jaar in staat stelde dit onderzoek te verrichten. Verder wil ik hen, evenals de Academische Stichting Leuven (ASL), bedanken voor het ter beschikking stellen van reiskredieten die mij toelieten buitenlandse verblijven te ondernemen en internationale conferenties bij te wonen.

Mijn tandheelkunde-collega's, Katleen Vandamme en prof. Joke Duyck, wil ik van harte bedanken voor hun enthousiasme en voor hun snelle en uitgebreide antwoorden op mijn vele botkamer-vragen! Prof. Geert Carmeliet en Christa Maes wil ik graag bedanken voor het ter beschikking stellen van experimentele data en voor het delen van de kennis rond angiogenese en botheling. I would like to thank prof. Allen Goodship for providing experimental data and for sharing his vast knowledge on all aspects of fracture healing. I would also like to thank Andriy Andreykiv for introducing me to the world of user subroutines. Finally, it is with much pleasure that I thank Alf Gerisch for our successful collaboration. Alf, this book would not have looked the same without your help. You were my reference for any and all numerical and mathematical problems. It was great to have such a colleague and a friend only an e-mail away. I hope we can continue this collaboration for a long time to come.

Al mijn voormalige en huidige collega's van de afdeling wil ik bedanken voor de fijne sfeer en voor de hulp. Onze secretaresse, Rita, verdient hier een speciale vermelding. Zij slaagde er steeds weer in om het onmogelijke waar te maken en wanneer het mij eens even te veel werd, stond haar deur altijd open.

In de afgelopen jaren zijn er nog een hele hoop andere mensen geweest die van mijn doctoraat een heel fijne en leerrijke periode hebben gemaakt. Caroline en Hilde, onze wekelijkse alma-bezoekjes waren een fijne traditie en ideale uitlaatklep. Alle collega AAP/BAP vertegenwoordigers, ik vond het enorm leuk en boeiend om mij ook met de andere aspecten van onderzoek en onderwijs aan onze Alma Mater te kunnen bezighouden. Bedankt voor de hulp die ik daarbij van jullie kreeg. A few years ago, a student committee of the European Society of Biomechanics was initiated which gave students all over the world the opportunity to actively participate in the organisation and meet new people in the field. Damien, Sebas, I had a great time, thanks.

Vriendinnetjes van de volleybal vroeger en nu, jullie waren (zijn) een super toffe en prettig gestoorde bende waar ik mij volledig thuis voelde. Ons strijdlied zal ik nooit meer vergeten. Tanja, de duizenden kilometers samen in de auto waarin we doctoraats- en andere ergernissen konden ventileren hebben mij door heel wat moeilijke momenten gehaald. Jo, ik moet toegeven dat ik dingen van u geleerd heb die zelfs buiten de volleybal heel nuttig zijn,

bedankt.

Mijn familie wil ik bedanken voor de vele jaren van gesupporter bij al mijn activiteiten. Mama en papa, bedankt voor de kansen die jullie mij geboden hebben. Bedankt, ook aan zusjes, broertje, oma en pépé, voor jullie interesse en voor jullie fier-zijn op mij.

Als laatste wil ik graag iemand heel bijzonder bedanken. Kristof, na vier en half jaar van wetenschappelijke discussies hebben we dan toch een goed compromis kunnen vinden tussen jouw experimenteel en mijn theoretisch werk. Bedankt voor alle steun in de moeilijke momenten, je slaagde er altijd weer in de lach terug op mijn gezicht te brengen. Jouw liefde maakt mij sterk en geeft mij het zelfvertrouwen om de wereld aan te kunnen. Tot aan de maan ... en terug!

Bij botregeneratie zijn er naast de cellen en groeifactoren die in dit doctoraat aan bod komen, nog tal van andere spelers die, ook verderop in dit doctoraat, onbenoemd blijven maar wel allemaal een bijdrage leveren tot het goed verloop van het regeneratie proces. Zo zijn er ook tal van helpende handen die niet allemaal bij naam genoemd kunnen worden, maar toch hebben bijgedragen aan dit doctoraat. Aan iedereen, bedankt!

Eliksem, mei 2007
Lies

Abstract

Despite the extensive body of literature on bone regeneration, many questions remain on e.g. the regulatory mechanisms and potential treatment strategies of pathological regeneration cases. The hypothesis underlying this work states that mathematical models of bone regeneration can make a substantial contribution to this domain by proposing pathological regeneration mechanisms and designing therapies, which can subsequently be tested experimentally.
In the first part of this work, existing mechanoregulatory and bioregulatory models of bone regeneration are implemented and applied to both implant osseointegration and fracture healing set-ups. A quantitative comparison with experimental results is performed. Thorough sensitivity analyses are carried out to assess the influence of various modelling aspects on the simulation outcome. Shortcomings of these models are identified and suggestions for improvements are made.
In the second part of this work, a novel bioregulatory model of bone regeneration is developed in which several of the previously defined shortcomings are addressed. This model includes key aspects of the regeneration process such as intramembranous and endochondral ossification, angiogenesis and directed cell motion. The results obtained with this novel model are corroborated both qualitatively and quantitatively by comparison with experimental data for normal fracture healing. Cases of pathological fracture healing are simulated and experimentally testable therapeutic strategies are implemented.
The last part of this work describes the establishment of a mathematical framework, based on the previously developed bioregulatory model, in which the regulatory influence of both biological and mechanical factors is combined. This is the first model of bone regeneration in which the coupling between mechanical loading and angiogenesis is made in an explicit and mechanistic manner. Several examples are given to illustrate the added value of this approach in simulating normal and pathological bone regeneration.
In summary, this work demonstrates the potential of mathematical models in advancing the knowledge on bone regeneration and designing treatment strategies for pathological healing cases.

Beknopte Samenvatting

Ondanks de huidige kennis rond botregeneratie, blijven vele vragen onbeantwoord. De in dit werk vooruitgeschoven hypothese stelt dat wiskundige modellen een substantiële bijdrage kunnen leveren aan dit onderzoeksdomein door het voorstellen van pathologische regeneratiemechanismen en het ontwerpen van therapieën, die vervolgens experimenteel getest kunnen worden.
Het eerste deel van dit werk beschrijft de implementatie van bestaande mechano- en bioregulatorische modellen en de toepassing ervan op zowel implantaat osseointegratie als breukhelingssituaties. Een kwantitatieve vergelijking met de experimentele resultaten is uitgevoerd, evenals een grondige sensitiviteitsanalyse ter bepaling van de invloed van verschillende modelleringsaspecten op het simulatieresultaat. Tekortkomingen van deze modellen zijn geïdentificeerd en suggesties voor verbeteringen geformuleerd.
In het tweede deel van dit werk is een nieuw bioregulatorisch model voor botregeneratie ontwikkeld, dat aan verschillende van de hoger gedefinieerde tekortkomingen tegemoet komt. Dit model omvat verscheidene kernaspecten van het regeneratie proces zoals intramembraneuze en endochondrale botvorming, angiogenese en gerichte celmigratie. De simulatieresultaten zijn zowel op kwalitatief als kwantitatief niveau gecorroboreerd door vergelijking met experimentele data voor normale breukheling. Gevallen van pathologische breukheling zijn gesimuleerd en experimenteel testbare behandelingsstrategieën geïmplementeerd.
Het laatste deel van dit werk beschrijft de ontwikkeling van een wiskundig kader, gebaseerd op het eerder ontworpen bioregulatorisch model, dat de regulerende invloed van zowel biologische als mechanische factoren combineert. Dit is het eerste model van botregeneratie dat de koppeling tussen mechanische belasting en angiogenese maakt op een expliciete en mechanistische wijze. Verschillende voorbeelden illustreren de toegevoegde waarde van deze aanpak in de simulatie van normale en pathologische botregeneratie.
Samenvattend, dit werk demonstreert het potentieel van wiskundige modellen in het vergroten van de kennis omtrent botregeneratie en in het ontwerpen van behandelingsstrategieën voor pathologische helingsgevallen.

Table of Contents

Dankwoord - Acknowledgements i

Abstract v

Beknopte Samenvatting vii

Table of Contents xii

List of Figures xiv

List of Tables xv

List of Symbols and abbreviations xvii

1 General Introduction **1**
- 1.1 Bone composition . . . 1
- 1.2 Bone structure . . . 2
  - 1.2.1 Structure of bone . . . 2
  - 1.2.2 Bone formation and (re)modelling . . . 3
- 1.3 Bone regeneration . . . 4
  - 1.3.1 Implant osseointegration . . . 6
  - 1.3.2 Fracture healing . . . 8

2 Hypothesis and Objectives **11**
- 2.1 General hypothesis . . . 11
- 2.2 Objectives . . . 12
- 2.3 Methodology . . . 12
  - 2.3.1 Experimental aspects . . . 12
  - 2.3.2 Modelling aspects . . . 14
  - 2.3.3 Numerical aspects . . . 14

3 Mechanoregulatory models of bone regeneration **15**
3.1 Introduction . . . 16
3.1.1 Mechanoregulatory models for tissue regeneration . 16
3.1.2 Predictive power of mechanoregulatory models . . . 18
3.2 Hypothesis and Objectives . . . 19
3.2.1 Hypothesis . . . 19
3.2.2 Objectives . . . 20
3.3 Materials and Methods . . . 20
3.3.1 Repeated sampling *in vivo* bone chamber . . . 20
3.3.2 Modelling of the bone chamber . . . 26
3.3.3 Implementation of mechanoregulatory models . . . 28
3.3.4 Simulations and sensitivity analyses . . . 30
3.4 Results . . . 30
3.4.1 Experimental bone chamber studies . . . 30
3.4.2 Numerical bone chamber studies . . . 31
3.5 Discussion . . . 41
3.5.1 Simulation results . . . 41
3.5.2 Sensitivity analyses . . . 46
3.5.3 Simplifications . . . 48
3.5.4 Falsifiability of mechanoregulatory models . . . 50
3.6 Conclusion . . . 51

4 A Bioregulatory model of bone regeneration **53**
4.1 Introduction . . . 54
4.1.1 Mathematical models in biomedicine . . . 54
4.1.2 Applications in bone regeneration . . . 55
4.2 Hypothesis and Objectives . . . 56
4.2.1 Hypothesis . . . 56
4.2.2 Objectives . . . 57
4.3 Materials and Methods . . . 57
4.3.1 Rodent fracture models . . . 57
4.3.2 Mathematical model . . . 61
4.3.3 Numerical implementation . . . 62
4.3.4 Simulations and sensitivity analyses . . . 64
4.4 Results . . . 65
4.4.1 Experimental fracture healing models . . . 65
4.4.2 Mathematical fracture healing models . . . 67
4.5 Discussion . . . 78
4.5.1 Simulation results . . . 78
4.5.2 Sensitivity analyses . . . 81
4.5.3 Simplifications . . . 82
4.5.4 Applications in pathological fracture healing . . . 85
4.6 Conclusion . . . 87

5 A Bioregulatory model including angiogenesis 89
5.1 Introduction . . . 90
5.1.1 Angiogenesis and fracture healing . . . 90
5.1.2 Mathematical models of fracture healing . . . 91
5.2 Hypothesis and Objectives . . . 92
5.2.1 Hypothesis . . . 92
5.2.2 Objectives . . . 93
5.3 Materials and Methods . . . 93
5.3.1 Mathematical framework . . . 93
5.3.2 Parameters . . . 100
5.3.3 Simulation details . . . 104
5.3.4 Numerical implementation . . . 106
5.3.5 Simulations and sensitivity analyses . . . 106
5.4 Results . . . 106
5.4.1 Normal fracture healing . . . 106
5.4.2 Sensitivity analyses . . . 107
5.4.3 Pathological fracture healing . . . 111
5.5 Discussion . . . 115
5.5.1 Simulation results . . . 115
5.5.2 Sensitivity analyses . . . 118
5.5.3 Simplifications . . . 121
5.5.4 Applications in pathological fracture healing . . . 122
5.6 Conclusion . . . 124

6 Combining mechanoregulatory and bioregulatory models 127
6.1 Introduction . . . 128
6.1.1 Mechanical loading and fracture healing . . . 128
6.1.2 Mechanical loading and oral implant osseointegration 131
6.1.3 Mechanical loading and cells . . . 133
6.1.4 Conclusion . . . 137
6.2 Hypothesis and Objectives . . . 138
6.2.1 Hypothesis . . . 138
6.2.2 Objectives . . . 138
6.3 Materials and Methods . . . 139
6.3.1 Combined mechanobioregulatory model . . . 139
6.3.2 Numerical implementation . . . 139
6.3.3 Simulation details . . . 142
6.3.4 Simulations and sensitivity analyses . . . 146
6.4 Results . . . 146
6.4.1 Application in an *in vivo* bone chamber . . . 146
6.4.2 Application in fracture healing . . . 150
6.5 Discussion . . . 151
6.5.1 Application in an *in vivo* bone chamber . . . 151

6.5.2 Application in fracture healing 154
6.5.3 Simplifications 156
6.5.4 Sensitivity analyses 156
6.5.5 General considerations 157
6.6 Conclusions 159

7 Conclusions and future perspectives **161**
7.1 Summary 161
7.2 Conclusions 162
7.3 Future research 165
7.3.1 Modelling aspects 165
7.3.2 Experimental aspects 166

Bibliography **169**

Curriculum Vitae **i**

List of publications **iii**

Nederlandse samenvatting - Summary in Dutch **xi**

Appendix **xxx**

List of Figures

1.1 Features of long bones 3
1.2 The three phases of bone regeneration 5
1.3 The reparative phase of implant osseointegration 6
1.4 The reparative phase of fracture healing 9

2.1 Research flowchart 13

3.1 Overview of mechanoregulatory models 17
3.2 Composition and installation of the bone chamber 22
3.3 Overview of the histological analyses 25
3.4 Overview of the FE models 27
3.5 Adaptive tissue differentiation simulation scheme 29
3.6 Overview of the bone chamber study results 32
3.7 Tissue differentiation simulation results 34
3.8 3D Tissue differentiation simulation results 37
3.9 Simulation results for different implant displacements 38
3.10 Results for the convergence tests 40
3.11 Simulations without precursor cell diffusion 41
3.12 Simulations using one mechanical stimulus 42
3.13 Sensitivity analysis tissue phenotype transitions 43
3.14 Sensitivity analysis material properties 44
3.15 Contact type for screw-shaped implants 49

4.1 Schematic overview of the bioregulatory model 56
4.2 Overview of the experimental set-ups 59
4.3 Overview of the simulation domain and boundary conditions 63
4.4 Results of the semi-stabilised fracture model 66
4.5 Results of the standardised fracture model 67
4.6 Overview of the tissue and growth factor patterns 69
4.7 Temporal evolution of the growth factor density 70
4.8 Quantitative comparison between simulation and experiment 71

4.9 Results of the convergence test 72
4.10 Results sensitivity analysis 74
4.11 Results 3 mm fracture gap 75
4.12 Results 3 mm fracture gap (2) 76
4.13 Results pathological healing and therapy 77
4.14 Results for an atrophic nonunion 79
4.15 Model sensitivity to symmetry assumptions 83
4.16 Influence of callus shape on simulation results 84

5.1 Schematic overview of enhanced bioregulatory model 94
5.2 Geometrical model and boundary conditions 105
5.3 Spatiotemporal evolution tissue densities 108
5.4 Predicted and experimentally measured tissue fractions . . 109
5.5 Influence of initial fibrous tissue matrix density 110
5.6 Influence of cell migration on fracture healing 111
5.7 Predicted and experimentally measured tissue fractions . . 112
5.8 Influence of angiogenic process on fracture healing 113
5.9 Atrophic nonunion 114
5.10 Treatment strategies atrophic nonunion 116
5.11 Cartilage formation in the endosteal callus 118
5.12 Endothelial cell front 120

6.1 Schematic representation of the coupled model 140
6.2 Mechanical regulation of parameter values 140
6.3 Overview implementation coupled model 141
6.4 Geometrical domain and boundary conditions 144
6.5 Geometrical domain and boundary conditions (2) 145
6.6 Simulation results 30 μm implant displacement 147
6.7 Comparison with experiments study 2 148
6.8 Simulation results different implant displacements 149
6.9 Comparison with experiments study 3 150
6.10 Simulation results fracture overload 151
6.11 Load induced pathological fracture healing 152
6.12 Recapitulation of healing after stabilisation 153

7.1 Computational systems biology 164
7.2 Overview figure thesis contributions 168

List of Tables

3.1 Material properties 28
3.2 Tissue differentiation simulation results 35
3.3 Bone-to-implant contact 36
3.4 Tissue differentiation simulation results (2) 39

4.1 Quantitative comparison semi-stabilised model 68
4.2 Results sensitivity analysis 88

6.1 Material properties 142
6.2 Adaptation parameter value bone chamber 143
6.3 Adaptation parameter value fracture healing 145
6.4 Influence loading frequency bone chamber 148

List of symbols and abbreviations

2D	Two-dimensional
3D	Three-dimensional
ε	Strain
ν	Poisson coefficient
μ	Permeability $[m^4(Ns)^{-1}]$
σ	Stress $[Pa \ = \ Nm^{-2}]$
∇	$\frac{\partial}{\partial x}i + \frac{\partial}{\partial y}j + \frac{\partial}{\partial z}k$
$\nabla^2 = \triangle$	$\frac{\partial^2}{\partial x^2} + \frac{\partial}{\partial y^2} + \frac{\partial}{\partial z^2}$ (Laplacian)
ALP	Alkaline phosphatase
BAF	Bone area fraction
BC	Bone chamber
BD	Bone density
BIC	Bone-to-implant contact
BOIC	Bone-and-osteoid-to-implant contact
BMP	Bone morphogenetic protein
Ca^{2+}	Calcium ion
cAMP	Cyclic adenosine monophosphate
Cbfa1	Core binding factor 1
Col	Collagen
cp-titanium	Commercially pure titanium
CTGF	Connective tissue growth factor
E	Young's modulus $[Pa \ = \ Nm^{-2}]$
EC	Endothelial cell
ECM	Extracellular matrix
FEA	Finite element analysis

FGF	Fibroblast growth factor
FH	Fracture healing
HIF1-α	Hypoxia inducible factor α
HP	Hydrostatic pressure
IGF	Insulin-like growth factor
IOI	Implant osseointegration
MMA	Methyl metacrylate
MMP	Matrix metalloproteinase
MOL	Method of lines
mRNA	Messenger ribo nucleic acid
MSC	Mesenchymal stem cell
NO	Nitric oxide
ODE	Ordinary differential equation
OIC	Osteoid-to-implant contact
OP	Osteopontin
OSTC	Osteocalcin
PDE	Partial differential equation
PDGF	Platelet derived growth factor
PFD	Post fracture day
PFW	Post fracture week
PGE2	Prostaglandin 2
PlGF	Placental growth factor
pO_2	Oxygen pressure
rhBMP	Recombinant human bone morphogenetic protein
ROWMAP	Krylov-W code for the integration of large stiff ODE's
SD	Standard deviation
SE	Standard error of means
SO	Safranin O
TAF	Tissue area fraction
TD	Tissue differentiation
TDR	Taxis-Diffusion-Reaction
TGF-β	Transforming growth factor β
TIMP	Tissue inhibitor of matrix metalloproteinase
TNF-α	Tumour necrosis factor α
VEGF	Vascular endothelial growth factor
WT	Wild type

Chapter 1

General Introduction

Bone is a fascinating tissue, unique in its scarless regeneration capacity. It is often called an intelligent material as it is capable of adapting itself to changes in the mechanical and biological requirements it is subjected to. This general introduction starts with a short description of the composition, structure and (re)modelling activities of bone. Subsequently, some basic notions of bone regeneration are explained. Finally, some challenges for future bone regeneration research are discussed. As this introduction only provides general information on bone and bone regeneration, chapters 3 to 6 each start with a short literature section, summarising the State of the Art of a specific topic discussed in the respective chapter.

1.1 Bone composition

Bone is composed of an organic phase, an inorganic phase and **water**. The **organic phase** encompasses approximately 30 % of the bone volume, its most important constituent being collagen. Collagen is a protein able to organise itself into strong fibres. These fibres provide the necessary flexibility and tensile strength to bone. Beside collagen, the organic phase consists of proteoglycans and non-collagenous proteins such as osteocalcin and osteopontin. The **inorganic phase** predominantly exists of hydroxy apatite crystals. This mineral is deposited onto the collagenous matrix providing the bone with rigidity and compressive strength (Martin *et al.*, 1998).

A very small fraction of the bone's volume is taken by the cells that are responsible for the production, resorption and maintenance of the above described bone matrix. **Osteoclasts** are multinuclear cells that resorb the matrix. They first mineralise the adjacent bone with acids and then dissolve

its collagen with enzymes. Bone resorption takes place at a rate of tens of micrometres per day. **Osteoblasts** are mononuclear cells, differentiated from mesenchymal stem cells, that produce osteoid. This osteoid is laid down at a rate of 1 μm/day and is later calcified to produce mineralised bone. **Osteocytes** are former osteoblasts that have become buried in the bone matrix which they and their neighbours have produced. They sit in cavities called lacunae and are connected with other osteocytes through their cellular processes sticking out in the little canals connecting the lacunae, the canaliculi. Osteocytes are believed to play an important role in the sensing of mechanical loading by bone tissue. **Bone lining cells** are also former osteoblasts, but they are not buried in newly formed bone matrix. When bone matrix production ceases, they become quiescent and flattened against the bone surface. When matrix production is resumed, these cells can be reactivated.

1.2 Bone structure

1.2.1 Structure of bone

At a macroscopic scale, two different kinds of bone can be distinguished (Figure 1.1). **Cortical** or compact bone is present at the outer surface of bones, while **trabecular**, cancellous or spongious bone is situated at the inner. The latter is a highly porous open-celled structure consisting of interconnected plates and struts (called trabeculae) of bone tissue. The thickness of these plates and struts is of the order of 100 to 300 μm. The intertrabecular spaces (typically 300 to 1500 μm) are filled with marrow that contains blood vessels, nerves and various types of cells. In the case of long bones, trabecular bone is only present at the ends of the bone, while for short and flat bones, it is encountered in the entire inner volume.

At the microscopic level, two types of bone can be distinguished, based on the organisation of the tissue: lamellar bone and woven bone (Figure 1.1). **Lamellar bone** is slowly formed, highly organised bone, consisting of parallel layers or lamellae comprising an anisotropic matrix of mineralised crystals and collagen fibres. These lamellae are 3 to 7 μm thick. **Woven bone** is a quickly formed, poorly organised tissue in which collagen fibres and mineral crystals are more or less randomly arranged. Woven bone can be formed more quickly than lamellar bone, but is weaker. Almost all of the bone tissue in the adult skeleton consists of lamellar bone. Woven bone is only formed during rapid bone accretion, e.g. during implant osseointegration or fracture healing.

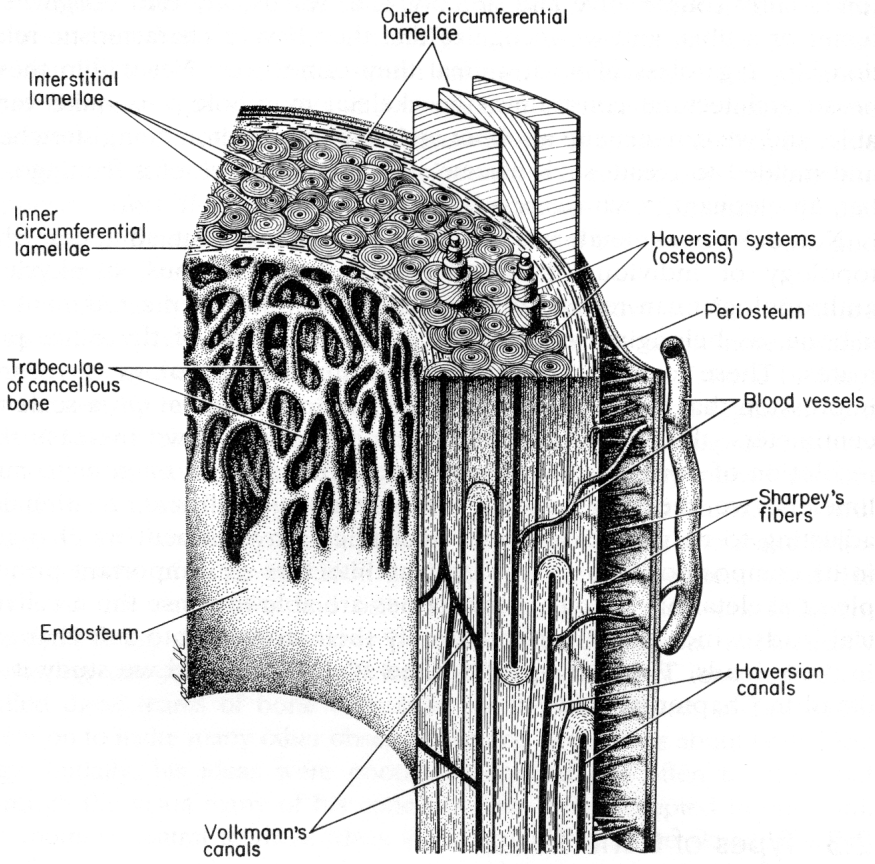


FIGURE 1.1: Schematic overview of different features present in long bones (reproduced from Martin *et al.* (1998)).

1.2.2 Bone formation and (re)modelling

Bone formation basically occurs in two steps. The first step is the **osteogenesis** in which osteoblasts deposit osteoid on a support. Depending on the supporting tissues, different osteogenic processes are distinguished. In intramembranous ossification, connective tissue provides the support for bone deposition. In the endochondral ossification process, osteoid is formed in cartilage that has been mineralised prior to the osteoblasts' invasion in the tissue. The third category of ossification processes is the appositional ossification, where previously formed bone tissue acts as support. The second step of

bone formation is the **mineralisation** of the osteoid. First, insoluble calcium phosphate salts are deposited in the osteoid. Subsequently, these salts are replaced by more stable hydroxyapatite crystals.

Two processes play a major role in the development and maintenance of a healthy and flexible skeleton: bone modelling and remodelling. **Bone modelling** encompasses the change in size and/or shape of the bones. This process is characterised by the independent actions of osteoclasts and osteoblasts. The rate of this process decreases dramatically once skeletal maturity is reached. The modelling process can be both resorptive and formative. Contrarily to bone modelling, **bone remodelling** is a process that usually does not affect the bone geometry. Furthermore, the actions of osteoclasts and osteoblasts are tightly coupled. Bone remodelling is a process that repairs microscopical damage, prevents accumulation of fatigue damage and provides the fine tuning to obtain optimal mechanical efficiency. The remodelling of cortical bone induces the formation of Haversian canals containing blood vessels for the supply of nutrients and the removal waste products. Each year, approximately 5 % of the total cortical bone volume and 25 % of the total trabecular bone volume undergoes remodelling.

1.3 Bone regeneration

Under most circumstances bone truly regenerates itself, whereas soft tissue wound healing results in scar formation (Glowacki, 1998). Bone regeneration involves complex physiological processes, involving the participation of many cell types, regulated by a myriad of biochemical and mechanical factors. The principle mechanisms underlying the healing around implants are comparable to those of fracture healing (Schenk and Herrmann, 1984; Gross, 1988; Plenk and Zitter, 1996; Overgaard *et al.*, 2000), although this view has triggered much debate since some authors have suggested that the presence of an implant induces a different healing mode (Schwartz *et al.*, 1997; Steflik *et al.*, 1998).

The regeneration response can be divided into primary and secondary healing (Overgaard *et al.*, 2000). **Primary healing** involves direct healing without the appearance of inflammation or the formation of callus tissue. Primary healing seems to occur only under optimal conditions, i.e. mechanical stability and the absence of gaps (in fracture healing the anatomical restoration is needed). When such conditions are present, the bone remodelling units will directly reestablish the haversian canals in the bone.

Secondary healing is the most common form of healing and takes place when the optimal conditions needed for primary repair are absent. The secondary healing of bone, whether it is in fracture healing or implant osseointegration, encompasses three overlapping phases: the inflammatory phase, the reparative phase and the remodelling phase (Einhorn, 1995, 1998; Hadjiargyrou *et al.*, 2002; Gerstenfeld *et al.*, 2003a; Overgaard *et al.*, 2000; Davies, 2003) (Figure 1.2).

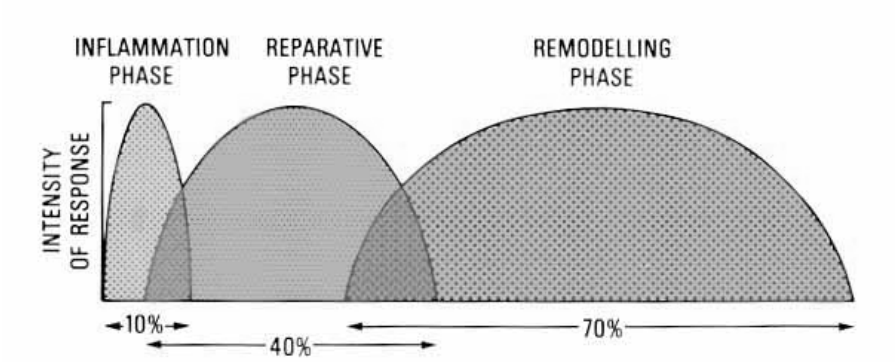


FIGURE 1.2: The three phases of bone regeneration (reproduced from Cruess and Dumont (1985)). The abscissa indicates the time in percentage of total healing time.

Following bone trauma (either from fracture or from the implantation procedure), the cortical bone, periosteum and surrounding soft tissues are damaged, rupturing numerous blood vessels. This blood rapidly coagulates to form a clot enclosing the trauma site. In this clot, activated and degranulating platelets provide a source of growth factors, playing an important role in the wound healing cascade. This is the start of the initial stage of bone regeneration, the **inflammation phase**. As a consequence of the vascular damage, the trauma site becomes hypoxic. Osteocytes at the trauma site become deprived of their nutrition and necrose, as do the damaged tissues in that area. This necrotic process triggers an immediate inflammatory response, bringing inflammatory cells, leukocytes and macrophages to the region. These are followed by the invasion of fibroblasts, mesenchymal stem cells and endothelial cells (Taguchi *et al.*, 2005). Growth factors and cytokines, important regulators of the healing process, are produced by the cells present in the regeneration area as well as released into this area from the surrounding tissues (damaged bone ends, muscles, periost, marrow) (Gerstenfeld *et al.*, 2003a; Malizos and Papatheodorou, 2005). The initially formed granulation

tissue is gradually being replaced by fibrous tissue. In this soft tissue matrix, mesenchymal stem cells will start differentiating, guided by cues from their microenvironment, such as the presence of biological factors (Einhorn, 1998) and the perceived mechanical stimuli (Carter *et al.*, 1998). This is the start of the **reparative phase** of bone regeneration. The processes enrolling during the reparative phase depend on the type of regeneration taking place (i.e. implant osseointegration, fracture healing etc.). This phase will be discussed separately for implant osseointegration and fracture healing in sections 1.3.1 and 1.3.2 respectively. Already during the reparative phase, the final remodelling phase begins with osteoclastic resorption of unnecessary or poorly placed parts of the regenerate and the formation of lamellar bone. This remodelling takes place for a prolonged period of time, gradually reverting the blood supply to a normal state and restoring the bone at the regeneration site to its original shape and strength.

1.3.1 Implant osseointegration

The reparative phase in implant osseointegration

In implant osseointegration, two different phenomena occur during the reparative phase, juxtaposing the bone to the implant surface: contact osteogenesis (osteoconduction and *de novo* bone formation) and distance osteogenesis (or appositional bone growth) (Figure 1.3).

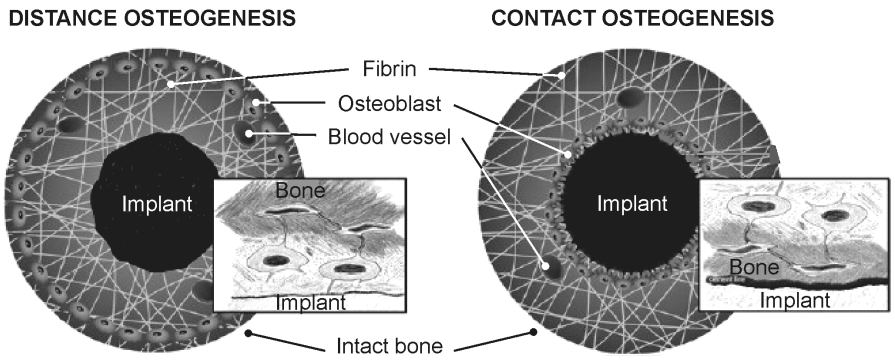


Figure 1.3: The two osteogenic processes occurring during the reparative phase of implant osseointegration: distance osteogenesis (left) and contact osteogenesis (right) (reproduced from Davies (2003)).

Contact osteogenesis is defined as the formation of bone into an endosseous healing site, resulting from the osteogenic cell recruitment and mi-

gration through a three-dimensional biological matrix (Davies, 2003). Migration of the potentially osteogenic population towards the implant surface (osteoconduction) occurs through the fibrin of the transient tissue matrix, potentiated and directed by biochemical cues present in the matrix. With the correct biochemical and mechanical stimuli, undifferentiated mesenchymal stem cells can be transformed into osteoblasts. These cells will then be available to synthesise *de novo* (woven) bone on the implant surface itself (and in doing so also stop migrating). The implant surface plays an important role in the process of contact osteogenesis, not only by inducing the release of biochemical factors from e.g. platelets, but also by maintaining the anchorage of the temporary scaffold through which the cells reach the implant surface. In **distance osteogenesis**, new bone is formed on the surfaces of old bone in the peri-implant site. The bone surfaces provide a population of osteogenic cells that lay down a new matrix that encroaches on the implant.

Challenges in implant osseointegration research

These above described tissue responses depend on several factors amongst which implant material and design, implant surface characteristics, anatomical site and mechanical conditions are the most relevant. Bone formation adjacent to endosseous implants with various design and surface characteristics and at different anatomical locations has extensively been studied in undisturbed healing conditions, i.e. without loading, in animal experiments (Akimoto *et al.*, 1999; Berglundh *et al.*, 2003; Botticelli *et al.*, 2003a,b, 2004; Franchi *et al.*, 2004, 2005; Rimondini *et al.*, 2005). To avoid adverse healing outcomes for oral implants, an initial uneventful healing period of several months has been advocated for decades. This protocol has commonly caused physiological, psychological or sociological challenges for patients who underwent implant treatment over the last 30 years. These challenges include avoiding any prosthesis wearing during the first weeks to ensure an unloaded healing condition, a transitional removable prosthesis wearing period with a loose denture compromising chewing ability, speech and aesthetics, and the necessity of a second surgery to expose the implant in the oral cavity after healing. Therefore, new protocols have emerged in recent years and focused on loading implants directly or soon after their placement.

The scientific literature on immediate implant loading is continuously increasing (Szmukler-Moncler *et al.*, 1998; Gapski *et al.*, 2003; Attard and Zarb, 2005), with a particular interest for refinements in implant design and surface characteristics, mainly in an attempt to speed up the biological healing response following implant placement. Conflicting data were obtained and could in part be assigned to implant design and loading protocol. Clinical and experimental trials investigating fracture healing provide evidence that

limited and well-controlled movement of fracture fragments stimulates callus formation and increases its mechanical stability (Goodship, 1992; Claes, 1998). Awareness of the initial mechanical conditions provides a firm basis for potential mechanical and biological approaches regarding the enhancement of fracture healing (Klein *et al.*, 2003).

Despite the fact that loading of implants immediately after their placement involves certain biological risks, the use of immediately loaded dental implants has been introduced in clinical routine over the last decade. It is no longer believed that immediate loading per se leads to fibrous encapsulation of implants (Szmukler-Moncler *et al.*, 2000). On the contrary, mechanical signals have a pronounced influence on the development and differentiation of mesenchymal cells (Carter, 1987). A certain amount of micro-strain can therefore even promote early peri-implant osteogenesis (Piattelli *et al.*, 1993; Simmons *et al.*, 1999, 2001; Meyer *et al.*, 2004; De Smet *et al.*, 2006; De Smet, 2006). Control of micro-motion at the bone-implant interface is probably one of the most significant biological requirements for a load-bearing implant. However, only a few well-controlled experimental studies have investigated the effect of mechanical load on tissue differentiation at the tissue-implant interface *in vivo*.

1.3.2 Fracture healing

The reparative phase in fracture healing

In fracture healing, the reparative phase can further be divided into two sub phases: the soft and the hard callus phase (Einhorn, 1995, 1998; Hadjiargyrou *et al.*, 2002; Gerstenfeld *et al.*, 2003a). The initially formed granulation tissue is gradually being replaced by fibrous tissue, forming the soft callus. In this soft callus, mesenchymal stem cells will start differentiating, guided by cues from their microenvironment, such as the presence of biological factors (Einhorn, 1998) and the perceived mechanical stimuli (Carter *et al.*, 1998). Direct differentiation towards osteoblasts is observed near the cortex, away from the fracture site. These osteoblasts produce woven bone matrix, the hard callus, in a process called intramembranous ossification. Mesenchymal stem cells differentiate into chondrocytes (cartilage forming cells) in the central fracture area where the soft callus will gradually take on the appearance of cartilage, mechanically stabilising the fracture zone. The chondrocytes mature towards hypertrophic chondrocytes, initiating biochemical preparations in the cartilage matrix to undergo calcification. This concludes the soft callus phase of healing. In the next phase, the hard callus phase, blood vessels invade the calcified cartilage, bringing along osteoblasts. These osteoblasts, receiving enough oxygen and subjected to the proper mechanical stimuli, will produce a hard callus tissue consisting of mineralised woven bone matrix in

a process called the endochondral ossification. When the fracture ends are connected by a bony callus, clinical union is reached.

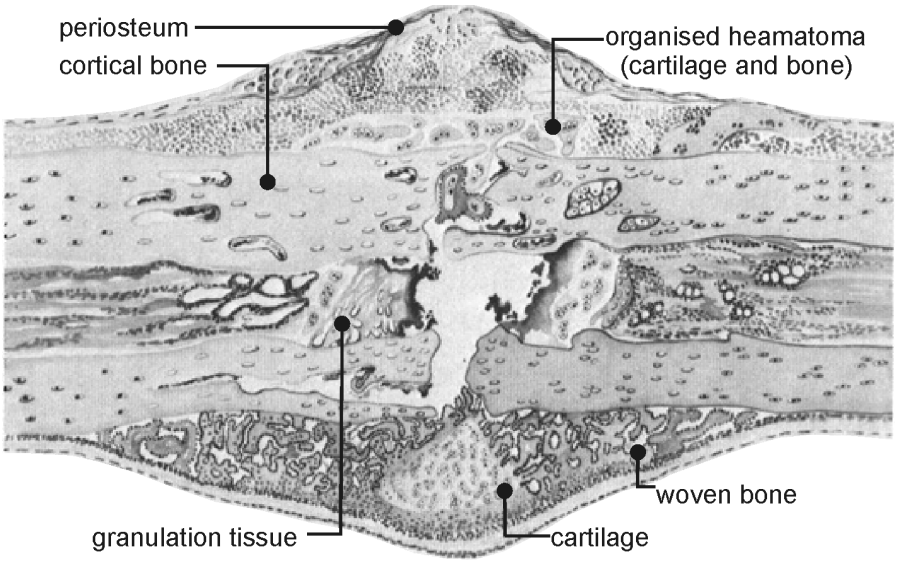


FIGURE 1.4: Schematic overview of the different tissues present in the callus area during the reparative phase of fracture healing (reproduced from Cruess and Dumont (1985)).

Challenges in fracture healing research

Nonunions, hypertrophic or atrophic, and synovial pseudarthrosis generally are differentiated based on radiographic and histological appearance (Rodriguez-Merchan and Forriol, 2004). Hypertrophic nonunions show abnormal vascularity and callus formation, with a horseshoe or elephant-foot (abundant callus) configuration on radiographs. Atrophic nonunions typically show little callus formation around a fibrous tissue-filled fracture gap. Synovial pseudarthrosis is defined as a nonunion in which a fluid-filled cavity with a synovial-like membrane is present at the fracture site. There is no universally accepted definition of nonunion of a fracture. If a fracture fails to heal within the time usually required (known from clinical experience), it is called a delayed union. Generally, failure of a fracture to heal in 6 to 8 months (in humans) constitutes nonunion. The fracture gap of a nonunion usually consists of fibrous tissue with varying amounts of cartilage.

Numerous adverse mechanical and biological factors influence the development of nonunion: excess motion, a large interfragmentary gap, loss of blood supply, severe periosteal and soft tissue trauma (An *et al.*, 1999; Cañadell and Forriol, 1997; Hulth, 1989; Marsh *et al.*, 1994; Landry, 2000; McKibbin, 1978; Oni *et al.*, 1989; Park *et al.*, 1999; Whiteside, 1978). General factors such as old age, cachexia and malnutrition, steroids or anticoagulants, anti-inflammatory agents, burns, and radiation may contribute to the establishment of nonunions but are not the primary causes (Aaron, 1996; Hulth, 1989). Classical treatment strategies for nonunions are aimed at restoring optimal mechanical circumstances to induce healing. Excess motion of the fracture fragments will be reduced by the use of plates, external or intramedullary fixators. However, the application of appropriate dynamic stimulation of the fracture has been shown to enhance the healing process (Goodship *et al.*, 1998; Kenwright and Gardner, 1998). The use of growth factors for enhancing fracture healing is a relatively novel treatment modality. Results of experimental and clinical studies have provided support for the clinical use of growth factors for treatment of acute and nonunion fractures, as reviewed by Southwood *et al.* (2004). Despite the large amount of information existing in literature, additional research is required to determine the exact mechanisms of nonunion and subsequently the optimal therapeutic strategies for each type of nonunion.

Chapter 2

Hypothesis and Objectives

2.1 General hypothesis

The previous chapter identified a clear need for continued research on the regulating factors of the bone regeneration processes in fracture healing and implant osseointegration. Most of the research conducted in this area is of experimental nature. However, despite the extensive set of experimental results that has been published, many aspects of the regeneration process still need to be examined. The last decades, the use of mathematical models in biology and medicine has increased enormously (Murray, 2002). Mathematical models can propose and test possible regeneration mechanisms and corroboration of these models by comparison with experimental data, contributes to the unravelling of the complex nature of the regeneration process. In the mathematical modelling of bone regeneration, a trend is observed towards the integration of both mechanical and biological regulating factors guiding the processes under investigation (Van der meulen and Huiskes, 2000).

The long-term goal of the research presented in this work, is the application of mathematical models in the research on possible causes and treatment of pathological bone regeneration. The hypothesis underlying this work is that **mathematical models are capable of making a substantial contribution to the bone regeneration research**. Models are able to simulate and predict both normal and pathological bone regeneration and can play a role in the design of possible treatment strategies for the latter. Furthermore, models can be applied in the design, guidance and support of (new) experiments. Finally, results from theoretical experiments can evoke interesting research questions and induce a new (more quantitative) look on the biology of bone regeneration.

2.2 Objectives

Specific objectives were formulated in order to assess the research hypothesis stated above. These general objectives are further broken down into specific objectives at the beginning of each of the following chapters. An overview of the coupling between the research presented in the different chapters is shown in figure 2.1

- *Implementation of existing mechanoregulatory and bioregulatory models*
  Existing mechano- and bioregulatory models were applied to different experimental set-ups of implant osseointegration and bone fracture healing. The experimental and numerical results were compared on a qualitative and quantitative basis. Thorough sensitivity analyses were carried out to assess the influence of the different model parameters on the simulation outcome. Shortcomings of the models were identified and suggestions for improvement were made. The results are described in chapters 3 and 4.

- *Development of a novel bioregulatory model*
  A novel mathematical bioregulatory model was developed based on the existing models, adding several indispensable key features of the bone regeneration process. Several of the shortcomings that were identified in chapter 4 were implemented in this model. Application of this model to the fracture healing set-ups allowed for a quantitative corroboration of the novel bioregulatory model (chapter 5).

- *Development of a novel mechanobioregulatory model*
  The concept of mechanoregulation of biological processes was integrated in the novel bioregulatory model described in chapter 5. Chapter 6 describes the establishment of a mathematical framework that allows to investigate the role of both mechanical and biological stimuli on the regeneration process. To illustrate the potential of the established mathematical framework, a simple mechanobioregulatory model was proposed and applications in both fracture healing and implant osseointegration were developed.

2.3 Methodology

2.3.1 Experimental aspects

Results from different animal experiments were used in the course of the studies presented in this thesis. An *in vivo* repeated sampling bone

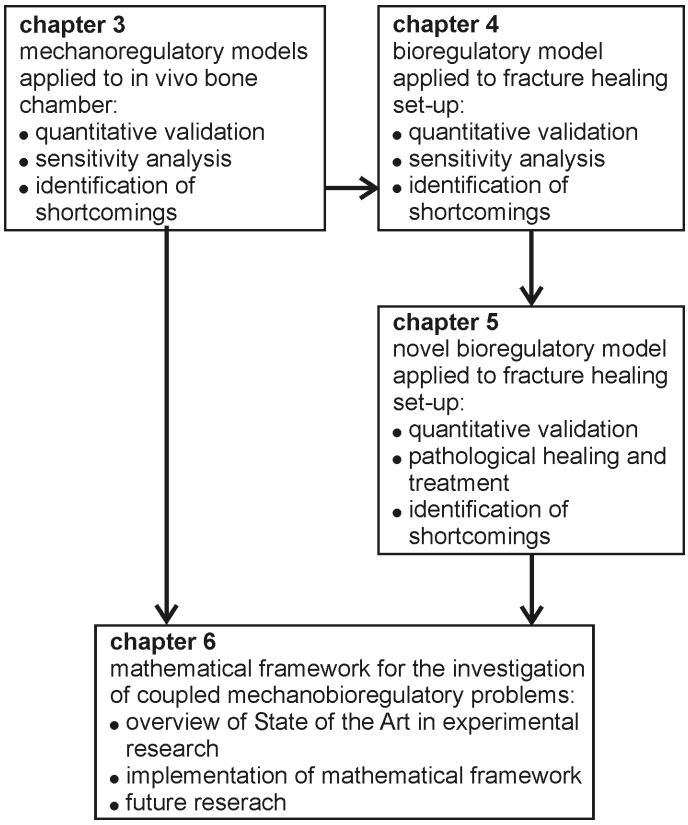


FIGURE 2.1: Flowchart showing the relation between the research presented in the different chapters of this thesis

chamber was developed by the BIOMAT research group (Prosthetic Dentistry, K.U.Leuven, Belgium) in collaboration with the MICAS group (ESAT, K.U.Leuven, Belgium) and the Division of Biomechanics and Engineering Design (Dept. Mechanics, K.U.Leuven, Belgium), featuring a unique peri-implant regeneration environment. Experimental results from this bone chamber model were provided by the BIOMAT research group. Furthermore, the results of a semi-stabilised murine fracture model were provided by the Laboratory of Experimental Medicine and Endocrinology (K.U.Leuven, Belgium (Maes *et al.*, 2006)) encompassing elaborate biological data on the angiogenic aspect of the fracture healing process. Finally, the standardised rodent femoral fracture model (Royal Veterinary College, London, UK (Harrison *et al.*, 2003)) provided quantitative data, obtained in standardised

regeneration sites, allowing for a quantitative comparison of the experimental and numerical results. The set-up of these experimental models, together with a summary of the most important results, are described in chapters 3 and 4.

2.3.2 Modelling aspects

In the framework of the research presented in this thesis, contributions were made to the development of the novel experimental set-up of the *in vivo* repeated sampling bone chamber. Furthermore, software was developed for the implementation of mechanoregulatory and combined mechanobioregulatory models. However, the main contribution and innovative aspect of this work is situated in the thorough assessment of existing mechano- and bioregulatory models and the development of a novel bioregulatory model and a mathematical framework for combined mechanobioregulatory models. Applications of these models in simulating pathological regeneration cases, demonstrate the potential of mathematical models in assisting, refining, inducing and developing experiments, thereby furthering the knowledge in the field of bone regeneration research.

2.3.3 Numerical aspects

The numerical implementation of the mechanoregulatory models was developed by the author in the framework of this thesis, using a combination of Matlab (The Mathworks, Inc.) code interacting with the finite element solver MSC.Marc through the application of Fortran user subroutines (chapter 3). The simulations with the bioregulatory models were carried out in a customised finite volumes code (chapter 4), especially derived for biological problems (courtesy of Dr. Gerisch, Martin-Luther University Halle-Wittenberg, Germany). The previous implementations were combined in a newly developed software framework (in the Matlab environment) to allow for the investigation of combined mechanobioregulatory problems (chapter 6). Further details on the different implementations are provided in the respective chapters.

Chapter 3

Mechanoregulatory models of bone regeneration: application in an *in vivo* bone chamber

This chapter describes the implementation of mechanoregulatory models to simulate peri-implant bone regeneration in an *in vivo* bone chamber. Different existing mechanoregulatory models are applied to this novel experimental set-up and the simulation results are compared with the experimental findings. The introduction gives a brief overview of the evolution of mechanoregulatory models and their application areas and the need for the study presented in this chapter is shown. Section 3.2 states the research hypothesis that was put forward during this study and identifies the different objectives. In section 3.3, first a description of the bone chamber is provided after which the implementation of the different mechanoregulatory models under investigation is explained. Subsequently, section 3.4 contains an overview of the experimental findings, followed by the simulation results for various testing conditions. A discussion of the results and the simplifications that were made during this study forms the content of section 3.5. Finally, the last section recapitulates the hypothesis and concludes with some potential solutions for the shortcomings encountered using mechanoregulatory models to simulate the events in the bone chamber.

3.1 Introduction

3.1.1 Mechanoregulatory models for tissue regeneration

It is well accepted that mechanical factors play a role in bone regeneration, whether it is within the framework of fracture healing or the integration of (oral) implants. Tissue differentiation constitutes a crucial step in the repair process, involving the differentiation of mesenchymal stem cells to tissue-specific cells, like osteoblasts and chondrocytes. Afterwards, the process of bone remodelling will adapt the external geometry and the internal structure of the newly formed bone. Many groups tried to qualify and quantify the exact contribution of the mechanical loading to these events, either by means of animal experiments (Moalli *et al.*, 2000; Søballe *et al.*, 1992a,b; Søballe, 1993) or numerical simulations (Bailón-Plaza and van der Meulen, 2001; Carter, 1987; Carter *et al.*, 1998; Claes and Heigele, 1999; Huiskes *et al.*, 1997; Kuiper *et al.*, 2000; Maheswari and Lauffenburger, 1998; Pauwels, 1960; Perren, 1979; Perren and Cordey, 1980; Prendergast *et al.*, 1997). In the field of prosthetic dentistry, there is a growing tendency towards immediate or early loading of oral implants. The mechanoregulatory effect discussed above may be expected to play an important role in the establishment of osseointegration of loaded oral implants. The question is in what way immediate loading will interfere with the normal healing response that will take place around an implant. Before a proper answer can be formulated, one needs to establish a reliable model to theoretically describe the interaction between tissue loading and differentiation.

The first theoretical models to describe the mechanoregulation of skeletal tissue differentiation were introduced by Pauwels (1960). He recognised that physical factors cause stress and deformation of the mesenchymal cells and that these stimuli could determine the cell differentiation pathway (Figure 3.1). He hypothesised that deviatoric stresses, which are accompanied by a change in cell shape, stimulate the formation of fibrous connective tissue. Hydrostatic stresses on the other hand are a specific stimulus for the formation of cartilaginous tissue. A specific stimulus for the formation of bone however is not present in the theory of Pauwels. According to Pauwels, bony tissue proceeds on the basis of a rigid framework of fibrous tissue, cartilage or bone (Pauwels, 1960).

Some years later, the concept of interfragmentary strain (IFS) was developed by Perren (1979) and Perren and Cordey (1980). They proposed that a tissue, with a certain failure strain, cannot be formed in a region that experiences strains higher than this level. This means that a fracture gap can only be filled with a tissue capable of sustaining the IFS without failure. The IFS

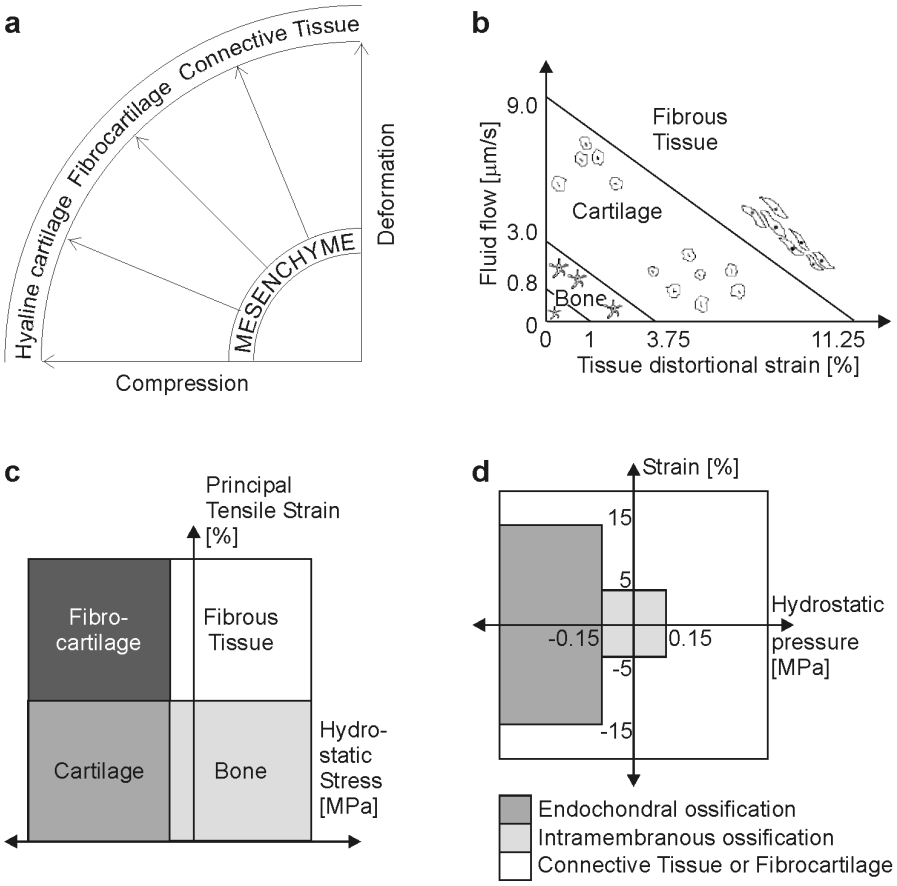


FIGURE 3.1: Differentiation schemes proposed by (a) Pauwels (1960), (b) Prendergast *et al.* (1997), (c) Carter *et al.* (1998) and (d) Claes and Heigele (1999).

concept provides a theoretical basis for evaluating fracture treatment strategies, but is not applicable for bone regeneration in general, since it disregards the structural and mechanical heterogeneity of the fracture callus.

Building on the theories of Pauwels (1960), Perren (1979) and Perren and Cordey (1980), many research groups have formulated a theoretical model relating tissue differentiation to mechanical loading. Carter (1987) and Carter *et al.* (1998) specifically discussed the importance of cyclic tissue loading and proposed a mechanical stimulus that takes into account the lo-

cal stress or strain history. The stress acting on the regenerating tissue is described in terms of hydrostatic stress and distortional strain. Direct bone formation is permitted in regions experiencing low hydrostatic stresses and low distortional strains. Carter however never provided any values for stimuli that favours bone formation. Claes and Heigele (1999) combined the result of their finite element analyses of the mechanical stimuli on ossifying surfaces during fracture healing with a histological analysis of a real callus geometry. From this, they derived a quantitative mechanoregulatory model relating magnitudes of hydrostatic pressure and principal strain to the bone formation process. Intramembranous bone formation occurred at the regenerating bone surface for hydrostatic pressures smaller than 0.15 MPa, while enchondral bone formation occurred when the compressive hydrostatic pressure exceeded this threshold.

The above mentioned theories all considered tissues as solid elastic materials. Prendergast *et al.* (1997) proposed a mechanoregulatory model for tissue differentiation, based on a poroelastic (biphasic) behaviour of the tissues. Maximal distortional strain and relative fluid velocity constitute the stimulus that controls the differentiation process. High values of both solid strain and fluid velocity favour fibrous tissue formation, while intermediate values lead to cartilaginous tissue. Bone can only be formed if the values are sufficiently low. Huiskes *et al.* (1997) quantified the upper and lower limits of the mechanical stimulus for the different tissue phenotypes, which yielded a mechanoregulatory diagram for tissue differentiation. The model was extended to include mesenchymal cell migration (by means of a diffusion equation), as a first step to incorporate the underlying cellular processes (Lacroix and Prendergast, 2002; Lacroix *et al.*, 2002b).

3.1.2 Predictive power of mechanoregulatory models

To answer the question "Does any particular simulation produce a better solution than another approach that has already been developed?", certain thoughts must be kept in mind. Currey (1995) formulated two problems with respect to this question. The first one is that since all models show qualitative agreement with some experimentally observed event but are not matched against each other, there is no telling which is better than the others. The second problem Currey (1995) pointed out is the tendency for simulations to be used with a single adaptation situation with no indication that the method is appropriate for any other one. Hart (2001) suggested that a uniform 'test suite' of example problems could be used to validate every simulation model and improve it incrementally.

Over the last years, efforts were made to meet the objections raised by Currey (1995) and others. The mechanoregulatory models were applied to various experimental situations to assess their validity. Lacroix and Prendergast (2002) successfully applied the model of Prendergast *et al.* (1997), that was calibrated originally with an experiment using a dynamic implant device in the femoral condyles of Labrador dogs (Søballe, 1993), to normal fracture healing. Isaksson *et al.* (2006a,b) compared the predictive power of different mechanoregulatory models, applying them to an identical experimental set-up of fracture healing. All models were able to simulate the course of normal fracture healing correctly. Contrarily, when using torsional loading, being a different mechanical condition than the one applied in the experiments the models were derived from, only the model of Prendergast *et al.* (1997) was able to successfully predict fracture healing. Applying the latter mechanoregulatory model to the experimental set-up of tibial distraction osteotomy (Isaksson *et al.*, 2006c), spatial and temporal tissue distributions as seen experimentally, as well as variations in predicted tissue distributions due to alterations in distraction rate and frequency were obtained. A variation of the same mechanoregulatory model was used by Idelsohn *et al.* (2006) to investigate mandibular distraction osteogenesis. Kelly and Prendergast (2005) applied the mechanoregulatory model of Prendergast *et al.* (1997) to simulate tissue regeneration in osteochondral defects and was able to capture patterns of cellular differentiation observed experimentally in this healing process. Continued efforts however remain necessary applying different mechanoregulatory models to one and the same experimental set-up, different from the one they were primarily designed for, to assess the scope of their predictive powers.

3.2 Hypothesis and Objectives

3.2.1 Hypothesis

The work reported in this chapter aimed to test the hypothesis that mechanoregulatory models are able to predict tissue formation around loaded titanium implants in an *in vivo* repeated sampling bone chamber. This novel experimental set-up was especially designed to control the mechanical load exerted on the differentiating tissues around an implant.
This chapter describes the steps that were followed in the implementation of the different mechanoregulatory models and their application in the simulation of various bone chamber experiments. The results obtained in the experimental and numerical studies are discussed and compared, and the results of a sensitivity analysis are shown, describing the influence of various parameter values that were chosen during the implementation of the model,

on the simulation outcome.

3.2.2 Objectives

1. The development of a finite element model of the bone chamber (section 3.3.2)
2. The implementation of the different mechanoregulatory models (section 3.3.3)
3. The simulation of various bone chamber experiments (section 3.4.2)
4. The comparison between the experimental and numerical results (sections 3.4.2 and 3.5.1)
5. Sensitivity analysis of the parameter values chosen during the implementation of the mechanoregulatory models (sections 3.4.2 and 3.5.2)

3.3 Materials and Methods

3.3.1 Repeated sampling *in vivo* bone chamber

Experimental set-up

A novel experimental set-up, designed to investigate tissue differentiation and bone formation adjacent to endosseous implants under controlled mechanical conditions, was developed by the department of Prosthetic Dentistry in collaboration with the division ESAT-MICAS and the division of Biomechanics and Engineering Design (BMGO) of the K.U.Leuven (Duyck *et al.*, 2004) (Figure 3.2). The experimental set-up constitutes a so called repeated sampling *in vivo* bone chamber, to be implanted in the proximal rabbit tibia. The model consists of two concentric perforated hollow TiAl6V4 cylinders with a centrally positioned c.p. titanium implant. The hollow cylinders, called outer and inner bone chamber, fit exactly into each other and have corresponding perforations, allowing blood inflow and tissue growth into the central cavity of the cylinders. The central implant that is stabilised in a sliding bearing accounting for the primary stability, can be loaded in a well-defined and highly controlled manner by means of an external loading device or actuator. This actuator consists of a piezo translator (preloaded closed loop LVPZT translator, P-841.60, ALT, The Netherlands), which can induce a displacement of up to 90 μm and a load cell (XFTC 100-M5M-1000N, FGP Sensors, France) with a capacity of 1000 N in tension and 100 N in compression. A closed loop control assures the required displacement, hereby inducing shear stresses and strains in the tissue surrounding the implant. The load can be applied with

a frequency of up to 90 Hz. The actuator is controlled by software written in TestPoint^{TM}. Variations in load parameters such as displacement, forces, frequency, duration and amount and distribution of load cycles are possible. The actuator can easily be mounted onto the outer hollow cylinder and be connected to the implant during the loading session.

Studies are carried out in groups of 10 6-months old female New Zealand white rabbits, all specific pathogen free (Pasteurella bacteria) and kept in quarantine for six weeks before the start of the study. The outer bone chamber was installed on the medial side of the proximal tibia. When the latter was osseointegrated (after 6 weeks), the inner bone chamber with central implant was put in place. Depending on the subject of the study, different implants with different surface characteristics were used. Most of the implants were c.p. Titanium (grade 2) drawn cylindrical or turned screw-shaped implants, with surface roughness (R_a) values between 0.45 μm and 0.70 μm. For one study a screw shaped implant with a specific surface texture, the Friadent® CELL-plus implant surface (FRIADENT GmbH, Mannheim, Germany) was used, resulting in a moderately roughened surface with a R_a value of 2.75 μm. The surgical procedure for outer and inner bone chamber installation is described in detail in Duyck *et al.* (2004) and Vandamme *et al.* (2006a). Due to its re-useability, multiple experiments can be performed in the same outer bone chamber. Though the number of experiments should be limited, in order to avoid infections in the bone chamber.

Experiments

The following experiments were conducted in the bone chamber, all of them applying immediate loading after implant installation.

1. Bone chamber study 1 looked into the influence of the load magnitude and the stimulation period on the tissue response around drawn cylindrical implants. Three different loading situations were investigated:
   (a) 30 μm implant displacement, 1 Hz, 400 cycles, twice a week for 6 weeks
   (b) 30 μm implant displacement, 1 Hz, 400 cycles, twice a week for 6 weeks, followed by 50 μm implant displacement, 1 Hz, 800 cycles, twice a week for 6 weeks
   (c) unloaded, 12 weeks
2. Bone chamber study 2 looked into the influence of the implant macro design (screw vs cylinder) and the implant displacement magnitude (0 vs 30 μm) on the tissue response in the bone chamber for a stimulation period of 9 weeks.

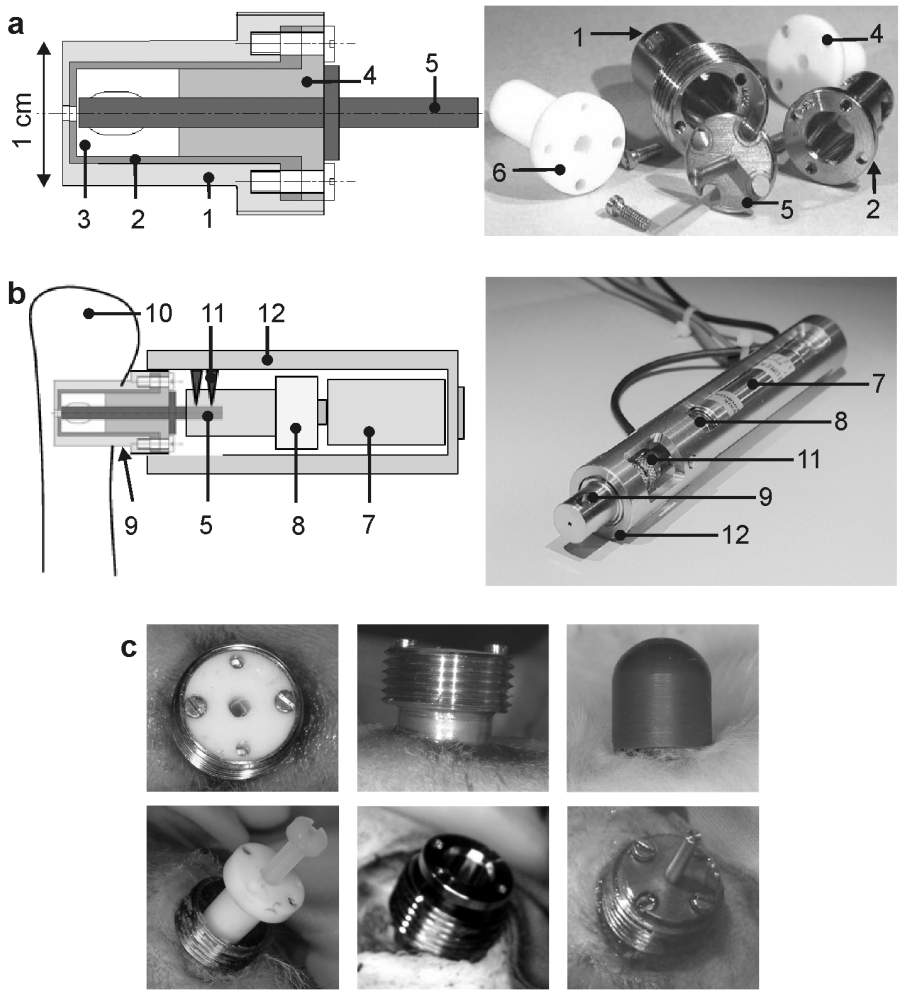


Figure 3.2: Overview of the composition and the installation of the bone chamber. (a) components of the bone chamber. 1: outer bone chamber; 2: inner bone chamber; 3: area for tissue differentiation; 4: teflon bearing stabilising the implant; 5: implant; 6: teflon plug used during the osseointegration period of the outer bone chamber. (b) the loading device. 7: piezo stack; 8: load cell; 9: bone chamber; 10: proximal tibia; 11: clamping device; 12: cage of the loading device. (c) surgical procedure for the installation of the outer bone chamber (top) and the inner bone chamber (bottom).

   (a) drawn cylindrical implant, 30 μm implant displacement, 1 Hz, 400 cycles, 3 times a week
   (b) turned screw shaped implant, 30 μm implant displacement, 1 Hz, 400 cycles, 3 times a week
   (c) turned screw shaped implant, unloaded

3. Bone chamber study 3 looked into the influence of the implant displacement magnitude on the tissue response in the bone chamber around drawn cylindrical implants for a stimulation period of 6 weeks.
   (a) unloaded
   (b) 30 μm implant displacement, 1 Hz, 800 cycles, twice a week
   (c) 60 μm implant displacement, 1 Hz, 800 cycles, twice a week
   (d) 90 μm implant displacement, 1 Hz, 800 cycles, twice a week

4. Bone chamber study 4 looked into the influence of the implant displacement magnitude on the tissue response in the bone chamber around roughened screw-shaped implants for a stimulation period of 9 weeks.
   (a) unloaded
   (b) 30 μ implant displacement, 1 Hz, 400 cycles, 3 times a week
   (c) 90 μ implant displacement, 1 Hz, 400 cycles, 3 times a week

Histological analysis

To evaluate the tissue differentiation and bone formation inside the bone chamber as well as in close vicinity and at the surface of the implant, the specimens were prepared for histological analysis on methylmetacrylate sections. Five sections at the level of the perforations with a thickness of 20 to 30 μm and stained with a combination of Stevenel's blue and Von Gieson's picrofuchsin were analysed (Figure 3.3). The applied stain colours mineralised bone red, osteoid green and fibrous tissue blue. Histological examinations were performed under the light microscope (Leitz Laborlux S, Wetzlar, Germany) at magnifications of $\times$ 40, $\times$ 100, $\times$ 125 and $\times$ 400. By means of a high-sensitivity colour video camera (AxioCam MRc5, Zeiss, Göttingen, Germany) mounted on the light microscope and by means of a colour image analyzing histometry software package (Image Pro Plus®, Media Cybernetics, MD, USA), the following histomorphometric parameters were recorded for each histological section (Figure 3.3):

- Tissue area fraction (TAF [%]): the whole tissue area (bone, bone marrow and fibrous tissue) expressed as a percentage of the entire bone chamber area

- Bone area fraction entire chamber (BAF entire chamber [%]): the whole spongy bone area (bone trabeculae and bone marrow) expressed as a percentage of the tissue area in the entire bone chamber
- Bone area fraction implant vicinity (BAF implant vicinity [%]): the whole spongy bone area expressed as a percentage of the tissue area within a 200 μm wide circular zone around the implant
- Bone density (BD [%]): summation of all individual bone trabeculae (both mineralised and non-mineralised/osteoid) expressed as a percentage of the total bone area (bone and bone marrow) in the entire bone chamber
- Bone-to-implant contact (BIC [%]): the fraction of mineralised bone in direct contact with the implant surface. Both the chance that contact occurred (incidence), as well as the amount of contact were calculated. The incidence was calculated as the number of sections from a certain loading condition in which contact occurred, divided by the total number of sections of that loading condition. The amount of contact was calculated for the subset of sections in which contact occurred.
- Osteoid-to-implant contact (OIC [%]): the fraction of non-mineralised bone in direct contact with the implant surface (incidence and amount)
- Bone-and-Osteoid-to-implant contact (BOIC [%]): the fraction of mineralised and non-mineralised bone in direct contact with the implant surface (incidence and amount).

Statistical analysis

Statistical analysis of the dataset was performed. For the evaluation of study 1, 2 and 4, a linear mixed model was used with the experimental animal as random effect and the loading condition (studies 1 and 2), implant design (study 4), number of histological section (all) and harvest number (studies 2 and 4) as fixed effects for the histomorphometric parameters TAF and BAF. For the evaluation of study 3, an analysis of variance (ANOVA) was performed with one of the histomorphometric parameters as dependent variable and as independent variable the experimental animal, loading condition and number of histological section. Due to the lack of normal distribution, logistic transformation of the data from all studies was performed for the parameters OIC and BIC. A logistic mixed model was used to calculate the chance that osteoid- or bone-to-implant contact occurred (incidence). Additionally, a linear mixed model, taking into account the amount of osteoid- and bone-to-implant contact, was used on the subset of data where implant contact

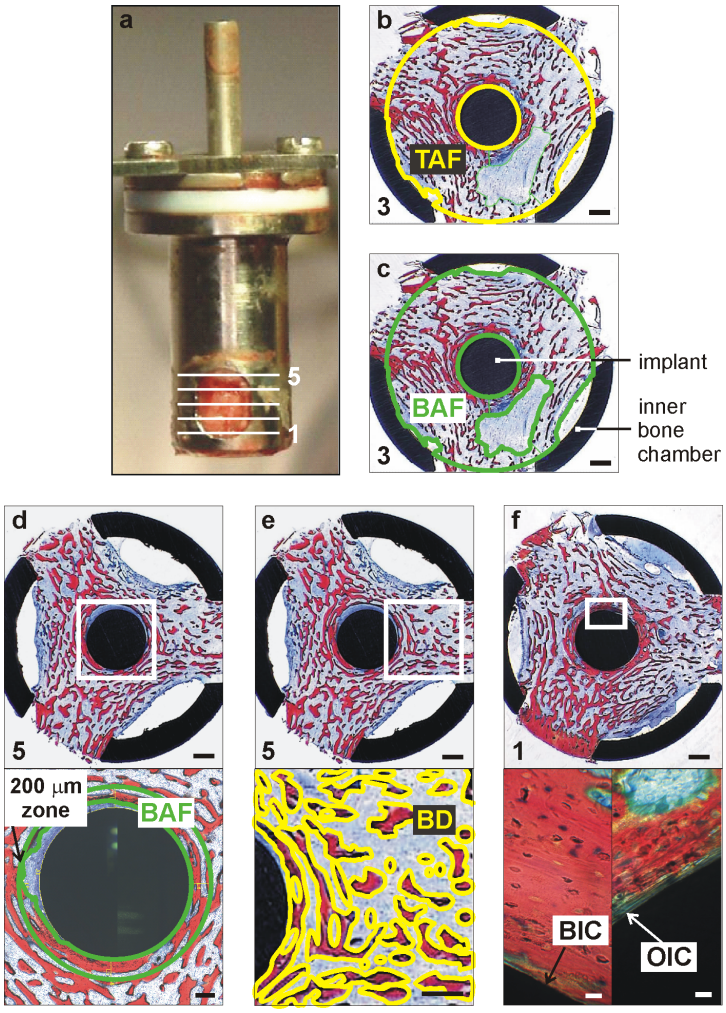


FIGURE 3.3: Overview of the histological parameters. (a) indication of the different sectioning planes. (b-f) indication of the different histological parameters. (b) TAF, scale bar = 500 μm. (c) BAF entire chamber, scale bar = 500 μm. (d) BAF implant vicinity, scale bars = 500 μm (top) & 200 μm (bottom). (e) BD, scale bars = 500 μm (top) & 200 μm (bottom). (f) BIC (bottom left) and OIC (bottom right), scale bars = 500 μm (top) & 20 μm (bottom).

was observed. The data were analysed with SAS/STAT statistical software (SAS Institute Inc., NC, USA). An α-level of 0.05 was chosen to determine the statistical significance. Post hoc multiple comparisons were done using Tukey-Kramer adjustments for significant tests (study 1) and the Bonferroni method for significant F-tests (studies 2 and 4).

3.3.2 Modelling of the bone chamber

Axisymmetric and simplified 3D finite element models were created of the bone chamber and both types of implants (Geris *et al.*, 2004, 2007). For the tissue differentiation simulations, FE models of only the tissue inside the chamber were used. The connection between the tissue and the bone chamber walls and teflon bearing were replaced by appropriate boundary conditions, based on the observations from animal experiments. The tissue was modelled to be connected to the implant and the bone surrounding the chamber. No tissue was observed in contact with the bottom of the chamber and no tissue was observed between the bottom of the chamber and the implant (Figure 3.4). At the perforation sites, free fluid flow (zero pressure) was allowed. Calculations with a model of the entire bone chamber, including the tissue surrounding the bone chamber gave results similar to the ones obtained from calculations performed with a model of only the tissue inside the bone chamber. The axial loading of the implant took place in a displacement controlled manner and was simulated by imposing displacement boundary conditions on the top nodes of the implant. Only one period of a sine function with a frequency of 1 Hz was used to simulate one loading event of the implant. For the 2D model the assumption of axisymmetry was made, while in reality the chamber geometry has only a 120^o rotational symmetry. Taking into account the symmetry of the displacement and fluid velocity fields within the chamber, only one sixth of the entire tissue in the chamber must be modelled in the 3D model. The used elements were biphasic 8-noded axisymmetric quadrilateral elements and biphasic 20-noded bricks, respectively.

All biological tissue were assigned biphasic material properties. According to the poroelasticity theory, tissues can be modelled as a mixture of solid and fluid constituents present at each material point. The stress $\boldsymbol{\sigma}$ acting on the tissue can be separated into a solid phase stress $\boldsymbol{\sigma}'$ and a pore pressure $\mathbf{p}$ ($\mathbf{I}$ representing the unity matrix):

$$\boldsymbol{\sigma} = \boldsymbol{\sigma}' - p\mathbf{I}.$$

All analyses were performed with MSC.Marc/Mentat (Version 2005r2, Palo Alto, USA), using its soil mechanics capabilities. The FE code assumes incompressibility of the solid and fluid constituents (requiring only the defini-

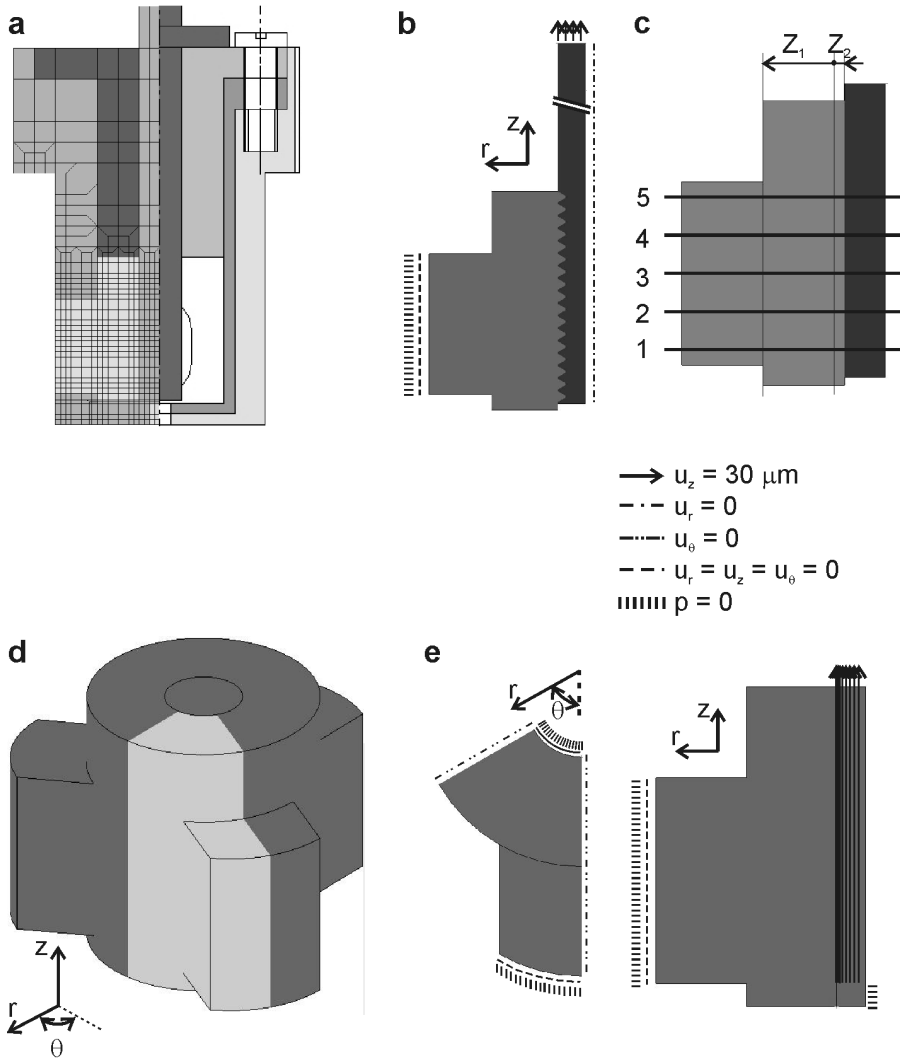


FIGURE 3.4: Overview of the FE models. Top row: 2D axisymmetric finite element model of the entire bone chamber (a) and the tissue inside the chamber (b-c). (b) Overview of the boundary conditions and (c) areas for the calculation of the histological parameters. Bottom row: (d) simplified 3D finite element model of the tissue inside the bone chamber and (e) indication of the boundary conditions.

tion of the material's permeability as an additional material characteristic compared to the linear elastic formulation). Prendergast *et al.* (1996) have demonstrated the validity of this code with respect to the biphasic theory, developed by Mow *et al.* (1980). The material properties used are taken from Lacroix and Prendergast (2002) and are summarised in Table 3.1. The tissue that will be formed through endochondral ossification in the model of Claes and Heigele (1999) was treated as cartilage (Isaksson *et al.*, 2006a), and will be represented that way in the remainder of this chapter.

Table 3.1: Material properties used in the adaptive tissue differentiation simulations.

	Gran. Tissue	Fibrous Tissue	Carti-lage	Immature Bone	Mature Bone
Young's modulus $[MPa]$	0.2	1[1]	10	1000	6000[2]
Permeability $[m^4(Ns)^{-1}]$	1e-14	1e-14[1]	5e-15[3]	1e-13	3.7e-13[4]
Poisson's ratio	0.17	0.17	0.17[5]	0.3	0.3

3.3.3 Implementation of mechanoregulatory models

Figure 3.5 shows an overview of the practical implementation of the adaptive tissue differentiation process, using the mechanoregulatory model of Prendergast *et al.* (1997) as an example. At the start of the simulations, the bone chamber is assumed to be filled with granulation tissue. Precursors cells are modelled to invade the bone chamber from the marrow surrounding the bone chamber. Only where a sufficient precursor cell concentration is present, tissue differentiation based on the local mechanical stimuli, can take place. Migration and proliferation of the cells was modelled as a diffusive process, uncoupled to the actual adaptation routine (Lacroix and Prendergast, 2002).

$$\frac{dC}{dt} = D\nabla^2 C$$

where D represents the diffusion coefficient and C the current cell concentration. The migration speed was determined based on the the total tissue

[1] Hori and Lewis (1982)
[2] Claes and Heigele (1999)
[3] Armstrong and Mow (1982)
[4] Ochoa and Hillberry (1992)
[5] Jurvelin *et al.* (1997)

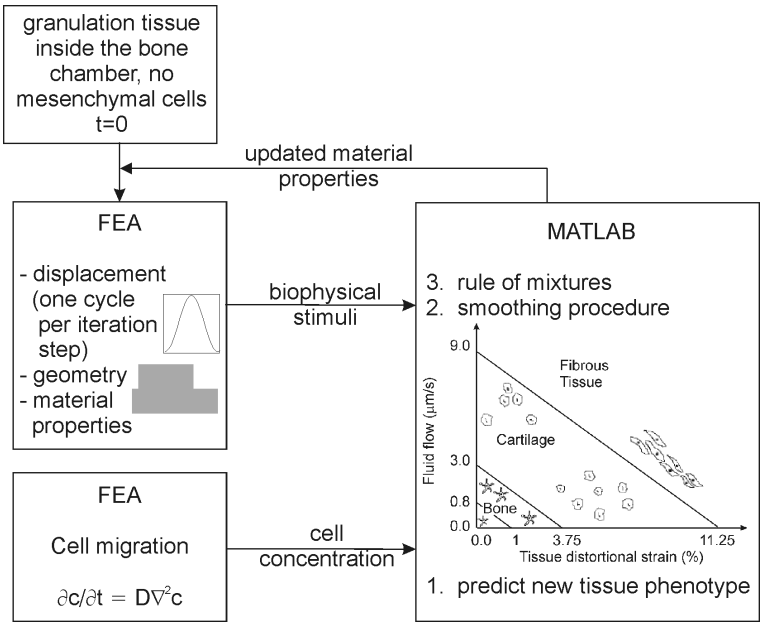


FIGURE 3.5: Schematic overview of the adaptive tissue differentiation simulation. Each iteration starts with the determination of the biophysical stimuli in a FE analysis. Matlab determines new phenotypes based on the stimuli using the mechanoregulatory model under investigation and determines, after mixing and smoothing, the new material properties.

volume measured in the bone chamber at different points after implant installation. After a simulated period of nine weeks, 95 % of the bone chamber was covered by precursor cells (corresponding to the TAF of animal study 2).

The precursor cells were allowed to differentiate into fibroblasts, chondrocytes or osteoblasts and produce their respective extracellular matrix types, depending on the local biophysical stimuli and the mechanoregulatory model under investigation. To account for predicted changes in cell phenotype and the time required for matrix production, a smoothing procedure was used when calculating the new element material properties.

$$E_{n+1} = \frac{1}{10} \sum_{i=n-9}^{n} E_i$$

E_i represents the Young's modulus predicted at iteration i and E_{n+1} represents the new Young's modulus predicted solely based on the local biophysical

stimuli. The latter value was further adapted to take into account the local concentration of precursor cells C present in the element:

$$E_{n+1} = \frac{C_{max} - C}{C_{max}} E_{gran} + \frac{C}{C_{max}} E_{n+1}.$$

E_{gran} represents the Young's modulus of the undifferentiated granulation tissue and E_{n+1} now represents the final Young's modulus. After the assignment of the new material properties, a new iteration could start.

This simulation scheme was followed for the three mechanoregulatory models under investigation: the model of Prendergast *et al.* (1997), the model of Carter *et al.* (1998) and the model of Claes and Heigele (1999). These models were already discussed in section 3.1.1. The values for the tissue phenotype boundaries were not specified for the model of Carter *et al.* (1998). Isaksson *et al.* (2006a) conducted a numerical study to determine appropriate values for the tissue phenotype boundaries. Those values were adopted in this study.

3.3.4 Simulations and sensitivity analyses

A number of simulations were performed to assess the predictive power of the mechanoregulatory models under investigation for the bone chamber set-up. Both the influence of the implant geometry and the magnitude of the displacement were investigated. The histomorphometric parameters mentioned in section 3.3.1 were calculated from the simulation results and compared to the experimental data. Additional analyses were carried out to assess the sensitivity of the simulation results to various features of the mechanoregulatory models and to the assumptions that were made during the construction of the FE model. Convergence tests were performed on the mesh density to ensure that the obtained simulation results were independent of the element size. The simplification of applying only one period of a sine function per iteration step, instead of the 400 to 800 periods that were applied in the animal experiments, was tested. The impact of the diffusion analysis and of individual mechanical stimuli on the simulation outcome was verified. Also the sensitivity of the simulation results to the value of the parameters determining the transition from one tissue phenotype to another was investigated.

3.4 Results

3.4.1 Experimental bone chamber studies

This section summarises the most important results from the bone chamber studies discussed in section 3.3.1 (Figure 3.6). Comparing the loaded and

the unloaded healing at different points in the healing process (6 weeks vs 12 weeks, study 1), it was shown that loading had a positive effect on tissue differentiation and bone formation around cylindrical drawn titanium implants after 12 weeks (Figure 3.6a: TAF, BAF) (Vandamme *et al.*, 2006a). Moreover, controlled implant displacement up to 50 μm had an accelerating effect on tissue mineralisation at the implants' surface (Figure 3.6a: BIC).

Investigation of different implant geometries (screw vs cylindrical shape, study 2) showed that implant loading enhanced bone formation in the implant surroundings for both designs (Figure 3.6b: BAF). At the implant surface itself, the screw-shaped implant design promoted osseointegration compared to the cylindrical implant (Figure 3.6b: BIC) (Vandamme *et al.*, 2006b).

Investigation of the effect of implant surface roughness (turned vs roughened, studies 2 and 4) revealed that under non-loading, roughened implants promote osseointegration compared to turned devices (Figure 3.6d: BIC) (Vandamme *et al.*, 2006c). In the presence of loading, the topographic dependency of the osteogenic activity at the interface was overruled by the loading-related bone response, revealing no significant differences in osseointegration incidence between turned and roughened implants.

Looking at different loading magnitudes (0 vs 30 vs 60 vs 90 μm, study 3) for a cylindrical implant, bone density increased with increasing implant displacement magnitude (Figure 3.6c: BD) while the chance to have bone-to-implant contact decreased in case of displacement at the tissues-implant interface (Figure 3.6c: BIC) (Duyck *et al.*, 2006). Looking at different loading magnitudes (0 vs 30 vs 90 μm, study 4) for a roughened screw-shaped implant, an improved bone reaction with increasing implant displacement magnitude in the surroundings as well as at the interface of the implant was seen (Figure 3.6d: BAF, BIC) (Vandamme *et al.*, 2006d).

3.4.2 Numerical bone chamber studies

Simulation results

2D simulations After a simulated healing period of 9 weeks (mimicking the loading conditions of studies 2 and 4 with a 30 μm implant displacement), the results showed a bone chamber filled with a mixture of (im)mature bone, cartilage and fibrous tissue for all of the implemented differentiation models and for both types of implant geometries (Figure 3.7a). The results obtained with the models of Carter *et al.* (1998) and Claes and Heigele (1999) for the cylindrical implant were very similar, predicting cartilage formation along and mainly at the apex of the implant. Using the model of Lacroix and Prendergast (2002),

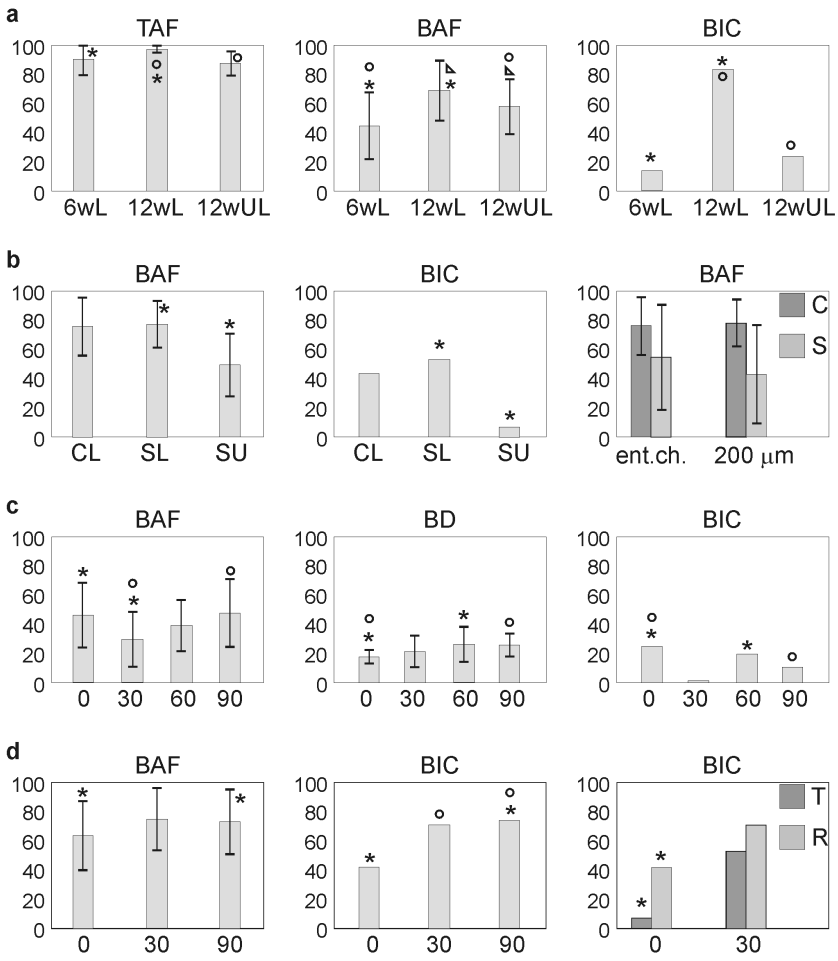


Figure 3.6: Overview of the results from the different bone chamber studies. TAF, BAF and BD: avg±SD; ⋆,○: $p < 0.05$. (a) Study 1: TAF, BAF and BIC incidence. 6wL: 6 weeks loaded; 12wL: 12 weeks loaded; 12wUL: 12 weeks unloaded. (b) Study 2: BAF, BIC incidence and BAF for both the entire bone chamber and the 200 μm peri-implant circular zone. CL: cylinder loaded; SL: screw loaded; SU: screw unloaded. (c) Study 3: BAF, BD and BIC incidence. 0, 30, 60 and 90 μm implant displacement. (d) Study 4: BAF, BIC incidence and BIC incidence for turned and rough screw-shaped implants. 0, 30 and 90 μm implant displacement.

cartilage was predicted to form alongside the central part of the implant, extending towards the chamber perforations. Calculation of the histomorphometric parameters BAF and BIC incidence from the simulation outcome for the cylindrical implant resulted in values that varied widely between the different differentiation models. All models predicted a BAF value which was lower in the implant vicinity than in the entire chamber. Qualitatively this was corroborated by the animal experiments (study 2 and 4). Quantitatively, these values did not correlate well with the experimental findings (Figure 3.7c; Table 3.2). Furthermore, while in the experiments more bone was found near the chamber bottom (Figure 3.8b), this was not captured by any of the models. The predicted values for BAF were closest to the experimental values for the model of Carter *et al.* (1998), while the model of Prendergast *et al.* (1997) predicted the lowest values for BAF of all the models. Contrarily, the model of Prendergast *et al.* (1997) predicted the highest incidence of bone-to-implant contact of all the models. However, this value was still lower than the experimentally observed one. Similar to the experimental data, implant geometry did not strongly influence the predicted tissue distribution pattern for the models of Carter *et al.* (1998) and Claes and Heigele (1999). Contrarily, for the model of Prendergast *et al.* (1997) a substantial difference was noticed in the predicted tissue distribution patterns for the two implant geometries. For all models, there was a substantial increase in the predicted BIC incidence for the screw-shaped implant compared to the cylindrical implant. The much higher values in case of a screw-shaped implant resulted from the fact that the tissue in between the implant threads experienced very low mechanical stimuli, which favoured the differentiation towards bone. Interestingly, a higher incidence and a significantly higher amount of bone-to-implant implant contact in the case of the screw-shaped implant was also found in the animal experiments. All differentiation models predicted a certain amount of cartilage tissue, while no cartilage was found in reality.

In a new set of numerical simulations, cartilage formation was replaced by fibrous tissue formation in the description of the differentiation models to try to obtain better correspondence to the experimental results. The predicted differentiation patterns were similar to the ones obtained previously, except for the formation of fibrous tissue instead of cartilage (Figure 3.7b). Still, no good correlation between the measured and predicted values for the histological parameters was found (Table 3.2).

3D simulations The results from the 3D simulations using the model of Prendergast *et al.* (1997), also showed a bone chamber filled with a mixture of (im)mature bone, cartilage and fibrous tissue (figure 3.8a). In the bottom half of the chamber, bone-to-implant contact was observed along the entire

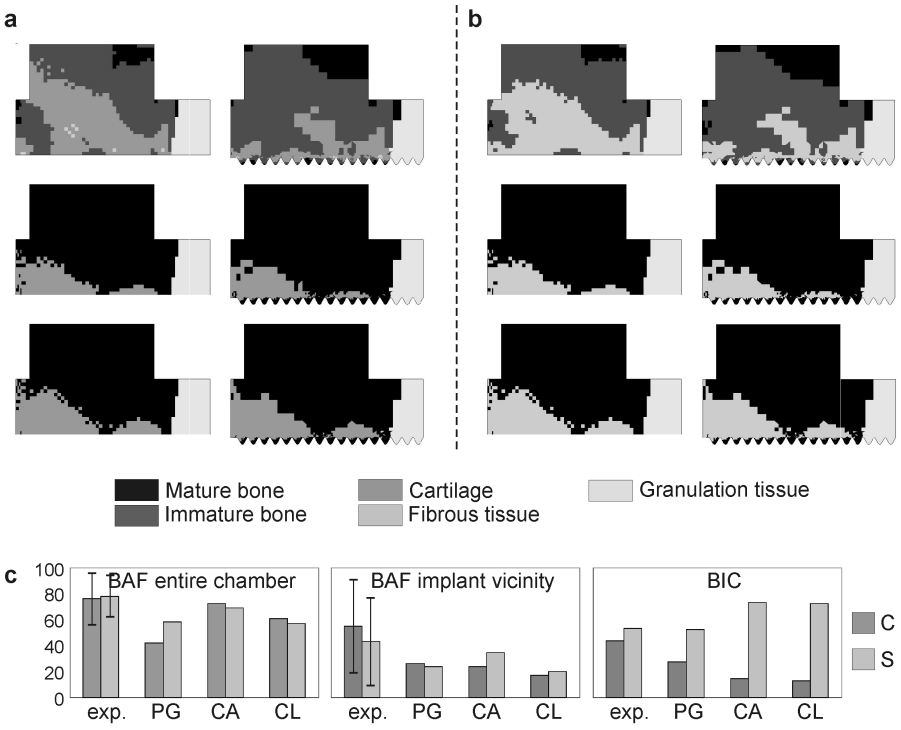


Figure 3.7: Results for tissue differentiation simulations for different implant geometries (cylinder C and screw-shaped S implant) with an implant displacement of 30 μm, using the model of Lacroix and Prendergast (2002) (top - PG), Carter *et al.* (1998) (middle - CA) and Claes and Heigele (1999) (bottom - CL). (a) simulation results for the original models. (b) simulation results after cartilage differentiation was removed from the models. (c) Comparison of BAF and BIC incidence, observed in experimental study 2 (avg±SD) and calculated from the simulations using the original models.

implant circumference. Higher up in the chamber, soft tissue dominated the interfacial tissue composition. The highest soft tissue concentrations were found in the areas adjacent to the chamber perforations, while in the areas in between the perforations, bone was predominantly present. The spatial evolution of the BAF calculated for the entire chamber showed a good qualitative and quantitative correspondence with the experimental data (Figure 3.8b). This was not the case for the BAF calculated in a 200 μm wide circular zone around the implant (data not shown). Calculating the values for bone-to-implant contact for the 3D simulations (Table 3.3), showed an enhanced

TABLE 3.2: Histological parameters BAF and BIC incidence obtained from bone chamber study 2 (avg±SD) and tissue differentiation simulations for cylindrical vs. screw-shaped implants. PG: model of Prendergast *et al.* (1997); CA: model of Carter *et al.* (1998); CL: model of Claes and Heigele (1999); 1: original model; 2: without cartilage formation; nt: without diffusion of precursor cells.

	C			S		
	BAF	BAF 200 μm	BIC incidence	BAF	BAF 200 μm	BIC incidence
exp.	76.39 (19.98)	54.89 (36.24)	43.75	77.75 (16.02)	43.21 (33.90)	53.33
PG1	41.92	26.29	27.48	58.18	23.65	52.45
PG2	37.42	17.33	19.54	56.04	23.81	50.25
PG1nt	45.43	15.34	14.57	47.75	55.48	76.39
PG2nt	28.74	42.63	46.56	51.83	39.72	71.5
CA1	72.42	23.9	14.57	69.02	34.74	73.30
CA2	72.7	23.9	14.57	69.80	34.77	73.26
CA1nt	40.96	1.0	0.0	41.87	9.92	70.61
CA2nt	41.76	1.0	0.0	44.96	11.19	70.35
CL1	60.9	16.93	12.91	57.05	20.01	72.54
CL2	61.18	16.93	12.91	57.20	20.87	72.56
CL1nt	21.64	1.0	0.0	25.02	6.47	65.88
CL2nt	22.88	1.0	0.0	25.08	7.01	64.67

correspondence (with respect to the 2D simulations) between the experimentally observed and numerically predicted values for the BIC incidence. The amount of BIC however was overestimated in the simulations.

Using 3D models, it is possible to explore the effect of different boundary conditions for cell inflow and relate this to certain experimentally observed phenomena. Figure 3.8c shows several histological sections obtained from the same bone chamber, where the bone ingrowth through one of the pores is diminished at the bottom of the chamber (only few trabeculae present) and even absent (no trabeculae) higher up along the implant. Bone ingrowth through the other perforations is normal. This leads to the hypothesis that one of the perforations might have been facing the cortex, therefore being shielded from the marrow. To test this hypothesis, a simulation was designed where the inflow of precursor cells, necessary for tissue differentiation to occur, was blocked in one of the perforations. A tissue distribution was predicted,

similar to the one experimentally observed, with bone present at the bottom of the chamber and gradually less bone present when going higher up in the chamber.

Table 3.3: Comparison of experimentally observed (bone chamber study 2, avg±SD) and numerically calculated values for bone-to-implant contact.

	experiments	2D model	3D model
incidence [%]	43.75	27.48	54.2
amount [%]	11.24	/	50.48
	(7.72)		(32.7)

Implant displacement magnitude Simulations for different implant displacements were performed, using the mechanoregulatory model of Lacroix and Prendergast (2002). The predicted tissue distribution patterns showed an increasing bone area in the main part of the bone chamber after 9 weeks, for an increasing implant displacement. The increase in bone area for implant displacements of 60 and 90 μm takes place mainly in the periphery of the chamber, meanwhile reducing the bone-to-implant contact to zero. For the models of Carter *et al.* (1998) and Claes and Heigele (1999), the bone fraction reduced when the implant displacement increased, as did the bone-to-implant contact. Table 3.4 shows the values for the histological parameters after 6 weeks of loading. The experimentally observed trend (study 3) for higher bone fractions for higher implant displacements was only encountered in simulations using the model of Lacroix and Prendergast (2002). The experimentally observed variations in BIC were not predicted by any of the mechanoregulatory models.

Sensitivity analyses

Convergence test Convergence tests were carried out to determine an appropriate mesh density. Both the reaction forces acting on the implant during displacement and the range of several mechanical stimuli calculated in the bone chamber were compared for different mesh densities (table in Figure 3.10). This showed that the mesh used in the simulations was sufficiently refined to obtain mesh independent results. This was further corroborated by the similarity in tissue differentiation simulation results obtained with the different mesh densities (Figure 3.10). The difference in the maximum values is obtained in a singular point of the mesh.

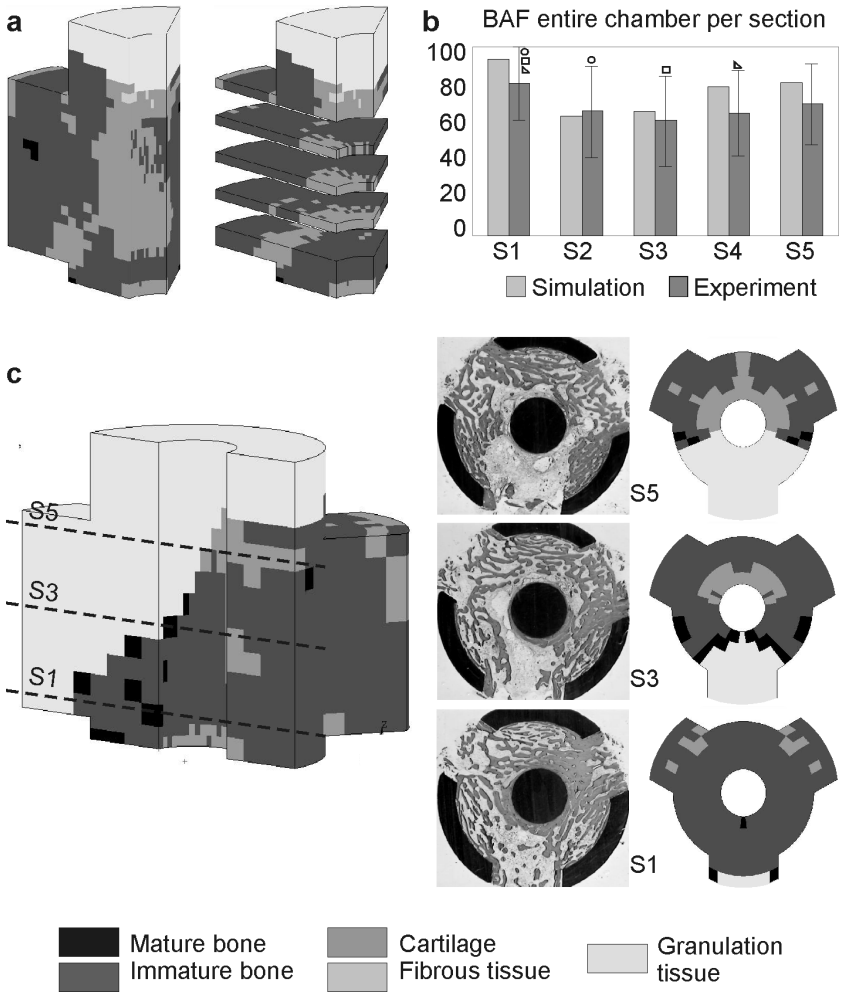


FIGURE 3.8: 3D Tissue differentiation simulation results using the model of Lacroix and Prendergast (2002). (a) Tissue distribution in the chamber (30 μm implant displacement). (b) experimentally measured (study 2, avg±SD, $p < 0.05$) and numerically calculated BAF at different heights along the implant (sections shown in Figure 3.4). (c) Simulation results in case precursor cell invasion through one of the perforations was inhibited. Right: experimental results from study 2 are depicted adjacent to corresponding sections from the FE model. The black zones in the histological sections are parts of the inner bone chamber, the dark grey zones are mineralised trabeculae.

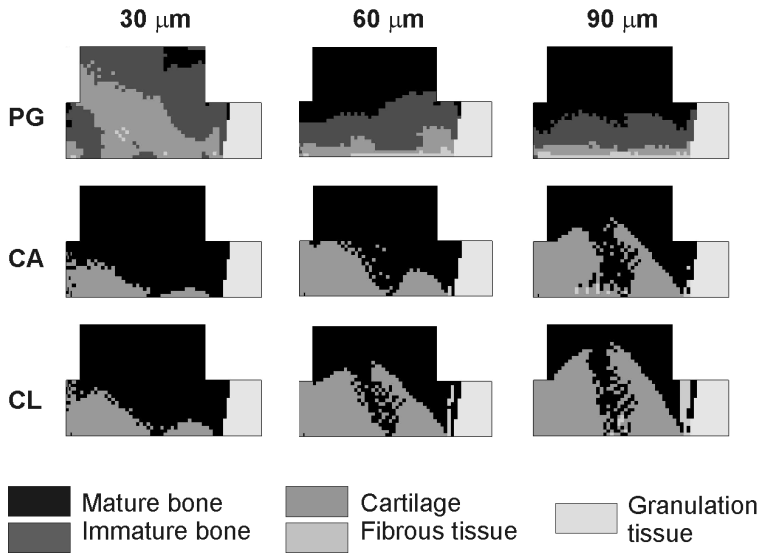


Figure 3.9: Simulation results for three different magnitudes of implant displacement: 30 μm, 60 μm and 90 μm. Results are shown for the different tissue differentiation models under investigation: the model of Lacroix and Prendergast (2002) (top), Carter *et al.* (1998) (middle) and Claes and Heigele (1999) (bottom).

Precursor cell diffusion All of the 2D analyses mentioned in the previous paragraph, were repeated leaving out the diffusion of the precursor cells, as in the original papers from Carter *et al.* (1998) and Claes and Heigele (1999). The analyses iterated until the predicted tissue pattern in the bone chamber did no longer change substantially between two consecutive iterations. For the models of Carter *et al.* (1998) and Claes and Heigele (1999), soft tissue formation alongside the entire implant, extending far into the periphery of the chamber, was predicted (Figure 3.11). Using the model of Lacroix and Prendergast (2002), quite different tissue distribution patterns were predicted depending on the implant geometry. For the cylindrical implant, soft tissue formation was predicted alongside almost the entire implant, whereas for the screw-shaped implant soft tissue formation was predicted to occur mainly in the perforations and alongside the bottom part of the implant. The histological parameters were determined for these simulation results (Table 3.2) but the correlation between these parameters and the ones obtained form the experiments was worse than when precursor cell differentiation was taken into account.

TABLE 3.4: Histological parameters BAF and BIC incidence obtained from bone chamber study 3 (avg±SD) and tissue differentiation simulations for different magnitudes of implant displacement. PG: model of Prendergast *et al.* (1997); CA: model of Carter *et al.* (1998); CL: model of Claes and Heigele (1999); 1: original model; 2: without cartilage formation.

	BAF			BIC		
	30	60	90	30	60	90
exp.	29.71 (18.83)	39.62 (17.62)	47.88 (23.31)	1.4	19.64	10.72
PG1	41.61	52.68	56.66	30.13	0	0
PG2	32.51	54.60	59.37	15.89	0	0
CA1	57.38	40.18	31.44	17.88	7.95	11.92
CA2	57.94	40.60	33.41	17.88	7.95	3.97
CL1	51.41	28.32	17.83	13.91	7.95	5.96
CL2	50.86	30.35	27.40	13.91	9.93	5.96

Mechanical stimulus Tissue differentiation simulations were also performed using only one mechanical stimulus. Deviatoric strain, maximal principal strain and fluid flow were tested in their capabilities to predict tissue differentiation in the bone chamber. The stimulus value indicating a transition from one phenotype to another was taken from Isaksson *et al.* (2006a) and shown in Figure 3.12. When a measure of strain (deviatoric strain or maximal principal strain) was used, the chamber was predicted to be filled with immature bone. Contrarily when a hydrostatic stimulus (fluid flow) was used, a large part of the chamber was predicted to be filled with soft tissue (cartilage and fibrous tissue).

Phenotype boundary values Varying the boundary values for the tissue phenotype transitions in the model of Lacroix and Prendergast (2002), had some effect on the overall tissue distribution pattern that was predicted in the simulations. Changing the boundary value between mature and immature bone led to a higher amount of bone present in the chamber for a lower value of the boundary. When this boundary value was raised however, more mature bone was predicted to form in the perforations but the main part of the chamber remained filled with soft tissue. Lowering the boundary value between immature bone and cartilage did not generate much effect. Increasing the boundary value however showed a bone chamber mainly filled with immature bone. Changing the boundary values between cartilage and fibrous tissue did not influence the simulation outcome. In summary, for this partic-

	coarse	medium	fine
# elements	376	1504	6016
$\Delta r = \Delta z$ [mm]	0.25	0.125	0.0625
max Freac [N]	2.51e-1	2.50e-1	2.50e-1
avg dev str [%]	2.12e-3	2.11e-3	2.11e-3
max dev str [%]	8.28e-3	1.08e-2	1.47e-2
avg fl fl [μm/s]	1.59e-8	1.55e-8	1.44e-8
max fl fl [μm/s]	5.95e-7	1.92e-6	1.36e-6

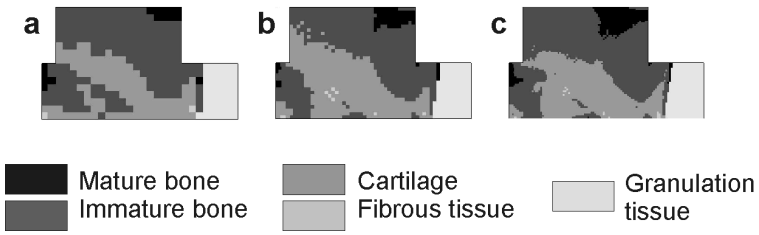


Figure 3.10: Results for the convergence tests. Number of elements, maximal reaction force on the implant during displacement, average and maximal deviatoric strain (dev str) and fluid flow (fl fl) are given in the table. The results for the tissue differentiation simulations using the model of Lacroix and Prendergast (2002) for an implant displacement of 30 μm are show for different mesh densities: (a) coarse, (b) medium and (c) fine mesh. The simulations presented in this chapter are obtained with the medium mesh density

ular experimental environment, the model appears to be highly sensitive to the value of the boundary between immature bone and cartilage.

Material properties Varying the values for the Young's modulus of mature and immature bone in the model of Lacroix and Prendergast (2002) had a substantial influence on the predicted tissue distribution patterns when the stiffness of both mature and immature bone was reduced (Figure 3.14). Reducing the stiffness of only mature or immature bone separately, did not alter the predicted tissue distribution pattern substantially. With less stiff material properties for immature and mature bone, the predicted tissue values for the histological parameters BAF and BIC incidence corresponded better to the ones experimentally observed, than those predicted using the material properties reported in Table 3.1. This enhanced qualitative and quantitative correspondence remained when the differentiation towards cartilage was removed from the mechanoregulatory model (Figure 3.14d).

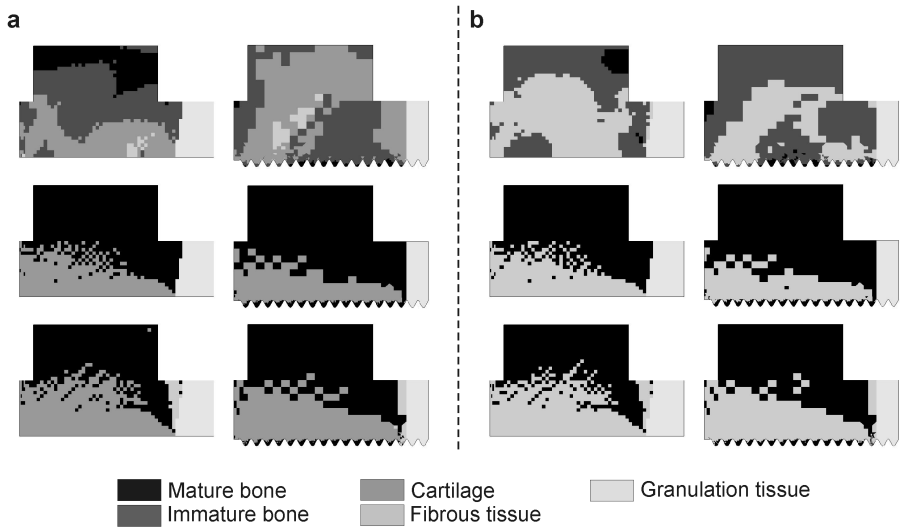


FIGURE 3.11: Results for tissue differentiation simulations without precursor cell diffusion (30 μm implant displacement) for different implant geometries (cylinder and screw-shaped implant), using the model of Lacroix and Prendergast (2002) (top), Carter *et al.* (1998) (middle) and Claes and Heigele (1999) (bottom). (a) simulation results with cartilage. (b) simulation results without cartilage.

3.5 Discussion

3.5.1 Simulation results

2D simulations

Different mechanoregulatory models for tissue differentiation were applied to simulate tissue formation in the bone chamber for different implant geometries. Large qualitative and quantitative differences were found between the tissue patterns, predicted by the models of Carter *et al.* (1998) and Claes and Heigele (1999) on the one hand and the model of Lacroix and Prendergast (2002) on the other hand. The model of Carter *et al.* (1998) yielded the best approximation to the experimentally observed BAF in the entire chamber (bone chamber studies 2 and 4). The highest incidence of bone-to-implant contact for a cylindrical implant was predicted by the model of Lacroix and Prendergast (2002), however, still substantially lower than the experimentally observed incidence. Similar to the experimental observations, all mechanoregulatory models predicted a higher bone-to-implant

	mat bone ↓ immat bone	immat bone ↓ cartilage	cartilage ↓ fibrous tis
a: deviatoric strain [%]	0.05	2.5	5
b: max princ strain [%]	0.05	2.5	5
c: fluid flow [μm/s]	0.6	2.5	5

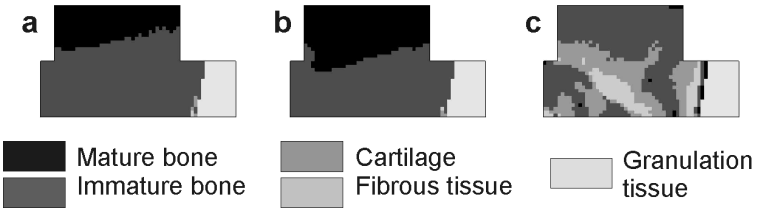


Figure 3.12: Tissue differentiation simulations (30 μm implant displacement) using one mechanical stimulus: (a) deviatoric strain, (b) maximal principal strain and (c) fluid flow. The boundary values for the tissue phenotype transitions are indicated in the table (top) (Isaksson *et al.*, 2006a).

contact incidence for the screw-shaped implant, compared to the cylindrical implant. Furthermore, no substantial difference in BAF value for the entire chamber was observed, nor predicted by the models of Carter *et al.* (1998) and Claes and Heigele (1999). Using the model of Lacroix and Prendergast (2002), a substantial increase in the amount of BAF was predicted for the screw-shaped implant compared to the cylindrical implant, resulting in a better quantitative agreement with the experimental observations.

Since cartilage tissue was not observed in any of the bone chamber experiments (Duyck *et al.*, 2006; Vandamme *et al.*, 2006a,b,c,d), the numerical simulations were repeated using adapted versions of the differentiation models, where cartilage formation was replaced by fibrous tissue formation. Because fibrous tissue has a lower stiffness and a higher permeability than cartilage (see Table 3.1) this adaptation to the models may affect the load transfer from the implant to the surrounding tissues, therefore also affecting the prediction of bone formation. However, the predicted (bone) tissue distribution patterns were similar to the ones obtained with the original models, with the (obvious) exception of fibrous tissue replacing the previously predicted cartilage. The adapted models did not lead to a better correlation between the predicted and the observed bone area fractions.

	mat bone ↓ immat bone	immat bone ↓ cartilage	cartilage ↓ fibrous tis
a	S x 0.5	-	-
b	S x 1.5	-	-
c	-	S x 0.8	-
d	-	S x 1.2	-
e	-	-	S x 0.8
f	-	-	S x 1.2

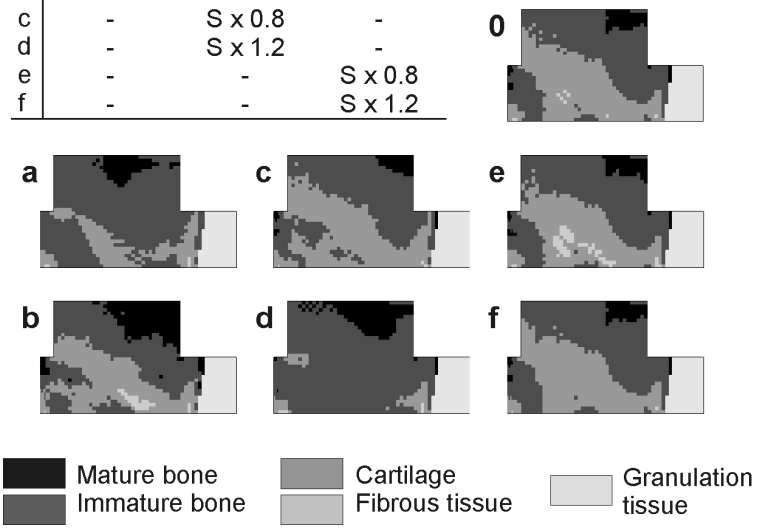


FIGURE 3.13: Results of the sensitivity analysis on the boundary values for tissue phenotype transitions using the model of Lacroix and Prendergast (2002). The tested values of the phenotype transition boundaries for the differentiation stimulus are indicated in the table (top) (Lacroix, 2000). (0) simulation result with boundary values determined by Huiskes *et al.* (1997).

The absence of cartilage in the bone chamber may be related to mechanical and/or biological factors by which the bone chamber environment differs from e.g. fracture healing. The bone chamber provides a mechanical environment that is much more isolated than the fracture callus. The implant is only loaded three times a week and in between consecutive loading events, the tissues inside the bone chamber experience no loading at all, whereas in the fracture callus, there is a more continuous exposure to mechanical loading. This difference in the amount of daily and weekly loading events may have affected the tissue response and its effect is not captured in the current mechanoregulation models. Furthermore, the amount of tissue damage induced when installing a new inner bone chamber, is much lower than the amount of damage associated with a bone fracture. This difference in tissue damage could lead to a quite different inflammatory response and subsequent regeneration process at the

	E-modulus mat bone [MPa]	E-modulus immat bone [MPa]
a	2000	1000
b	6000	500
c	2000	500
d	2000	500

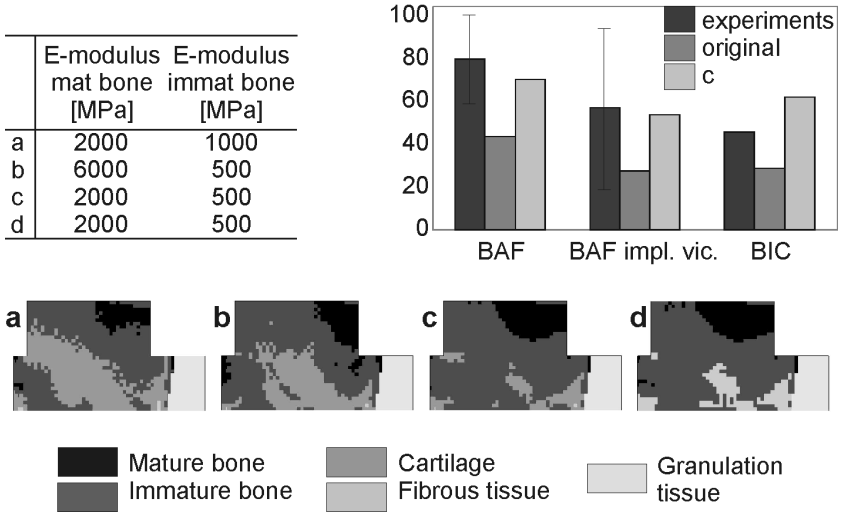


Figure 3.14: Influence of bone material properties on the simulation outcome for the model of Lacroix and Prendergast (2002) (30 μm implant displacement). Left: the different combinations of material properties used in the simulations with the model of Lacroix and Prendergast (2002) (for combination d also cartilage was removed from the model). Right: comparison of BAF (avg $\pm$SD) and BIC incidence for bone chamber study 2 (cylindrical implant), simulations with the material properties of Table 3.1 and simulations with material properties combination c in the left table.

trauma site (Barnes, 1999). Also, a good vascularisation in the bone chamber may have favoured direct bone formation, instead of cartilage formations (and its subsequent ossification) (Street *et al.*, 2000, 2002; Uchida *et al.*, 2003). Finally, it is likely that all the biological factors that may have regulated tissue differentiation in the bone chamber, originated form the bone marrow. Bone marrow derived cells have been shown to differentiate into osteoblasts during bone fracture repair (Taguchi *et al.*, 2005).

The effect of other model adaptations, besides the removal of cartilage, was explored as well. Adding the prerequisite to the (original) models that bone formation could only occur on preexisting bony surfaces (Claes and Heigele, 1999; Isaksson *et al.*, 2006c) resulted in a bone chamber entirely filled with mature bone, except for a very thin layer of fibrous tissue, covering the entire implant and shielding the bone from any mechanical load (results not shown).

3D simulations

The 3D simulations resulted in a better correspondence to the experimental observation on the bone-to-implant contact incidence and the spatial distribution of the bone area fractions at different locations in the bone chamber. This could be attributed to the correct representation of the geometry of the perforations. In the simplified axisymmetric model, there is a 360^o opening in the chamber whereas in reality there are only 3 oval perforations at 120^o from each other. In the simulations, less bone is observed immediately opposed to the perforations due to higher values for the fluid flow in that region. In the histological analyses however, the distribution of the tissues with respect to their relative position to the perforations was not quantified and therefore a quantitative validation of this numerical observation was not possible. In the longitudinal plane through the implant axis and the middle of a perforation (i.e. corresponding to the plane of the 2D axisymmetric model), the predicted tissue distribution pattern was not substantially different from the one predicted with the 2D simulations. Therefore, 2D simulations are a sufficient measure to assess the global behaviour of the mechanoregulatory models.

Whereas 2D simulations are sufficient to asses the global behaviour, 3D simulations allow for a more detailed investigation into the spatial distribution of the tissue at different locations in the bone chamber. An example was given where the invasion of precursor cells, from the marrow into the chamber, was blocked in one of the perforations . The resulting tissue distribution pattern showed bone formation opposed to this sealed perforation near the bottom of the implant, but little to no bone formation higher up in the chamber. This particular tissue distribution pattern was also observed in some of the harvested inner bone chamber samples. It was hypothesised then that this phenomenon had been caused by a erroneous positioning of the outer bone chamber upon installation in the rabbit's tibia, whereby one of the perforations was facing the inner cortex instead of the bone marrow. Using 3D simulations, this hypothesis could be confirmed.

Implant displacement magnitude

Looking at the effect of implant displacement, no good qualitative or quantitative correspondence for the BAF and BIC incidence values observed experimentally and predicted numerically was obtained with the models of Carter *et al.* (1998) and Claes and Heigele (1999). Using the model of Lacroix and Prendergast (2002), the experimentally observed trend for higher bone fractions with higher implant displacements was confirmed. However, the experimentally observed values for BIC incidence could not be predicted by this model either. The counterintuitive numerical result indicating higher

bone area fractions for higher implant displacements could be explained by the influence of the fluid flow on the differentiation process. For the 30 μm implant displacement, large pressure gradients are present at the interface between cartilage and bone, causing high fluid flows in the cartilage tissue, preventing the tissue from differentiating further towards bone. For higher implant displacements, a layer of fibrous tissue is formed adjacent to the implant, shielding the remainder of the chamber from the mechanical load and therefore allowing bone to be formed.

3.5.2 Sensitivity analyses

Precursor cell diffusion

Removing the precursor cell diffusion from all differentiation models, allowed to determine an equilibrium situation between mechanical stimuli and tissue distribution patterns, without simulating the ingrowth process into the chamber. The tissue in the upper part of the chamber was excluded from the differentiation process as it was not yet present in the bone chamber after nine weeks. It was modelled as granulation tissue to allow for a better comparison with the results obtained using the original models (Figure 3.7). The differentiation loop as presented in Figure 3.5 was reiterated until the obtained tissue distribution patterns stabilised. The correlation between the predicted and observed tissue distribution patterns however did not improve compared to the previous simulations.

Mechanical stimulus

All the mechanoregulatory models consist of two types of stimuli, one related to the volumetric deformation, accounting for the change in size, and one related to the deviatoric deformation, accounting for the change in shape. The contribution of each type of stimulus was investigated. Using only the deviatoric stimulus, the whole chamber was predicted to be filled with (im)mature bone. Contrarily, using a hydrostatic stimulus, mainly fibrous tissue and cartilage formation was predicted. Using maximal principal strain as a stimulus, a tissue distribution pattern was predicted, similar to the one obtained with the deviatoric stimulus. For none of the predicted tissue patterns however there was an improvement in the quantitative correspondence with the experimental results compared to the simulations where both stimulus types were combined.

Phenotype boundary values

All of the mechanoregulatory models have already been shown to be (sometimes even highly) sensitive to the boundary values of the tissue phenotype

transitions. Lacroix (2000) showed that for the application to fracture healing, the value of the boundary between fibrous tissue and cartilage on the one hand and cartilage and immature bone on the other hand, had a high impact on the predicted outcome. Lowering the threshold for the formation of the stiffer tissue caused a too slow decrease in interfragmentary strains and too high fluid flows, resulting in a nonunion. Isaksson *et al.* (2006a) showed that the simulation outcome for the models of Carter *et al.* (1998) and Claes and Heigele (1999) was highly sensitive to the chosen boundary values. Similar sensitivity tests were carried out for the bone chamber set-up and these results reported by Lacroix (2000) and Isaksson *et al.* (2006a) were largely confirmed. Only for the model of Lacroix and Prendergast (2002), no influence was observed when the boundary value for the transition between cartilage and fibrous tissue was altered. The largest influence however was observed when the boundary value for the transition between cartilage and immature bone was increased, predicting a substantial increase in the amount of bone formation in the chamber. This indicates that for an implant displacement magnitude of 30 μm, many elements in the bone chamber experience a mechanical stimulus that is only slightly too high for bone formation to occur.

Material properties

Sensitivity of the simulation outcome to the chosen values of the material properties was extensively tested by Lacroix (2000). It was shown that the Young's modulus and permeability of the biological tissues was important, especially in the case of the soft tissues (fibrous tissue and cartilage). For the application of the model of Lacroix and Prendergast (2002) to the bone chamber set-up, the influence of the Young's modulus on the tissue distribution pattern was assessed. The analyses indicated that there was a substantial influence of the stiffness of the bone tissue on the simulation outcome. Lowering the stiffness for both the mature and immature bone combined generated an enhanced quantitative correspondence with the experimental results. This result emphasises the need for adequate characterisation of not only the biological processes taking place in the bone chamber, but also of the tissues that are being formed. The values for the bone stiffness used in this study were determined from literature in Lacroix (2000) and used in the majority of the tissue differentiation simulations reported in the literature up till now. They were based on direct measurements on callus tissue by Augat and Claes (1997). However, depending on the density and anatomical location, a wide range of stiffness values for trabecular bone can be found, ranging from 85 MPa up to 2000 MPa (Ulm *et al.*, 1997; Keaveny *et al.*, 1994). Experimental tests should be carried out on the tissue formed inside the bone chamber, to determine its mechanical properties.

3.5.3 Simplifications

Boundary conditions

In the course of this study, several simplifications were made for the FE model of the bone chamber. The boundary conditions were derived based on experimental observations. No fixed contact between the tissue and the bottom of the bone chamber was observed. Contrarily, a solid connection of the tissue inside the chamber to the tissue surrounding the outer bone chamber was observed and modelled likewise. No tissue was observed under the implant and in the perforation in the bottom of the bone chamber. Calculation of the mechanical stimuli in a FE model incorporating the tissue under the implant and the bottom perforation, showed a very high value for these stimuli, affecting the tissue in the entire bottom area of the bone chamber. It could very well be that under these extreme mechanical conditions, no tissue will be formed at all or that present tissues will be resorbed. None of the investigated mechanoregulatory models incorporated the effect of tissue resorption due to excessive mechanical stimuli. For this reason, the FE model did not incorporate any tissue under the implant or in the bottom perforation.

Tissue-implant contact

The composition of the new tissue formed inside the bone chamber was clearly dependent on the mechanical conditions. Comparable results for the observed bone area fractions in the loaded situation for both implant geometries, significantly differing from the results obtained in an unloaded situation, show that transmission of mechanical stimuli from the implant to the surrounding tissue is taking place (Vandamme *et al.*, 2006a,b). From these observations it is concluded that a bond between the implant and the surrounding tissues exists.

The contact option in the finite element program used for this study (MSC.Marc/Mentat), allows the user to determine the value of the maximal tensile strength upon which bond between the implant and the surrounding tissues is broken. For the shear strength only two options are given: zero ('touch contact') or infinite ('glue contact') shear strength. A detailed literature survey on the experiments determining the values of maximum tensile and shear strength, as well as a study of the influence of the modelling options in MSC.Marc/Mentat on the mechanical stimuli experienced by the tissues surrounding the implant can be found in Van Oosterwyck (2000). For an axially loaded screw-shaped implant, the largest difference in mechanical stimuli in the peri-implant tissue was found between the models with zero and infinite shear strength over the full length of the implant.

When simulating the tissue differentiation taking place in the bone chamber around a cylindrical implant, the only possible option is a 'glue contact', representing a rigid bond between the implant and the tissue. In case of a 'touch contact', no transfer of mechanical stimuli would take place since the implant is only displaced in the axial direction. For the screw-shaped implant, also a rigid bond between the implant and the surrounding tissue was modelled during the simulations. For this implant geometry, another set of differentiation simulations were carried out using the zero shear strength option ('touch contact'). The differentiation outcome did not differ substantially from the one shown in Figure 3.7 and Table 3.2. Comparison of the experimentally measured and numerically calculated reaction forces on the implant during displacement (both around 25 N after 9 weeks) further indicated that the assumption of 'glue contact' between implant and surrounding tissues was acceptable for the purpose of this study.

	glue contact (a)	touch contact (b)	Experiment avg (SD)
BAF entire chamber [%]	58.18	61.22	77.75 (16.02)
BAF 200 μm zone [%]	23.65	21.80	43.21 (33.90)
BIC [%]	52.45	57.71	53.33

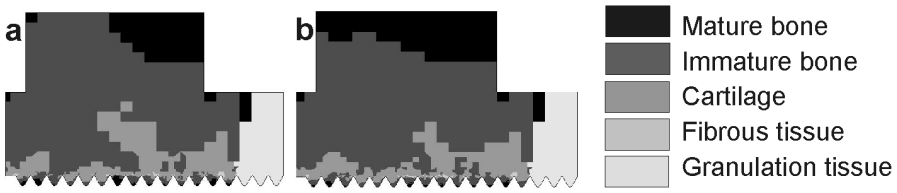


FIGURE 3.15: Influence of the tissue-implant contact conditions on the simulation outcome (30 μm implant displacement). (a): rigid bone ('glue contact'); (b): no bond ('touch contact'). The table shows the comparison with experimental results from bone chamber study 2 (avg±SD).

Number of displacement cycles per loading event

In the animal experiments, at each loading event, the implant was displaced 400 times (800 in study 3), following a sinusoidal curve. In the simulations, only 1 displacement cycle was modelled per loading event. Calculation of the mechanical stimuli when modelling 20 displacement cycles showed that maximal mechanical stimuli occurred in the first displacement cycle due to the poroelastic nature of the tissues. Running differentiation simulations where 20 displacement cycles per loading event were modelled, gave rise to results

that were a quasi perfect match to the ones shown in Figure 3.7 (Geris *et al.*, 2003).

3.5.4 Falsifiability of mechanoregulatory models

The goal of this study was to corroborate both qualitatively and quantitatively each of the presented mechanoregulatory models (Prendergast *et al.*, 1997; Carter *et al.*, 1998; Claes and Heigele, 1999) for a situation other than the one they were primarily designed for or mainly applied to (the model of Prendergast *et al.* (1997) was originally derived from an implant osseointegration set-up), namely secondary fracture healing. The application of mechanoregulatory models to different *in vivo* cases of tissue formation is an essential part of the falsification of these theories (Currey, 1995). In his philosophy of the Critical Rationalism, K. Popper stated that good scientific theories must have a large number of potentially falsifying hypotheses. Theories that lack potential falsifiers leave little room for refutation and therefore have little predictive power (Prendergast, 2004). Prendergast (2004) formulated some potential falsifiers for his mechanoregulatory tissue differentiation theory, among which are histological studies of real tissue forming situations that show different tissue patterns as the ones predicted from the simulation. So far, the mechanoregulatory theory developed by Prendergast *et al.* (1997) and calibrated with a loading experiment using an implant device in canine femoral condyles (Huiskes *et al.*, 1997) has already been shown to hold in situations of normal and pathological fracture healing (Lacroix and Prendergast, 2002; Isaksson *et al.*, 2006a,b) and distraction osteogenesis (Isaksson *et al.*, 2006c). However, in this study, the three considered mechanoregulatory models could only partially be corroborated by the experimental findings.

The question that arises now is whether these tissue differentiation models can be applied to implant osseointegration in an *in vivo* bone chamber in the first place. The fact that the predicted tissue patterns do not correspond to the ones observed does not prove the theories and their underlying principles to be false, but could indicate that for this experimental set-up other factors are equally or perhaps more important than the ones encompassed in the models. Although mechanical stimuli favouring the formation of cartilage are shown to be present in the chamber, no cartilage formation has been observed in any of the bone chamber experiments. Possible explanations could be found in the presence (or absence) of growth factors and good vascularisation of the tissues in the bone chamber, as explained earlier in this discussion (Section 3.5.1). Therefore, the characterisation of the cellular and molecular mechanisms that lead to bone formation in the bone chamber, which may be different to the ones found during secondary fracture healing, will be important to explain

the observed discrepancy between model and experiment. At the same time, it will contribute to the demarcation of the application area of the models.

3.6 Conclusion

In summary, no clear qualitative or quantitative correlation was obtained between all of the experimentally observed and numerically simulated tissues and tissue distribution patterns for any of the investigated mechanoregulatory models. However, depending on the model under investigation, certain aspects of the experimental observations could be captured by some of the models:

- An increased BIC incidence for screw-shaped implants compared to cylindrical implants, also experimentally observed, was predicted by all models
- A higher BAF for the entire chamber compared to the 200 μm circular zone around the implant was predicted by all models and observed experimentally.
- No substantial difference between the BAF for cylindrical or screw-shaped implants was predicted by the models of Carter *et al.* (1998) and Claes and Heigele (1999) nor measured experimentally.
- Using 3D simulations with the model of Prendergast *et al.* (1997), the experimentally observed spatial distribution throughout the chamber of the BAF was predicted

However, also a substantial influence of a number of model parameters such as material properties and the boundary values of tissue phenotype transitions on the simulation outcome was demonstrated. Therefore, the hypothesis of this study, that the mechanoregulatory models of Prendergast *et al.* (1997), Carter *et al.* (1998) and Claes and Heigele (1999) are able to simulate the histodynamics of bone tissue formation in the bone chamber, could not be fully confirmed. A better characterisation of the experimental set-up and the introduction of biological factors in the mechanoregulatory models could lead to a better correspondence between experimental observations and simulation results. The next two chapters will discuss an existing (chapter 4) and a novel (chapter 5) bioregulatory model for bone regeneration. The coupling between the mechanics and the biology will be discussed in chapter 6.

Chapter 4

A Bioregulatory model of bone regeneration: application in fracture healing

In this chapter an existing bioregulatory model was implemented in a custom code and applied to experimental fracture healing set-ups in order to facilitate a quantitative comparison between simulation results and experimental observations, complementing the qualitative comparisons reported in literature. The introduction describes mathematical models developed for different biomedical problems and the different modelling techniques that were used for that purpose. The research hypothesis underlying this study and the different objectives that were formulated are stated in section 4.2. The next section describes the two rodent fracture models that provided the experimental results presented in this chapter, followed by a brief summary of the bioregulatory model under investigation and finally the details of the custom code, especially designed for the implementation of biological problems. Section 4.4 contains a summary of the experimental findings of the two experimental set-ups and the results obtained simulating normal and pathological fracture healing cases. A discussion of these results and the simplifications that were made during this study forms the content of section 4.5. The last section summarises the most important conclusions of the study reported in this chapter and contains a number of potential improvements to the mathematical model under investigation.

4.1 Introduction

4.1.1 Mathematical models in biomedicine

The majority of the research activities in the field of tissue differentiation and regeneration is experimental. The underlying biology of these processes is extremely complex and remains partially unknown. Theoretical biology can make a significant contribution in further unravelling the interactions between the different influencing factors. Considerable research efforts have been devoted to the development of theoretical models of soft tissue growth and repair. Sherratt and Murray (1990) described epidermal wound healing, hypothesising that a single chemical with a simple regulatory effect can account for epidermal mitosis. Later, different aspects of soft tissue regeneration have been elaborated: angiogenesis in wound healing (Pettet *et al.*, 1996), extracellular matrix dynamics (Dallon *et al.*, 1999), cell kinetics in corneal epithelial wound healing (Gaffney *et al.*, 1999) and wound contraction (Tranquillo and Murray, 1992). All of these models consist of a continuum system of partial differential equations (PDE).

Tumour growth and its underlying processes of angiogenesis and invasion have also been the subject of extensive theoretical research. Suggestions for anti-cancer therapies have been formulated, based on the prevention of the tumour angiogenic process (Levine *et al.*, 2001; McDougall *et al.*, 2002; Plank *et al.*, 2004). This field of research is one of the most active areas within mathematical and theoretical biology (Alarcon *et al.*, 2005). Many approaches, ranging from the use of continuum models to the use of cell centred[1] models and various hybrid forms, are being followed to investigate diverse aspects of tumour growth and development. A review of continuum modelling in cancer research can be found in Preziosi (2003) and a review of the various applications of cell centred models in cancer research is given in Moreira and Deutsch (2002). A small number of these models is mentioned below in this section.
Systems of partial differential equations, describing the spatiotemporal evolution of various cellular concentrations, tissue densities and protein concentrations are used by many groups (Anderson and Chaplain, 1998; Levine *et al.*, 2001; McDougall *et al.*, 2002). Anderson and Chaplain (1998) and Sun *et al.* (2005) combine this continuum formulation with a discrete (cell-centred) representation of the vasculature, allowing for a representation of capillary growth, branching and anastomosis. In McDougall *et al.* (2002) the work of Anderson and Chaplain (1998) is extended to incorporate the fluid flow through the capillaries to model the nutrient supply and the delivery of chemotherapeutic drugs to the tumour. Turner and Sherratt (2002) use a cell centred model (extended Potts model) to study the influence of malignant cell

phenotypes on cancer invasiveness. All of the aforementioned models focus on one scale, without addressing the question of how the phenomena occurring at different scales are coupled. The framework proposed by Alarcon *et al.* (2005) allows for the formulation of multi-scale models of tumour growth, capable of integrating a hierarchy of processes occurring at different scales.

4.1.2 Applications in bone regeneration

A simple model for wound healing in bone has been proposed by Adam (1999) and Arnold and Adam (1999). Bailón-Plaza and van der Meulen (2001) have developed a more extensive mathematical model describing the reparative phase of the secondary fracture healing process. The processes of cell proliferation, differentiation, intramembranous and endochondral ossification as described in section 1.3 are all represented in this mathematical model. For further details the reader is referred to the original paper. A schematic representation of the model is given in Figure 4.1. Briefly, the model constitutes 7 variables, namely the concentration of mesenchymal stem cells, chondrocytes and osteoblasts, the concentration of an osteogenic and a chondrogenic growth factor and the density of a combined fibrous/cartilaginous extracellular matrix (ECM) and a bone ECM. The cell densities change due to cell migration, proliferation, differentiation, endochondral replacement and cell removal, while the changes in the matrix density are the result of synthesis. Most of these processes are mediated by the osteogenic and chondrogenic growth factors. The concentration of growth factors changes due to diffusion, synthesis and decay.

Many studies into possible biological causes of delayed or nonunion are carried out in genetically modified mice (Colnot *et al.*, 2003; Gerstenfeld *et al.*, 2003b; Maes *et al.*, 2006). When a mathematical model capable of simulating normal fracture healing in mice is available, genetic modifications can be incorporated into the model and the simulation outcome compared to the experimental findings. Starting from that basis, potential therapeutic strategies can be designed and tested *in silico* before they are tested *in vivo*. However, in order to obtain clinically relevant results when looking at pathological fracture healing and therapeutic strategies, a quantitative validation of the model is indispensable. Bailón-Plaza and van der Meulen (2001) compared the simulation outcome of their model to the data available in literature, on a qualitative basis. A good qualitative agreement was found. Up to this point, no quantitative comparison between numerical simulation results and experimental measurements has been made for this model.

[1] The word cell refers in this context to either an individual biological cell (e.g. endothelial cells) or a (small) cluster of cells (Alarcon *et al.*, 2005).

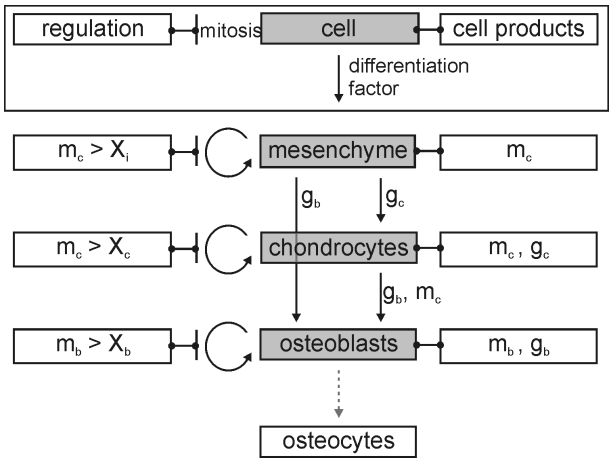


Figure 4.1: Schematic overview of the model of Bailón-Plaza and van der Meulen (2001) (reproduced from Bailón-Plaza and van der Meulen (2001))

4.2 Hypothesis and Objectives

4.2.1 Hypothesis

The long-term goal of this research is to identify possible causes of pathological fracture healing and to investigate different therapies to avoid or reverse pathological healing. Prior to that, a mathematical model needs to be established that can predict the biological processes, observed during normal fracture healing in a quantitative way. The research hypothesis underlying the study described in this chapter is that the bioregulatory model of Bailón-Plaza and van der Meulen (2001) is able to capture several important aspects of the fracture healing process, allowing for the investigation of possible causes of pathological healing. The application of the mathematical model of Bailón-Plaza and van der Meulen (2001) to a mouse model of semi-stabilised fracture healing and a standardised rodent fracture model, and the comparison between the experimental and numerical results for both set-ups will be described. A set of parameter values, slightly different from the values reported by Bailón-Plaza and van der Meulen (2001), was derived to give an optimal correspondence between the experimentally observed and numerically predicted process of fracture healing. Additionally, the sensitivity of the numerical predictions to the different model parameters was assessed for this bioregulatory model. Finally, several cases of pathological fracture healing and examples of treatment by the administration of growth factors were simulated

to demonstrate the potential therapeutic value of mathematical modelling of fracture healing. This study forms the basis for the further development of the mathematical model, supported by experimental observations, as described in chapter 5.

4.2.2 Objectives

- The development of geometrical models of the experimental fracture healing models (section 4.3.2)
- The implementation of the bioregulatory model of Bailón-Plaza and van der Meulen (2001) (section 4.3.3)
- The simulation of normal fracture healing (section 4.4.2 and 4.5.1)
- Qualitative and quantitative comparison of the simulation results with the experimental findings (section 4.4.1 and 4.5.1)
- Sensitivity analysis of the parameter values (section 4.4.2 and 4.5.2)
- The simulation of pathological fracture healing and examples of simulations of treatment strategies (section 4.4.2 and 4.5.4)

4.3 Materials and Methods

4.3.1 Rodent fracture models

Two distinct experimental fracture healing set-ups were used in the course of this study, a semi-stabilised murine tibial fracture and a standardised rodent femoral fracture. Both set-ups were developed for different research purposes and both models provide useful information on different aspects of the fracture healing process. The semi-stabilised model was developed in the Laboratory for Experimental Medicine and Endocrinology (Prof. G. Carmeliet) of the K.U.Leuven. This model did not provide a standardised fracture environment that would allow for a reproducible quantification of tissue distribution throughout the callus area, but provided a lot of data on the biological aspects of the healing process such as angiogeneses and the presence of growth factors. In the development of the femoral rodent fracture at the Royal Veterinary College London (Prof. A. Goodship), special attention was paid to the development of a standardised fracture environment where the quantification of the tissue distribution throughout the callus was possible in a reproducible manner for all specimens of the experiment. However, additional information on the angiogenic process and the presence of growth factors was absent from the latter.

Semi-stabilised murine tibial fracture model

A transverse bone fracture was induced in the left tibia of 11-week old mice (n = 34), under pentobarbital anesthesia (100 mg/kg intraperitoneal). A longitudinal incision of approximately 8 mm was made in the skin, on the anterior side of the lower leg, to expose the proximal tibia. Micro-pincers were used to induce the fracture in the proximal tibia, at approximately 0.5 cm distal from the knee, taking care not to injure the surrounding soft tissues. The fracture was semi-stabilised by an intramedullary fixating pin (a thin-walled needle, 0.4 mm diameter), which was inserted into the tibia at the proximal articular surface and which longitudinally spanned the main part of the bone through the marrow (Figure 4.2). To avoid gross displacement of the tibia halves, the fibula was cut at mid-diaphysis. Mice were sacrificed at several time points after fracture induction (post fracture day PFD 3, 8, 13, 21). The experiments were conducted with the approval of the Ethical Committee of the Katholieke Universiteit Leuven.

Histomorphometric analysis was conducted using a a Zeiss Axiovert microscope and a Kontron image analyzing system (KS400 V 3.00, Kontron Electronik, Germany). Measurements were done on 2 to 6 sections of 4 to 6 mice per group (cartilage: n = 6 at PFD 8, n = 5 at PFD 13; bone: n = 5 at PFD 8, n = 4 at PFD 13). Skin and surrounding tissues were carefully removed and the tibia was isolated. For assessment of the cartilage content of the callus, the tibia was fixed in 2 % paraformaldehyde overnight at 4^o C. After decalcification, bones were dehydrated in a graded ethanol series, embedded in paraffin and sectioned (thickness 5 μm). To visualise the cartilage proteoglycans, sections were stained with 0.1 % Safranin O (SO) combined with Fast green stain, colouring the proteoglycans red. Intensity of SO staining as well as cell morphology were used to qualify tissue as cartilage. Determination of the percentage of cartilage in the callus was performed by computer quantification of the manually marked callus and the cartilage areas. For assessment of the bone area, callus mineralisation was visualised by treating undecalcified MMA sections (thickness 4 μm) with a 5 % silver nitrate ($AgNO_3$) solution for 1 hour in strong light (Von Kossa staining, colouring mineralised bone black). Soft tissues were stained light blue with a hematoxylin counterstain. The bone area was calculated, using a macro, as the surface area of mineralised tissue divided by the surface area of a manually selected region of interest. The latter encompassed the entire callus area, but excluded the original cortical bone and the area formerly occupied by the needle. Additional histological analyses were carried out on the specimen harvested at PFD 8, to determine the tissue distribution in the callus in terms of the total area occupied by bone tissue (not only the mineralised tissue but also the spaces between the

trabeculae), cartilage and fibrous tissue.

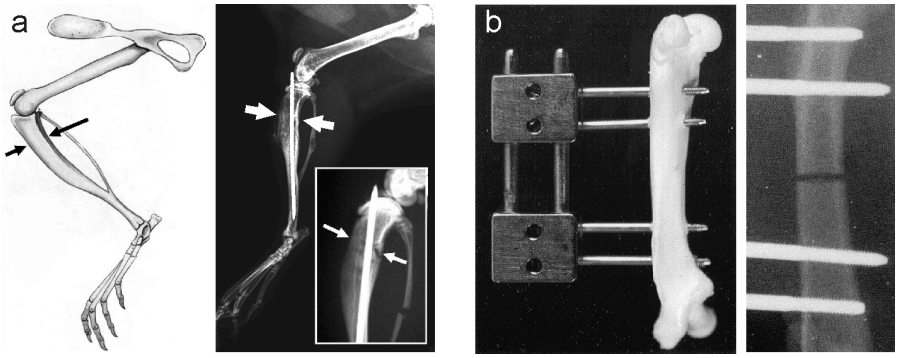


FIGURE 4.2: (a) model of a semi-stabilised murine tibia fracture. Left: schematic view of the site of fracture induction in the proximal diaphysis of the murine tibia (arrows). Right: radiograph illustrating the tibia fracture model and its semi-stabilisation by an intramedullary pin. The insert shows a magnified view of the fracture site. (b) model of a standardised rodent femoral fracture. Left: in vitro model of the fixator set-up. Right: radiograph illustrating the femoral fracture and its stabilisation by the fixator.

Standardised rodent femoral fracture model

A mid-diaphyseal femoral osteotomy was created in 12-week-old male Wistar rats (body weight 450-550 gr, n=16) and stabilised with a precision miniature external fixator in a unilateral, single plane configuration. The fixator was applied to the craniolateral aspect of the femur using four threaded M1.2 stainless steel pins. Surgery was performed under general anesthesia using aseptic techniques, in accordance with U.K. Government, Home Office regulations. Consistent positioning of the fixator pins was ensured using a drill locator template. A bone-fixator distance of 8.0 mm was created using a precision spacer. After pin placement, a transverse osteotomy was created midway between the proximal and distal pins using an oscillating diamond bone saw, with saline irrigation throughout. The bone fragments were distracted to leave an osteotomy gap of either 0.5 mm or 3.0 mm, this being provided using a precision spacer and maintained by locking the fixator blocks on to the connecting bars (Figure 4.2).

Rats were sacrificed at several time points after fracture induction (post fracture week PFW 1, 3, 5, 9, n=4 at each time point) and the healing was

assessed by means of radiography, dual-energy X-ray absorptiometry, histology and mechanical testing. For the sample preparation for histology, care was taken to minimise the variance in histologic appearance of the longitudinal sections caused by the asymmetry and heterogeneity of the repair callus, by standardising the plane of section in relation to defined anatomical landmarks. After death, the osteotomised femora were excised and dissected free of surrounding musculature. Two reference pins (diameter 1.0 mm) were inserted, one in each fragment, midway between and perpendicular to the fixator pins (i.e., craniomedial-caudolateral plane). Pin position was determined consistently using a custom-made locating device attached to the fixator. The fixator was next removed and replaced with a holding device to maintain osteotomy alignment during processing.

Bones were fixed in alcoholic Bouin solution for 2 days, followed by decalcification in 5 % nitric acid-based solution, and then impregnated and embedded in paraffin wax. After removal of all pins, longitudinal sections (5 μm) were cut in the craniomedial-caudolateral plane using a Reichert-Jung microtome. Sections were retrieved for histologic analysis only when the reference pin tracks traversed the bone with maximum diameter. These were stained with Masson's Blue Trichrome (blue or green: collagen and bone, light red or pink: cytoplasm, dark brown to black: cell nuclei). The tissue distribution was evaluated using a Leica microscope at 50×, 100×, and 200× magnification. In particular, the appearance of callus (periosteal-endosteal) was documented, specifically with reference to ongoing chondrogenesis, intramembranous ossification, and endochondral ossification. Evidence of cortical union via end-to-end or periosteal bridging was recorded. Based on preliminary validation studies, histomorphometric parameters, which could be quantified precisely, were recorded. Measurements were performed at 50× magnification using a video image display, digital bit pad (CalcComp Drawing Board III, Osteometrics, Inc., Atlanta, GA, U.S.A.), and commercial bone histomorphometry software (Osteomeasure, Osteometrics Inc.). The area (mm^2) occupied by specific tissues (bone, cartilage, fibrous tissue, and marrow) in defined regions was obtained by tracing the tissue perimeter. Spaces within woven bone were measured as 'void' and subtracted from the total bone area to give the area of woven bone per se. The area of each tissue was expressed as a percent of the total tissue area in a region. These specific regions in which analysis was performed were the periosteal, the endosteal and the intercortical callus region, indicated in Figure 4.3.

4.3.2 Mathematical model

Model structure

The mathematical model for secondary fracture healing presented by Bailón-Plaza and van der Meulen (2001) describes the temporal and spatial change of the densities of the fibrous/cartilaginous extracellular matrix (ECM), the bone ECM, mesenchymal stem cells, chondrocytes and osteoblasts as well as the change of the concentration of a chondrogenic and an osteogenic growth factor. An optimal vascular and mechanical environment is assumed for 'normal' secondary fracture healing to proceed (Bailón-Plaza and van der Meulen, 2003).

In more detail, the mathematical model consists of seven highly coupled nonlinear partial and ordinary differential equations, forming a system of the taxis-diffusion-reaction type. Its general structure is represented by the following system of equations.

$$\begin{aligned} \frac{\partial c_m}{\partial t} =& \nabla \cdot \left[D_{cm}\left(\vec{c}\right) \nabla c_m - c_m \sum_{i=1}^{6} f_i\left(\vec{c}\right) \nabla c_i \right] + f_0\left(c_m, \vec{c}\right) \\ \frac{\partial \vec{c}}{\partial t} =& D \Delta \vec{c} + \vec{g}\left(c_m, \vec{c}\right) \end{aligned} \tag{4.1}$$

t represents the time, $\vec{x}$ the space and $c_m\left(t, \vec{x}\right)$ the non-dimensional density of the mesenchymal stem cells. $\vec{c}(t, \vec{x})$ represents a vector of six non-dimensional concentrations or densities of chondrocytes, osteoblasts, ECM and growth factors, respectively. The diffusion coefficients $D_{cm}\left(\vec{c}\right)$ and D (non-negative diagonal matrix), the taxis coefficients $f_i\left(\vec{c}\right)$ and reaction terms $f_0\left(c_m, \vec{c}\right)$ and $\vec{g}\left(c_m, \vec{c}\right)$ are further explained in Appendix 7.3.2. The system 4.1 must be complemented by suitable initial and boundary conditions to ensure the existence, uniqueness and non-negativity of a solution $\left(c_m\left(t, \vec{x}\right), \vec{c}\left(t, \vec{x}\right)\right)$. Appendix 7.3.2 contains the detailed non-dimensionalized equations of the mathematical model and the values of all of the parameters used in this study. Most of the values of the model parameters were derived by Bailón-Plaza and van der Meulen (2001) from experimental results reported in literature. However, for some parameters the value could not be derived from experimental results and their value was estimated. For a number of these estimated parameters, the value was adapted in this study to obtain a better correspondence between the experimental data and the simulation results.

Geometrical domain

The geometry of the fractures was simplified to the generic geometry presented in Figure 4.3. In case of the semi-stabilised murine fracture, the dimensions were obtained from the experimental model and from literature (Turner *et al.*, 2001). The gap size was taken to be 0.4 mm. The intramedullary needle (diameter 0.4 mm) stabilising the fracture was assumed to be positioned in the centre of the medullary canal. The presence of this needle was further assumed not to affect the normal secondary healing process. Due to assumed symmetry of the fracture callus, only one quarter of the cross-section was considered. This quarter area was further simplified since the custom finite volumes code requires the geometry to be constructed of rectangular shapes, resulting in the simplified generic model domain as depicted in Figure 4.3 (bottom middle). The above described simplifications were also made upon creation of the generic geometry of the standardised rodent femoral fracture (Figure 4.3b). For that experimental set-up, the dimensions were obtained from the histological data at PFW 3, when the callus had reached its maximal size. The inner diameter of the femur was 1 mm, the width of the cortex 0.5 mm. Models were created for a fracture gap of 0.5 mm and 3 mm (the latter is not shown in Figure 4.3).

Initial and boundary conditions

Boundary conditions are indicated in Figure 4.3 and their value and duration were based on the value and duration reported by Bailón-Plaza and van der Meulen (2001). Mesenchymal stem cells were allowed to enter the fracture site from the surrounding tissues and the intramedullary space (0.02×10^6 cells/ml) during the first 3 days, followed by a no-flux boundary condition for the remainder of the simulation period (Gerstenfeld *et al.*, 2003a). Chondrogenic and osteogenic growth factors were assumed to originate from respectively the fractured bone ends and the cortex away from the fracture site (Barnes, 1999; Dimitriou *et al.*, 2005a) (200 ng/ml during 20 days). At the start of the simulation ($t = 0$), the initial fibrous/cartilaginous ECM density was set to 0.01 g/ml for the entire fracture area. All other initial densities and concentrations were set to zero.

4.3.3 Numerical implementation

The seven variables $(c_m(t, \vec{x}), \vec{c}(t, \vec{x}))$ in the model 4.1 are non-negative. This qualitative property of the solution must be inherited by its numerically computed approximation because, amongst others, erroneous negative values for the concentrations might render otherwise stable reaction terms unstable. Besides ensuring non-negativity, the algorithm used for the numerical

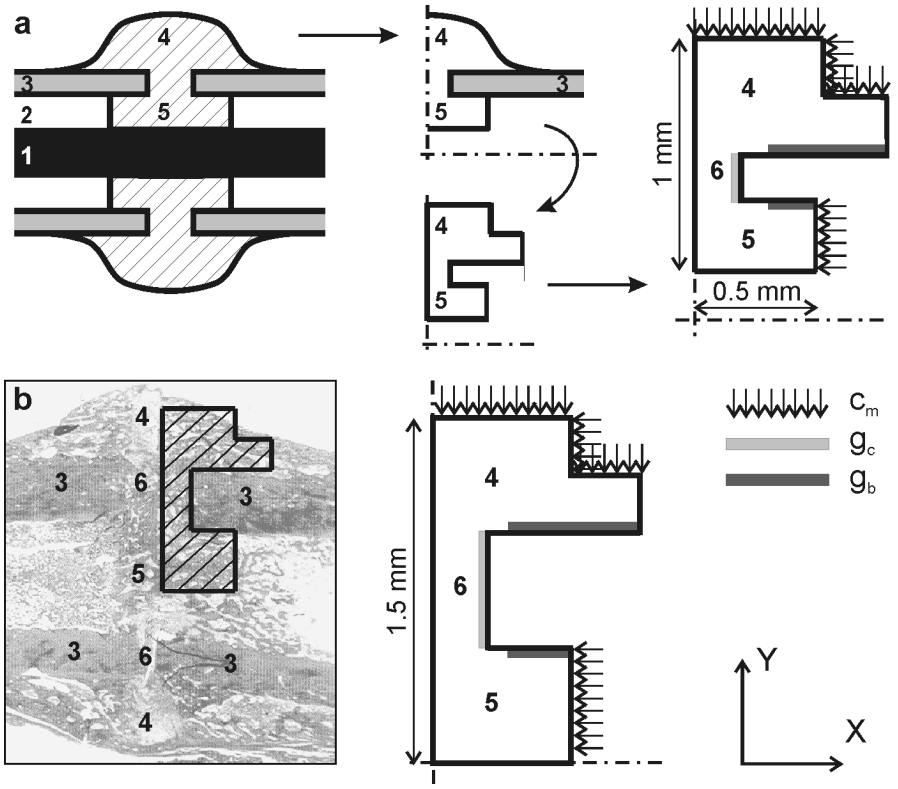


FIGURE 4.3: Generic geometric model of a semi-stabilised murine tibia fracture (top) and of a standardised rodent femoral fracture (bottom). 1: needle; 2: marrow cavity; 3: cortical bone; 4: periosteal callus; 5: endosteal callus; 6: intercortical callus. Due to symmetry reasons only one quarter was used. For the simulation, the geometry was further simplified to a construction of rectangles. The boundary conditions are indicated on the right figures.

solution of the model must respect conservation of mass. The finite volumes technique was employed (in the spatial discretisation) for its inherent mass conservation properties. The method of lines (MOL) was applied to separate the spatial and temporal discretization (Hundsdorfer and Verwer, 2003). This approach is widely used in the numerical solution of systems of partial differential equations. The approach consists of three steps: the selection of a spatial grid, followed by the spatial discretisation (semi-discretisation, as all but one dimension are discretised) leading to an initial value problem for an ordinary differential equation (ODE) system and finally, the time integra-

tion of this large ODE system. In the first step, the spatial domain Ω was covered with an equidistant computational grid. After convergence tests the grid size was fixed at 0.01 mm in both directions. On this grid, the diffusion and reaction terms in system 4.1 were discretised using respectively the standard second order central difference approximation and pointwise evaluation, which were found to be sufficient in terms of accuracy and to ensure non-negativity of the solution of the resulting ODE system. Contrarily, the discretisation of the taxis term in system 4.1 required the application of upwinding techniques with nonlinear limiter functions (van Leer limiter) to guarantee accurate, non-negative solutions of the MOL-ODE system (Gerisch, 2001; Gerisch and Chaplain, 2005). The order of the spatial approximation is two in general. For the time integration of the resulting stiff MOL-ODE system the code ROWMAP (Weiner *et al.*, 1997) was used. The method's built-in automatic step size control ensures the error caused in each time step (local error) to remain below a user-prescribed tolerance while keeping the computational cost as low as possible.

4.3.4 Simulations and sensitivity analyses

With this simulation approach extensive single and multi-parameter studies were conducted in order to assess the influence of the value and duration of the initial and boundary conditions, and of the value of other model parameters on the simulation results. All parameters were tested at 10, 50, 100, 200 and 1000 % of their original value. The percentages of cartilage and bone in the callus were calculated from the percentages of grid cells with respectively an average fibrous/cartilaginous ECM and an average bone ECM density higher than 0.05 g ml^{-1} indicating a substantial density of the respective tissue in the grid cell. Furthermore, a challenged fracture with an interfragmentary gap of 3 mm, leading to an delayed healing observed by Harrison *et al.* (2003) was simulated. Finally, a few examples were developed to illustrate the potential of this model in simulating pathological situations. A nonunion due to insufficient growth factor production and its treatment by administering the osteogenic growth factor were simulated. Atrophic nonunions in mice experiments caused by a lack of mesenchymal stem cells were also simulated, together with possible treatment therapies.

4.4 Results

4.4.1 Experimental fracture healing models

Semi-stabilised murine tibial fracture

After an initial inflammatory and angiogenic response, considerable amounts of cartilage were formed along the fracture line and newly formed woven bone was deposited adjacent to the cortex. At PFD 8, the replacement of the cartilaginous callus with bone and vascular elements was actively in progress. By PFD 13, the cartilage had almost disappeared from the callus, which at that stage was mainly composed of a highly spongy type of bone with little soft callus tissue left. Histological analysis at various time points after fracture induction showed the changes in the amounts of cartilage and bone in the fracture callus in a quantitative way. At PFD 3 and 21, hardly any cartilage was present in the callus. For PFD 8 and 13 the amount of cartilage was quantified to be respectively 9.0 % $\pm$ 1.6 (standard error of means, SE) and 2.1 % $\pm$ 0.7 (Figure 4.4). The amount of bone increased throughout the entire healing period. It was quantified to be 19.2 % $\pm$ 2.0 at PFD 8 and 37.1 % $\pm$ 4.2 at PFD 13, as is shown in Figure 4.4. To allow for a better comparison with the simulation results, extra histological analyses were carried out on the PFD 8 sections. The amount of soft tissue, encompassing both cartilage and fibrous tissue, and the total bone area (not just the mineralised tissue) were calculated. At PFD 8, the percentage of soft tissue in the total callus area amounted to 29.6 % $\pm$ 2.7 and the percentage of bone in the total callus area 38.6 % $\pm$ 2.3.

Standardised rodent femoral fracture

For the 0.5 mm osteotomy, healing occurred via indirect repair, involving both intramembranous ossification along periosteal and endosteal surfaces and endochondral ossification of the soft callus, in and immediately adjacent to the osteotomy. By 5 weeks, an advancing cuff of periosteal woven bone extended from both fragments, resulting in partial or complete bony bridging, with little cartilage persisting in the osteotomy gap. Remote from the osteotomy, the periosteal callus was remodelling to lamellar bone at this time. Data for the histomorphometric parameters quantified at each end point are illustrated in Figure 4.5. For the 3.0 mm osteotomy, the osteotomy gap was occupied by organising hematoma one week postoperatively. The transected cortical ends were sharply demarcated, with a small number of empty osteocyte lacunae. There was thickening of the outer, fibrous layer of the periosteum, with intramembranous bone formation. Loose fibrous tissue, containing small islands of cartilage, was present in the periosteal region of the osteotomy. This extended outward to infiltrate the surrounding musculature and into

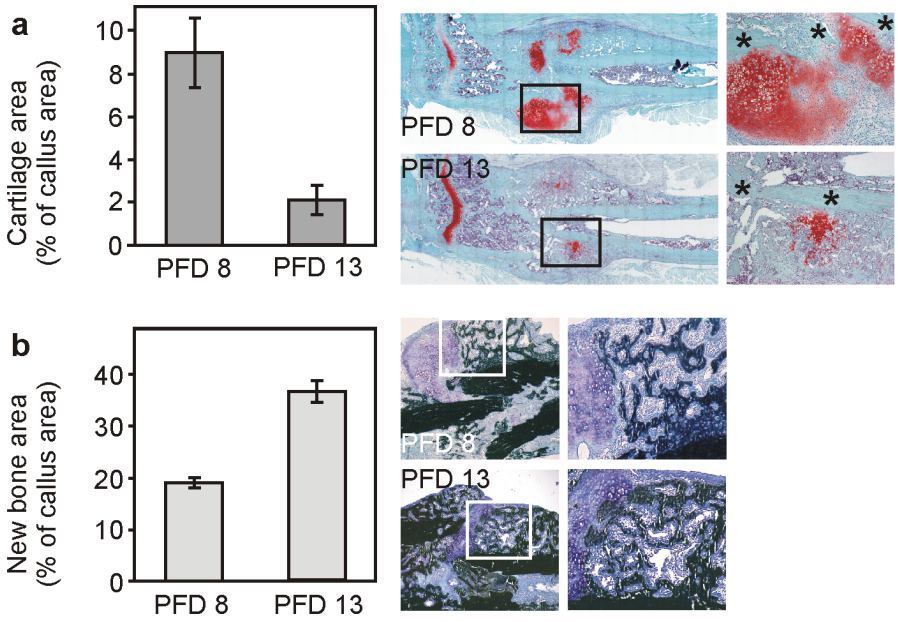


Figure 4.4: Histological results of the semi-stabilised fracture model. Left: Histomorphometric measurements of cartilage (a) and bone (b) areas at PFD 8 and 13 (n = 6, avg±SE). Right: examples of histological sections showing cartilage (a) in red (Safranin O) and mineralised bone (b) in black (Von Kossa). Asterisk: bone.

the osteotomy gap, where it merged with the interfragmentary hematoma. Three weeks postoperatively, the osteotomy was filled with loose fibrous tissue mixed with fibrocartilage and small islands of hyaline cartilage. Small outgrowths of woven bone arose from the transected cortices. The cortical ends had an irregular outline. Periosteal callus extended for most of the diaphyseal length. Five weeks postoperatively, the cortical ends had a rounded appearance, with an occasional outgrowth of woven bone. A narrow band of woven bone extended between the transected cortices of each fragment, appearing to 'seal' the medullary canal from the osteotomy, which was occupied by loose, hypocellular fibrous tissue. Data for the histomorphometric parameters quantified at each end point are illustrated in Figure 4.5.

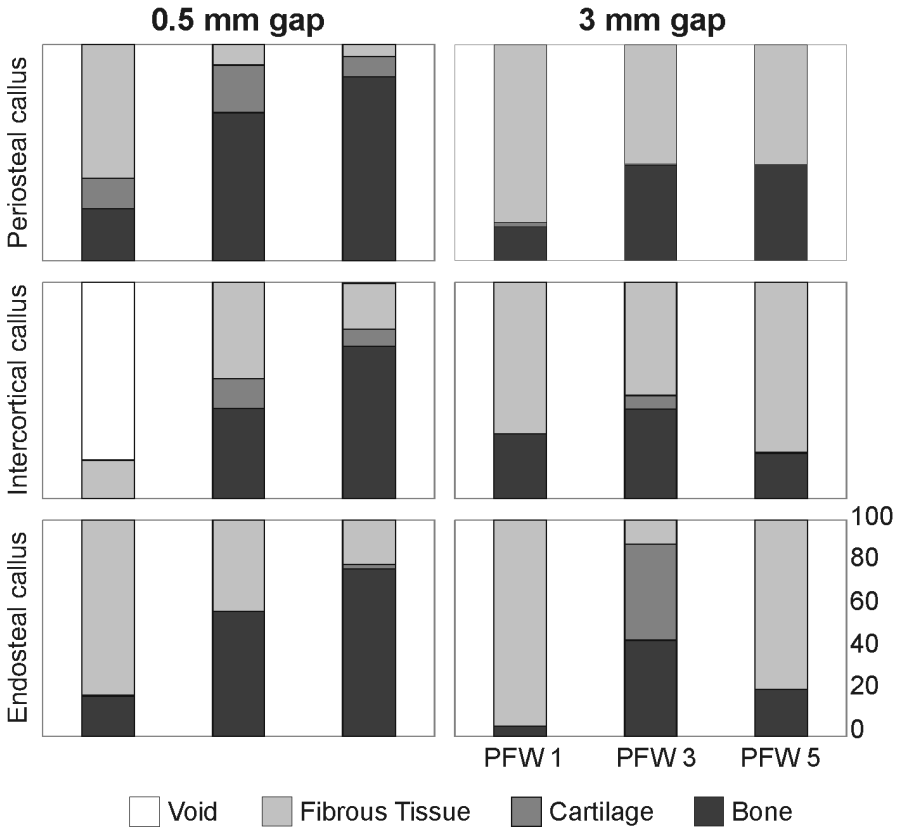


FIGURE 4.5: Histomorphometric measurements for the standardised rodent femoral fracture model with 0.5 mm (left) and 3 mm (right) gap sizes, showing the tissue fractions [%] in the different parts of the callus (as indicated in Figure 4.3) at post fracture weeks 1, 3 and 5.

4.4.2 Mathematical fracture healing models

Simulation results

Semi-stabilised murine fracture model Using the parameter set presented by Bailón-Plaza and van der Meulen (2001) a full ossification of the semi-stabilised murine fracture callus was predicted by day 6 (Table 4.2). After adapting certain parameter values (Appendix 7.3.2), the obtained tissue pattern of fracture healing (Figure 4.6) corresponded well to the pattern observed experimentally. A steep moving front of mesenchymal stem cells migrated throughout the callus within 3 days. Simultaneous diffusion of the

chondrogenic growth factor caused these cells to differentiate into chondrocytes depositing a cartilage matrix in the periosteal and endosteal callus by PFD 8 and 13 respectively. Meanwhile, alongside the periosteal and endosteal cortices the release of osteogenic growth factor caused the differentiation of the mesenchymal stem cells into osteoblasts, depositing bone matrix. This process of intramembranous bone formation was observed from PFD 4 onwards. Endochondral replacement of hypertrophic chondrocytes (related to a high cartilage density in the model) by osteoblasts started at day 8 in the most peripheral part of the periosteal callus, gradually proceeding towards the endosteal callus. The rise in osteoblast concentration preceded the rise in bone ECM density. A complete ossification was observed at PFD 14 for the external callus and PFD 20 for the intramedullary callus. There was a good qualitative comparison between the experimentally measured and numerically predicted temporal evolution in the density of the cartilage and bone matrix. Comparing the numerically predicted values for the soft tissue and bone matrix density with the results from the extra histological analyses at PFD 8, showed also a reasonable quantitative correspondence between these results.

Table 4.1: Comparison of experimentally observed and numerically calculated values for callus areas occupied by bone and soft tissue at PFD 8 for the semi-stabilised murine fracture model.

	bone [%]	soft tissue [%]
experiments	29.6	38.6
(SE)	(2.7)	(2.3)
simulations	36.45	28.37

An overview of the change over time of the concentrations of the osteogenic and chondrogenic growth factor in the callus is presented in Figure 4.7, together with the experimentally determined temporal evolution of these generic growth factors as determined by Cho *et al.* (2002). There is a good correspondence between the numerical and experimental results. Both graphs show chondrogenic growth factor expression in the first half of the healing process. Osteogenic growth factors are expressed during intramembranous ossification in the first half of the healing process, but mainly during the endochondral ossification process taking place in the second half of the healing process.

Standardised rodent fracture model Applying the mathematical model to simulate fracture healing in the standardised rodent fracture model leads to a spatiotemporal evolution of the different tissues in the callus, similar to

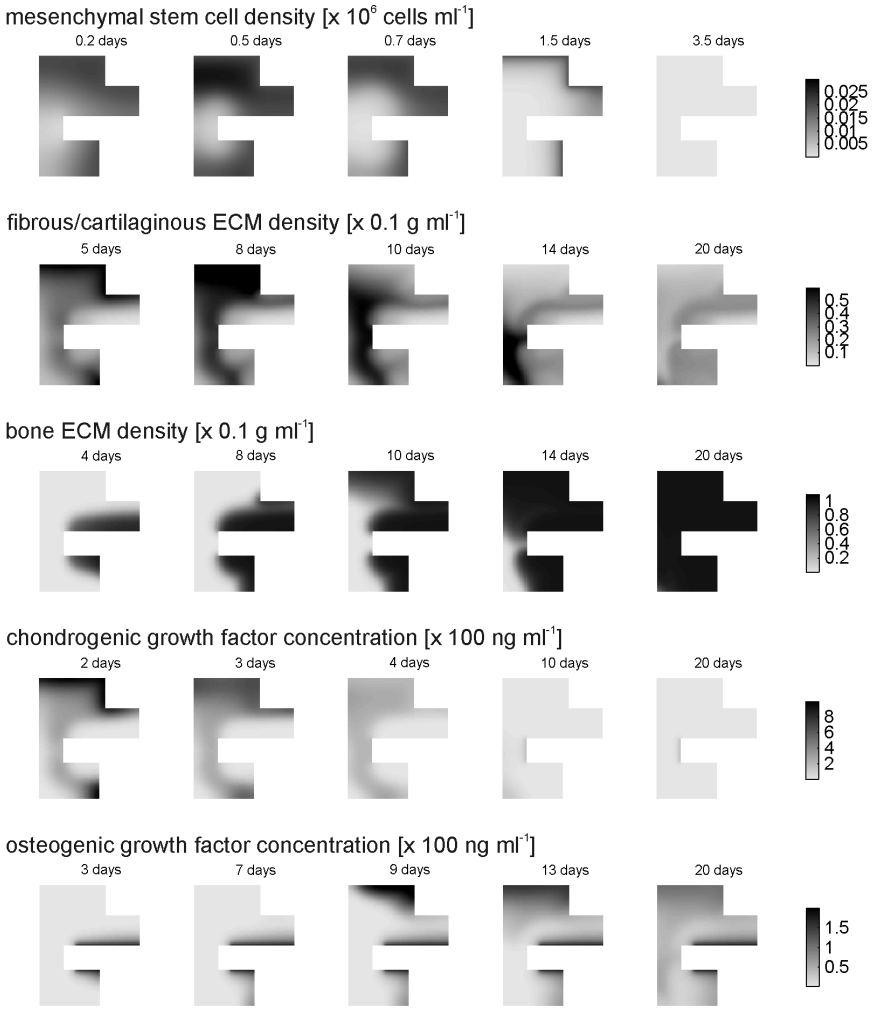


FIGURE 4.6: Overview of the change over time (in days post fracture) of the mesenchymal stem cell density (top), the fibrous/cartilaginous and bone ECM density (middle) and the chondrogenic and osteogenic growth factor concentration (bottom) for the semi-stabilised murine fracture model.

the one shown in Figure 4.6. The experimentally measured and numerically calculated temporal evolution of the hard and soft tissue fractions in different regions of the callus area is depicted in Figure 4.8. The bars represent the experimentally measured callus fraction occupied by bone (top), cartilage alone

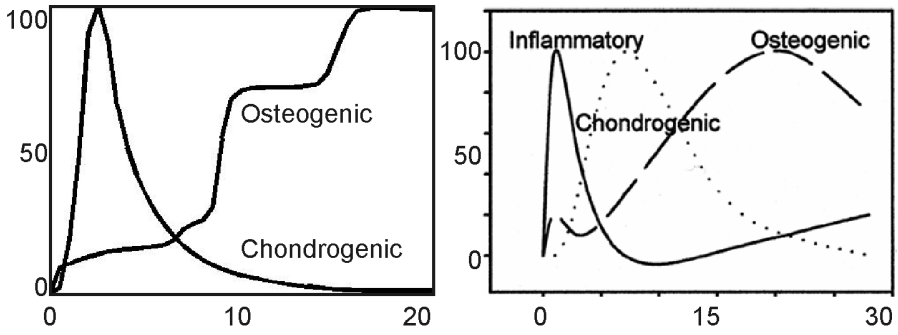


Figure 4.7: Change over time (days post fracture) of the average concentration of chondrogenic and osteogenic growth factors in the callus of the semi-stabilised murine fracture (expressed as % of maximum). Left: simulation results. Right: adapted from Cho *et al.* (2002).

(middle) and both cartilage and fibrous tissue (bottom) at PFW 1, 3 and 5. The predicted area occupied by bone increases towards the end of the healing period whereas the area occupied by fibrous/cartilaginous matrix tissue increases and subsequently decreases again. As observed experimentally, the periosteal callus is the first zone where healing is completed, followed by the endosteal zone. The healing process in the intercortical zone starts up last. Although the order of events corresponds to the order observed experimentally, the time scale does not. Furthermore, as the mathematical model does not make a distinction between fibrous tissue and cartilage, a good comparison with the experimental data is not possible for the soft tissues. Experimentally, the fibrous tissue fraction gradually decreases throughout the healing process, resulting in an overall decrease of the soft tissue content as shown in Figure 4.8 (bottom). This evolution is not captured by the soft tissue variable in the model.

Sensitivity analyses

Convergence test Convergence tests were carried out to determine an appropriate mesh density. The spatiotemporal evolution in bone and soft tissue matrix density and the temporal evolution in bone and soft tissue fractions were compared for different mesh densities (Figure 4.9). For the coarsest grid tested, the endochondral ossification process started one day later than for the finer meshes, resulting in a higher maximal cartilage fracture. The mesh density used in these simulations ($\triangle x = \triangle y = 0.01$ mm) was sufficiently refined to obtain mesh independent results.

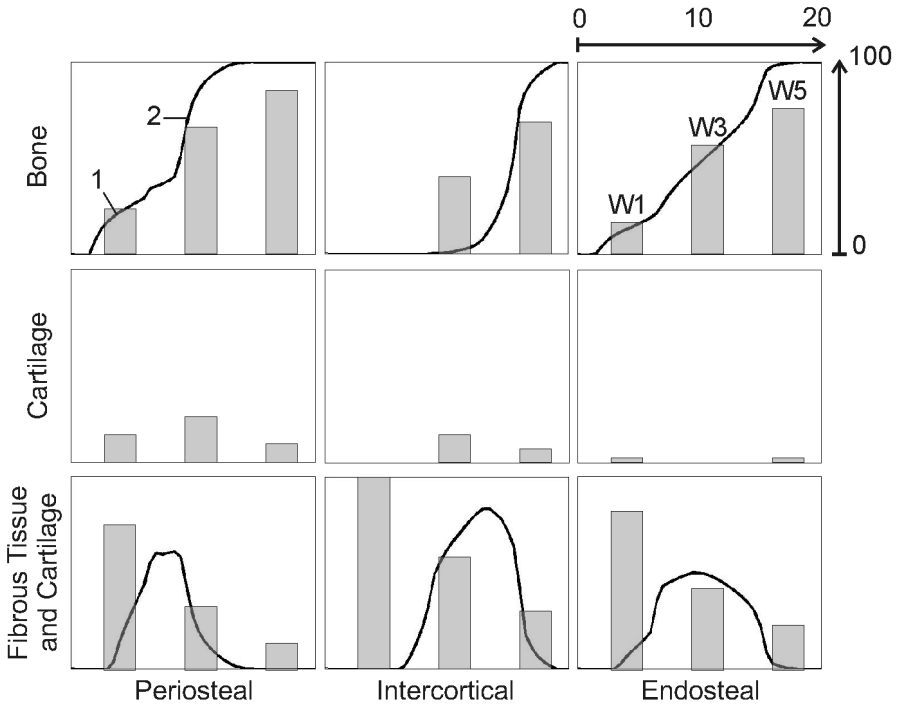


FIGURE 4.8: Quantitative comparison between predicted (continuous line) and experimentally measured (bars) fractions [%] of bone (top) and soft tissue (middle and bottom) for the standardised rodent fracture model at various time points post fracture. In the upper left figure the rise in bone fraction due to intramembranous (1) and endochondral ossification (2) are indicated.

Parameter sensitivity Sensitivity analyses showed a large influence of a small group of parameters. The results for this small group of parameters are summarised in Table 4.2 on page 88. The evolution of the soft and hard tissue matrix density over time for the different values of these parameters is shown in Figure 4.10. The multi-parameter analyses did not lead to additional insight (over the single-parameter analyses) into the interaction between different parameters and their influence on the simulation outcome and therefore will not be further discussed. Perturbations in the parameters linked to the proliferation of chondrocytes (A_{co}) and osteoblasts (A_{bo}) directly affected the buildup of the fibrous/cartilaginous and bone ECM. This also indirectly affected the process of endochondral bone formation since the latter only starts when the fibrous/cartilaginous ECM reaches a certain density. The parameters used in the expressions for the chondrogenic growth factor production

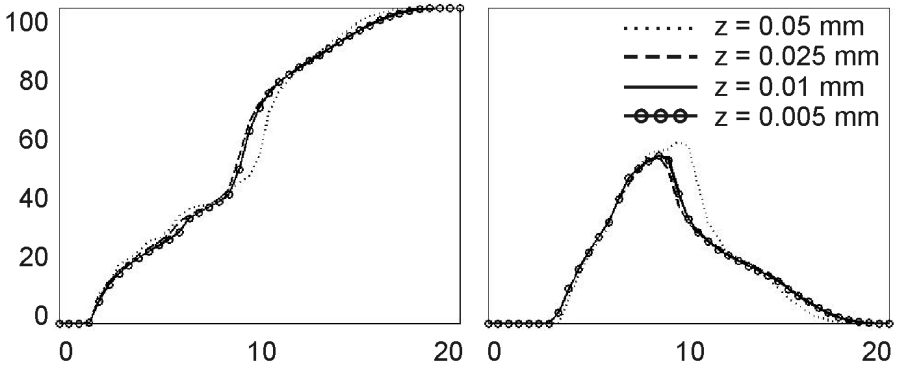


Figure 4.9: Influence of element size ($\triangle$x = $\triangle$y = z) on the simulation outcome for the semi-stabilised murine fracture set-up. Temporal evolution (in days post fracture) of the bone (left) and soft tissue (right) fractions [%] in the callus.

rate (G_{gc}) and the chondrogenic and osteogenic growth factor decay rate (d_{gc}, d_{gb}) influenced the formation of the cartilage matrix. A low value for chondrogenic growth factor production rate or a high value for chondrogenic growth factor decay rate resulted in a slower buildup of the cartilage matrix. In extreme cases this even led to the inhibition of chondrogenesis resulting in callus ossification through intramembranous ossification. Low values for the osteogenic growth factor decay enforced the process of intramembranous ossification (not shown in Figure 4.10). Again, in extreme cases, this completely inhibited chondrogenesis.

Varying the cartilage matrix synthesis and degradation rates (P_{cs}, κ_c) affected the density of the fibrous/cartilaginous matrix. A slow buildup of the matrix slowed down the process of endochondral ossification or, in extreme cases, even inhibited it completely. Endochondral ossification was further found to depend strongly on the parameter values for chondrocyte replacement (B_{ec}, Figure 4.10) and cartilage matrix degradation (Q_{cd2}). A high value for these parameters maintained a high chondrocyte concentration and cartilage matrix density and simultaneously inhibited endochondral replacement to start. A low value for B_{ec} allowed endochondral replacement to start for a very low fibrous/cartilaginous ECM density, resulting in very fast healing through endochondral ossification.

Finally, the time period during which the mesenchymal stem cells (c_{m_bc}) were allowed to enter the callus and their initial concentration applied at the

boundaries of the callus were found to be important parameters in obtaining reasonable results. High values for the initial concentration accelerated both endochondral and intramembranous ossification, while low values led to an insufficient number of stem cells, chondrocytes and osteoblasts to produce sufficient matrix densities. Long release periods of stem cells ($c_{m_bc_dur}$) merely steepened the propagation fronts of the processes running throughout the callus. Short release periods allowed insufficient infiltration of the cells into the callus generating similar effects as observed for too low values of c_{m_bc}. Varying the duration and the concentration of the initial growth factor release (g_{c_bc}, g_{b_bc}) or the location of initial chondrogenic growth factor release did not have a significant influence on the simulation outcome.

Pathological healing and therapy

Increased gap size Increasing the fracture gap size in the simulations leads to a delayed fracture healing response as observed experimentally in the standardised rodent fracture model. The experimentally observed and numerically simulated bone and soft tissue fractions for both the 0.5 mm and 3 mm gap are depicted in Figure 4.11. When healing is achieved for the 0.5 mm gap, no successful healing is yet predicted for the 3 mm gap, similar to the experimental observations. Allowing the numerical analyses to continue up till 5 weeks after fracture, still no bridging of the fracture gap is predicted. Whereas experimentally, a constant or even decreasing amount of bone is observed further on in the healing process, this value keeps rising steadily in the simulations. The graphs for the different model variables in Figure 4.12 show a substantial acceleration of the healing response around PFD 40. This sharp change in the variables is due to the increase in the concentration of the mesenchymal stem cells. At the beginning of the simulations, stem cells differentiate towards chondrocytes in the central part of the callus around the fracture line. However, a small fraction (not visible in the graph) remains undifferentiated and is able to proliferate. Under the influence of the osteogenic growth factor present in the callus, the stem cells will differentiate towards osteoblasts, accelerating the ossification process.

Growth factor deficiency A case of fracture nonunion, caused by a deficiency in the osteogenic growth factor production, was modelled by decreasing the value of the corresponding model parameter (10 % of the reference value of G_{gb}). The administration of an osteogenic growth factor by injection of a carrier that gradually releases its content into the callus area was simulated. To this end, an exponentially decreasing growth factor concentration was applied as a boundary condition starting at PFD 20 (Seeherman *et al.*, 2003). The maximum concentration was set at 200 μg/ml, which is comparable to the concentrations examined in experimental studies (Southwood *et al.*, 2004). A

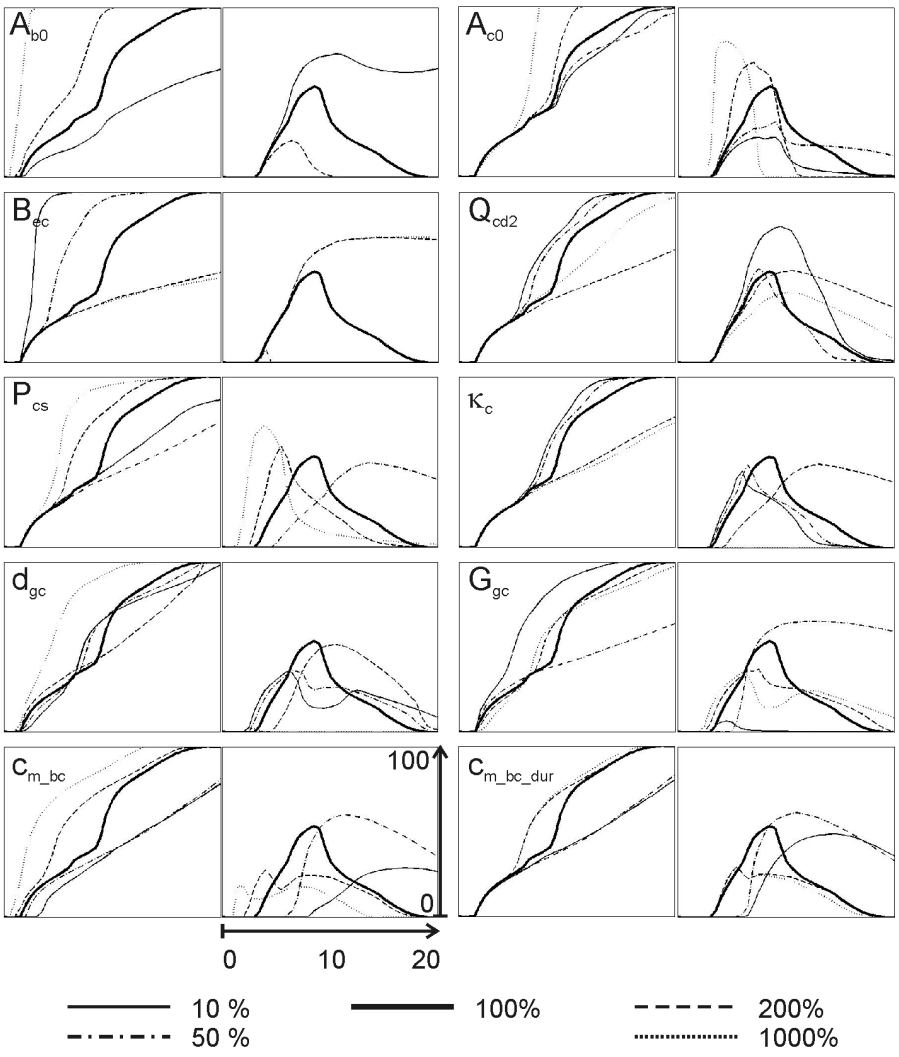


Figure 4.10: Temporal evolution (days post fracture) of cartilage (right) and bone (left) fractions [%] in the callus for five levels of those parameters that have a substantial influence on the simulation outcome (semi-stabilised murine fracture).

deficiency in osteogenic growth factor production led to a nonunion. After 3 weeks, intramembranously formed bone was present but endochondral ossification did not take place, leaving a dense cartilage matrix occupying the main

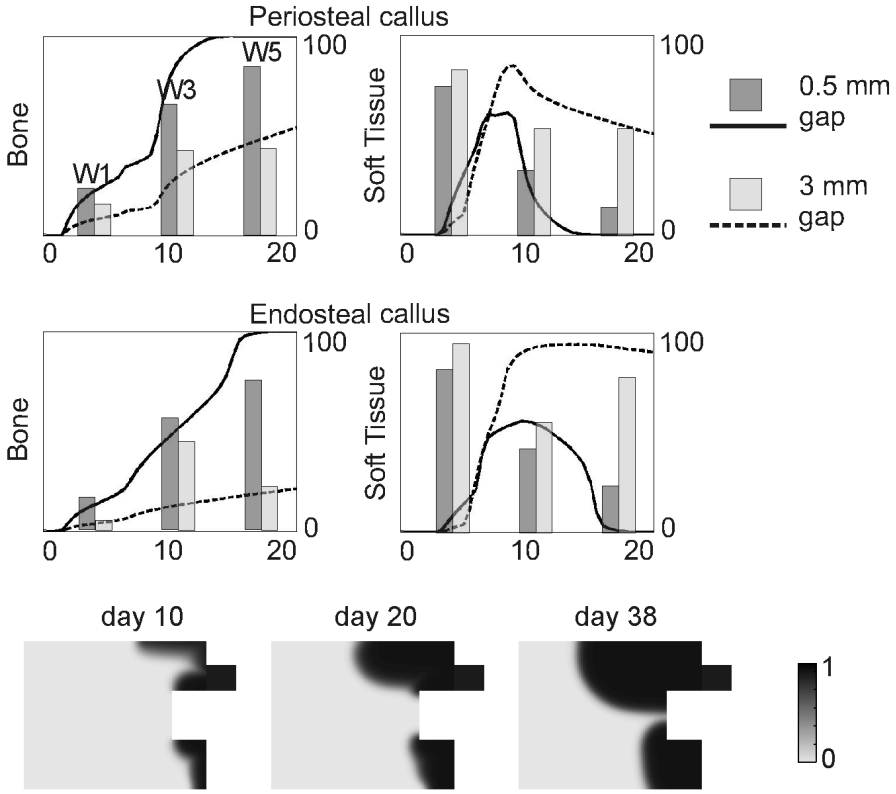


FIGURE 4.11: Experimental (bars) and simulation (continuous line) results for the standardised rodent fracture model with an interfragmentary gap of 3 mm. The temporal evolution (days post fracture) of the bone (left) and soft tissue (right) fractions [%] are shown for the periosteal (top) and endosteal (bottom) callus. Bottom: temporal evolution of the bone matrix density [× 0.1 g/ml] for several time points post fracture.

part of the callus (Figure 4.13, PFD 20). An osteogenic growth factor was gradually released to the callus tissue from an injectable carrier (Figure 4.13, top right). Upon administration of the growth factor, the endochondral ossification process precipitated, replacing the cartilage by bone, as shown in Figure 4.13 from PFD 20 on. This resulted in a fully ossified callus 3 weeks later. The residual amount of cartilage still present in the callus area at day 40 is located in the endosteal callus around the fracture line. This corresponds to the area where the injected osteogenic growth factor was unable to penetrate. Osteogenic growth factor produced by the newly formed osteoblasts

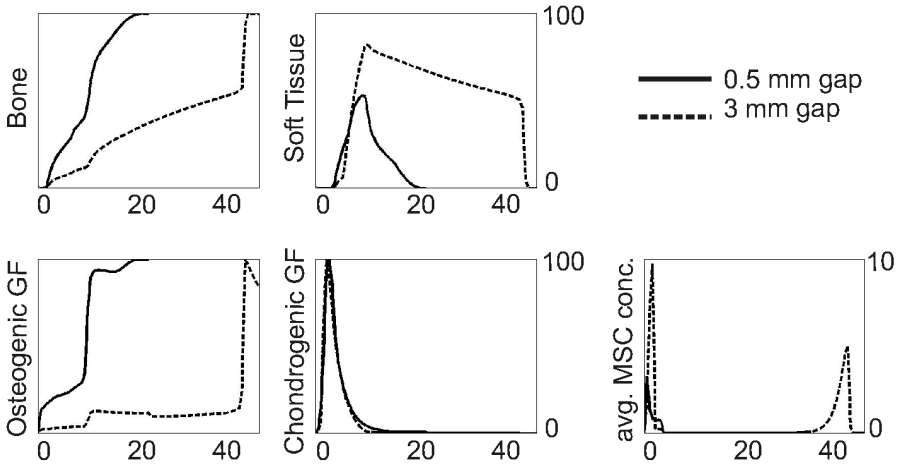


Figure 4.12: Temporal evolution (days post fracture) of the biological variables of the fracture healing process for the standardised rodent fracture with an interfragmentary gap of 0.5 mm and 3 mm. Top: bone (left) and cartilage (right) fractions in the callus [%]. Bottom: average concentrations of the osteogenic (left) and chondrogenic (middle) growth factors [$\times$ 100 ng/ml], and the average density of the mesenchymal stem cells (right) [$\times$ 10^6 cells/ml].

surrounding this residual cartilage zone will slowly but steadily cause the remaining cartilage to be replaced. A dose-effect was observed (Figure 4.13, bottom), where the amount of residual cartilage in the callus increased with decreasing concentrations of the injected growth factor.

Atrophic nonunion The atrophic nonunion model described by Brownlow *et al.* (2001, 2002); Reed *et al.* (2002, 2003); Kokubu *et al.* (2003); Makino *et al.* (2005) and Niikura *et al.* (2006) was simulated as well. In this experimental set-up, a challenged fracture was created by stripping the periosteum and curetting the marrow canal over a distance comparable to the bone's diameter (2 mm for rats) both proximally and distally, thereby compromising the supply of mesenchymal stem cells to the fracture gap. Fracture nonunion was observed although experimentally normal growth factor concentrations in the first week after fracture and good vascularisation of the callus tissue were demonstrated. In the simulations, the geometrical domain was enlarged in the craniocaudal direction to encompass the area where, in the experiments, the periosteum was stripped and the marrow canal curetted (Figure 4.14 top). Mesenchymal stem cells were no longer modelled to enter the fracture callus from the surrounding tissues, but only from the remain-

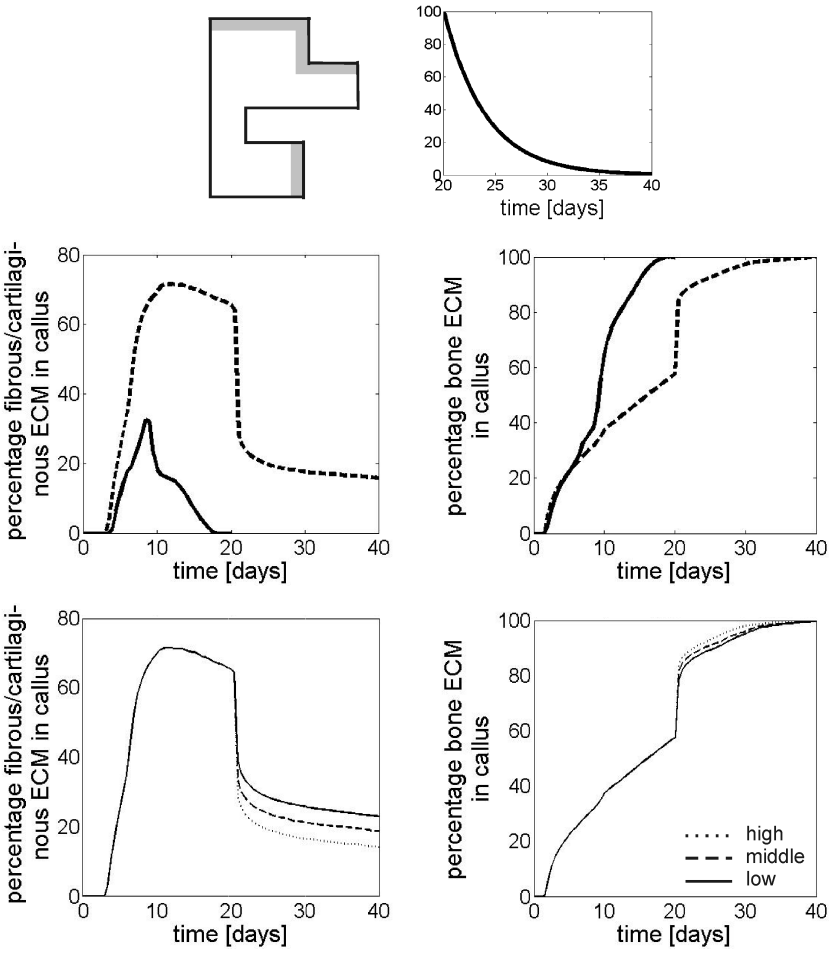


FIGURE 4.13: Top left: the grey zones in the simplified fracture model indicate the sites where the osteogenic growth factor, released from the carrier, was applied from PFD 20 onwards. Top right: curve showing the retention of the growth factor (percentage) in the carrier. Middle: cartilage (left) and bone (right) fractions in the callus for normal and impaired fracture healing, treated with the administration of an osteogenic growth factor (g_b = 200 μg/ml) starting at PFD 20. Bottom: cartilage (left) and bone (right) fractions in the callus for three concentrations of the administered growth factor (2, 20 & 200 μg/ml).

ing marrow and periosteum. Due to this lack of precursor cells, no healing response (bone or cartilage formation) whatsoever was induced in the callus area (Figure 4.14).

At the injection of mesenchymal stem cells into the callus at PFD 20, a sharp increase in the soft tissue matrix was predicted. This injection of mesenchymal stem cells was modelled similar to the injection of growth factors in the the previous nonunion case (Figure 4.14 top), with $c_m = c_{m_ini}$. Corresponding to the experimental observations (Brownlow *et al.*, 2001), the growth factors that were present in the callus area immediately after fracture were no longer present at that point. In the absence of growth factors, the mesenchymal stem cells did not differentiate into chondrocytes or osteoblasts. The increase in the amount of soft tissue in the callus area was due to the production by mesenchymal stem cells as this was allowed by the model equations (Bailón-Plaza and van der Meulen, 2001). When mesenchymal stem cells were administered in combination with an osteogenic growth factor, the precursor cells differentiated towards osteoblasts, which subsequently deposited bone matrix throughout the entire callus. When upon initiation of the atrophic nonunion simulations, additional mesenchymal stem cells were administered immediately (modelled as an initial condition), the fracture healing process was predicted to proceed slower than normal (Figure 4.14 right), but both intramembranous and endochondral ossification processes were observed. A dose-effect was observed in these last simulations, whereby the progress of the healing process increased for higher administrated stem cells concentrations.

4.5 Discussion

4.5.1 Simulation results

Semi-stabilised murine fracture model

The predicted progress of the semi-stabilised murine fracture healing, as shown in Figure 4.6, is in good agreement with the change over time in the amount of cartilage present in the callus, as measured experimentally (Figure 4.4). However, these experimental results cannot be compared in a quantitative way with the simulation results presented in Figure 4.6 since, in the mathematical model, the variable describing the cartilage matrix density also encompasses the density of the fibrous tissue matrix. The latter is formed in the callus along with cartilage during the reparative phase (Cruess and Dumont, 1985) of fracture healing. Qualitatively a good agreement can be observed.

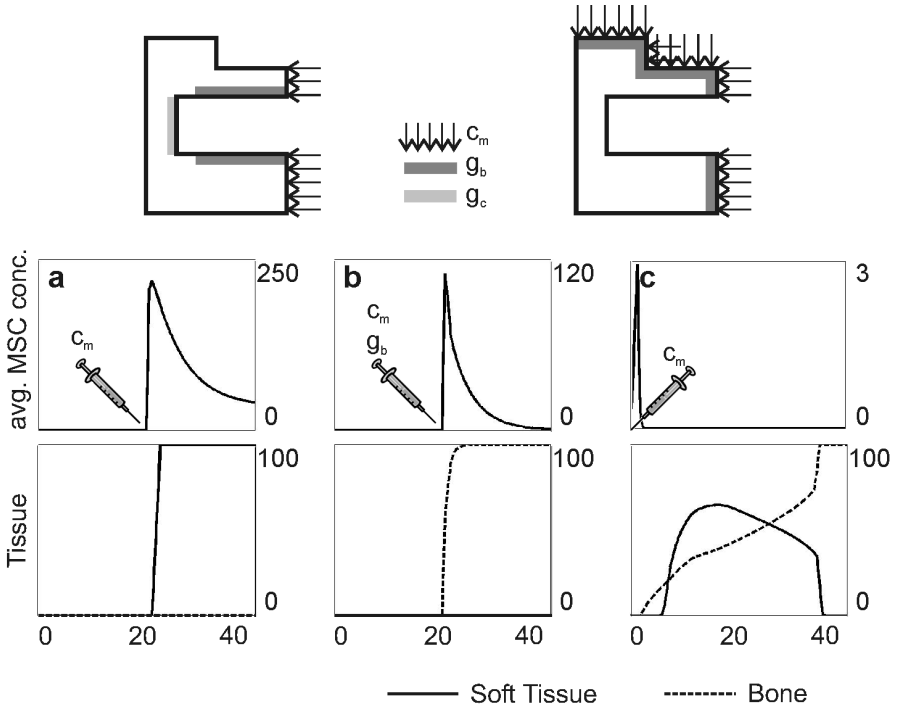


FIGURE 4.14: Modelling of a atrophic nonunions (Brownlow *et al.*, 2001, 2002; Makino *et al.*, 2005) and their subsequent treatment with the injection of (a) mesenchymal stem cells at PFD 20, (b) mesenchymal stem cells and an osteogenic growth factor at PFD 20 and (c) mesenchymal stem cells immediately after fracture induction. The top row shows the geometry and boundary conditions for atrophic nonunion (left) and the boundary conditions for therapy simulation (right). The middle row shows the temporal evolution (days post fracture) in the average density of mesenchymal stem cells in the callus ares [$\times$ 10^6 cells/ml], the bottom row shows the temporal evolution of the soft tissue and bone fractions in the callus [%].

Additional histological analyses were carried out for PFD 8, allowing for a quantitative comparison between experiments and simulations for that particular time point. Beside the amount of cartilage, also the amount of fibrous tissue in the callus was determined. A reasonable quantitative correspondence is evident between the histologically determined and numerically predicted values for the bone and soft tissue fraction (all fractions occupy 30 to 40 % of the callus area, Table 4.1).

The change in concentration of the growth factors over time can be compared with the findings of Cho *et al.* (2002) who analyzed the expression of members of the TGF-β superfamily during murine fracture healing. The expression of chondrogenic growth factors was reported to start in the first week after fracture. Osteogenic growth factor expression was observed mainly in the second half of the healing process. This corresponds to the simulation results presented in Figure 4.7.

Standardised rodent fracture model

More elaborate quantitative comparison is possible using the results from the standardised rodent fracture model. Looking at the bone fraction in different callus regions, a good quantitative correspondence could be observed (Figure 4.5, top). The ossification process starts first in the periosteal callus, followed by the endosteal callus and subsequently the intercortical callus. As the amounts of fibrous tissue and cartilage are represented by a single variable in the model, the evolution of the combined variable was also determined from the experimental results. A substantial difference exists between the experimentally determined and numerically predicted temporal evolution of the soft tissue fraction. Separation of the soft tissue variable into a variable representing the fibrous tissue density and one representing cartilage density would allow for a better comparison between the experiments and simulations.

Although the predicted bone fractions are comparable to the ones experimentally observed, the time frame in which these bone fractions are predicted to be formed is substantially different. For the standardised rodent fracture model, complete healing is achieved after 3 weeks in the simulations and only after 5 weeks in the experiments. There are several explanations for this observation. One of them is that the model does not capture cell maturation and the time that elapses between the differentiation of mesenchymal stem cell towards osteoblast and the production of extracellular matrix by the mature osteoblast (Bruder and Scaduto, 2005). Furthermore, the parameter values have been derived based on both *in vivo* and *in vitro* experiments on different animal models and cell lines reported in the literature, or have been estimated when no information was available. When applying their model on another animal model than the rat model it was developed for, Bailón-Plaza and van der Meulen (2003) assumed that the differences between the healing response in animals were geometrical and temporal, but not biological. Consequently they scaled the temporal parameter values from the original model, in order to match the time scale of the healing process under investigation. A similar procedure could be applied here, scaling the temporal parameters by three-fifth. As this study focusses on the feasibility of the

model in simulating the correct sequence of the processes in fracture healing, the temporal scale was not adapted.

4.5.2 Sensitivity analyses

Parameter values

The sensitivity analysis indicates the importance of the values of the parameters describing the proliferation of chondrocytes and osteoblasts, the synthesis and degradation of both types of ECM, the growth factor production and decay rates and the initial concentration of mesenchymal stem cells. Whereas these parameter values are constants in the model, in reality they can be a function of many other variables. For instance, in the sensitivity analysis, endochondral ossification is found to depend strongly on the values for chondrocyte replacement (B_{ec}) and cartilage matrix degradation (Q_{cd2}). Experimental studies show that endochondral replacement is mediated by many other factors. Enomoto-Iwamoto *et al.* (1998) showed that BMP signalling is required for expression of the hypertrophic phenotype in chondrocytes. Gerstenfeld *et al.* (2003b) reported that the inflammatory factor TNF-α in mice mediates both chondrocyte apoptosis and the expression of proresorptive cytokines that control endochondral tissue remodelling by osteoclasts. Colnot *et al.* (2003) showed that matrix metalloproteinase 9 (MMP-9) mediates vascular invasion of the hypertrophic cartilage callus. MMP-9 deficient mice exhibit a large persisting cartilage callus after fracture. Furthermore, Street *et al.* (2002) described that inhibition of the vascular endothelial growth factor (VEGF) causes the fracture healing process to arrest at the soft callus phase in mice. Based on these findings, the parameter B_{ec} and Q_{cd2} could be expressed as a function of BMP, TNF-α, MMP-9 and/or VEGF concentrations. In this way, it would become possible to model compromised endochondral ossification due to the deficiency or absence of one of the aforementioned factors.

A distinction can be made between physical and non-physical, measurable and non-measurable parameters. Half of the parameters shown in Table 4.2 (A_{b0}, d_{gc}, d_{gb}, P_{cs}, κ_c) are based on experimental observations. Notably, these experimental observations are obtained from both *in vivo* and *in vitro* set-ups and are measured for different species, cell lines etc. Other parameter values have a physical meaning (A_{c0}, G_{gc}) and could be measured, but no experimental data is available yet. Experiments could be designed to determine their value, however, caution must be exerted as these parameters in turn depend on several other parameters. For instance, in measuring the proliferation rate of cells, the presence or absence of certain growth factors in the medium (Lieberman *et al.*, 2002) and the stiffness of the substrate (Ghosh *et al.*, 2007)

have a substantial influence on the outcome of the experiment. A last category of parameters are those without a physical meaning (i.e. not related to one specific process such as proliferation or decay). These are, for example, the chondrocyte replacement (B_{ec}) and the cartilage matrix degradation (Q_{cd2}). They represent a cluster of processes which are not included separately in the model for reasons of simplicity. However, as mentioned higher in this section, it is possible to express the underlying processes by introducing additional variables.

Boundary conditions

The source of the chondrogenic growth factor was assumed to coincide with the degrading fractured ends of the cortex. Sensitivity analyses showed that varying its location effected no change in the simulation outcome. This was not the case for osteogenic growth factors as intramembranous ossification was observed immediately next to the boundaries where osteogenic growth factors were released. However, experimental observations have shown that condensation and osteoblastic differentiation of mesenchymal stem cells inside the marrow, reactivation of the osteoblasts lining the cortical bone surface and subsequent intramembranous ossification, is also only taking place near the cortex away from the fracture site Barnes (1999). As processes in the marrow and cortex are not included in the mathematical model, these events are captured by the boundary conditions applied at the location.

4.5.3 Simplifications

Geometrical domain

The growth and degradation of the callus is not captured by this model. When constructing the geometric model (Figure 4.3), the craniocaudal, dorsoventral and mediolateral asymmetry of the mouse tibia was not taken into account, as a generic model of a fracture callus is sufficiently accurate for the purpose of this study. Additional simulations were carried out to assess the influence of this assumption on the numerical results. Figure 4.15 shows the results for the spatiotemporal change in the bone matrix density for situations where the craniocaudal (b) and dorsoventral or mediolateral (c) asymmetry was modelled. No change in the predicted outcome was observed. However, where in the simulation the geometrical asymmetry is imposed, in reality, the asymmetry in the local biological and mechanical factors will cause asymmetry in the regeneration response, leading to the geometrical asymmetry of the fracture callus. In order to capture this phenomenon, growth and degradation of the callus area would have to be included in the model.

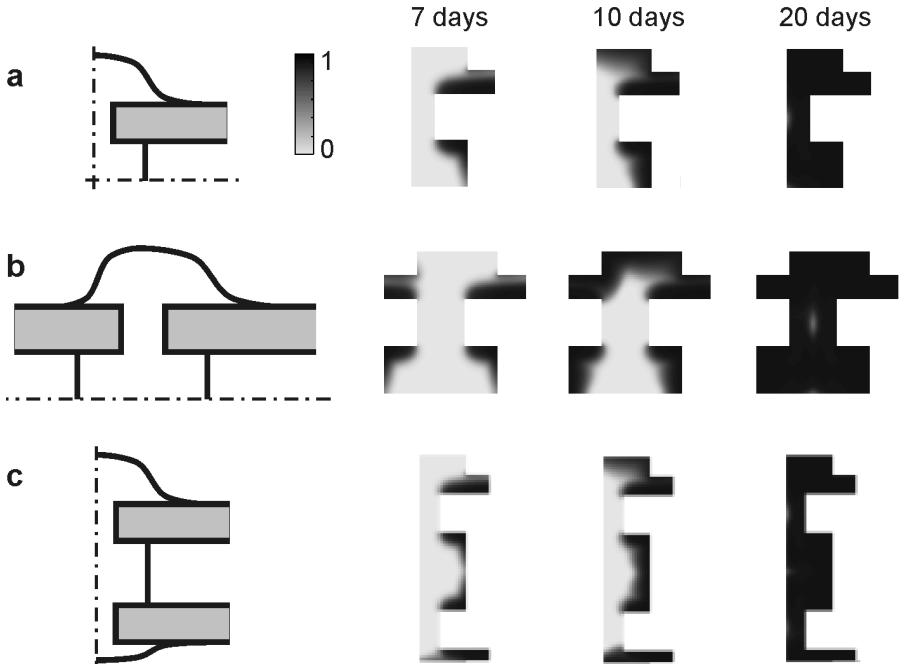


FIGURE 4.15: Influence of the asymmetrical callus geometry on the simulation outcome, shown by the temporal evolution (days post fracture) of bone matrix density [× 0.1 g/ml]. (a) axisymmetric model of standardised rodent fracture. (b) model of craniocaudal asymmetry. (c) model of dorsoventral or mediolateral asymmetry.

Callus shape

The boundary of the external callus was not accurately modelled since in its present state, the custom code requires the geometry to be constructed out of rectangular shapes. Analyzing the simulation results demonstrates that, despite the rectangular boundaries, the propagation fronts in the callus assume curved shapes due to the diffusion present in the model (e.g. Figure 4.16a, day 10). Approximating the curved callus shape by a stepped geometry, thereby increasing the computational cost (CPU time × 6), does not lead to substantially different results.

Presence of intramedullary needle

The position of the intramedullary needle was assumed central in the medullary canal. However, in reality, the position of this needle in the

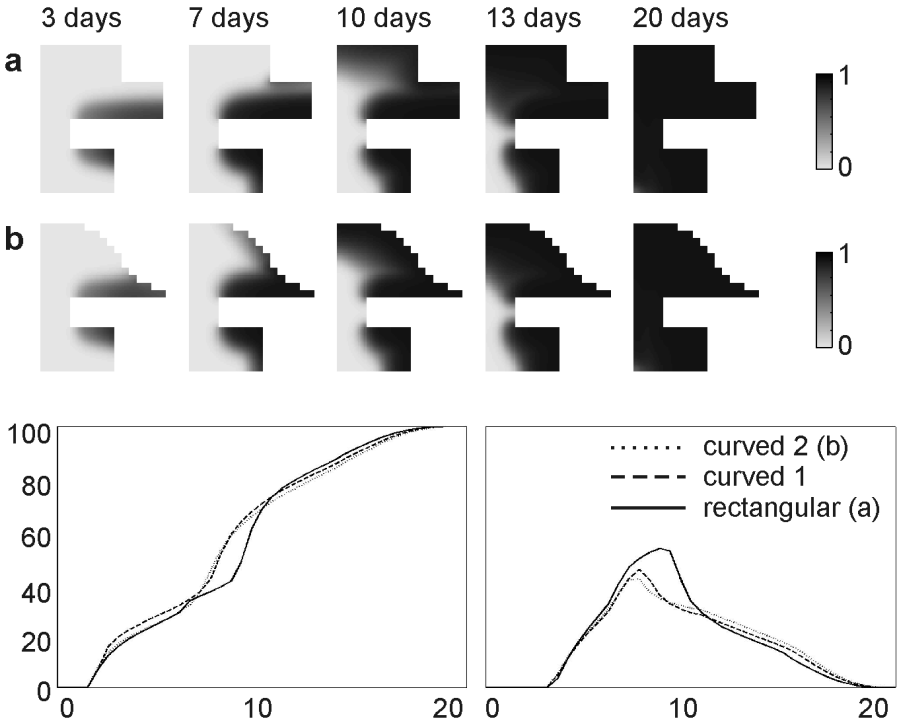


Figure 4.16: Influence of the callus shape on the simulation results. (a) temporal evolution (days post fracture) of bone matrix density [× 0.1 g/ml] for a rectangular geometry. (b) temporal evolution of bone matrix density [× 0.1 g/ml] for more curved geometry. Bottom: comparison of the temporal evolution of bone (left) and soft tissue (right) fractions in the callus [%] for the rectangular geometry shown in a, the curved geometry shown in b and an intermediate geometry.

medullary canal may vary between different animals. Furthermore, it was assumed that the presence of the needle does not influence the progress of healing. The needle fills the main part of the medullary canal on the distal side of the tibia. More importantly, on the proximal side where the fracture was induced, a medullary space is maintained between the endosteum and the needle. This allows a rapid regeneration of the medullary arterial supply (Cruess and Dumont, 1985). Therefore, it is still valid to assume an optimal vascular environment, similar to Bailón-Plaza and van der Meulen (2001), despite the presence of the intramedullary needle.

4.5.4 Applications in pathological fracture healing

Pathological healing cases

Increased gap size To demonstrate the feasibility of modelling pathological healing situations and the potential therapeutic value of mathematical models, three cases of delayed or nonunion were modelled. The first example was the model of delayed healing due to an enlarged osteotomy gap as reported by Harrison *et al.* (2003). Similar to the experiments, the numerical simulations show a lack of bony bridging at the time when full ossification of the 0.5 mm gap callus is observed. However, the endochondral ossification process is still active and, although at a very slow rate, cartilage is being degraded and replaced by bone. Given enough time, the simulation will finally predict successful healing (Figure 4.12). This is opposed to the experimental observations. At PFW 5, the cortical bone ends had a rounded appearance and a narrow band of woven bone appeared to seal the medullary canal from the remainder of the callus. No indication could be observed that normal fracture healing processes such as endochondral ossification were still active. The factors that are responsible for the observed phenomena of rounding of the cortices by osteoclasts and sealing of the medullary canal by a layer of woven bone are not yet identified.

Growth factor deficiency A second example shows a case where the endochondral ossification process is compromised due to a reduced production rate of osteogenic growth factor. This effect was counteracted by supplementing an additional amount of osteogenic growth factor, which was gradually released to the callus. Upon administration of the growth factor, the ossification process resumed. At locations where the concentration of the supplied growth factor was sufficiently high, ossification took place immediately (Figure 4.13). The part of the endosteal callus closest to the fracture line however where the growth factors did not penetrate, only slowly started to ossify. The concentration of the applied growth factors (corresponding to the amount of growth factors that were injected), determined the penetration depth of the growth factors.

Atrophic nonunion A final example was based on the experiments by Brownlow *et al.* (2001, 2002) and Makino *et al.* (2005). The lack of healing response, which was shown by these researchers to be caused by a lack in mesenchymal stem cells in the callus area, could be simulated with the mathematical model under investigation. Currently, research is being carried out to find a treatment for this type of atrophic nonunions. One possible strategy is the administration of mesenchymal stem cells, either alone or in combination with growth factors, directly into the callus area. Different treatment

strategies were modelled (Figure 4.14). The administration of mesenchymal stem cells alone did not lead to successful healing in the simulations due to the lack of growth factors in the callus region. The combined administration of osteogenic growth factors and mesenchymal stem cells solved this problem, resulting is a successful ossification of the entire callus. Another tested strategy was the administration of the mesenchymal stem cells at the beginning of the healing process. This resulted in a, albeit slower, successful healing of the fracture. The simulations further indicate that there is a dose-dependency of the healing period on the cell concentration. A smaller amount of precursor cells led to a slower healing process. Translating this to the clinical practice indicates that in situations where the risk for atrophic nonunion development is present (e.g. due to excessive trauma to periost and marrow (Marsh *et al.*, 1994; Marsh, 1998)), injection of mesenchymal stem cells at the beginning of the healing process, could substantially reduce this risk.

Design of treatment strategies

One of the most interesting applications of these models is the study of pathological situations of fracture healing (delayed or nonunions) and the optimisation of the treatment of these pathological cases. A few simple examples were presented, showing cases of pathological healing and simple treatment strategies. No attempt was made here to validate these simulations of therapeutic strategies, although evidence can be found in the literature that e.g. the administration of BMP's (by gradually releasing them from a carrier) indeed enhances bridging in cases of delayed healing (Southwood *et al.*, 2004). In order to test the validity of the model for the study of pathological cases and their treatment, additional experiments will have to be run for these cases. This however makes it necessary to extend the model with these factors that actually cause delayed healing or nonunions, such as (improper) angiogenesis or mechanical loading. As to the former, transgenic mouse models can help to unravel the governing role of angiogenic factors in normal and pathological fracture healing, and to incorporate these factors in the mathematical model (the creation of which is the subject of next chapter). As to the latter, the incorporation of the (stimulating) effect of mechanical loading on cell differentiation and ossification will be discussed in chapter 6. Obviously, incorporating more cytokines and growth factors in the model, leads to a higher degree of complexity. An additional problem is the fact that the mutual interactions between these influencing factors have yet to be fully unravelled, so that their implementation in the mathematical model is not straightforward. On the other hand, the model can help to identify possible interactions, by running simulations for different possible sets of interactions, and retaining these interactions that lead to a reasonable course of fracture healing (i.e. corroborated by experimental findings).

4.6 Conclusion

In order to establish a combined experimental and theoretical framework for the further study of pathological fracture healing and fracture healing in genetically altered mice, the mathematical model of Bailón-Plaza and van der Meulen (2001) was applied to a semi-stabilised murine tibial fracture model and a standardised rodent femoral fracture model, and the experimental and numerical results were compared for both cases. The model was implemented in a custom code, paying special attention to the requirements of mass conservation and non-negativity of the variables. With the set of parameter values given in appendix 7.3.2, a good qualitative agreement was obtained between simulated results and experimental data for several important aspects of the normal fracture healing process such as the global spatial and temporal evolution of the cartilage and bone matrix and the temporal evolution in the growth factor concentrations. This qualitative agreement was further corroborated by experimental results reported previously in literature. A quantitative comparison between simulation results and experimental data, showing a reasonable agreement for the bone matrix, is hampered by the coupling of cartilage and fibrous tissue in one mathematical variable. Cases of pathological healing (delayed union and nonunion) were described, indicating the possibilities of mathematical models to investigate causes of pathological healing. Furthermore, an example was given to demonstrate the potential therapeutic value of mathematical models.
However, several essential regulators of the fracture healing process, such as angiogenesis and directed cell migration are lacking in this model. Also the combination of the fibrous and cartilaginous matrix in one mathematical variable and the phenomenological description of the endochondral ossification, prevent a thorough quantitative comparison between simulation and experiments. In order to obtain results that are more suitable for clinical applications, these shortcomings need to be addressed.
The structure of the numerical implementation of the mathematical model enables easy extension of the code to incorporate more cells and tissue types, such as fibroblasts and endothelial cells (chapter 5), and other influencing factors, such as mechanical loading (Bailón-Plaza and van der Meulen, 2003) (chapter 6), angiogenesis (chapter 5) or additional growth factors (chapter 5). These model extensions are discussed in the next chapters.

Table 4.2: Summary of the most important results of the sensitivity analyses. The upper rows indicate the parameter and its tested value, expressed as a percentage of the original value (Exp: results from experiments and from Hadjiargyrou *et al.* (2002); B: reference parameter set used in this study, BP: parameter set from Bailón-Plaza and van der Meulen (2001)). The next rows indicate the starting day for intramembranous ossification (IMOS) and endochondral ossification (ECOS). The next rows show the time and place of bridging of the callus by bone (E: external; I: intramedullary). The final rows indicate when full ossification was reached within the simulation period (/: no full ossification was reached in the simulated period) and by which process this was mainly achieved (EC: endochondral ossification; IM: intramembranous ossification; B: both)

	Exp	B	BP	A_{co}				A_{bo}				G_{gc}		d_{gc}		d_{gb}		P_{cs}		κ_c		B_{ec}				Q_{cd2}		c_{m_bc}				$c_{m_bc_dur}$	
%				10	50	200	1000	10	50	200	1000	10	50	200	1000	10	50	10	50	200	1000	10	50	200	1000	200	1000	10	50	200	1000	10	50
IMOS	4	3	1	3	3	3	3	4	3	3	2	3	3	3	3	3	3	3	3	3	3	3	3	3	3	3	3	6	4	3	2	3	3
ECOS	8	8	1	7	7	6	6	9	7	6	/	5	14	9	3	/	5	/	9	9	/	2	4	14	/	8	7	/	14	4	2	12	12
bridge		10	2	10	10	10	8	/	10	8	3	11	/	18	8	4	7	20	/	/	18	4	5	/	/	/	/	/	/	5	3	/	/
	E	E	E	E	E	E	EI		E	E	EI	EI		EI	EI	E	E	EI			EI	E	E							E	E		
fullOS	21	20	6	/	/	12	8	/	19	11	3	16	/	21	15	9	15	/	/	/	/	7	15	/	/	/	/	/	/	18	14	/	/
	EC	EC	EC			EC	EC		EC	IM	IM	IM		EC	IM	IM	EC					EC	EC							EC	B		

Chapter 5

A novel Bioregulatory model of bone regeneration including angiogenesis: application in fracture healing

In this chapter the development of a novel bioregulatory model is elaborated. In this model, a number of the currently existing models' shortcomings are overcome. The introduction discusses the influence of angiogenesis on the fracture healing process, followed by a concise description of the most recently published fracture healing models and their limitations. Section 5.2 states the research hypothesis that was put forward during this study and identifies the different objectives. In section 5.3 the novel bioregulatory model with all its variables, parameters and underlying assumptions is discussed in detail. Section 5.4 shows simulation results obtained with this model, both for normal and pathological healing cases. These results and the simplifications that were made in the design of the model are discussed in section 5.5. To conclude this chapter, the most important findings are recapitulated together with suggestions for future improvements of the model.

5.1 Introduction

5.1.1 Angiogenesis and fracture healing

Many local and systemic factors active during fracture healing have direct or indirect osteogenic and angiogenic functions (Carano and Filvaroff, 2003). These factors include members of the fibroblast growth factor (FGF), transforming growth factor (TGF), bone morphogenetic protein (BMP) and vascular endothelial growth factor (VEGF) families. Endogenous VEGF is a key player in bone repair, where its temporal and spatial expression pattern corresponds to the one observed during long bone development (Street *et al.*, 2002). VEGF is essential for normal angiogenesis and appropriate callus architecture. More and more evidence is found to support the hypothesis that blood vessel invasion has a key role in tissue repair and VEGF production is the major coupling mechanism between angiogenesis and osteogenesis during fracture healing (Street *et al.*, 2002). VEGF expression is induced in osteoblasts by various stimuli (overview in Carano and Filvaroff (2003)). In turn, VEGF regulates recruitment, survival and activity of endothelial cells, osteoblasts and osteoclasts (Street *et al.*, 2002; Mayr-Wohlfart *et al.*, 2002; Midy and Plouet, 1994; Deckers *et al.*, 2000). Furthermore, VEGF has been observed to play a major role in cartilage maturation and resorption. Produced by hypertrophic chondrocytes, it initiates the endochondral ossification cascade by recruiting and/or differentiating cells that resorb cartilage and by attracting osteoblasts (Colnot *et al.*, 2003; Maes *et al.*, 2002).

Impaired angiogenesis plays an important role in the occurrence of nonunions and mal-unions. Inhibition of the activity of VEGF or one of its homologues (e.g. placental growth factor PlGF) disrupts the repair process and results in delayed union or nonunion. Fracture healing experiments in $PlGF^{-/-}$ knock-out mice (Maes *et al.*, 2006), show a reduced osteoblastic differentiation of mesenchymal progenitor cells and a persistent cartilaginous matrix without any sign of endochondral ossification. Angiogenesis, bone formation and callus mineralisation decrease when VEGF activity is inhibited in a mouse model of secondary fracture healing (Street *et al.*, 2002). Severe vascular damage accompanying the skeletal injury during fracture, leading to an ischemic regeneration site, results in delayed union or nonunion (Lu *et al.*, 2007) with little cartilage or bone formation. In a distraction osteogenesis set-up, acute distraction (causing acute mechanical overload) disrupts the angiogenic process, preventing normal osteogenesis and resulting in fibrous nonunion (Fang *et al.*, 2005). In the same experimental set-up, fibrous nonunion also occurs when proliferation of endothelial cells is blocked by an anti-angiogenic agent.

5.1.2 Mathematical models of fracture healing

Over the last decade, a number of mathematical models describing bone regeneration have been proposed. The first models were mechanoregulatory models, predicting bone formation based on local mechanical stimuli, in many cases making a distinction between the effect of deviatoric and hydrostatic stimuli. Several mechanoregulatory models were proposed and tested for various experimental situations, as discussed in section 3.1. None of these models however takes the biological aspects of bone regeneration into account. Bailón-Plaza and van der Meulen (2001) proposed a bioregulatory model of bone regeneration. This model assumes an ideal mechanical and vascular environment and describes fracture healing as a process regulated solely by osteogenic and chondrogenic growth factors. The two-dimensional continuum model (system of partial differential equations), permits a detailed qualitative and quantitative comparison of the predicted spatiotemporal distribution of the different tissues with the *in vivo* experimental observations. In chapter 4, this bioregulatory model was corroborated by applying the model to a semi-stabilised murine tibial fracture and a standardised rodent fracture setup and comparing the simulation results with the experimental observations (Geris *et al.*, 2006). In that study also a first attempt was made to model situations of pathological fracture healing and to demonstrate the potential therapeutical value of bone regeneration models.

Some of the most recent models in literature try to combine both mechanical and biological factors. Bailón-Plaza and van der Meulen (2003) adapted their bioregulatory model and made a number of the model parameters dependent on the local mechanical environment. A fuzzy logic model was proposed by Shefelbine *et al.* (2005) to simulate fracture healing, based on local mechanical factors, as described by Claes (1998), and the local vascularity. To model the progress of angiogenesis in the fracture callus, a number of very basic, mechanoregulatory fuzzy rules were applied. Finally, Gómez-Benito *et al.* (2005) presented a model describing fracture healing in terms of the evolution of the densities of different cell types in a growing callus. However, the only regulatory component is the local mechanical environment, neglecting again the influence of biological factors.

All of the aforementioned models lead to reasonable simulation results for normal fracture healing. However, there are still a number of limitations connected to these models when the simulation of pathological healing is envisaged.

- Most models only consider the influence of either the biology or the mechanics on the regeneration process

- Cell migration, if present at all, is mostly treated as a simple diffusion process
- None of the models (except the model of Shefelbine *et al.* (2005) in a very crude way) includes the angiogenic process in the description of fracture healing
- The model of Bailón-Plaza and van der Meulen (2001, 2003) does not make a distinction between the fibroblasts and chondrocytes, nor between the fibrous tissue component and the cartilaginous tissue component of the soft tissue callus.
- Endochondral ossification is described in a very phenomenological way by all models, as cartilage simply being replaced by bone without any reference to the underlying mechanisms.
- None of the aforementioned models (except the model of Gómez-Benito *et al.* (2005)), modelled the growth and degradation of the fracture callus.

5.2 Hypothesis and Objectives

5.2.1 Hypothesis

In view of the long-term goal of the research presented in this work, being the application of mathematical models in the research into possible causes and treatment of pathological bone regeneration, this chapter builds on the framework that was presented in the previous chapter. The work presented in this chapter aims to meet some of the shortcomings identified in chapter 4 and section 5.1.2. The hypothesis underlying this study is that the incorporation of several model extensions such as angiogenesis, extended cell migration and fibroblasts/fibrous tissue allows for a better description of both normal and pathological bone regeneration. The main goals for the work described in this chapter are:

1. The development of an enhanced bioregulatory model.
2. The investigation of possible causes of pathological fracture healing among others due to impaired angiogenesis.

In order to achieve these goals, the model presented here has started from the model proposed by Bailón-Plaza and van der Meulen (2001) and has extended it to include a description of the angiogenic process. Further modifications have been carried out to separate the descriptions of cartilage and fibrous tissue. Finally, the description of cell migration has been elaborated on to

incorporate chemotaxis as a migratory mechanism. The experimental system to which the model has been applied is the standardised externally fixated rodent fracture, developed by Harrison *et al.* (2003) (see chapter 4). The parameter values used for this model have been based on estimates obtained from experimental observations, if possible. Finally, a few of the pathological situations described in section 5.1.1 due to impaired angiogenesis were simulated.

5.2.2 Objectives

- The development of an extended bioregulatory model, including a description of angiogenesis, cell migration and fibrous tissue formation (section 5.3.1).
- The derivation of model's parameter values (sections 5.3.2 and 5.3.3).
- The corroboration of the model's predictions by comparison with experimental data (sections 5.4.1 and 5.5.1)
- The simulation of pathological cases of fracture healing (sections 5.4.3 and 5.5.4)

5.3 Materials and Methods

This section describes in detail the different aspects of the novel bioregulatory model. Section 5.3.1 describes the functional forms and equations of the mathematical model followed by section 5.3.2 describing the derivation of the parameter values. The next sections (5.3.3 and 5.3.4) provide the simulation details and a description of the numerical implementation. Finally, section 5.3.5 gives an overview of the simulations that were carried out using the enhanced bioregulatory model.

5.3.1 Mathematical framework

The presented mathematical model is built on the model proposed by Bailón-Plaza and van der Meulen (2001). That model describes fracture healing as the spatiotemporal variation in density of seven variables: mesenchymal stem cells (c_m), chondrocytes (c_c), osteoblasts (c_b), a combined fibrous/cartilaginous extracellular matrix (m_c), bone extracellular matrix (m_b) and a generic osteogenic (g_b) and chondrogenic (g_c) growth factor. The model was extended with the following variables:

- the density of endothelial cells (c_v), a vascular matrix (m_v) and a generic angiogenic growth factor (g_v) for the description of angiogenesis

- a variable representing the concentration of fibroblasts (c_f) and one describing the fibrous tissue density(m_f), thereby separating the variable from the model of Bailón-Plaza and van der Meulen (2001) representing the combined fibrous/cartilaginous extracellular matrix into two variables, the fibrous tissue (m_f) and the cartilage matrix (m_c) respectively.

The mathematical model describing the interactions of these variables is a PDE model of taxis-diffusion-reaction type. The following section discusses the individual taxis and diffusion coefficient functions and the reaction terms. A schematic overview of the mathematical models is presented in Figure 5.1.

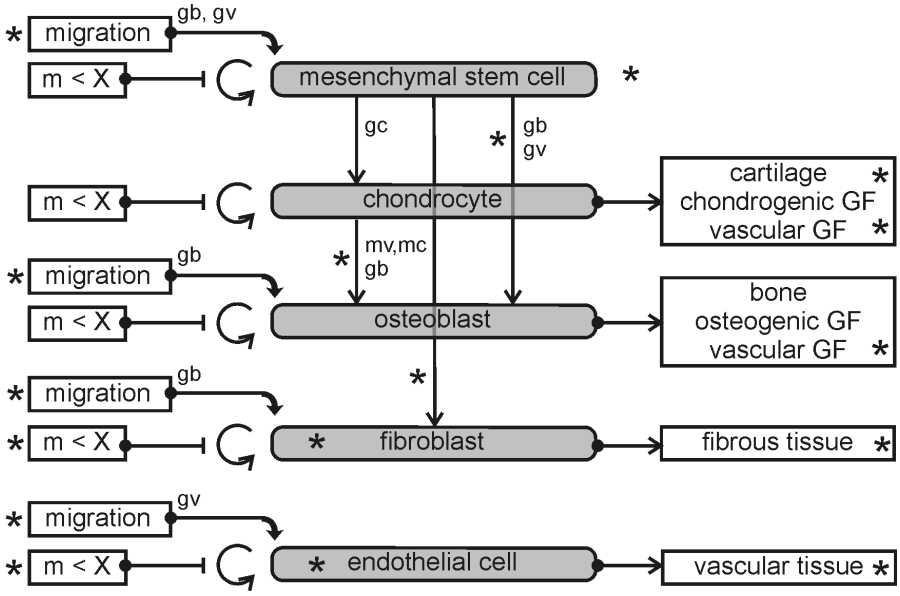


Figure 5.1: Schematic overview of enhanced bioregulatory model. Asterisks indicate model extensions compared to Bailón-Plaza and van der Meulen (2001).

Mesenchymal stem cells

The migration of mesenchymal stem cells is a combination of random and directed motion (Pountos and Giannoudis, 2005). The random motion was modelled as a haptokinetic process. The form of the haptokinetic coefficient was taken from Olsen *et al.* (1997), based on Dickinson and Tranquillo

(1993). The latter model was corroborated by the experiments performed by Kuntz and Saltzman (1997) and Lutolf *et al.* (2003). Random motion is influenced by the total matrix density, defined as $m = m_f + m_c + m_b + m_v$, such that in the absence or abundance of extracellular matrix, cells cease to move.

$$D_m = \frac{D_{hm} m}{(K_{hm}^2 + m^2)} \tag{5.1}$$

Chemotaxis was modelled using a receptor-kinetic form, giving a maximum chemotactic response at a particular growth factor concentration, as was observed in experiments by Lind *et al.* (1996), Fiedler *et al.* (2004, 2005) and Metheny-Barlow *et al.* (2004). The chemotactic response of mesenchymal stem cells depends both on osteogenic and angiogenic growth factors.

$$C_{m_{CT}} = \frac{C_{kCTm}(g_b + g_v)}{(K_{kCTm}^2 + (g_b + g_v)^2)} \tag{5.2}$$

The haptotactic coefficient was taken from Olsen *et al.* (1997), based on a kinetic analysis of a model mechanism for the cell-surface-receptor-extracellular-ligand binding dynamics (Sherratt, 1994).

$$C_{m_{HT}} = \frac{C_{kHTm}}{(K_{kHTm} + m)^2}$$

The proliferation of stem cells, as well as the other four cell types, is modelled by a logistic growth function, whereby the proliferation rate depends on the surrounding matrix density (Olsen *et al.*, 1997; Weinberg and Bell, 1985; Yoshizato *et al.*, 1985).

$$A_i = \frac{A_{i0} m}{(K_i^2 + m^2)} \qquad \text{for} \quad i = m, f, c, b, v \tag{5.3}$$

The differentiation of mesenchymal stem cells towards osteoblasts is mediated by the presence of osteogenic and angiogenic growth factors (Street *et al.*, 2002; Mayer *et al.*, 2005; Midy and Plouet, 1994). For high chemical concentrations, a saturation effect was modelled to take place (Bailón-Plaza and van der Meulen, 2001).

$$F_1 = \frac{Y_{11} g_b}{(H_{11} + g_b)} \times \frac{Y_{12} g_v}{(H_{12} + g_v)}$$

A similar function, depending on the concentration of the chondrogenic growth factor, was used to model the differentiation towards chondrocytes.

$$F_2 = \frac{Y_2 g_c}{(H_2 + g_c)}$$

Fibroblasts

Fibroblasts invade the callus area from the surrounding tissues, but also differentiate from mesenchymal stem cells. The main regulator of that process seems to be mechanical load whereby a high mechanical load stimulates the formation of fibroblasts (Prendergast *et al.*, 1997; Carter *et al.*, 1998). However, since this model does not explicitly treat the mechanical influences on fracture healing, the differentiation rate of mesenchymal stem cells towards fibroblasts was taken to be a constant (F_4). Very few studies report on the actions and functions of fibroblasts and fibrous tissue during fracture healing (Chai *et al.*, 1999; Bland *et al.*, 1999; Maheswari *et al.*, 1999). Therefore, fibroblast migration and proliferation were described in a similar way as for the other cell types. The random motion of fibroblasts was modelled by means of a constant diffusion rate. For the directed migration of fibroblasts up the gradient of osteogenic growth factor concentrations, a receptor-kinetic form as given by equation 5.2, but only depending on g_b and not on g_v, was used. Upon the initiation of endochondral ossification, fibroblasts are removed from the callus (Zhang *et al.*, 2001). This decay was modelled using replacement function F_3 (see equation 5.4), to be discussed next, together with a proportionality factor d_f.

Chondrocytes

Endochondral replacement refers to the removal of mineralised cartilage and formation of bone. When chondrocytes exit their proliferative cycle, they will mature towards hypertrophic chondrocytes (Rossi *et al.*, 2002). Exactly what causes the exit from the proliferative cycle and the subsequent differentiation towards hypertrophy is not well known. It involves amongst others a growth factor dependent triggering of proteins that induce growth arrest and proliferation slowdown (Enomoto-Iwamoto *et al.*, 1998; Laplantine *et al.*, 2002; Rossi *et al.*, 2002). According to Einhorn (1998), the initiation of cartilage mineralisation is triggered by the abundance of cartilage. Combining these factors leads to the simplified representation of hypertrophic chondrocytes as chondrocytes that are no longer proliferating in the presence of a dense cartilage matrix (consistent with function 5.3 where the proliferation rate decreases for increasing matrix densities). Hypertrophic chondrocytes in the matrix start producing VEGF, attracting endothelial cells into the mineralised matrix, increasing vascularity and triggering matrix metalloproteinases (MMP's) to degrade the cartilage matrix (Gerber *et al.*, 1999; Colnot *et al.*, 2003). These endothelial cells are closely followed by osteoblasts laying down bone matrix. All these facts combined resulted in the following function for

the endochondral replacement of chondrocytes:

$$F_3 = \frac{m_c^6}{(B_{ec}^6 + m_c^6)} \times \frac{m_v^6}{(B_v^6 + m_v^6)} \times \frac{Y_3 g_b}{(H_3 + g_b)} \tag{5.4}$$

The first factor in this expression refers to the hypertrophy of the chondrocytes, the second factor to the invasion of blood vessels and the third factor to the attraction of osteoblasts, all of which are indispensable in the process of endochondral ossification.

Osteoblasts

The functional form 5.4 was used to describe both the disappearance of chondrocytes from the cartilage and the introduction of new osteoblasts into the callus. These osteoblasts closely follow the endothelial cells upon the invasion of the mineralised cartilage by blood vessels (Einhorn, 1998). The migration of osteoblasts is mainly due to chemotaxis, again using a functional form similar to 5.2, but only depending on g_b and not on g_v. Upon production of bone matrix, osteoblasts gradually become entrapped by the matrix they are producing. When an osteoblast is completely surrounded by bone matrix, it will either mature and become an osteocyte or die (apoptosis). In both cases, this removes the osteoblast from the active matrix producing population and was modelled by a constant decay term.

Endothelial cells

Endothelial cells migrate in and towards the callus from the intact vasculature surrounding the fracture zone. This migration has a random movement component, modelled identical to the haptokinesis of mesenchymal stem cells (functional form 5.1), and a directed movement component. Chemotactic migration up a gradient of vascular growth factor concentration was modelled again using the functional form 5.2, but this time only depending on g_v and not on g_b (Terranova *et al.*, 1985), whereas haptotactic migration up a gradient of vascular tissue density was modelled using a constant haptotactic coefficient (Anderson and Chaplain, 1998). No distinction was made between tip cells, which have migratory capacities, and the quiescent endothelial cells, which do not. However, upon production of a collagenous vascular matrix, the endothelial cells become embedded and cease to migrate. This was modelled as the disappearance of endothelial cells with a constant decay rate. In that way, the variable c_v is representing the active cell pool, while the quiescent endothelial cells are enclosed in the vascular matrix, represented by variable m_v.

Extracellular matrix

The spatiotemporal evolution of matrix densities was modelled according to Bailón-Plaza and van der Meulen (2001) and Olsen *et al.* (1997). Extracellular matrix production was assumed proportional to the cell density of the matrix producing cells, whereby the production rate decreases as the surrounding matrix density increases. The soft tissues (fibrous tissue and cartilage) have an additional degradation component, reflecting the removal of the respective tissue during the endochondral ossification process.

Growth factors

In most of the aforementioned processes, the local concentration of growth factors plays a key role. Growth factors are able to migrate inside the callus area, simulated here by a diffusion process with a constant diffusion rate (Anderson and Chaplain, 1998). Chondrogenic growth factors are produced by chondrocytes, up to a certain saturation concentration, after which the production rate levels off. For normal matrix densities, the production saturates and even decreases again for higher matrix densities. When chondrocytes become hypertrophic (simulated in this model by reaching a certain cartilage density, as previously elaborated), they cease to produce chondrogenic growth factors, and as they are removed during the endochondral ossification process, the production of chondrogenic growth factors drops to zero.

$$E_{gc} = \frac{G_{gc} g_c}{(H_{gc} + g_c)} \times \frac{m}{\left(K_{gc}^3 + m^3\right)}$$

Removal of chondrogenic growth factors was modelled by a decay function (d_{gc}) representing denaturation and irreversible binding (Bailón-Plaza and van der Meulen, 2001). The production and decay of osteogenic growth factor was modelled in a similar way, except that the osteogenic growth factor production rate is not limited by matrix density.

$$E_{gb} = \frac{G_{gb} g_b}{(H_{gb} + g_b)}$$

Angiogenic growth factors are produced both by osteoblasts and hypertrophic chondrocytes. The production rate is proportional to the present growth factor concentration (up to a saturation level) and also saturates for high vascular densities, leading to the following function for the production rates by osteoblasts E_{gvb} and hypertrophic chondrocytes E_{gvc}:

$$E_{gvb} = \frac{G_{gvb} g_v}{(H_{gv} + g_v)} \times \frac{m_v}{\left(K_{gv}^3 + m_v^3\right)}$$

$$E_{gvc} = \frac{G_{gvc} g_v}{(H_{gv} + g_v)} \times \frac{m_v}{\left(K_{gv}^3 + m_v^3\right)} \times \frac{m_c^6}{(B_{ec}^6 + m_c^6)}$$

The final factor in the last equation refers again to the hypertrophy of the chondrocytes. The removal of vascular growth factor from the callus area, both through natural decay (d_{gv}) and through consumption by endothelial cells (d_{gvc}), was modelled by a simple uptake function (Anderson and Chaplain, 1998).

System of equations

Summarised, this leads to the following system of equations:

$$\begin{aligned}
\frac{\partial c_m}{\partial t} &= \nabla \left[D_m \nabla c_m - C_{m_{CT}} c_m \nabla (g_b + g_v) - C_{m_{HT}} c_m \nabla m \right] \\
&\quad + A_m c_m \left[1 - \alpha_m c_m \right] - F_1 c_m - F_2 c_m - F_4 c_m \\
\frac{\partial c_f}{\partial t} &= \nabla \left[D_f \nabla c_f - C_f c_f \nabla g_b \right] + A_f c_f \left[1 - \alpha_f c_f \right] + F_4 c_m \\
&\quad - F_3 d_f c_f \\
\frac{\partial c_c}{\partial t} &= A_c c_c \left[1 - \alpha_c c_c \right] + F_2 c_m - F_3 c_c \\
\frac{\partial c_b}{\partial t} &= -\nabla \left[C_b c_b \nabla g_b \right] + A_b c_b \left[1 - \alpha_b c_b \right] + F_1 c_m + F_3 c_c - d_b c_b \\
\frac{\partial c_v}{\partial t} &= \nabla \left[D_v \nabla c_v - C_{v_{CT}} c_v \nabla g_v - C_{v_{HT}} c_v \nabla m_v \right] + A_v c_v \left[1 - \alpha_v c_v \right] \\
&\quad - d_v c_v \\
\frac{\partial m_f}{\partial t} &= P_{fs} \left(1 - \kappa_f m_f \right) c_f - Q_f m_f m_c c_b \\
\frac{\partial m_c}{\partial t} &= P_{cs} \left(1 - \kappa_c m_c \right) c_c - Q_c m_c c_b \\
\frac{\partial m_b}{\partial t} &= P_{bs} \left(1 - \kappa_b m_b \right) c_b \\
\frac{\partial m_v}{\partial t} &= P_{vs} \left(1 - \kappa_v m_v \right) c_v \\
\frac{\partial g_c}{\partial t} &= \nabla \left[D_{gc} \nabla g_c \right] + E_{gc} c_c - d_{gc} g_c \\
\frac{\partial g_b}{\partial t} &= \nabla \left[D_{gb} \nabla g_b \right] + E_{gb} c_b - d_{gb} g_b \\
\frac{\partial g_v}{\partial t} &= \nabla \left[D_{gv} \nabla g_v \right] + E_{gvb} c_b + E_{gvc} c_c - g_v \left(d_{gv} + d_{gvc} c_v \right)
\end{aligned}$$

5.3.2 Parameters

Parameter values

The parameter values were derived from literature where possible and estimated when no relevant data was available.

- **Random Motion and Haptokinesis**
  Microscopic studies of random movement of various cell types report diffusion constants D in the orders of magnitude of 10^{-8} to 10^{-10} cm^2/s, depending on the cell type under investigation and the experimental conditions (Gruler and Bültmann, 1984; Friedl *et al.*, 1998; Rupnick *et al.*, 1988). For the haptokinetic coefficient (functional form 5.1) used in this model, the maximum rate of cell motility occurs at a matrix density of $m = K_{hm}$ or $m = K_{hv}$ for mesenchymal stem cells and endothelial cells respectively, yielding a value of $D_{hi} = 2K_{hi}D$ (i=m,v). K_{hm} and K_{hv} were chosen positive and higher than the initial matrix density. Random movement of fibroblasts was modelled with a constant diffusion coefficient, using the reported values above.

- **Chemotaxis**
  Many experimental studies have investigated the chemotactic response of mesenchymal stem cells (Fiedler *et al.*, 2004, 2005), fibroblasts (Seppä *et al.*, 1982; Postlethwaite *et al.*, 1987), osteoblasts (Lind *et al.*, 1996; Mayr-Wohlfart *et al.*, 2002) and endothelial cells (Stokes *et al.*, 1990; Li *et al.*, 2005a) to various growth factors. Most of them report bell-shaped curves representing the migratory response to increasing growth factor concentrations. Maximal chemotactic response is reported for growth factor concentrations of 1 to 10 ng/ml. Based on the reported chemotactic coefficients for the different cell types, the values of the parameters involved in the description of chemotaxis were determined.

- **Haptotaxis**
  In the absence of any available data for the haptotactic coefficients involved, the parameters were assigned values in the same order of magnitude as those of the chemotactic coefficients (Anderson and Chaplain, 1998; Bailón-Plaza and van der Meulen, 2001).

- **Proliferation**
  Bailón-Plaza and van der Meulen (2001) derived for their model the values of the parameters of the proliferation function 5.3 for mesenchymal stem cells, chondrocytes and osteoblasts. Due to lack of dedicated experimental data, these values were also adopted for the description of fibroblast and endothelial cell proliferation.

- **Differentiation**
  Bailón-Plaza and van der Meulen (2001) examined, in the absence of quantified cell differentiation rates, different values for the parameters describing mesenchymal cell differentiation in a sensitivity analysis. The function representing the endochondral replacement (Bailón-Plaza and van der Meulen, 2001) was extended to encompass the influence of the angiogenic process. A parameter B_v was introduced, indicating that the endochondral replacement can only proceed when the vascularisation is increasing. The differentiation of mesenchymal stem cells towards fibroblasts is mainly controlled by mechanical load. Since the mechanical aspect of the healing process is not considered here, the differentiation rate was modelled as a constant F_4. The value of this parameter was chosen rather low, due to the assumption of ideal mechanical circumstances. Therefore, the majority of the fibroblasts present in the callus, is there as a result of the fibroblast migration from the surrounding tissues into the callus area.

- **Cell decay**
  The rate of cell (osteoblast, fibroblast and endothelial) removal is not available from literature, and has been estimated by Bailón-Plaza and van der Meulen (2001) in a linear stability analysis. Their estimates were adopted in this model.

- **Matrix synthesis and degradation**
  Matrix synthesis rate was modelled to decrease proportionally with the increase of the corresponding matrix density. When the matrix density reaches its maximum value, the production will arrest. Initial production rates (P_{is}, i=f,c,b,v) were taken from Bailón-Plaza and van der Meulen (2001), based on the estimates calculated by Olsen *et al.* (1997).

- **Growth Factor Diffusion**
  The diffusion coefficient of a chemical in an aqueous solution can be determined from its molecular weight, using a relation developed by Vander *et al.* (1998). Taking into account typical molecular weights of osteogenic and chondrogenic growth factors (Joyce *et al.*, 1990), this leads to values for the diffusion coefficients in the order of magnitude of 10^{-8} cm^2/s. These values are corroborated by reported diffusion coefficients of various growth factors (Filion and Popel, 2004; Thorne *et al.*, 2004). Reported diffusion coefficients for angiogenic growth factors (Helm *et al.*, 2005; Ambrosi *et al.*, 2004) are in the order of magnitude of 10^{-7} cm^2/s.

- **Growth Factor Production**
  No experimental data is available on the production rates of growth factors. Therefore, a range of values for the magnitude of the production rate was explored numerically. The other parameter values (H_{gi}, i=c,b,v) were chosen in such a way that the saturation level for the production occurs around typical growth factor concentration levels.

- **Growth Factor Decay and Consumption**
  Typical values for the half life of growth factors involved in fracture healing are around and below 30 min. (Coffey *et al.*, 1990; Dasch *et al.*, 1989; Edelman *et al.*, 1993; Shima *et al.*, 1995). A half-life of 10 min. corresponds to a decay constant of 100 day^{-1}. Consumption of the angiogenic growth factor by endothelial cells was modelled by a simple uptake function, of which the rate was determined numerically due to the lack of experimental data.

Scaling and non-dimensionalisation

The following scalings were chosen for the non-dimensionalisation of the model variables:

$$\begin{aligned}
\tilde{t} &= \frac{t}{T}, \quad \tilde{x} = \frac{x}{L}, \quad \tilde{y} = \frac{y}{L}, \quad \tilde{c_m} = \frac{c_m}{c_0}, \quad \tilde{c_f} = \frac{c_f}{c_0}, \\
\tilde{c_c} &= \frac{c_c}{c_0}, \quad \tilde{c_b} = \frac{c_b}{c_0}, \quad \tilde{c_v} = \frac{c_v}{c_0}, \quad \tilde{m_f} = \frac{m_f}{m_0}, \quad \tilde{m_c} = \frac{m_c}{m_0}, \\
\tilde{m_b} &= \frac{m_b}{m_0}, \quad \tilde{m_v} = \frac{m_v}{m_0}, \quad \tilde{g_c} = \frac{g_c}{g_0}, \quad \tilde{g_b} = \frac{g_b}{g_0}, \quad \tilde{g_v} = \frac{g_v}{g_0}
\end{aligned}$$

Typical time and length scales for fracture healing in rodent studies are $T = 1$ day and $L = 3.5$ mm (Harrison *et al.*, 2003). A representative concentration of the collagen content in the tissues under investigation is $m_0 = 0.1$ g/ml. Typical growth factor concentrations are in the order of magnitude of 10^{-9} M (Nogami and Oohira, 1984; Joyce *et al.*, 1990). Taking into account the order of magnitude of the atomic mass of the growth factors, this results in a non-dimensionalisation value of $g_0 = 100$ ng/ml. Based on geometrical constraints, Bailón-Plaza and van der Meulen (2001) derived a typical value for cell density at the beginning of the healing process: $c_0 = 10^6$ cells/ml.

The model parameters were non-dimensionalised as follows (tildes referring to non-dimensionalised parameters):

$$
\begin{aligned}
\tilde{D}_{hm} &= \frac{D_{hm}T}{L^2 m_0}, \quad \tilde{K}_{hm} = \frac{K_{hm}}{m_0}, \quad \tilde{C}_{kCTm} = \frac{C_{kCTm}T}{L^2} \\
\tilde{K}_{kCTm} &= \frac{K_{kCTm}}{g_0}, \quad \tilde{C}_{kHTm} = \frac{C_{kHTm}T}{L^2 m_0}, \quad \tilde{K}_{kHTm} = \frac{K_{kHTm}}{m_0} \\
\tilde{A}_{m0} &= \frac{A_{m0}T}{m_0}, \quad \tilde{K}_m = \frac{K_m}{m_0}, \quad \tilde{Y}_{11} = Y_{11}T \\
\tilde{H}_{11} &= \frac{H_{11}}{g_0}, \quad \tilde{Y}_{12} = Y_{12}, \quad \tilde{H}_{12} = \frac{H_{12}}{g_0} \\
\tilde{Y}_2 &= Y_2 T, \quad \tilde{H}_2 = \frac{H_2}{g_0}, \quad \tilde{F}_4 = F_4 T \\
\tilde{D}_f &= \frac{D_f T}{L^2}, \quad \tilde{C}_{kf} = \frac{C_{kf}T}{L^2}, \quad \tilde{K}_{kf} = \frac{K_{kf}}{g_0} \\
\tilde{A}_{f0} &= \frac{A_{f0}T}{m_0}, \quad \tilde{K}_f = \frac{K_f}{m_0}, \quad \tilde{Y}_5 = Y_5 T \\
\tilde{H}_5 &= \frac{H_5}{m_0}, \quad \tilde{B}_v = \frac{B_v}{m_0}, \quad \tilde{B}_{ec} = \frac{B_{ec}}{m_0} \\
\tilde{Y}_3 &= Y_3 T, \quad \tilde{H}_3 = \frac{H_3}{g_0}, \quad \tilde{d}_f = d_f \\
\tilde{A}_{c0} &= \frac{A_{c0}T}{m_0}, \quad \tilde{K}_c = \frac{K_c}{m_0}, \quad \tilde{C}_{kb} = \frac{C_{kb}T}{L^2} \\
\tilde{K}_{kb} &= \frac{K_{kb}}{g_0}, \quad \tilde{A}_{b0} = \frac{A_{b0}T}{m_0}, \quad \tilde{K}_b = \frac{K_b}{m_0} \\
\tilde{d}_b &= d_b T, \quad \tilde{D}_{hv} = \frac{D_{hv}T}{L^2 m_0}, \quad \tilde{K}_{hv} = \frac{K_{hv}}{m_0} \\
\tilde{C}_{kCTv} &= \frac{C_{kCTv}T}{L^2}, \quad \tilde{K}_{kCTv} = \frac{K_{kCTv}}{g_0}, \quad \tilde{C}_{v_{HT}} = \frac{C_{v_{HT}}T m_0}{L^2} \\
\tilde{A}_{v0} &= \frac{A_{v0}T}{m_0}, \quad \tilde{K}_v = \frac{K_v}{m_0}, \quad \tilde{d}_v = d_v T \\
\tilde{P}_{fs} &= \frac{P_{fs}Tc_0}{m_0}, \quad \tilde{Q}_f = Q_f m_0 c_0 T, \quad \tilde{P}_{cs} = \frac{P_{cs}Tc_0}{m_0} \\
\tilde{Q}_c &= Q_c c_0 T, \quad \tilde{P}_{bs} = \frac{P_{bs}Tc_0}{m_0}, \quad \tilde{P}_{vs} = \frac{P_{vs}Tc_0}{m_0} \\
\tilde{D}_{gc} &= \frac{D_{gc}T}{L^2}, \quad \tilde{G}_{gc} = \frac{G_{gc}Tc_0}{g_0 m_0^2}, \quad \tilde{H}_{gc} = \frac{H_{gc}}{g_0} \\
\tilde{K}_{gc} &= \frac{K_{gc}}{m_0}, \quad \tilde{d}_{gc} = d_{gc}T, \quad \tilde{D}_{gb} = \frac{D_{gb}T}{L^2} \\
\tilde{G}_{gb} &= \frac{G_{gb}Tc_0}{g_0}, \quad \tilde{H}_{gb} = \frac{H_{gb}}{g_0}, \quad \tilde{d}_{gb} = d_{gb}T
\end{aligned}
$$

$$\begin{aligned}
\tilde{D}_{gv} &= \frac{D_{gv}T}{L^2}, \quad \tilde{G}_{gvb} = \frac{G_{gvb}Tc_0}{g_0 m_0^2}, \quad \tilde{H}_{gv} = \frac{H_{gv}}{g_0} \\
\tilde{K}_{gv} &= \frac{K_{gv}}{m_0}, \quad \tilde{G}_{gvc} = \frac{G_{gvc}Tc_0}{g_0 m_0^2}, \quad \tilde{d}_{gv} = d_{gv}T \\
\tilde{d}_{gvc} &= d_{gvc}Tc_0
\end{aligned}$$

This resulted in the following set of non-dimensional parameters values: $\tilde{D}_{hm} = 0.014$, $\tilde{K}_{hm} = 0.25$, $\tilde{C}_{kCTm} = 0.04$, $\tilde{K}_{kCTm} = 0.1$, $\tilde{C}_{kHTm} = 0.0034$, $\tilde{K}_{kHTm} = 0.5$, $\tilde{A}_{m0} = 1.01$, $\tilde{K}_m = 0.1$, $\tilde{\alpha}_m = 1$, $\tilde{Y}_{11} = 10$, $\tilde{H}_{11} = 0.1$, $\tilde{Y}_{12} = 2$, $\tilde{H}_{12} = 0.1$, $\tilde{Y}_2 = 50$, $\tilde{H}_2 = 0.1$, $\tilde{F}_4 = 0.001$, $\tilde{D}_f = 0.02$, $\tilde{C}_{kf} = 0.4$, $\tilde{K}_{kf} = 0.1$, $\tilde{A}_{f0} = 0.202$, $\tilde{K}_f = 0.1$, $\tilde{\alpha}_f = 1$, $\tilde{Y}_5 = 50$, $\tilde{H}_5 = 0.1$, $\tilde{B}_v = 0.3 \cdot 10^{-7}$, $\tilde{B}_{ec} = 1.5$, $\tilde{Y}_3 = 1000$, $\tilde{H}_3 = 0.1$, $\tilde{d}_f = 0.1$, $\tilde{A}_{c0} = 0.101$, $\tilde{K}_c = 0.1$, $\tilde{\alpha}_c = 1$, $\tilde{C}_{kb} = 1.4 \cdot 10^{-8}$, $\tilde{K}_{kb} = 0.01$ $\tilde{A}_{b0} = 0.202$, $\tilde{K}_b = 0.1$, $\tilde{\alpha}_b = 1$, $\tilde{d}_b = 0.1$, $\tilde{D}_{hv} = 0.00007$, $\tilde{K}_{hv} = 1$, $\tilde{C}_{kCTv} = 0.0306$, $\tilde{K}_{kCTv} = 0.025$, $\tilde{C}_{v_{HT}} = 10^4$, $\tilde{A}_{v0} = 0.202$, $\tilde{K}_v = 0.1$, $\tilde{\alpha}_v = 1$, $\tilde{d}_v = 0.1$, $\tilde{P}_{fs} = 0.2$, $\tilde{\kappa}_f = 1$, $\tilde{Q}_f = 1.5$, $\tilde{P}_{cs} = 0.2$, $\tilde{\kappa}_c = 1$, $\tilde{Q}_c = 1.5$, $\tilde{P}_{bs} = 2$, $\tilde{\kappa}_b = 1$, $\tilde{P}_{vs} = 2 \cdot 10^{-6}$, $\tilde{\kappa}_v = 10^6$, $\tilde{D}_{gc} = 0.005$, $\tilde{G}_{gc} = 50$, $\tilde{H}_{gc} = 1$, $\tilde{K}_{gc} = 0.1$, $\tilde{d}_{gc} = 100$, $\tilde{D}_{gb} = 0.005$, $\tilde{G}_{gb} = 500$, $\tilde{H}_{gb} = 1$, $\tilde{d}_{gb} = 100$, $\tilde{D}_{gv} = 0.5$, $\tilde{G}_{gvb} = 10^{-11}$, $\tilde{H}_{gv} = 1$, $\tilde{K}_{gv} = 10^{-6}$, $\tilde{G}_{gvc} = 10^{-3}$, $\tilde{d}_{gv} = 200$, $\tilde{d}_{gvc} = 200000$.

5.3.3 Simulation details

Geometrical domain

The numerical simulations with this model were performed on the standardised rodent fracture model that was discussed in section 4.3.1. The simplified axisymmetric representation of the callus geometry derived in the previous chapter, was also used for this study (Figure 5.2). The expansion and regression of the callus geometry was not simulated in this study. The grid size was chosen sufficiently small to obtain grid independent results (cf. previous chapter, section 4.4.2).

Initial conditions

At the start of the simulation, the entire callus area is filled with a loose fibrous tissue matrix ($\tilde{m}_{f_ini} = 0.1$). Resulting from the haemorrhage, vascular growth factor is present throughout the callus ($\tilde{g}_{v_ini} = 10$). All other variables were assumed to be zero initially.

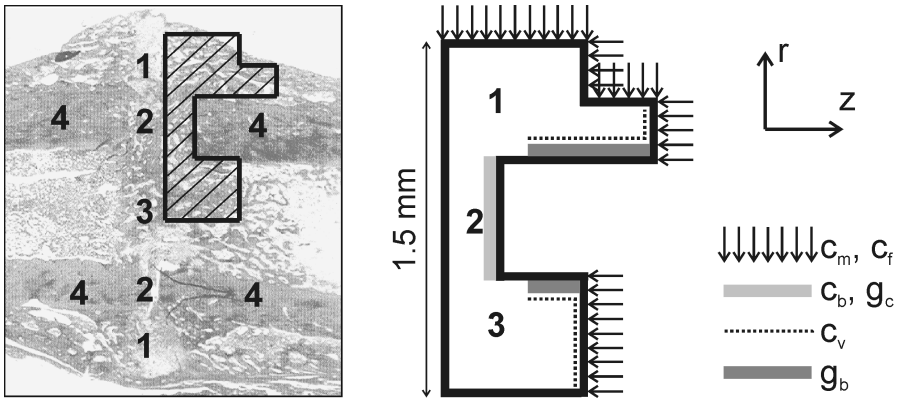


FIGURE 5.2: Left: geometrical domain deduced from the real callus geometry at post fracture week 3. Right: Dirichlet boundary conditions. 1: periosteal callus; 2: intercortical callus; 3: endosteal callus; 4: cortical bone.

Boundary conditions

The mathematical model is closed by prescribing suitable boundary conditions. No-flux boundary conditions are applied for all components of the PDE system with diffusion or taxis terms, except for the the situations, described below, where Dirichlet boundary conditions are prescribed for certain components on specific parts of the boundary and for a specified period of time. Mesenchymal stem cells and fibroblasts are released into the callus tissue at the beginning of the healing process from three possible sources: the periosteum, the surrounding soft tissues and the marrow space at the site of the damaged cortical tissue (Gerstenfeld *et al.*, 2003a). The experimental model under investigation in this study did not compromise any of these sources, therefore all sources were adopted here ($\tilde{c}_{m_bc} = 0.02$ & $\tilde{c}_{f_bc} = 0.02$ during first 3 days) (Figure 5.2). Osteoblasts were modelled to originate from the degrading bone ends, only in the very beginning of the healing process ($\tilde{c}_{b_bc} = 1$ during the first 4 days). Contrarily, the intact vasculature in the cortical bone and marrow cavity are a source of endothelial cells throughout the entire regeneration process ($\tilde{c}_{v_bc} = 10^{-4}$) (Gerstenfeld *et al.*, 2003a). Chondrogenic and osteogenic growth factors were assumed to originate from respectively the fractured bone ends and the cortex away from the fracture site (Barnes, 1999; Dimitriou *et al.*, 2005a) ($\tilde{g}_{c_bc} = \tilde{g}_{b_bc} = 20$ during respectively 5 and 10 days).

5.3.4 Numerical implementation

In the previous chapter, the spatial domain was considered to be two dimensional instead of axisymmetric, similar to the implementation reported in Bailón-Plaza and van der Meulen (2001). The results shown in this chapter are obtained using an enhanced version of the customised code discussed in chapter 4. The axisymmetric structure of the problem was exploited to properly reduce the model to an equivalent problem in 2D space, leading subsequently to an efficient spatial discretisation (Gerisch and Geris, 2007). The results obtained in the previous chapter were verified with this improved code and the difference between the solutions calculated with the different versions is negligible for the mathematical model of Bailón-Plaza and van der Meulen (2001) (Gerisch and Geris, 2007). This is however no longer the case for the novel model presented in this chapter due to the importance of the cellular migration. For the time integration of the resulting stiff MOL-ODE system, again the code ROWMAP (Weiner *et al.*, 1997) was used. The method's built-in automatic step size control ensures the error caused in each time step (local error) to remain below a user-prescribed tolerance while keeping the computational cost as low as possible.

5.3.5 Simulations and sensitivity analyses

The simulation results obtained with the enhanced mathematical model were compared with the histological measurements from the experiments. The added value of including angiogenesis and an elaborate description of cell migration is demonstrated. Furthermore, the influence of the value of the parameters connected to these phenomena on the simulation outcome is assessed in a sensitivity analysis. Finally, a few examples were developed to illustrate the potential of this model in simulating pathological situations. Several pathological healing situations involving impaired angiogenesis that were simulated, are discussed. Furthermore, similar to the previous chapter, murine experiments of atrophic nonunions caused by a lack of mesenchymal stem cells (section 4.4.2 on page 4.4.2) (Brownlow *et al.*, 2001, 2002; Kokubu *et al.*, 2003) were simulated, together with possible treatment strategies.

5.4 Results

5.4.1 Normal fracture healing

Using the parameters as described in section 5.3.2, the model predicts full ossification of the callus at 4 weeks post fracture. Figure 5.3 shows the spatiotemporal evolution of the fibrous tissue, cartilage, bone and vascular tissue extracellular matrix density. Mesenchymal stem cells, fibroblasts and growth

factors invade the callus area from the surroundings. Near the cortex, away from the fracture site, mesenchymal stem cells differentiate directly towards osteoblasts under the influence of the osteogenic growth factor. Intramembranous ossification can be observed from post fracture day (PFD) 5 onward. In the remainder of the callus, mesenchymal stem cells differentiate into chondrocytes, guided by the presence of chondrogenic growth factors. The predominant tissue types present in the callus after 1 week are fibrous tissue and cartilage. When the cartilage matrix reaches its maximum density (from PFD 14 onwards), chondrocytes start producing vascular growth factor. This attracts endothelial cells into the callus, causing cartilage degeneration, followed by a rise in the concentration of osteoblasts, producing bone matrix.

In the experiments reported by Harrison *et al.* (2003), the distribution of fibrous tissue, bone and cartilage for different zones of the callus were determined at post fracture days (PFD) 7, 21 and 35. These values are represented by the bars in Figure 5.4. In the same figure, the temporal evolution of these matrix densities, as predicted by the model, is shown. The fibrous tissue density decreases, as the bone matrix density increases towards the end of the healing period. Meanwhile, the cartilage matrix density increases and subsequently decreases again. As observed experimentally, the ossification process enrolls most rapidly in the periosteal callus. The healing process in the intercortical zone starts up last. Although the predicted order of events corresponds to the order observed experimentally, the time scale does not. Whereas in the experiments successful healing is established 5 weeks after fracture, the simulations predict successful healing after 4 weeks. Furthermore, the amount of cartilage in all zones is overestimated by the simulations. However, qualitative results on cartilage formation correspond between the simulations and experiments. In the endosteal zone, the smallest amount of cartilage formation, compared to the other callus areas, is found for both experiments and simulations. Moreover, similar to the experimental observations, the cartilage formation in the intercortical zone is observed to start at a later time point than in the periosteal callus.

5.4.2 Sensitivity analyses

Fibroblasts and fibrous tissue

Sensitivity analyses were carried out to assess the influence on the simulation outcome of the value of the parameters involved in the description of fibroblasts/fibrous tissue, cell migration and angiogenesis. The model shows robustness for small changes in the parameters connected to fibroblasts and fibrous tissue. Large changes in those parameters (> 1000 % or < 10 % of the original value) that lead to a markedly increased number of fibroblasts or en-

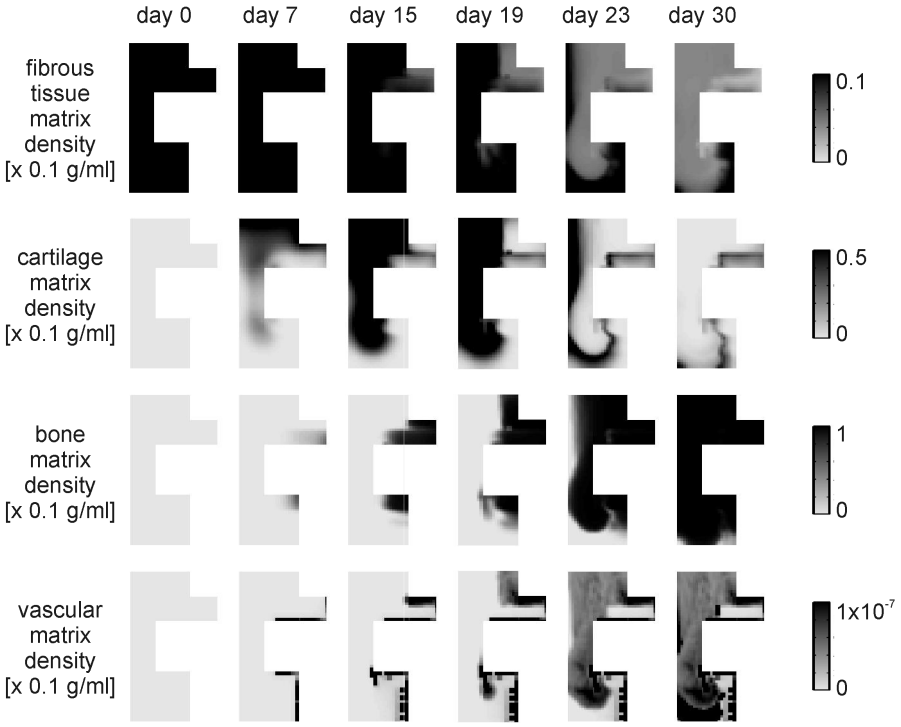


Figure 5.3: Spatiotemporal evolution (days post fracture) of fibrous tissue, cartilage, bone and vascular matrix density.

hanced fibrous tissue density in the callus area, have an influence on the speed of the healing process and the location of the bony bridging of the fracture. Similar observations were made for the influence of the value of the initial fibrous tissue density on the simulation outcome. Figure 5.5 shows various distributions (varying around $\tilde{m}_{f_ini} = 0.1$) of the initial fibrous tissue density at the start of the healing process. Successful healing is obtained in all three cases, however increased soft tissue matrix densities slow down the ossification front (by decreasing the random motion of endothelial cells, see functional form 5.1). When the highest fibrous tissue matrix density is situated in the central part of the callus (Figure 5.5b), bridging occurs in the periosteal callus with an ossification front moving inwards towards endosteal callus where the remaining (high density) soft tissue matrix is delaying complete ossification. When lowering the overall fibrous tissue density, compared to the previous example (Figure 5.5c), cartilage rapidly forms in the periosteal and endosteal callus. Proliferation and diffusion of endothelial cells in the periosteal region

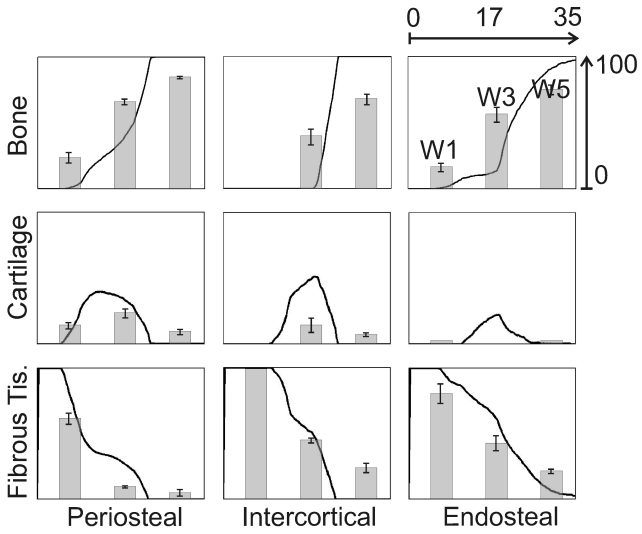


FIGURE 5.4: Predicted (continuous line) and experimentally measured (bars, avg±SE) tissue fractions [%] for the periosteal (top), intercortical (middle) and endosteal callus (bottom). The bars represent the histological measured values at post fracture week 1, 3 and 5.

is decreased in the first phase of healing due to insufficient substrate density (see Functional forms 5.1 and 5.3). This causes endochondral ossification to start up in the endosteal callus (closest to the source of endothelial cells, i.e. the intact vasculature in the cortex), followed by bony bridging of the fracture gap at that location. Ossification of the periosteal callus is delayed.

Endothelial cell migration

The migration of endothelial cells, modelled as a combination of directed and random motion, is an important aspect of this model. Figure 5.6 shows the predicted endothelial cell concentration and bone matrix density at various time points in the healing process for three models, only differing in their description of endothelial cell migration. Figure 5.7 shows the temporal evolution of the various tissue fractions in different parts of the callus. Using only random motion, endothelial cells slowly cover the entire callus area. Successful healing is established five weeks after fracture, bridging the fracture gap simultaneously at the periosteal and endosteal callus. Adding chemotaxis causes the cells to react to the vascular growth factor produced by the chondrocytes, resulting a in rapid invasion and subsequent degradation of the

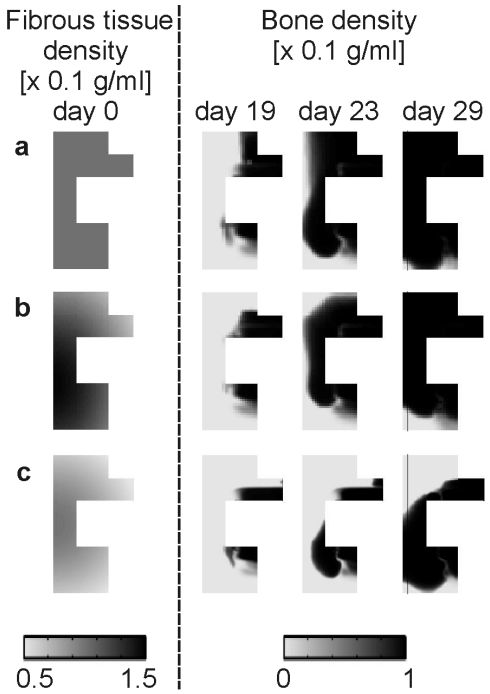


Figure 5.5: Influence of initial fibrous tissue matrix density on the progress of the healing process. (a) reference situations (cf. Figure 5.3). (b-c) various initial fibrous tissue distributions. Left: fibrous tissue density [× 0.1 g/ml] at start of simulations. Right: temporal evolution (days post fracture) of bone density [× 0.1 g/ml].

cartilage matrix. Successful healing is predicted after less than three weeks, bridging occurring on the external side of the periosteal callus. Including also haptotaxis in the migration of endothelial cells causes the cells to align on a front between the degrading cartilage and newly formed bone.

VEGF consumption

The sensitivity analyses further indicated that the consumption of the vascular growth factor by the endothelial cells is essential for a normal fracture healing process. Consumption of the growth factor by the endothelial cells ensures the presence of a chemical gradient (of vascular growth factor) leading the endothelial cells further towards the source of the endothelial growth factor production (i.e. hypertrophic chondrocytes). As the concentration of

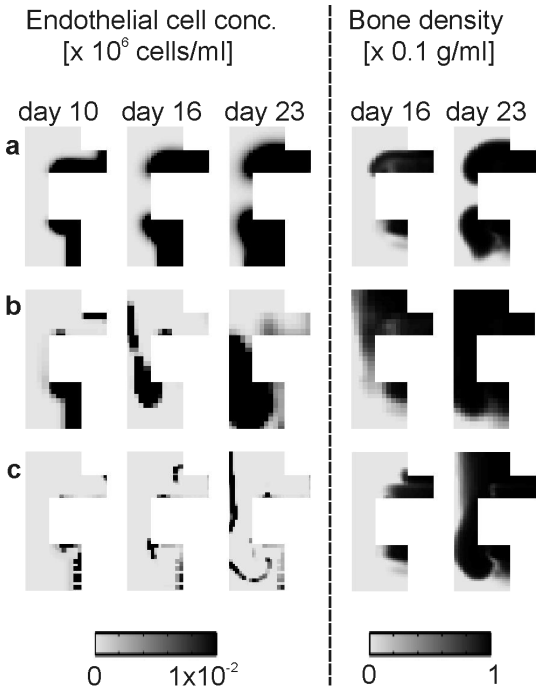


FIGURE 5.6: Influence of migration of endothelial cells on fracture healing, shown by predicted endothelial cell concentration (left) and bone density (right) at various post fracture time points. (a) only haptokinesis. (b) haptokinesis and chemotaxis. (c) haptokinesis, chemotaxis and haptotaxis.

chondrocytes producing vascular growth factor is lower in the endosteal zone, the healing process in this region is less affected by changes in the consumption rate (results not shown). The production of the vascular growth factor and its presence at the beginning of the healing process also have an important influence on the simulation outcome. These results are reported in the next section.

5.4.3 Pathological fracture healing

Impaired angiogenesis

Angiogenesis is crucial for the predicted normal fracture healing process as shown in Figure 5.8. A reduced production (10 % of reference value of $\tilde{G}_{gvc}$) of vascular growth factor by hypertrophic chondrocytes will cause a very slow invasion of the cartilage matrix by the endothelial cells (Figure 5.8a). In-

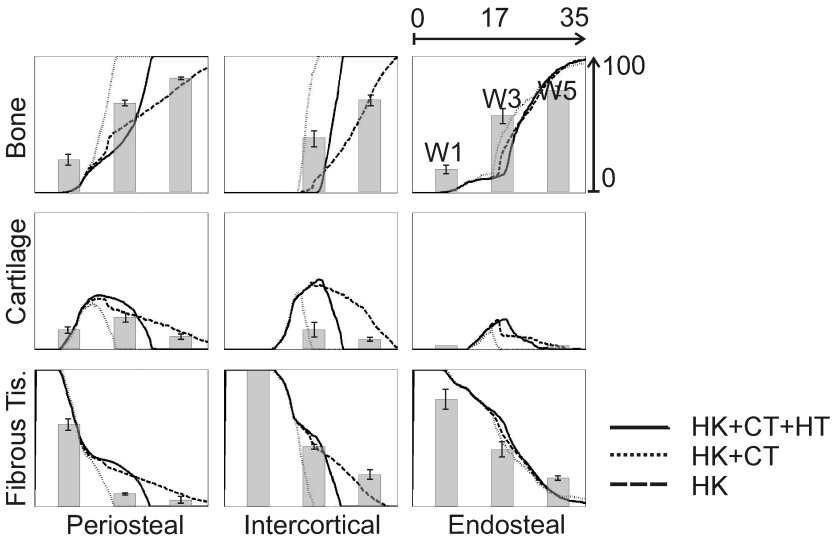


Figure 5.7: Predicted (continuous line) and experimentally measured (bars, avg±SE) tissue fractions [%] for the periosteal (top), intercortical (middle) and endosteal callus (bottom). The bars represent the histological measured values at post fracture week 1, 3 and 5. The dashed and dotted lines represent situations with different descriptions of endothelial cell migration. HK: haptokinesis; CT: chemotaxis; HT: haptotaxis.

tramembranous ossification is unaffected by this reduced production. Successful healing through endochondral ossification takes place after 5 weeks, with bridging occurring simultaneously in the periosteal and endosteal callus zone. Reducing the production of vascular growth factor by the hypertrophic chondrocytes even further (1 % of reference value of $\tilde{G}_{gvc}$) (Figure 5.8b) prevents any endochondral ossification or the initiation thereof, constituting a nonunion. Removing the initial condition for the vascular growth factor (i.e. initial concentration of vascular growth factor equal to 0: $\tilde{g}_{v_ini} = 0$), with a normal vascular growth factor production rate by hypertrophic chondrocytes, also leads to a lack of healing response. A little intramembranous bone formation is observed near the presence of the intact vasculature (Figure 5.8c), but there are no signs of endochondral ossification, nor the initiation thereof, in a period of 5 weeks after fracture.

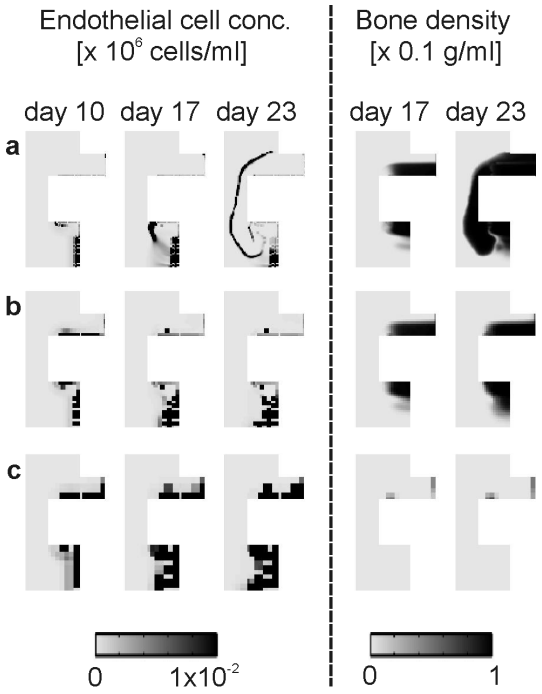


FIGURE 5.8: Influence of the angiogenic process on fracture healing, shown by predicted endothelial cell concentration (left) and bone density (right) at various post fracture time points. (a) reduced production of vascular growth factor by hypertrophic chondrocytes. (b) further reduced production of vascular growth factor by hypertrophic chondrocytes. (c) absence of vascular growth factor in callus at day 0.

Atrophic nonunion

The atrophic nonunion model described by Brownlow *et al.* (2001, 2002) and Makino *et al.* (2005) (discussed in section 4.4.2) was simulated with the extended bioregulatory model. Due to a lack of mesenchymal stem cells, no cartilage or bone formation was observed in the callus over a period of 12 weeks after fracture. Furthermore, comparable to the experimental findings, vascularisation of the callus area progressed continuously during this period (Figure 5.9). This aspect of the experimental findings could not be reproduced using the model of Bailón-Plaza and van der Meulen (2001) as shown in the previous chapter.

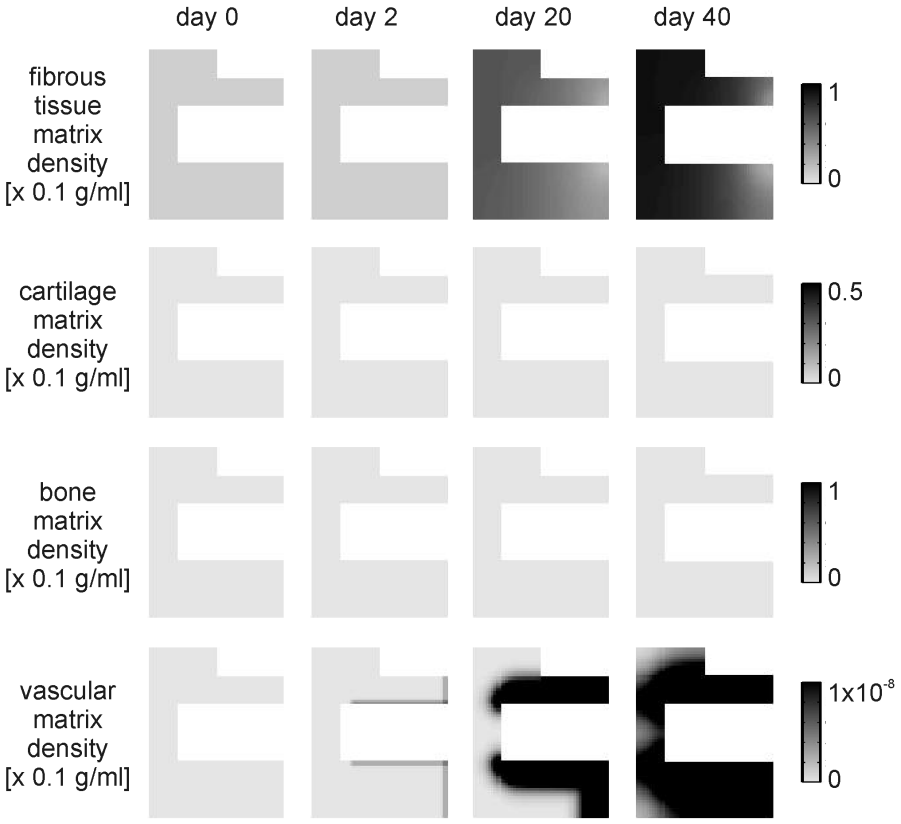


Figure 5.9: Spatiotemporal evolution (days post fracture) of fibrous tissue, cartilage, bone and vascular matrix density in an atrophic nonunion model.

Several treatment strategies were tested in this atrophic nonunion model. Figure 5.10 shows for each strategy the temporal evolution of the different tissues in the callus and the spatial distribution of the bone matrix in the callus after three weeks of treatment. Application of mesenchymal stem cells alone ($c_{m_bc} = 0.02 \times 10^6$ cells/ml, simulated as indicated in Figure 4.14 top) did not induce any healing response due to the lack of growth factors present in the callus area. Addition of osteogenic growth factors ($g_{b_bc} = 2$ μg/ml, simulated as indicated in Figure 4.14 top) did not induce any healing response either, as osteoblast differentiation from mesenchymal stem cells requires the presence of both osteogenic and vascular growth factors in this model (section 5.3.1). Upon addition of vascular growth factor ($g_{v_bc} = 2$ μg/ml, simulated as indicated in Figure 4.14 top), the fracture healing process was resumed (Fig-

ure 5.10a). However, as the cells and growth factors were applied outside the callus area, this resumed healing response was limited to the external part of the periosteal callus as the mesenchymal cells and growth factors were unable to penetrate deeper into the callus. Application of the mesenchymal stem cells into the callus area itself ($c_{m_bc} = 0.02 \times 10^6$ cells/ml in all grid cells) and the growth factors at the boundaries resulted in a much delayed healing response with successful healing established only 9 weeks after treatment (Figure 5.10b). Application of the mesenchymal stem cells as well as growth factors into the callus area itself, allowed for a renewed healing response in the entire callus area (Figure 5.10c). Immediate application of mesenchymal stem cells into the callus area at the initiation of the challenged fracture was able to restore a more or less normal healing process if the initially applied concentration of mesenchymal stem cells was sufficiently high ($c_{m_ini} = 0.02 \times 10^6$ cells/ml in all grid cells) (Figure 5.10d). When this concentration was too low ($\leq 0.002 \times 10^6$ cells/ml in all grid cells), the healing response arrested at the soft callus phase with no endochondral ossification taking place (Figure 5.10e). Enhancing the proliferative capacities of the small pool of mesenchymal stem cells present after fracture ($\tilde{A}_{m0} \times 10$), had a similar effect as the immediate application of additional mesenchymal stem cells, namely the occurrence of a (slightly delayed) normal healing response (Figure 5.10f).

Note that the greyscale plots in Figures 5.10c and d show a complete coverage of the fracture area with high density bone matrix while in the graph above, the bone component does not reach 100 %. This is due to the fact that the fibrous tissue is not degraded when bone forms through intramembranous ossification.

5.5 Discussion

5.5.1 Simulation results

The presented model is able to capture essential features of the fracture healing process and demonstrates that angiogenesis and directed cell motility are key factors in the establishment of a successfully healed fracture. Fracture healing is described using a continuum system of equations, representing the spatiotemporal evolution of concentrations or densities of several cell types, extracellular matrix types and growth factors (Figures 5.3 and 5.4). Parameter values were derived from literature if available and the model was applied to a highly quantified (in terms of tissue distribution) experimental set-up.

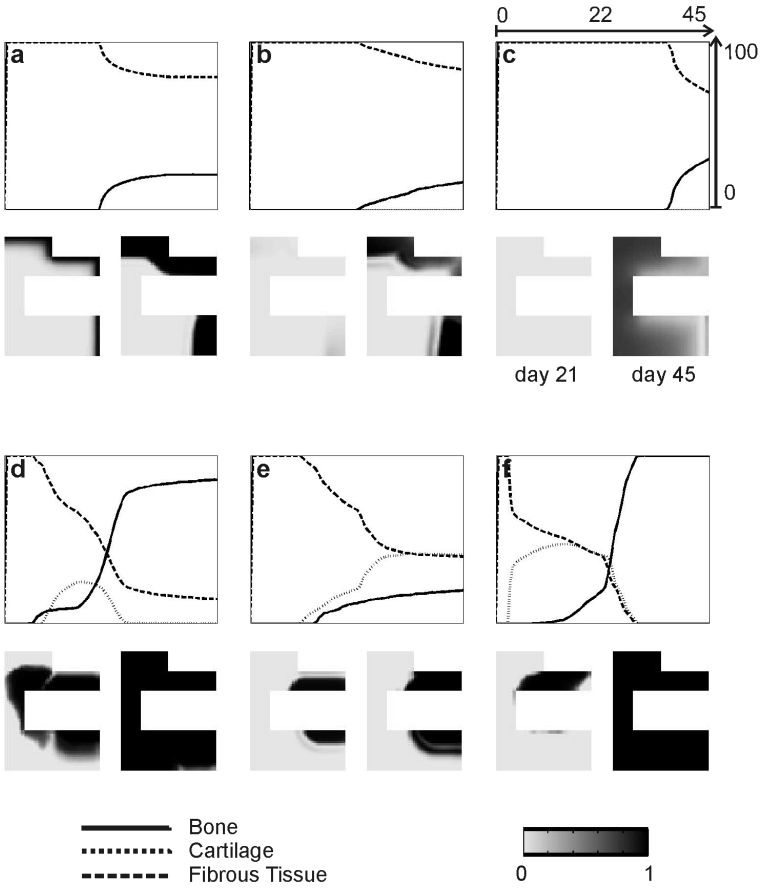


Figure 5.10: Treatment strategies for the atrophic nonunion model of Brownlow *et al.* (2001) and Makino *et al.* (2005). For every strategy, the temporal evolution (days post fracture) of the tissue fractions in the callus (graph) as well as the final bone matrix density [$\times$ 0.1 g/ml] (greyscale plot) are shown. (a) administration of mesenchymal stem cells, osteogenic and vascular growth factors (at the boundaries) at PFD 20. (b) administration of MSC (into the callus area) and osteogenic and vascular GF (at the boundaries) at PFD 20. (c) administration of MSC, osteogenic and vascular GF (into the callus area) at PFD 20. (d) administration of mesenchymal stem cells at fracture initiation. (e) administration of MSC (in a lower concentration than for (d)) at fracture initiation. (f) enhancement of the MSC's proliferation rate in response to the application of a GF administered at fracture initiation.

Standardised rodent fracture model

Comparison with the experimental results obtained by Harrison *et al.* (2003), shows a good agreement between the theoretically predicted and experimentally observed changes in the distribution of different tissues in the callus. Similar to the experimental observations, the transitions between the different tissue types were predicted to initiate first in the periosteal callus, followed by the endosteal callus and the intercortical callus. As to the latter zone, the transitions occur very rapidly. Compared to the results presented in the previous chapter, more realistic healing patterns were observed, due to the addition of angiogenesis and directed cell migration, as will be elaborated on in the next section. Furthermore, contrarily to the results obtained with the model of Bailón-Plaza and van der Meulen (2001), a quantitative comparison with the experimental observations of all the experimentally measured tissue fractions in the callus (bone, cartilage and fibrous tissue) was possible, due to the addition of fibroblasts and fibrous tissue as separate variables to the model.

In the experiments, hardly any cartilage was observed in the endosteal zone. This was opposed to the model's predictions, although the amount of cartilage predicted to form in this zone was substantially lower, compared to the other callus regions. Most of the mesenchymal stem cells present in the endosteal zone originate from the bone marrow. Bone marrow derived cells have been shown to differentiate towards osteoblasts during fracture healing (Taguchi *et al.*, 2005). This preference of the precursor cells was not captured by the model. A possible way to achieve this in the model would be to add a boundary condition for the osteogenic growth factors in the marrow cavity. When doing so, a substantial decrease in the amount of cartilage was encountered in the endosteal callus, with a maximum endosteal cartilage fraction of 5 % (Figure 5.11). Additionally, this caused a slowdown of the ossification process in the endosteal callus area.

Another discrepancy between the experimental observations and the model's predictions is the time frame. Whereas it takes 5 weeks in the experiments to establish successful healing, the model predicts a fully ossified callus after 4 weeks already. This however is an improvement compared to the model of Bailón-Plaza and van der Meulen (2001) which predicts full callus ossification in less than 20 days. There are several explanations for the observed discrepancy in the absolute timing of the healing events. One reason is that the model does not capture the maturation of the cell and the time that elapses between the differentiation of mesenchymal stem cell towards osteoblast and the production of extracellular matrix by the matured osteoblast (Bruder and Scaduto, 2005). Another reason is the fact that the parameter

values have been derived based on both *in vivo* and *in vitro* experiments on different animal models and cell lines reported in the literature, or have been estimated when no information was available. As the relative order of the events is correct, alteration of all time-dependent parameter values would suffice to change the absolute time frame of the simulated healing period to that of the experiments (Bailón-Plaza and van der Meulen, 2003).

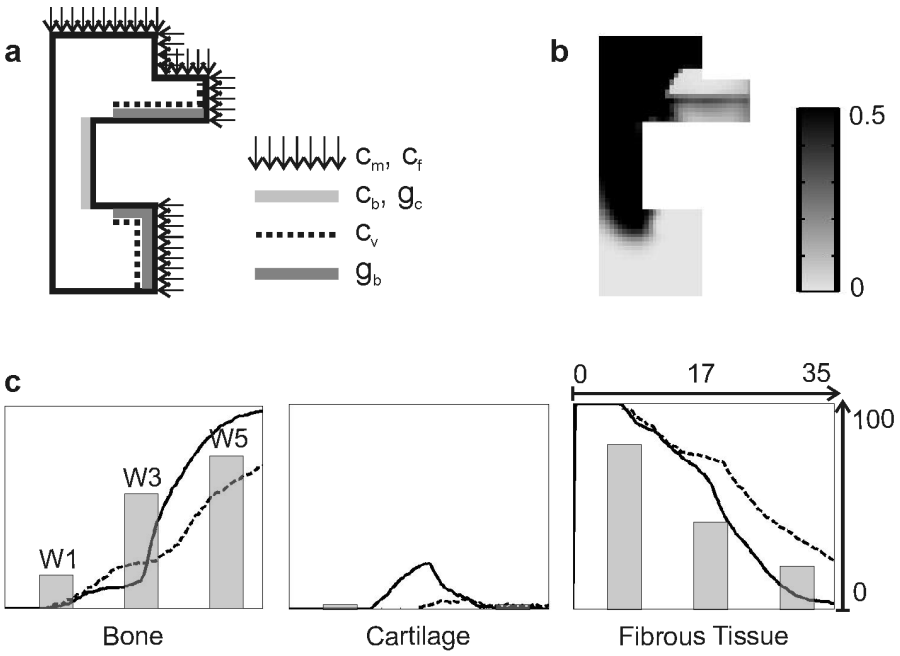


Figure 5.11: Cartilage formation in the endosteal callus. (a) boundary conditions. (b) cartilage density [× 0.1 g/ml] at 23 days after fracture, i.e. when the cartilage fraction in the callus reaches its maximal value. (c) temporal evolution (days post fracture) of tissue fractions in endosteal callus for simulations with the boundary conditions shown in Figure 5.2 (continuous line) and with additional boundary condition for the osteogenic growth factor (dashed line).

5.5.2 Sensitivity analyses

Fibroblasts and fibrous tissue

Sensitivity analyses indicated robustness of the model's predictions for small changes in the parameter values related to the description of fibroblasts and

fibrous tissue formation. Larger changes (> 1000 % or < 10 % of the original value) that lead to substantial increases in the fibrous tissue density, influence the speed of the healing process and the location of the bony bridging. Rapid formation of soft tissue matrix inhibits endothelial cell proliferation and migration into the callus, resulting in delayed ossification at that location. An example was given, showing different distributions of the initial fibrous tissue density, resulting in different healing patterns. However, due to lack of experimental data concerning the spatial distribution of the fibrous tissue density, all of the analyses reported in this chapter were carried out with a constant initial fibrous tissue density, as discussed in section 5.3.3.

The numerically observed inhibition of cell migration due to increased soft tissue matrix density is not corroborated by experimental observations. Migration of (endothelial) cells depends both on chemical (e.g. matrix ligand and cell integrin receptor levels) and mechanical (e.g. stiffness of the substrate) cues from the environment (Zaman *et al.*, 2006). Moreover, cell migration often depends on the proteolytic activity from broad-spectrum matrix metalloproteinase (MMP) (Zaman *et al.*, 2006) to clear a path through the existing matrix. Incorporation of these MMP's as additional variable in the model, could further enhance the model's description of cell migration.

Endothelial cell migration

The addition of angiogenesis and directed motion of cells to the model of Bailón-Plaza and van der Meulen (2001) resulted in more realistic healing patterns. Directed motion of endothelial cells is essential to derive the correct pattern of endothelial cell distribution throughout the callus. As observed in Figure 5.6, in the absence of directed motion, endothelial cells spread throughout the entire callus. Although the time scale corresponds to that of the standardised fracture set-up (Figure 5.7), the spatial evolution of the tissue fractions (e.g. location of callus bridging) and the endothelial cells (e.g. alignment at ossification front) in the callus does not (Figures 5.6 and 5.12). Chemotaxis alone causes a fast endochondral ossification in response to the vascular growth factors, produced by the chondrocytes, with a wide spread ossification front moving from the periosteal callus towards the endosteal callus. Haptotaxis is responsible for the alignment of the endothelial cells in the zone between the degrading cartilage and the newly formed bone, as experimentally observed (Maes, 2004) (Figure 5.12). This alignment causes an ossification front that moves, perpendicular to the cortex, from the distal callus areas towards the centre, similar to the experimental findings (Harrison *et al.*, 2003; Maes, 2004). These results are an improvement of the results obtained with the model of Bailón-Plaza and van der Meulen (2001) for a comparable experimental setting (Geris *et al.*, 2006). With the latter model, periosteal

bridging of the callus was achieved through an ossification front parallel to the cortex, which moved inwards from the external edges of the callus.

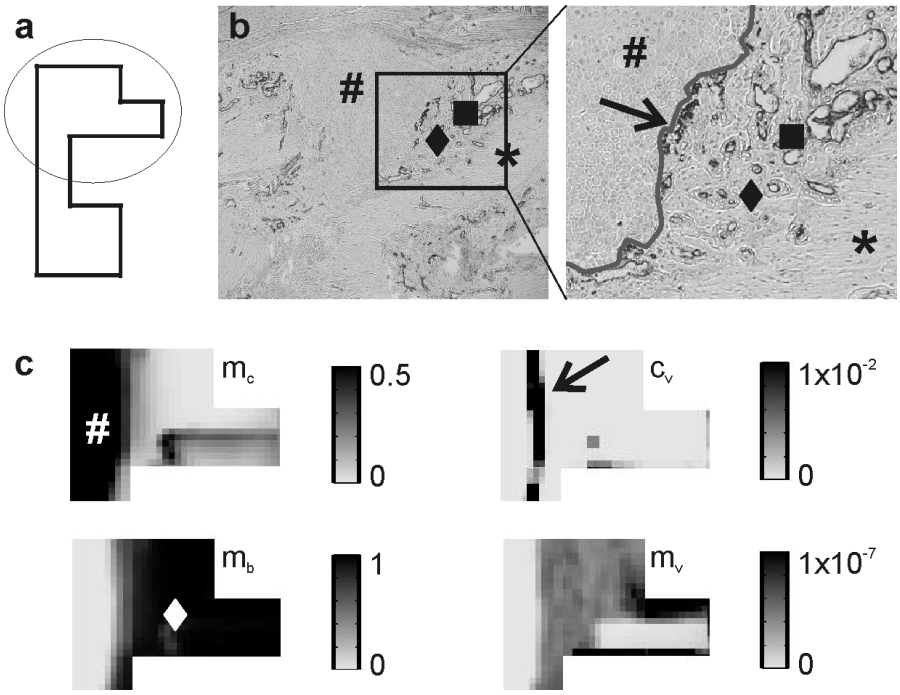


Figure 5.12: The invasion of cartilage by endothelial cells during endochondral ossification. (a) schematic indication of region of interest. (b) histological results at PFD 8 for vascularisation (CD31 staining). The endothelial cells are dark. (c) simulation results at PFD 22 showing the bone (bottom left), cartilage (top left) and vascular (bottom right) matrix density [$\times$ 0.1 g/ml] and the concentration of endothelial cells [$\times$ 10^6 cells/ml] (top right) during the endochondral ossification process. m_c: cartilage matrix; m_b: bone matrix; m_v and square: vascularisation; c_v: endothelial cells; #: soft tissue; asterisk: old cortical bone fragment; diamond: new bone.

VEGF consumption

As chemotaxis is an essential part of the cell's migratory mechanism, the presence of a chemical gradient is needed for the good progression of fracture healing. Consumption of the vascular growth factor by endothelial cells ensures the maintenance of this gradient, guiding the endothelial cells towards

the source of the vascular growth factor production (i.e. the hypertrophic chondrocytes). A decrease in the consumption rate of vascular growth factor by endothelial cells (10 % of reference value of $\tilde{d}_{gvc}$) insufficiently reduces the concentration of vascular growth factors at the location of the endothelial cells, leading to a loss of the directional cue that guides them. Endothelial cell migration is disturbed (Nagy and Senger, 2006), leading to a disturbance in the angiogenic and hence endochondral ossification process. As the concentration of chondrocytes producing vascular growth factor is lower in the endosteal callus, endothelial cell migration in this region is less disturbed. Endochondral ossification starts up in the endosteal callus followed by bony bridging in that region.

5.5.3 Simplifications

Influence of mechanics

The influence of mechanical loading has not been incorporated yet in the current model. However, several cellular processes are known to depend on the experienced mechanical stimuli. Cell migration (Michaeli *et al.*, 1994), cell proliferation (Kaspar *et al.*, 2000), cell differentiation (Jagodzinski *et al.*, 2004), matrix synthesis (Bancroft *et al.*, 2002) and growth factor production (Sakai *et al.*, 1998; Pufe *et al.*, 2005) have been shown to be influenced by mechanical loading (a detailed overview will be presented in section 6.1.3 on page 133). Furthermore, recent data suggests that mechanical loading interferes with angiogenesis, rendering this interaction one of the key regulators for successful bone formation during distraction osteogenesis and fracture healing (Amir *et al.*, 2006; Fang *et al.*, 2005; Lienau *et al.*, 2005). Too high mechanical loads inhibit the formation of a vascular network, thereby inhibiting bone formation to occur. The incorporation of the mechanical aspect of fracture healing into the model is the next obvious extension of the model and the subject of chapter 6.

Activation states

As already mentioned in section 5.3.1, endothelial cell activation states were not explicitly addressed in this model. Endothelial cells can generally be divided according to two activation states, the active and the quiescent state. At the early stage of the angiogenic process, active endothelial cells are able to migrate and proliferate. Later on, they organise into blood vessel structures and become quiescent. When fractures occur, the quiescent endothelial cells can revert back to their active state as their organised matrix is disrupted (Lee and Gotlieb, 1999).

Similar to the lack of activation states, the differentiation from one cell type to another was not modelled to go through any transitory state. For example, osteogenic differentiation of mesenchymal stem cells passes through many intermediate states: osteoprogenitor, pre-osteoblast, transitory osteoblasts, secretory osteoblasts and the final state of maturation, the osteocyte (Bruder and Scaduto, 2005). All of these intermediate cell states have their specific functions. While in the model, osteoblasts are able to migrate, proliferate, produce matrix and express growth factors at the same time, in reality, all these functions are performed by different osteoblast intermediates. For chondrocytes, a distinction was made between the normal chondrocyte and its terminally differentiated state, the hypertrophic chondrocyte, by means of the cartilage matrix density. Activation states and differentiation intermediates could be included in the model by either extending the model framework to include new variables for every state (leading to a huge number of variables), or to include for each cell type a discrete value, indicating its activation or differentiation state.

Other aspects

Other important aspects of fracture healing which could be added to the model in the future include the role of oxygen gradients and oxygen concentration (Glowacki, 1998; Cramer *et al.*, 2004), the role of matrix metalloproteinases (Colnot *et al.*, 2003; Ortega *et al.*, 2004; Henle *et al.*, 2005) and the interaction between the different growth factors (Peng *et al.*, 2002).

5.5.4 Applications in pathological fracture healing

Impaired angiogenesis

Different pathological conditions due to impaired angiogenesis, as reported in literature were tested on the model. Depending on the level of reduction of the vascular growth factor production by hypertrophic chondrocytes, delayed healing and even non-healing was predicted (Figure 5.8a,b). Street *et al.* (2002) observed a decreased angiogenesis and bone formation when they inhibited VEGF activity in a mouse model of secondary fracture healing. Experiments using placental derived growth factor (PlGF) knock-out mice (PlGF is a VEGF homologue), show a persistent cartilaginous matrix and no sign of endochondral ossification (Maes *et al.*, 2006). Using these knock-out mice, the authors also observed a significant decrease in the amount of other vascular growth factors (e.g. VEGF) available at the beginning of the healing process, after the inflammation phase. This experimental situation was modelled by taking the initial concentration of vascular growth factor equal to zero. It resulted, similar to the experimental observations, in a persistent cartilaginous

matrix, with only a small amount of intramembranous bone, formed close to the cortex.

Atrophic nonunion

Pathological healing and therapy Pathological situations, unrelated to problems with the angiogenic process were also simulated with the model. Applying the extended bioregulatory model to the atrophic nonunion model of Brownlow *et al.* (2001, 2002) and Makino *et al.* (2005), the model was able to capture the essential aspects of the experimental model: a lack of cartilage and bone development due to the absence of mesenchymal stem cells and complete vascularisation of the interfragmentary tissue eight weeks after fracture as shown in Figure 5.9.

Different treatment strategies were simulated to reestablish the healing response. Immediate application of mesenchymal stem cells at fracture initiation allowed for a normal fracture healing process if a sufficient initial cell concentration was present. Application of mesenchymal stem cells together with osteogenic and vascular growth factors to the boundaries of the callus area, after establishment of the nonunion (PFD 20), was able to initiate a healing response. The application to the boundaries of the callus was modelled to simulate the release from a carrier, containing cells and growth factors, that was placed (injected) close to the callus area (cf. page 73). However, the healing response for this strategy was limited by the mesenchymal stem cells' and growth factors' ability to penetrate the callus tissue. Applying the mesenchymal stem cells directly in the callus area (injection into the callus) allowed for a renewed healing response in the entire callus area. Injection of only the mesenchymal stem cells directly into the callus area, at the same time keeping the growth factors at the boundary, resulted in a delayed healing response, starting again at the boundaries of the callus area, as the mesenchymal stem cells migrated towards the boundaries in response to the growth factor gradient.

Makino *et al.* (2005) demonstrated the prevention of atrophic nonunion development in the challenged fracture set-up, by the immediate application of rhBMP-7 (tested in a single dosage). BMP's are able (amongst others) to promote both proliferation of progenitor cells and differentiation of mesenchymal stem cells towards osteoblasts (Peng *et al.*, 2004; Luo *et al.*, 2004; Luu *et al.*, 2007). As cellular proliferation is not growth factor dependent in this model, the proliferation rate was enlarged ($\tilde{A}_{m0} \times 10$) to test its influence on the simulation outcome. The applied increase in mesenchymal stem cell proliferation was able to sufficiently enlarge the available pool of mesenchymal stem

cells for normal fracture healing to occur. Similar to the experimental observation, successful healing was obtained four weeks after fracture. Addition of the growth factor dependency of cell proliferation to the model would allow to test additional aspects of various growth factor related treatment strategies.

Osteoblast differentiation As mentioned above, only the addition of mesenchymal cells together with both osteogenic and vascular growth factors was able to recapitulate the healing response as, in the mathematical model, osteoblastic differentiation from mesenchymal stem cells depends both on the presence of osteogenic and vascular growth factors at the same time (section 5.3.1). *In vitro* experiments have shown osteoblastic differentiation to be solely influenced by osteogenic growth factors (Thies *et al.*, 1992; Ahrens *et al.*, 1993; Rickard *et al.*, 1994). However, *in vivo*, vascular invasion is a prerequisite for endochondral bone formation and fracture healing (Bolander, 1992). Angiogenesis related factors may therefore affect osteoblast function or differentiation and vice versa (Guenther *et al.*, 1986; Sato and Rifkin, 1988; Villenueva and Nimni, 1997; Kasperk *et al.*, 1997; Deckers *et al.*, 2000). Osteoblasts are also able to produce paracrine factors that influence endothelial cell function (Folkman and Shing, 1992; Fiorelli *et al.*, 1994). In this cross-talk between endothelial cells and osteoblasts, vascular endothelial growth factor (VEGF), which acts as an angiogenic factor, may play an important role (Wang *et al.*, 1997; Gerber *et al.*, 1999). Clearly, there is still room for further investigation into the mechanisms behind the osteoblastic differentiation. In future research, the expressions for the differentiation of mesenchymal stem cells will be revised.

Experimental corroboration Experiments investigating various treatment strategies for this type of atrophic nonunions are underway (Prof. Keita Ito, personal communication). As the applied concentrations of mesenchymal stem cells and growth factors are quantified in the model, experiments can be designed mimicking the simulated therapies. Information from these experiments on growth factor concentrations and spatial distribution, and on the spatiotemporal evolution of the cells and tissue fractions in the callus, will allow for a comparison between experimental observations and numerical predictions on a qualitative as well as on a quantitative level. Furthermore, this information will facilitate a thorough assessment of the model's potential in designing treatment strategies.

5.6 Conclusion

The main goals for this chapter were (1) the development of an enhanced bioregulatory model and (2) the investigation of possible causes and treat-

ment strategies of pathological fracture healing. An enhanced bioregulatory model, incorporating a number of the bone regeneration key features such as intramembranous and endochondral ossification, angiogenesis and cell migration has been established and its results have been successfully corroborated by comparison with experimental data. A good qualitative agreement between the experimentally observed and numerically predicted results has been demonstrated together with an enhanced quantitative agreement compared to the previous existing mathematical models discussed in chapter 4. Furthermore, due to the presence of angiogenesis, this model has exhibited augmented potential for the investigation of pathological regeneration cases . The sensitivity analysis shows a relative robustness of the model's predictions for small changes in the parameters related to the evolution in fibroblasts/fibrous tissue, angiogenesis and cell migration. Larger changes in these parameters influence the speed of the healing process and the location of bridging. This demonstrates the need for additional experimental data to evaluate these parameters and points at the same time to possible pathologies. Cases of pathological fracture healing due to impaired angiogenesis have been simulated, corresponding to experimental studies reported in literature. The predicted results are similar to the experimental observations. Furthermore, the model's potential therapeutic value has been tested on an atrophic nonunion model. Several experimentally testable treatment strategies, involving the application of mesenchymal stem cells and growth factors at different stages in the healing process, have been simulated, predicting a (dose-dependent) resumption of the healing process.
In the course of the simulations a number of potential improvements to the model have been identified that would further enhance the model's capabilities in simulating pathological healing and treatment strategies. One of these improvements, the incorporation of the influence of mechanical loading on the healing process, is treated in the next chapter.

Chapter 6

Combining mechanoregulatory and bioregulatory models: application in an *in vivo* bone chamber and in fracture healing

To conclude the research presented in this thesis, a combination was made of the mechanoregulatory principles presented in chapter 3 and the novel bioregulatory model elaborated in the previous chapter. The introduction to this chapter describes the State of the Art of experimental research on the influence of mechanical loading on fracture healing and oral implant osseointegration in general and on cellular behaviour in particular. The research hypothesis underlying the work presented in this chapter and the different objectives that were formulated, are stated in section 6.2. Section 6.3 describes the combined mechanobioregulatory model and its numerical implementation. Applications of this model to simulate bone regeneration in the *in vivo* bone chamber and semi-stabilised murine fracture set-up are shown and discussed in sections 6.4 and 6.5 respectively. The last section summarises the most important conclusions of the study reported in this chapter and gives suggestions for further development of the coupled mechanobioregulatory model.

6.1 Introduction

6.1.1 Mechanical loading and fracture healing

This sections discusses the influence of mechanical loading on the fracture healing process. Different aspects of mechanical loading are highlighted and discussed.

Mechanical stability

As discussed in section 1.3 (page 4), under optimal circumstances, including an anatomical restoration of the fractured bone, a fracture heals without the formation of a callus in a process called primary healing. Under less optimal circumstances, secondary fracture healing takes place, the first steps constituting inflammation and the formation of a fracture callus. The initial phase of fracture healing was shown to be specifically sensitive to the mechanical conditions (Klein *et al.*, 2003; Miclau *et al.*, 2000; Schell *et al.*, 2005; Lienau *et al.*, 2005, 2006). Comparing the callus for different fracture fixation stabilities, differences were observed both morphologically and in the rate of callus development. Even though the less rigid fixation did not always result in delayed healing, a less optimal healing path was always taken to achieve healing (Schell *et al.*, 2005). This includes a reduced initial vascularisation (Lienau *et al.*, 2005, 2006) and a strongly increased callus volume (Klein *et al.*, 2003).

After the formation of the soft callus, mesenchymal stem cells start differentiating towards chondrocytes or osteoblasts, guided by the biochemical (Einhorn, 1998) and mechanical (Goodship and Kenwright, 1985; Kenwright and Gardner, 1998; Le *et al.*, 2001; Thompson *et al.*, 2002) cues they perceive. During endochondral ossification, the mechanical environment influences the amount of cartilage formation and the speed of the healing response. By stabilising the bone fragments with respect to each other (e.g. through the use of external fixation), the interfragmentary movement is reduced as well as the amount of cartilage formed in the callus (Kenwright *et al.*, 1991; Goodship and Kenwright, 1985; Le *et al.*, 2001; Thompson *et al.*, 2002; Claes *et al.*, 2002; Schell *et al.*, 2005).

Since Rhinelander (1974) demonstrated that different patterns of fracture vascularisation arise under stable versus unstable fixation conditions, it has become well-accepted that mechanical instability in the fracture healing zone leads to an inhibition of vascularisation and formation of excessive fibrocartilage, causing a delayed healing response (Carter *et al.*, 1998; Claes,

1998; Miclau *et al.*, 2000; Lienau *et al.*, 2005). The effects of different axial movements, fracture gap sizes (Claes *et al.*, 2002) and fixation stabilities (Lienau *et al.*, 2005) on tissue differentiation and vascularisation were quantified. Different mechanisms were proposed that cause tissue avascularity under high interfragmentary movement. Based on purely mechanical arguments, newly formed vessels could rupture under high tissue strains or collapse under high hydrostatic pressure (Carter *et al.*, 1998). Looking at the biology, avascularisation could be caused by an imbalance in the upregulation of genes coding for angiogenic and anti-angiogenic proteins. Miclau *et al.* (2000) showed a clear influence of the fixation on the expression of angiogenic genes in mesenchymal stem cells at the fracture site. Similarly, mechanically induced upregulation of anti-angiogenic genes was also suggested to develop and maintain avascular zones in tendons (Pufe *et al.*, 2003, 2005).

Interfragmentary movement

The interfragmentary movement is composed of axial and shear components as a consequence of the combined axial and torsional movement of the bone fragments. These different components were studied separately in literature. Controlled axial micromovement was shown to enhance fracture healing (shorter average healing times) in comparison with rigid fixation (Goodship and Kenwright, 1985; Kenwright *et al.*, 1991; Kenwright and Gardner, 1998). Bending of the fracture site allows to distinguish between compression and tension load and a greater amount of new bone formation at the compressive side of the fracture callus was observed (Henté *et al.*, 2004). These results were contradicted by another study (Smith-Adaline *et al.*, 2004) where finite element models were used to assess the magnitude and spatial distribution of strains within the fracture gap. Results from that study suggested that tensile strains suppressed chondrogenesis during the mechanical stimulation period. After stimulation ended, however, increased chondrogenesis was observed in the zones were tensile strains were present during stimulation (the authors hypothesised this could be through a strain induced increase in the pool of mesenchymal precursor cells) followed by rapid bone formation. In contrast, in areas providing a compressive environment during stimulation, bone was formed primarily via intramembranous ossification. The results of this study are in disagreement with most aspects of the mechanoregulatory models discussed in section 3.1.1 on page 16.

Shear interfragmentary movement was demonstrated to adversely effect, delay or even impede fracture healing (Loboa *et al.*, 2001; Augat *et al.*, 2003) as well as to enhance it (Park *et al.*, 1998; Bishop *et al.*, 2006). A possible explanation for this contradiction could be found in the differences in local

mechanical conditions e.g. translational vs. torsional shear set-ups or differences in loading magnitude, resulting in differences in callus makeup and tissue formation (Bishop *et al.*, 2003, 2006). Mechanical models have shown that translational shear leads to regions of compressive pressure in oblique fractures (Pauwels, 1960; Loboa *et al.*, 2001) which were proposed to stimulate cartilage formation. Pure torsion theoretically leads to no local pressure generation and therefore no cartilage stimulation.

Magnitude and timing of the stimulus

The optimal magnitude of the mechanical stimulus to enhance the healing process was quantified in several animal models (Claes *et al.*, 1997; Wolf *et al.*, 1998; Schell *et al.*, 2005). As it was observed that applying mechanical stimuli with higher strain rates could trigger enhanced osteogenic responses in intact bone (O'Connor and Lanyon, 1982) and limit the loss of bone mass in osteoporotic bone (Smith *et al.*, 1989), the effect of strain rate in fracture healing was investigated (Goodship *et al.*, 1998). The application of a short term interfragmentary cyclic micromovement applied at a high strain rate ($\geq$ 40 mm/s) at the beginning of the healing process, induced a greater amount of periosteal callus than the same stimulus applied at a low strain rate (2 mm/s). Applying the high strain rate stimulus at a later stage in the healing process, inhibited healing. Several other studies confirm the beneficial effect of immediate or early mechanical intervention (Chao *et al.*, 1998; Miclau *et al.*, 2002, 2004) whilst other demonstrate the need for a short delay between fracture and application of loading (Wallace *et al.*, 1994; Claes *et al.*, 2002; Gardner *et al.*, 2006). An adequate description and comparison of the biological and mechanical environment for the different experimental set-ups might help to interpret these apparently contradictory results. In any case, it was shown that both the magnitude and the rate of the stimulus as well as the time postfracture the stimulus is initiated have an effect on the healing process.

Fracture geometry

Not only the movement in the fracture is important, also its geometry. One of these geometrical aspects is the gap size which, together with other mechanical conditions, determines the strain experienced by the developing tissue in the fracture area. Claes *et al.* (1997) and Augat *et al.* (1998) compared the influence of different gap sizes (1, 2 and 6 mm) and interfragmentary strain magnitudes (7 and 31 %) in a sheep osteotomy model. They concluded that larger interfragmentary movements and strains stimulated larger callus formation for small gaps but not for larger gaps. Inferior healing resulting in a significant reduction in the bending stiffness of the healed bones was ob-

served for larger gap sizes, independent of the interfragmentary movement magnitude. Harrison *et al.* (2003) compared different osteotomy gap sizes in mice (0.5 and 3 mm) under comparable mechanical environments imposed through external fixation. For smallest gap size, normal fracture healing was observed with a restoration of the torsional strength to that of intact bone by 9 weeks postoperatively. However, by increasing the osteotomy gap size, the pattern and progression of the repair process were very different. A consistent pattern of atrophic fibrous pseudarthrosis was seen. The fragment ends remodelled to form an osseous cap over the medullary cavities with rounding of the fragment ends and a joint between the fragment ends of fibrous connective tissue. This was an established pattern and could be described as a syndesmosis (formation of a fibrous joint).

Conclusion

The influence of all of the above described aspects of mechanical loading on fracture healing boils down to an alteration of the local mechanical environment of the regenerating tissues and cells. The expression of this alteration in terms of geometry, stability or stimulus type and magnitude is mainly made by clinicians. However, the quantification of the local mechanical environment is indispensable to gain further insight into the role of mechanical loading in fracture healing.

6.1.2 Mechanical loading and oral implant osseointegration

As discussed in the first chapter of this work (section 1.3.1 on page 6), it is no longer believed that immediate loading of implants per se leads to fibrous encapsulation of the implants and consequently, failure of the osseointegration process. Many studies showed good results for immediately loaded implants. However, excessive implant displacement, ranging from 150 μm to 500 μm, was shown to inhibit successful osseointegration of the implants (Søballe *et al.*, 1992b; Søballe, 1993; Pilliar *et al.*, 1986). The exact threshold is different for every situation and depends on the implant's design and surface state. Additional factors such as initial stability, host bone quality, occlusal forces and splinting are also important (reviewed by Szmukler-Moncler *et al.* (1998), Gapski *et al.* (2003) and Nkenke and Fenner (2006)). Care must be taken in comparing different experimental results to each other, as most of the aforementioned factors are highly variable between different studies (Hobkirk *et al.*, 2006).

Implant design

The most commonly used implant designs are screws and cylinders. In general, screw-shaped implants develop higher mechanical retention as well as a greater ability to transfer compressive forces (Skalak, 1985; Wolfe and Hobkirk, 1989; Lefkove and Beals, 1990; Randow *et al.*, 1999). They minimise micromotion of the implant and improve the initial stability, both requirements for successful immediate loading. Additionally, the thread increases the surface area which accounts for a further reduction of the peri-implant stresses, improving osseointegration and reducing crestal bone loss (Misch, 1999). Despite its lower initial stability and mechanical retention properties, favourable clinical results were reported for cylindrical implants when a delayed loading regime was used (Wheeler, 1996).

Apart from the geometrical design, experimental and clinical studies showed that the surface coating plays an important role in timing (Kirsch and Donath, 1984), amount of integration (Buser *et al.*, 1991) and micromotion tolerance (Szmukler-Moncler *et al.*, 1996; Søballe *et al.*, 1992b; Søballe, 1993). Contrarily, other studies observed no significant influence of the surface roughness on the survival rate of immediately loaded implants (Evans *et al.*, 1996; Corso *et al.*, 1999).

Finally, implant length may also influence the outcome of immediate implant loading. However, no consensus is reached yet on the critical length and diameter of immediately loaded implants (Schnitman *et al.*, 1997; Buser *et al.*, 1988; Lefkove and Beals, 1990; Chiapasco *et al.*, 1997).

Loading-related factors

As already indicated above, primary stability of the immediately loaded implant seems to be the key factor in determining the outcome of the osseointegration process. If an implant is placed in soft spongy bone with poor initial stability, often a connective tissue encapsulation is formed, similar to the pseudarthrosis observed in unstabilised fractures (Brunski *et al.*, 1979; Schroeder *et al.*, 1981; Hansson *et al.*, 1983; Spector, 1988; Albrektsson and Sennerby, 1991; Aspenberg *et al.*, 1992; Roberts, 1993; Szmukler-Moncler *et al.*, 1998).

Consensus exists that immediate occlusal loading of dental implants is possible (Aparicio *et al.*, 2003; Cochran *et al.*, 2004; Misch *et al.*, 2004). However, controlling the functional forces is essential for successful osseointegration. Vertical forces applied during function are less detrimental for implant stability than oblique or horizontal forces. Therefore, bruxism (grinding and/or

clenching) is considered as a possible contraindication for immediate implant loading (Balshi and Wolfinger, 1997; Jaffin *et al.*, 2000; Colomina, 2001).

Primary stability of the implant can be enhanced by splinting. Various modes of splinting were introduced (Hashimoto *et al.*, 1988; Sagara *et al.*, 1993; Akagawa *et al.*, 1993; Nikellis *et al.*, 2004; van Steenberghe *et al.*, 2004), all showing favourable results. Splinting seems to allow the implants to withstand early functional loading and keeps micromotion below the critical threshold (Szmukler-Moncler *et al.*, 1998).

Conclusion

As discussed at the end of section 6.1.1, the influence of all of the above described aspects of mechanical loading on implant osseointegration boils down to an alteration of the local mechanical environment of the regenerating tissues and cells. The expression of this alteration in terms of implant design and initial stability is mainly made by clinicians to compare various treatment strategies. Again, as mentioned earlier, the quantification of the local mechanical environment could provide further insight into the effectiveness of the different treatment strategies.

6.1.3 Mechanical loading and cells

This section describes different experiments undertaken to assess the influence of mechanical load on individual cells and their behaviour. The description is divided according to the biological entity under investigation: mesenchymal stem cells, osteoblasts, chondrocytes and endothelial cells.

Mesenchymal stem cells and osteoblasts

Markers The influence of mechanical loading on bone cells and mesenchymal stem cells is monitored through the measurement of gene upregulation, collagen production and the presence of signaling molecules. Ca^{2+}, cAMP and NO are second messengers transducing extracellular signals to the cell interior and hence are important signaling molecules that are often measured to determine the immediate cell response to stimuli. Prostaglandin E_2 (PGE2) is an important mediator in the regulation of bone metabolism. Alkaline phosphatase (ALP) activity is measured to precede bone matrix mineralisation and is used to assess osteoblast activity. Additionally, ALP is a marker of the various stages of osteoblast differentiation (from mesenchymal stem cells into osteoblasts). Mesenchymal stem cell differentiation to osteoblasts is often studied by measuring the mRNA levels of osteoblast

marker genes such as core binding factor 1 (Cbfa1 - transcriptional activator of osteoblast differentiation), osteopontin (OP - non-collagenous protein promoting osteoblast attachment and migration), osteocalcin (OSTC - non-collagenous protein upregulated at the onset of mineralisation), collagen type I (Col - collagen is the most abundant extracellular protein in connective tissues such as bone, cartilage and fibrous tissue) (Frank *et al.*, 2002; Jacobs *et al.*, 1998; Jaiswal *et al.*, 1997; Mizuno and Kuboki, 2001; Pittenger *et al.*, 1999; Plant and Tobias, 2001; Yang and Karsenty, 2002; Zhang *et al.*, 1995). All of the studies mentioned in the following paragraphs measured one or several of the aforementioned markers.

Fluid flow induced shear Many studies investigated the effect of various types of fluid flow (steady, pulsatile and oscillatory) on osteoblasts (Owan *et al.*, 1997; Jacobs *et al.*, 1998; You *et al.*, 2000; Donahue *et al.*, 2003a,b; Bacabac *et al.*, 2004; Batra *et al.*, 2005; Mullender *et al.*, 2006; Vezeridis *et al.*, 2006; Kamioka *et al.*, 2006; Ponik *et al.*, 2007), osteocytes (Vezeridis *et al.*, 2006; Kamioka *et al.*, 2006; Ponik *et al.*, 2007) and mesenchymal stem cells (Li *et al.*, 2004; Kreke *et al.*, 2005; Knippenberg *et al.*, 2005) in parallel plate flow chambers. Fluid flow induced shear stress was shown in this experimental set-up to stimulate the production of numerous intracellular and extracellular signaling molecules in the cells, indicating enhanced proliferation and differentiation. 3D perfusion flow systems showed a positive effect of fluid flow on the osteogenic differentiation of mesenchymal stem cells and on osteoblast matrix production and mineralisation (Bancroft *et al.*, 2002; Holtorf *et al.*, 2005; Datta *et al.*, 2006). Both 2D and 3D studies confirmed the dominant effect of fluid flow induced shear strain over substrate strain in the cells' response to mechanical loading (Owan *et al.*, 1997; Smalt *et al.*, 1997; Tanaka *et al.*, 2005).

Tensile and compressive strain Osteoblasts cyclically strained showed increased osteoblast proliferation and type I collagen propeptide production, accompanied by a decreased level of ALP activity and OSTC release (Kaspar *et al.*, 2000). Although cyclic strain was observed to permit early aspects of osteoblast activation, it was also observed to delay in part later biochemical parameters associated with mineralisation (Knoll *et al.*, 2005). Osteoblastic precursors seeded in a 3D type I collagen gel subjected to uniaxial cyclic strain showed enhanced proliferation and osteoblast differentiation (Ignatius *et al.*, 2005).
Cyclical mechanical stimulation of mesenchymal stem cells (8% strain) increases ALP and OSTC levels and upregulates Col I and III synthesis and Cbfa1 expression, all of which are signs of osteoblast differentiation (Jagodzinski *et al.*, 2004). However, differentiation of mesenchymal stem cells

along a chondrogenic lineage was also observed under cyclic strain conditions (10% strain) (McMahon *et al.*, 2006; Kearney *et al.*, 2006). Kurpinski *et al.* (2006) suggested that not only does mechanical strain play an important role in MSC differentiation and proliferation, but that the effects of mechanotransduction depend on the orientation of cells with respect to the strain axis strained membrane. Furthermore, a definitive influence of the substrate material (stiffness, surface characteristics, topography, surface chemistry and treatment) was observed, causing differences in cell proliferation, differentiation and migration depending on the substrate stiffness (Anselme, 2000; Ghosh *et al.*, 2007; Walboomers *et al.*, 2004).

Chondrocytes

Hydrostatic pressure Chondrocytes respond to hydrostatic pressure changes by altering their synthetic capacity depending on the type, timing and mode of pressure (Lippiello *et al.*, 1985; Parkkinen *et al.*, 1993; Lammi *et al.*, 1994; Smith *et al.*, 1996; Takano-Yamamoto *et al.*, 1991; van Kampen *et al.*, 1985; Sironen *et al.*, 2002). The expression of aggrecan increases during relatively low, intermittent pressure and decreases under more strenuous and static pressure (Parkkinen *et al.*, 1993; Hall *et al.*, 1991). Type II collagen and aggrecan (two major structural components of cartilage) mRNA expression can have different expression patterns depending on the loading profile (Smith *et al.*, 2000). Furthermore, it was reported that reduced pO_2 (oxygen pressure) and different settings of intermittent hydrostatic pressure increased the proliferation, collagen secretion and phenotype stability of chondrocytes (Hansen *et al.*, 2001). Continuous hydrostatic pressure was shown to activate genes involved in growth arrest and cellular adaptation and/or differentiation (Sironen *et al.*, 2002). Contrarily, cyclic hydrostatic pressure was also observed to downregulate the expression of matrix metalloproteinase MMP-13 and type I collagen and upregulated the expression of TIMP-1 (metalloproteinase inhibitor) indicating a slowdown of chondrocyte differentiation towards hypertrophy and a chondroprotective influence on cartilage tissue (Wong *et al.*, 2003).

Shear stress, tensile and compressive strain Shear stress was shown to influence the regulation of matrix metalloproteinases (Yokota *et al.*, 2003) and the production of NO, aggrecan and type II collagen in a dose and time dependent manner (Lee *et al.*, 2003, 2002). Cyclic strain was demonstrated to have a dose-dependent effect on chondrocyte viability and proteoglycan synthesis (Akagi *et al.*, 2006). Cyclic strain was further suggested to negatively regulate (i.e. inhibit) the terminal differentiation of chondrocytes through the signal pathway of TGFβ (Ohno *et al.*, 2005). Chondrocyte proliferation and expression of hypertrophic chondrocyte markers (Cbfa1, MMP13,

type X collagen, VEGF and connective tissue growth factor CTGF), cartilage matrix proteins, MMP's and TIMP's are all influenced by cyclic tensile strain in a dose-dependent manner (Lahiji *et al.*, 2004; Honda *et al.*, 2000; Wong *et al.*, 2003; Ohno *et al.*, 2005). 3D experimental set-ups under various loading conditions have shown dose-dependent reactions of chondrocytes in terms of proliferation, growth factor expression and matrix macromolecule production (Grad *et al.*, 2006; Maeda *et al.*, 2005; Hunter *et al.*, 2002).

Tissue level *In vivo* and *ex vivo* studies have investigated the effect of mechanical loading on cartilage development and endochondral ossification. Tagil and Aspenberg (1999) observed the differentiation of mesenchymal stem cells into chondrocytes and the formation of a cartilage layer in a bone conduction chamber under the influence of a compressive hydrostatic stress. Sundaramurthy and Mao (2006) observed the formation of a secondary ossification centre in a cartilage rabbit femoral condyle explant under cyclic loading.

Endothelial cells

In vivo The principal mechanical forces sensed by endothelial cells are the shear stress of flowing blood on their apical surface, and the circumferential stress resisting blood pressure, which induces stretch in the cell body (Tarbell and Pahakis, 2006). These two classes of mechanical stimuli were tested both *in vivo* and *in vitro* to assess their influence on endothelial cell gene expression, initiation of signaling cascades and changes in phenotype. *In vivo* experiments demonstrated increased expression of VEGF expression and endothelial cell proliferation in response to fluid flow induced shear strain (Egginton *et al.*, 2001; Rivilis *et al.*, 2002) whereas mechanical stretch was shown to induce VEGF expression, endothelial cell proliferation and VEGF-independent production of MMP-2 (Zhou *et al.*, 1998; Egginton *et al.*, 2001; Rivilis *et al.*, 2002; Shukla *et al.*, 2004).

In vitro Both 2D and 3D *in vitro* experiments have identified the distinct (dose and time dependent) influence of shear stress on the expression of growth factors such as platelet derived growth factor PDGF, fibroblast growth factor FGF, BMP and TGF-β and the expression of endothelial cell adhesion molecules (Malek and Izumo, 1995; Chen *et al.*, 2001; McCormick *et al.*, 2001; Wasserman *et al.*, 2002; Vara *et al.*, 2006). Furthermore, these experiments showed that the shear stress induced production of NO (Malek and Izumo, 1995; Coyle and Kader, 2007; Duerrschmidt *et al.*, 2006; Wessel *et al.*, 2006; Tao *et al.*, 2006; Zhang *et al.*, 2006) and MMP-9 (Chen *et al.*, 2001; Garcia-Cardena *et al.*, 2001; Wasserman *et al.*, 2002;

Sun *et al.*, 2007), the activation of endothelial cell integrins (Orr *et al.*, 2006), alignment and elongation of endothelial cell (Kadohama *et al.*, 2006) and inhibition of apoptosis were mediated by multiple mechanisms (Dimmeler *et al.*, 1997; Hermann *et al.*, 1997; Jin *et al.*, 2001; Taba *et al.*, 2003; Bongrazio *et al.*, 2006). Prolonged subjection to laminar shear stress and pulsatile flow was shown to have an inhibitory effect on the proliferation of endothelial cells whereas disturbed flow and reciprocal oscillatory flow enhanced the endothelial cells' turnover in comparison with static loading conditions (Davies *et al.*, 1986; Levesque *et al.*, 1990; Mitsumata *et al.*, 1997; Li *et al.*, 2005b). Several studies demonstrated a significant increase of endothelial cell migration by laminar shear stress in wound healing (Sprague *et al.*, 1997; Wu *et al.*, 1995), whereas disturbed flow had less effect. In summary, laminar shear stress induces the upregulation of atheroprotective genes, whereas disturbed flow upregulates pro-atherosclerotic genes (Chien *et al.*, 1998; Brooks *et al.*, 2002; Li *et al.*, 2005b).

6.1.4 Conclusion

Despite the extensive body of literature that discusses the influence of mechanical loading on various aspects of the bone regeneration process, many questions remain. Most of the above described studies investigate a single or a few magnitudes of various global mechanical stimuli, but hardly ever investigate a whole range of magnitudes of these stimuli or quantify this load at the local tissue level. Furthermore, the relation between the mechanical stimuli experienced by the cells (micro) and the load exerted on the regenerate (macro) is still largely unknown. Several mechanisms have been proposed in the literature coupling the global load on the tissue to the local load experienced by the osteocytes in healthy bone (You *et al.*, 2001). However, little information is available on this coupling in regenerating tissues.
Often apparently contradictory results are encountered as well. Several aspects of the experimental set-ups are often overlooked when comparing various studies to each other. A detailed comparison of all aspects of the experimental set-up would probably yield an explanation for the apparent contradictions, leading to a further enhancement of the knowledge on bone regeneration.
In summary, caution must be exerted in the transfer of the previously discussed experimental results to mathematical models and numerical simulations described hereafter.

6.2 Hypothesis and Objectives

6.2.1 Hypothesis

In this chapter, it is hypothesised that a combination of mechanical and biological regulators in a mathematical model of bone regeneration allows for improved predictive capabilities and simulation outcomes, compared to models regulated by either mechanical or biological factors alone. A literature survey was performed looking at the effect of mechanical loading on biological processes, both at the tissue level (in fracture healing as well as in implant osseointegration) and the cellular level. Referring back to the general conclusion drawn from that literature survey, no clear-cut answers to how mechanical loading influences the regenerative processes are provided by the experimental studies. Most of the processes involved in bone regeneration seem to depend (either directly or indirectly) on mechanical loading. A mathematical model can be used to investigate how the influence of mechanical loading on various cellular processes (proliferation, differentiation, growth factor production) affects the global regeneration process. Furthermore it can provide new insights into the regeneration process in general and the coupling between mechanics and biology in particular, e.g. by identifying the dominant stimulus type present in the regenerate or the major coupling mechanisms between mechanics and biology.
The work presented in this chapter does not aim to provide answers to the above questions nor does it aspire at proposing a 'complete' mechanobioregulatory model. It rather seeks to develop a mathematical framework that allows to investigate the role of both mechanical and biological stimuli on the regeneration process. To illustrate the potential of such coupled mathematical models, a mechanobioregulatory model was proposed, based on the novel bioregulatory model described in the previous chapter and, as a first example, with a simple coupling between the mechanics and the biology. A number of biological parameters values were made dependent on the local mechanical stimuli. This combined mechanobioregulatory model was applied to both the *in vivo* bone chamber and the semi-stabilised murine fracture model and several cases of normal and pathological bone regeneration were simulated.

6.2.2 Objectives

- The development of a combined mechanobioregulatory model (section 6.3.1).
- The implementation of the combined model (section 6.3.2).
- The simulation of peri-implant bone regeneration (sections 6.4.1 and 6.5.1)

- The simulation of normal and pathological cases of fracture healing (sections 6.4.2 and 6.5.2)

6.3 Materials and Methods

This section describes the development of the coupled mechanobioregulatory model. The model was applied to simulate bone regeneration in the *in vivo* repeated sampling bone chamber and in fracture healing. The former set-up has been described in detail in chapter 3 (section 3.3.1 on page 20). The results of bone chamber studies 2 and 3, in which different implant displacements were tested, served as a basis for comparison with the simulation results. The experimental fracture healing set-up has been described in detail in chapter 4 (section 4.3.1 on page 57). As no information on the mechanical aspects of either of the fracture healing set-ups described in chapter 4 was available, the geometry of the semi-stabilised murine fracture was used and a comparison was made between bone regeneration under normal, non-loading and overloading conditions.

6.3.1 Combined mechanobioregulatory model

As this chapter's aim is to illustrate the potential of the coupling between mechanics and biology in the current framework, rather than providing a 'complete' mechanobioregulatory model, a simple coupling was proposed in which only the proliferation rate of osteoblasts and endothelial cells varied based on a local mechanical stimulus (Figures 6.1 and 6.2). In a certain range of magnitude of the mechanical stimulus, proliferation was enhanced, whereas for stimuli outside this range, proliferation decreased (Bailón-Plaza and van der Meulen, 2003). Due to lack of dedicated experimental information, the stimulus boundaries, determining the value of the proliferation rates, were based on the previously existing models (Prendergast *et al.*, 1997), assisted by finite element calculations of the stimulus' magnitude inside the regenerating tissue.

6.3.2 Numerical implementation

Figure 6.3 shows an overview of the implementation of the coupled mechanobioregulatory bone regeneration model. At the start of the simulations, the domain (i.e. the bone chamber or the fracture callus) was assumed to be filled with a low density fibrous tissue.

The first step of the analysis was a loading step. Based on the mechanical stimuli obtained from this FE analyses, the parameters of the bioregulatory

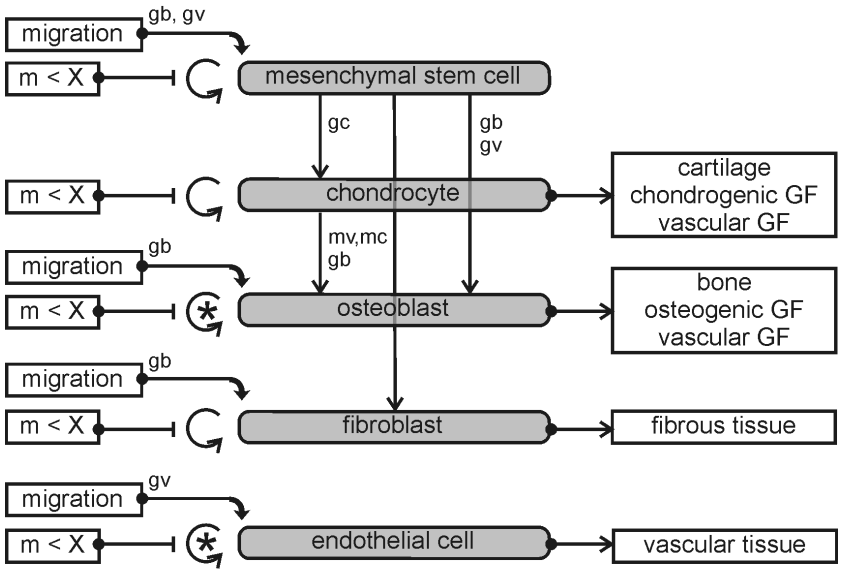


Figure 6.1: Schematic representation of the coupled mechanobioregulatory model. Asterisks indicate the processes depending on the mechanical stimuli (proliferation of osteoblasts and endothelial cells).

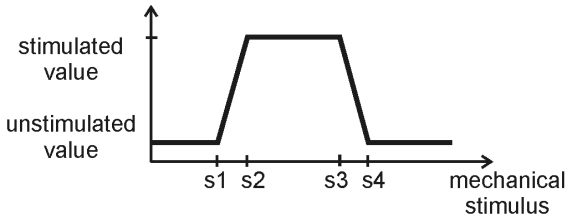


Figure 6.2: Relation between the value of the parameters from the bioregulatory model and the magnitude of the mechanical stimulus.

model were adapted according to the rules proposed in section 6.3.1. The biological analyses was allowed to run for a predefined time, depending on the regeneration process under investigation. Consequently, prior to the next loading step, the new material properties of the tissues in the domain were determined. Depending on the local bone (b), cartilage (c) and fibrous tissue (f) densities, the Young's modulus E, Poisson coefficient ν and permeability μ of each grid cell (i) in the domain were derived, using the following rules:

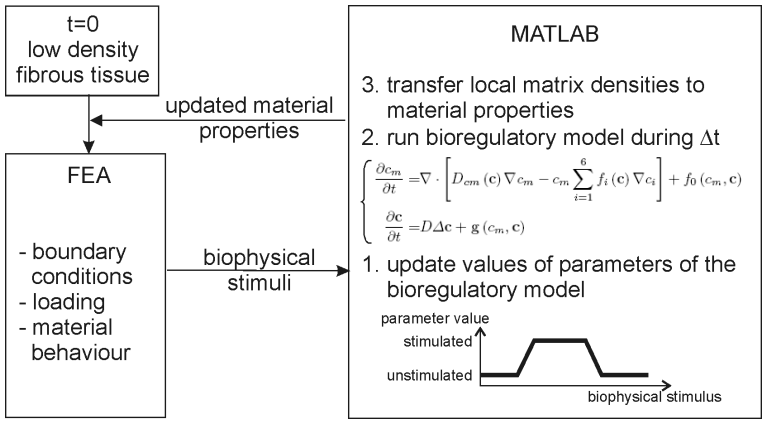


FIGURE 6.3: Overview of the implementation of the coupled mechanobioregulatory model

$$E(i) = \frac{\left(\frac{m_b(i)}{m_{b_ref}}E_b\right)m_b(i) + \left(\frac{m_c(i)}{m_{c_ref}}E_c\right)m_c(i) + \left(\frac{m_f(i)}{m_{f_ref}}E_f\right)m_f(i)}{m_b(i) + m_c(i) + m_f(i)} \quad (6.1)$$

$$\nu(i) = \frac{\nu_b m_b(i) + \nu_c m_c(i) + \nu_f m_f(i)}{m_b(i) + m_c(i) + m_f(i)} \quad (6.2)$$

$$\mu(i) = \frac{\mu_b m_b(i) + \mu_c m_c(i) + \mu_f m_f(i)}{m_b(i) + m_c(i) + m_f(i)}. \quad (6.3)$$

The reference matrix density refers to the density the tissue reaches when it is the dominant tissue type in the domain. These values were based on the simulation results obtained with the bioregulatory model (Table 6.1). All biological tissues were assigned biphasic material properties. All material properties used in the following simulations are summarised in Table 6.1.

The implementation of the coupling between the model's biology and mechanics was carried out in Matlab (The Mathworks Inc.). The implementation of the bioregulatory models was already described in section 5.3.4. Finite el-

[1]Hori and Lewis (1982)
[2]Claes and Heigele (1999)
[3]Armstrong and Mow (1982)
[4]Ochoa and Hillberry (1992)
[5]Jurvelin *et al.* (1997)

Table 6.1: Material properties used in the simulations with the coupled mechanobioregulatory model.

	Fibrous Tissue	Cartilage	New Bone	Cortical Bone	Titanium
Young's modulus $[MPa]$	1[1]	10	1000[2]	6000	110000
Permeability $[m^4(Ns)^{-1}]$	1e-14[1]	5e-15[3]	1e-13	3.7e-13[4]	-
Poisson's ratio	0.17	0.17[5]	0.3	0.3	0.3
m_{ref} [× 0.1 g/ml]	0.1	0.5	0.5	-	-

ement analyses were carried out in MSC.Marc (Version 2005r2, Palo Alto, USA), using its soil mechanics capabilities.

6.3.3 Simulation details

***In vivo* bone chamber**

For the application of the mechanobioregulatory model to the *in vivo* bone chamber, only the tissue in the inner bone chamber was considered. Figure 6.4 shows the domain used in the simulations.

The boundary conditions applied during the mechanical analyses are indicated in Figure 6.4c and correspond to those applied during the simulations with the mechanoregulatory models discussed in chapter 3. Axial loading of the implant took place in a displacement controlled manner and was simulated by imposing a displacement boundary condition on the top nodes of the implant. The chamber was modelled to be filled with a low density fibrous tissue matrix at the beginning of the simulations. An appropriately small element size ($\triangle$r = $\triangle$z = 0.0625 mm) was chosen to obtain mesh independent results (sections 3.4.2 and 4.4.2). An identical mesh was used in the finite element and the finite volume calculations, whereby the element size was driven by the demands of the latter as the finite volume calculations of the bioregulatory model required a higher mesh density to obtain mesh independent results. The elements in the finite element calculations were biphasic 8-noded axisymmetric quadrilateral elements.

The boundary conditions applied during the simulations with the bioregulatory model are also indicated in Figure 6.4c. Mesenchymal stem cells,

fibroblasts, osteoblasts, endothelial cells and osteogenic as well as vascular growth factors, all originating from the marrow cavity, enter the bone chamber through the perforations. The preference of bone marrow derived stem cells to differentiate towards osteoblasts (Taguchi *et al.*, 2005) is modelled by not applying any chondrogenic growth factors.

The biological simulations were allowed to run for 3 days in between consecutive loading events to simulate the experimental conditions. The biological parameter values were derived from the stimulus value calculated in the mechanical analyses, as indicated in Figure 6.2. As it was shown that cells are more responsive to fluid flow than substrate stress (Owan *et al.*, 1997; Smalt *et al.*, 1997; Tanaka *et al.*, 2005), the mechanical stimulus used in the simulations presented in this chapter, was fluid flow only. The values of the stimulus boundaries (s1 to s4 in Figure 6.2) and the values of the stimulated and unstimulated parameters are given in Table 6.2. These stimulus boundaries were determined based on the magnitude of the stimulus experienced by the tissues in the bone chamber at the beginning of the analyses.

TABLE 6.2: Stimulated and unstimulated parameter values and stimulus boundaries (Figure 6.2) for the bone chamber simulations.

	Unstimulated value	Stimulated value	s1 [μm/s]	s2 [μm/s]	s3 [μm/s]	s4 [μm/s]
$\tilde{A}_{b0}$	0.202	2.02	0.01	0.02	0.09	0.1
$\tilde{A}_{v0}$	0.202	2.02	0.01	0.02	0.09	0.1

Semi-stabilised murine fracture model

For the application of the mechanobioregulatory model to the semi-stabilised murine fracture healing model, the simplified geometry derived in chapter 4 (Figure 4.3 on page 63) was used (Figure 6.5).

The boundary conditions applied during the mechanical analyses are indicated in Figure 6.5b. The external surface of the callus and the cortex were assumed to be covered by fascia and hence impermeable for fluid (Einhorn, 1998). Axial loading of the regenerate took place in a force controlled manner and was simulated by imposing a force boundary condition on the top nodes of the cortex. The mice made full use of the fractured limb immediately after surgery, hence the applied load was assumed to correspond to the normal load in that limb. As no information is available on the normal load in mice

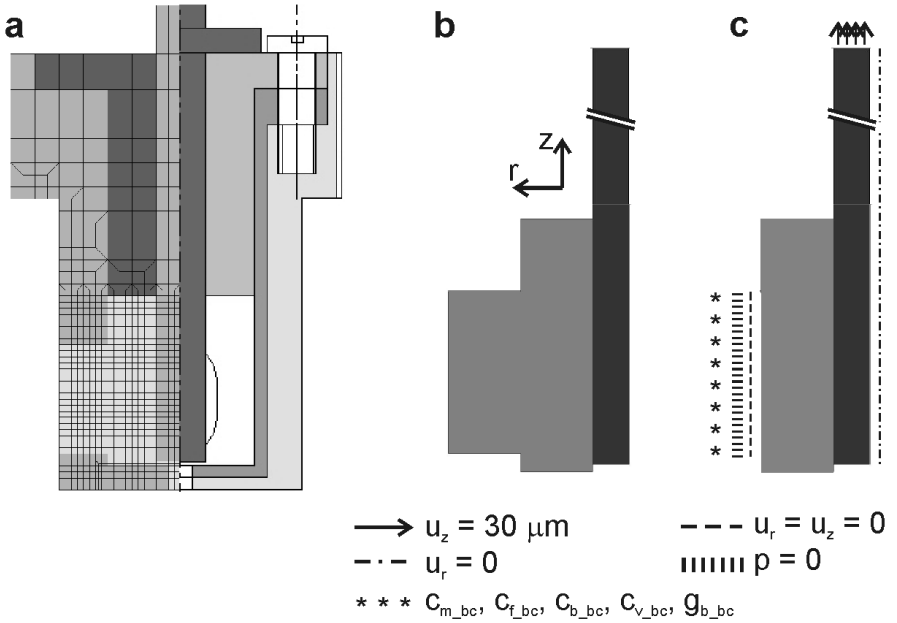


Figure 6.4: Overview of the geometrical domain and boundary conditions for the *in vivo* bone chamber applied in the simulations with the mechanobioregulatory model. (a) finite element model of the entire bone chamber and (b) tissue inside the chamber. (c) reduced model of tissue inside the chamber with indication of boundary conditions for the mechanical and biological analyses.

tibiae, twice the body weight was used (1.5 N). The callus was modelled to be filled with a low density fibrous tissue matrix at the beginning of the simulations. An appropriately small element size ($\triangle$r = $\triangle$z = 0.0125 mm) was chosen to obtain mesh independent results (sections 3.4.2 and 4.4.2), the element size driven by the demands of the finite volume calculations as explained higher. The elements in the finite element calculations were biphasic 8-noded axisymmetric quadrilateral elements.

The boundary conditions applied during the simulations with the novel bioregulatory models, as indicated in Figure 6.5a, are the ones discussed in the previous chapter (page 105).

As the mice were allowed to move freely, the fracture limb was continuously loaded. However, in a first set of simulations, the loading regimen was grossly simplified to 1 loading event per day. This means that the bioregulatory

model was allowed to run for 1 day in between consecutive loading events. The biological parameter values were derived from the stimulus value calculated in the mechanical analyses, as indicated in Figure 6.2. As it was shown that cells are more responsive to fluid flow than substrate stress (Owan *et al.*, 1997; Smalt *et al.*, 1997; Tanaka *et al.*, 2005), the mechanical stimulus used in the preliminary simulations presented in this chapter was the fluid flow. The values of the stimulus boundaries (s1 to s4 in Figure 6.2) and the stimulated and unstimulated parameters are given in Table 6.3. These stimulus boundaries were determined based on the values derived by Huiskes *et al.* (1997) for the mechanoregulatory model of Prendergast *et al.* (1997).

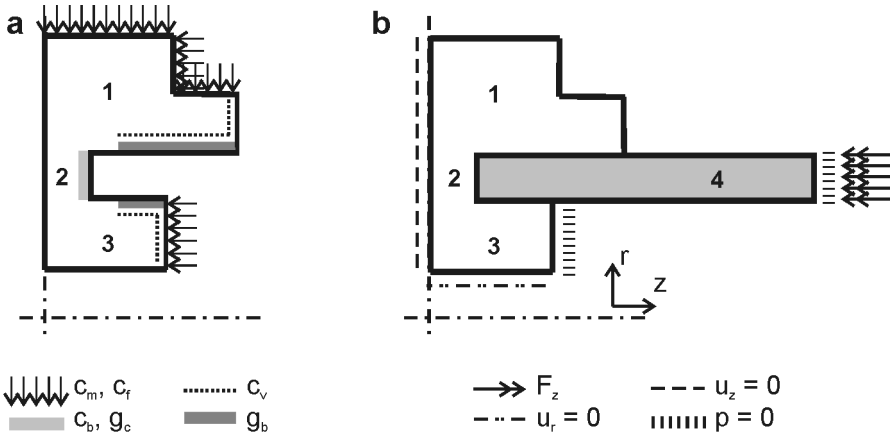


FIGURE 6.5: Overview of the geometrical domain and boundary conditions for the semi-stabilised murine fracture model. (a) Dirichlet boundary conditions for the bioregulatory model (b) boundary conditions for mechanical analysis. 1: periosteal callus; 2: intercortical callus; 3: endosteal callus; 4: cortex.

TABLE 6.3: Stimulated and unstimulated parameter values and stimulus boundaries (Figure 6.2) for the fracture healing simulations.

	Unstimulated value	Stimulated value	s1 [μm/s]	s2 [μm/s]	s3 [μm/s]	s4 [μm/s]
$\tilde{A}_{b0}$	0.0202	0.202	1	2	9	10
$\tilde{A}_{v0}$	0.0202	0.202	1	2	9	10

6.3.4 Simulations and sensitivity analyses

A number of simulations were performed to illustrate the potential of using coupled mechanobioregulatory models to simulate and predict tissue regeneration. For the *in vivo* bone chamber set-up, different magnitudes of implant displacement were simulated and compared to the experimental results reported in chapter 3. Furthermore, the influence of the loading frequency (once every 3 days vs. daily loading) was investigated. For the semi-stabilised murine fracture healing set-up, pathological healing due to non-loading, underloading and overloading was investigated. An example was presented where the healing process was resumed after restoration of a normal mechanical environment.

6.4 Results

6.4.1 Application in an *in vivo* bone chamber

The results presented in Figure 6.6 show the temporal evolution of the ingrowth of bone and vasculature in the bone chamber. Initially, only a low density fibrous tissue matrix was present in the chamber. Vasculature and bone invade the chamber over time and in regions with low bone density, the fibrous tissue density increases. Comparing these simulation results with the experimental data gathered in study 2 (section 3.3.1 on page 20) and the predictions of the mechanoregulatory model of Prendergast *et al.* (1997) (section 3.4.2 on page 31), a reasonably good agreement was observed for all the experimentally measured histological parameters, an improvement compared to the simulation results obtained with the mechanoregulatory model (Figure 6.7). The BAF in individual sections taken at different heights in the bone chamber was experimentally measured and numerically calculated whereby the location of the sections in the numerical calculations corresponded to those used in the histological measurements, as indicated in Figure 3.4 (page 27). With exception of section 5 where BAF increases again, the numerically predicted distribution corresponded to the one that was experimentally observed.
Daily loading of the implant caused a slightly slower ingrowth process (BAF and BIC) compared to loading the implant once every 3 days (Table 6.4). Loading the implant once every 2 or 4 days showed comparable values for BAF (i.e. compared to loading once every 3 days), but markedly smaller BIC values after 9 weeks of loading. After 6 weeks of loading, the lowest loading frequency showed the highest BIC value, but after 9 weeks of loading, its BIC value was the lowest of all loading frequencies.

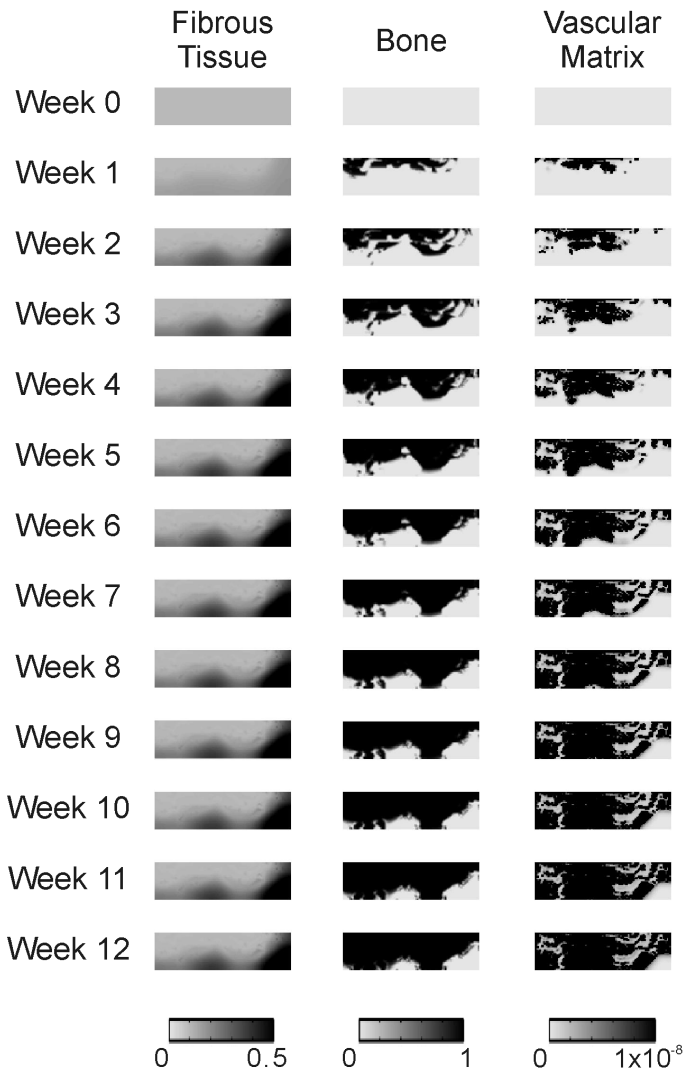


FIGURE 6.6: Simulation results for an implant displacement of 30 μm for different points in time. Fibrous tissue matrix density (left), bone matrix density (middle) and vascular tissue matrix density (right) [x 0.1 g/ml].

In order to assess the influence of the implant displacement on the regeneration process, different implant displacements, ranging from 0 μm up to 500 μm, were applied. Looking at the simulation results (Figure 6.8), a good

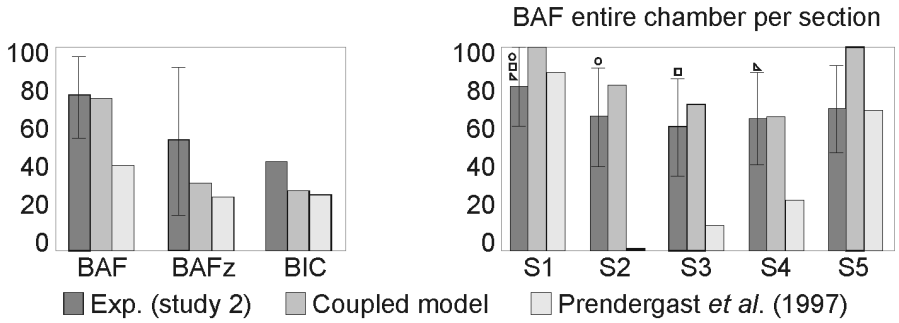


Figure 6.7: Comparison between experimental and simulation results, for both the coupled model and the mechanoregulatory model of Prendergast *et al.* (1997), for a 30 μm implant displacement after 9 weeks. Left: comparison of the different histological parameters (BAFz: BAF 200 μm peri-implant zone). Right: comparison of the evolution of the parameter BAF entire chamber (avg±SD) for different heights along the implant (S refers to section number as indicated in Figure 3.4). In the simulations, no BIC was observed for the non-loading case.

Table 6.4: Influence of the loading frequency ($\triangle$t indicates the time in between consecutive loading cycles in days) on the simulation outcome (BAF and BIC) for a 30 μm implant displacement in the bone chamber at 6 weeks (6W) and 9 weeks (9W) after implant installation.

	BAF 6W	BAF 9W	BIC 6W	BIC 9W
$\triangle t = 1$	56.61	69.95	4.46	25.89
$\triangle t = 2$	60.07	70.51	0.89	18.75
$\triangle t = 3$	63.06	74.80	3.57	29.46
$\triangle t = 4$	62.36	75.45	8.04	14.29

osseointegration of the cylindrical implant was observed for implant displacements between 30 μm and 90 μm. Non-loading showed hardly any ingrowth of bone in the chamber, whereas for the highest implant displacements little bone and hardly any BIC was observed due to the low proliferation capacity. Comparing these simulation results to the experimental results obtained in animal study 3 (page 20 - 6 week period), only the predictions for the 90 μm were corroborated (Figure 6.9). Although the simulations applying the mechanoregulatory model of Prendergast *et al.* (1997) were, contrarily to these applying the coupled model, able to capture the trend for higher values

of BAF for higher implant displacements, the non-loading case was incorrectly predicted to lead immediately to a fully ossified bone chamber (or no bone at all when resorption is included in the model). The evolution of the numerically predicted values of the BIC for 30 μm, 60 μm and 90 μm implant displacement, was similar (yet less pronounced) to the one experimentally observed and an improvement compared to the simulation results obtained with the mechanoregulatory models. The highest BIC for these loading cases was observed for the 60 μm displacement, followed by the 90 μm displacement and the lowest BIC was observed for the 30 μm implant displacement. The difference between experiments and predictions was the most pronounced for the non-loading case.

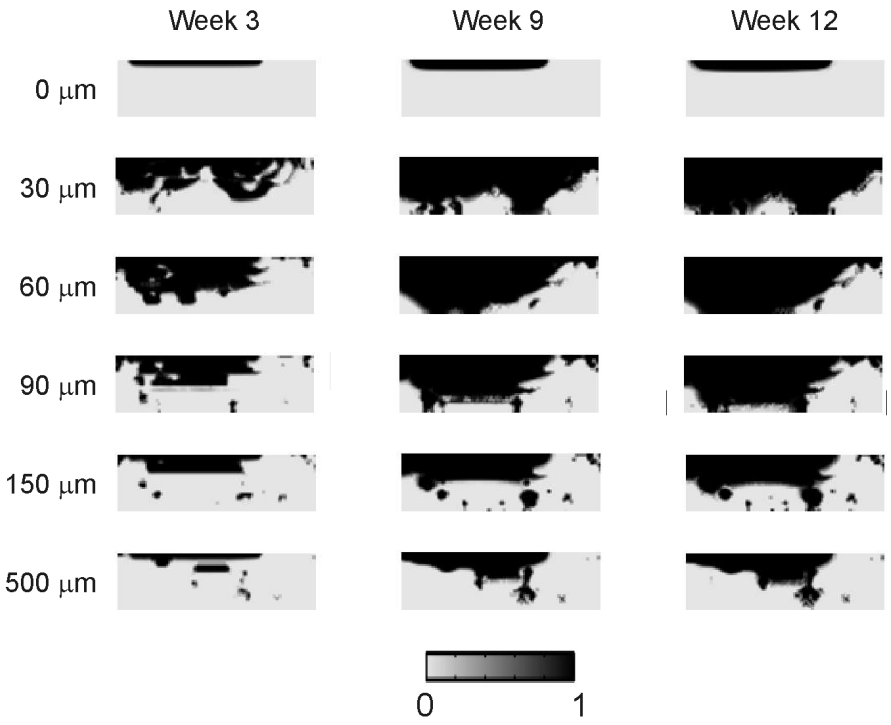


FIGURE 6.8: Simulation results for different implant displacements shown by bone matrix density for different time points (weeks) in the osseointegration process [× 0.1 g/ml]

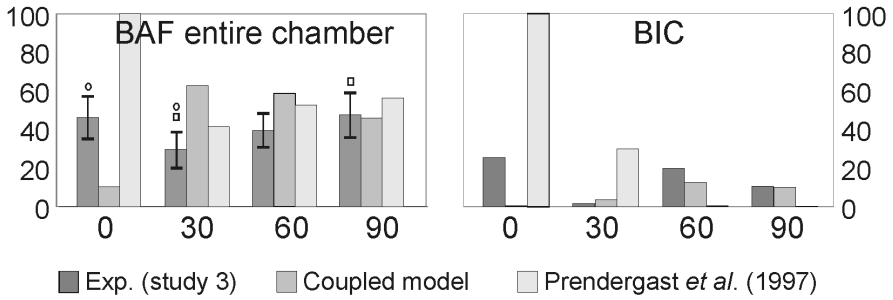


Figure 6.9: Quantitative comparison between the results of animal study 3 (avg±SD) and the simulation results, for both the coupled model and the mechanoregulatory model of Prendergast *et al.* (1997), for different implant displacements (after 6 weeks).

6.4.2 Application in fracture healing

The results presented in Figure 6.10 show the spatiotemporal evolution of the different tissues in the callus under overloading conditions (5 times normal load). Intramembranous ossification, starting around PFD 4 under normal loading conditions, was now reduced. Cartilage formation was proceeding as normal, filling the entire callus area as the parameters related to chondrocytes and cartilage were unaffected by the mechanical loading in this model. Endochondral ossification, starting around PFD 14 for normal loading conditions, was not observed in the simulations for overloading conditions. Furthermore, angiogenesis was strongly reduced, both in the zones where intramembranous ossification and the zones where endochondral ossification takes place under normal loading conditions. In Figure 6.11, the temporal evolution of the tissue distribution in the callus area is compared for different loading situations. Normal loading (Figure 6.11c) showed the development of a cartilage matrix and the subsequent degradation thereof in the endochondral ossification process. Non-loading (Figure 6.11a) and overloading (Figure 6.11d) conditions both led to a situation where the entire callus consisted of soft tissues. Underloading of the fracture callus (20 % of normal load, Figure 6.11b) led to some intramembranous bone formation, primarily in the endosteal callus.

After establishment of the nonunion at post fracture week 3 (corresponding to the normal healing time as shown in Figure 6.11), the excessive forces were reduced to test whether normal healing processes can be resumed. Reducing the forces that caused the avascular nonunion to a normal loading level, does not lead to the recapitulation of normal fracture healing as insufficient endothelial cells are present to initiate the endochondral ossification process

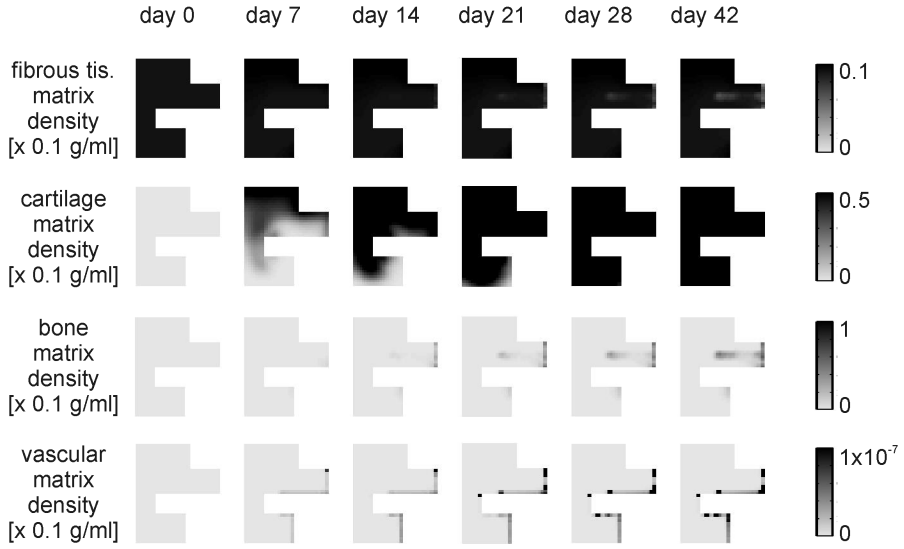


FIGURE 6.10: Spatiotemporal evolution (days post fracture) of fibrous tissue, cartilage, bone and vascular matrix density for an overloaded fracture.

(results not shown). However, reducing these forces to half the normal level (0.75 N), allows endochondral ossification to start, leading to successful healing within 3 to 4 weeks after stabilisation as shown in Figure 6.12. Endochondral ossification starts up in the endosteal callus and bridging of the fracture gap is observed endosteally 2 weeks after stabilisation. The ossification front moves outwards, slowly ossifying the entire callus area until full callus ossification was reached 25 days after stabilisation. Administration of osteogenic growth factors ($\tilde{g}_b = 10$ in all grid cells) caused an initially slower healing response, but endochondral ossification was observed in both periosteal and endosteal callus. Bridging of the fracture gap occurred simultaneously in periosteal and endosteal areas, full ossification of the callus was reached within 17 days after stabilisation.

6.5 Discussion

6.5.1 Application in an *in vivo* bone chamber

A mechanobioregulatory model was proposed, based on the bioregulatory model presented in the previous chapter, where the proliferation rate of osteoblasts and endothelial cells was made dependent on the magnitude of a

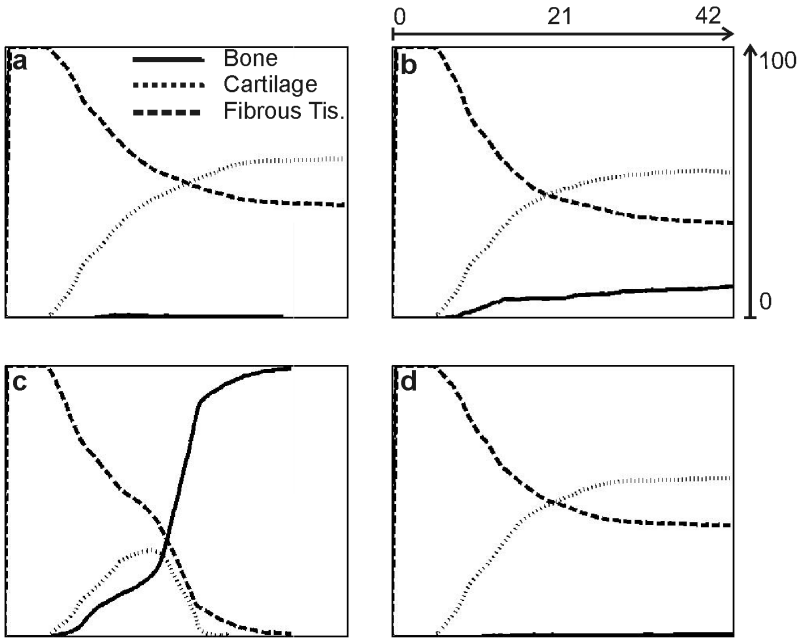


Figure 6.11: Temporal evolution (days post fracture) of tissue fractions in the callus [%] for normal and pathological fracture healing. (a) non-loading situation. (b) underloading situation (20 % of normal load). (c) normal loading situation. (d) overloading situation (5 times normal load).

mechanical stimulus, in this case fluid flow. No preliminary calibration study or sensitivity analysis was carried out to determine the optimal value of the parameters of the bioregulatory model, the value of the stimulated parameters or the stimulus boundaries for the bone chamber set-up.

An implant displacement of 30 μm yielded results that are roughly comparable to the experimental measurements and that are an improvement compared to the simulation results obtained with the mechanoregulatory models (chapter 3), both in terms of BAF, BIC (Figure 6.7a) and spatial distribution of BAF (Figure 6.7b) throughout the chamber. Under the non-loading condition (0 μm implant displacement, Figure 6.8), very little bone ingrowth in the chamber and no bone-to-implant contact was observed in the simulation results. For high implant displacements ($>$ 100 μm), again little bone ingrowth and a limited bone-to-implant contact was simulated. As the implant was almost entirely surrounded with fibrous tissue, this would in clinical terms constitute a failed implant osseointegration. These high implant dis-

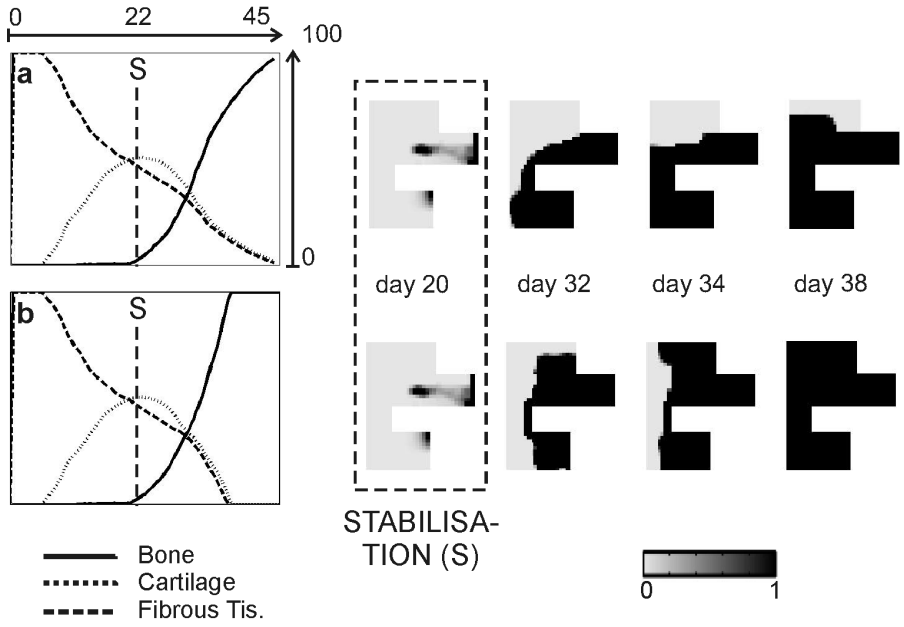


FIGURE 6.12: Recapitulation of normal healing after reduction of excessive motion to a normal mechanical environment. Left: temporal evolution (post fracture days) of the tissue fractions in the callus [%] (vertical dashed lines indicate stabilisation point at PFW 3). Right: bone matrix density in the bone chamber at various time points after stabilisation [× 0.1 g/ml]. Top: stabilisation of the fracture callus alone. Bottom: stabilisation of the fracture callus in combination with osteogenic growth factor administration at fracture stabilisation.

placements were not tested in the bone chamber, but are generally accepted as the upper limit of micromovements above which implant osseointegration does not occur (Søballe *et al.*, 1992b; Søballe, 1993; Pilliar *et al.*, 1986).

For the no and moderate implant displacements, a comparison was made with the results obtained in bone chamber study 3 (Figure 6.9) and the simulation results obtained using the mechanoregulatory model of Prendergast *et al.* (1997). For the moderate implant displacements, osseointegration of the implant was predicted in all cases. There is a good quantitative correspondence between the numerically predicted and experimentally observed BAF and BIC for the 90 μm implant displacement after 6 weeks of loading. Relative to the BIC incidence for the 90 μm displacement, the simulations for 60 μm and

30 μm displacement predicted a higher and a lower BIC incidence respectively. This was also observed experimentally and an improvement compared to the predictions of the mechanoregulatory models. The difference between simulations and experiment was most pronounced for the non-loading case where, contrarily to the simulation results, experimentally a high BAF and BIC incidence was observed. When comparing the different experimental results for the non-loading cases in all the animal studies (section 3.3.1 on page 20 and Figure 3.6 on page 32), it showed a substantial diversity in these observations. The results for the BAF from study 3, which were obtained at 6 weeks after implant installation, approach those of study 1, which were obtained after 12 weeks. No explanation could be found for the high BAF observed in study 3.

Comparing the BAF and BIC for the 30 μm implant displacement of studies 1 and 3 (Figure 3.6 on page 32, a.6WL and c.30 respectively), showed a substantial higher BAF and BIC for study 1. The only difference between these studies (apart from the animals) was the loading frequency, 3 times a week for study 1 compared to only twice a week for study 3. This could suggest that a higher loading frequency is beneficial for the implant osseointegration process. However, in the simulations the effect of loading frequency was shown not to be so straightforward (Table 6.4). Whereas a lower simulated loading frequency ($\triangle$t = 4) initially caused a higher BIC after 6 weeks of loading, this value was the lowest of all tested loading frequencies after 9 weeks of loading. In the simulations, the loading frequency did not substantially influence the amount of bone in the chamber, but did have a considerable effect on the predicted chance for bone-implant contact to occur. The optimal frequency for maximum bone and bone-to-implant contact after 9 weeks appeared to be loading the implant once every 3 days. Additional studies with chamber harvests at intermediate time points (e.g. weeks 1, 2 and 4 after installation), will allow for calibration and optimisation of the coupled model. Theoretical experiments can then be carried out to help to elucidate the cause of the aforementioned inter-study differences.

6.5.2 Application in fracture healing

As adverse mechanical loading affects the osteoblast's and endothelial cell's capacity to proliferate, both under- and overloading simulation results show the development of avascular nonunions (Figure 6.10). This corresponds to the experimental and clinical studies reported in literature where it is concluded that appropriate load is necessary for angiogenesis and osteogenesis (Glowacki, 1998; Kirchen *et al.*, 1995; Sarmiento *et al.*, 1977; Carter *et al.*, 1988; Lu *et al.*, 2007). Additionally, many other studies show the beneficial influence of appropriate loading of the callus on the heal-

ing response in general, as discussed in the introduction of this chapter (Goodship and Kenwright, 1985; Cheal *et al.*, 1991; Chao *et al.*, 1998; Claes, 1998; Kenwright and Gardner, 1998).

Additional analyses were carried out where, after the establishment of the avascular nonunion at PFW 3 (corresponding to normal healing times in mice), the excessive force on the callus was reduced to the normal force. Despite the formation of some bone close to the cortex away from the fracture line, no full recapitulation of the healing process (no endochondral ossification) was observed over a period of 6 weeks after stabilisation. However, reducing the force further to half the normal force, successful healing was observed 25 days after stabilisation as in the simulations. This simulation result corresponds to a myriad of clinical studies reporting on the resumption of the healing process after increasing the fracture's stability. Various techniques exist in clinical practice to successfully reduce the motion in an instable fracture as reviewed by Rodriguez-Merchan and Forriol (2004). The further reduction of the load to half the normal load was required in the simulations as, under normal load, a combination of the influences of both the cartilage density and the local mechanics on the cells' proliferation rate prevented adequate endothelial cell proliferation needed to initiate the endochondral healing process. Additional simulations are required to further investigate this phenomenon.
Besides internal and external fixation methods, biochemical enhancement of fracture healing has found its way to clinical practice. Several clinical studies report a substantial increase of the success rate in the treatment of fracture nonunions when, together with mechanical stabilisation, rhBMP-2 or 7 is administered to the fracture site (Ronga *et al.*, 2006; Zimmermann *et al.*, 2006; Dimitrou *et al.*, 2005b; Giannoudis and Tzioupis, 2005; Friedlaender *et al.*, 2001; Johnson and Urist, 1998). Preliminary simulation results indicate however that, without a proper mechanical reduction, osteogenic growth factors are unable to initiate successful healing. A combination of fixation and growth factor administration results in successful healing 17 days after stabilisation. The growth factor concentration administrated upon stabilisation was in the order of magnitude of the concentration applied at the boundaries at the beginning of the simulations. No sensitivity analyses were performed yet to assess the influence of this concentration on the simulation outcome. Further refinement of the coupled mechanoregulatory model, including the mechanodependency of other processes beside proliferation, and the performance of thorough sensitivity analyses, will allow for a further optimisation of the model's predictions and applicability in clinical practice.

6.5.3 Simplifications

As this chapter builds on the results obtained in the previous chapters, most of the simplifications that were made in those studies are also present here. The simplifications that were made in the construction of the FE model of the bone chamber regarding the applied boundary conditions, the shape and the way tissue-implant contact is modelled, are discussed in section 3.5.3. A discussion on the simplifications made in the composition of the geometrical domain of a fracture callus (assumption of axisymmetry, rectangular callus shape, fixed callus size) is given in sections 4.5.3 and 5.5.3. In a first step, a more realistic FE model could be created and coupled to the simplified geometry, to exclude any effect of singularities arising from the rectangular shape of the FE mesh on the simulation outcome. Section 5.5.3 further discusses several simplifications related to the bioregulatory model that forms the basis for the coupled mechanobioregulatory model.

Calculated tissue level mechanical stimuli are used to adapt the biological parameters, whereas in reality a substantial difference is measured between tissue level and cellular level stimuli. You *et al.* (2001) proposed a model to explain (and calculate) the observed strain amplification phenomenon in the osteocytes' skeleton. These osteocytes are considered the main mechanosensors in bone (Mullender and Huiskes, 1997; Burger and Klein-Nulend, 1999). However, mechanosensing by cells in a regenerating tissue yet remains to be unravelled. In order to realistically incorporate the events taking place at the different length scales (global and local), a multi-scale approach could be followed.

Finally, for the simulations shown in this chapter, only fluid flow was considered to influence biological processes. Additional mechanical stimuli and combinations of different types of stimuli will be tested in future research.

6.5.4 Sensitivity analyses

Several assumptions were made in the coupling of the mechanical and biological effects on bone regeneration. The stimulus boundary values for the adaptation of the biological parameter values were chosen, based on FE calculations of the mechanical stimuli experienced by the tissues in the case of the bone chamber and based on the values derived by Huiskes *et al.* (1997) for the model of Prendergast *et al.* (1997) in the case of the fracture healing set-up. Sensitivity analysis will have to be carried out to assess the influence of these boundary values on the predicted healing patterns.

The formula (6.1) that was used to calculate the material properties from the matrix densities, differs slightly from the formula proposed by Bailón-Plaza and van der Meulen (2003):

$$E(i) = \frac{E_b m_b(i) + E_c m_{c'}(i)}{m_b(i) + m_{c'}(i)} \quad \text{with} \quad m_{c'} = \left(\frac{c_c}{c_c + c_m}\right) m_c. \quad (6.4)$$

Only matrix densities were used in this chapter to calculate the material properties, as fibrous tissue was modelled as a separate variable in the applied bioregulatory model, in contrast to the bioregulatory model used by Bailón-Plaza and van der Meulen (2003). Furthermore, a reference was made to the normal matrix density, which is the density a certain tissue type has when it is the dominating tissue in the callus. This prevents the algorithm from assigning e.g. the full stiffness of bone to elements where only low density bone and no other tissues are present. In the early phase of fracture healing a small difference was observed between the two formulas 6.1 and 6.4. However, one week after fracture, this difference had disappeared and both algorithms led to similar simulation outcomes.

6.5.5 General considerations

Mathematical framework

The mathematical framework presented in this chapter, is the first mechanistic bone regeneration modelling framework that allows for a direct and explicit coupling between local mechanical stimuli and angiogenesis as well as chondrogenesis and osteogenesis. Previous models either considered ideal angiogenic circumstances (Bailón-Plaza and van der Meulen, 2003; Gómez-Benito *et al.*, 2005; Ambard and Swider, 2006), modelled the effects of mechanics on bone regeneration in a more phenomenological fashion (Simon *et al.*, 2004; Shefelbine *et al.*, 2005) or both (Prendergast *et al.*, 1997; Carter *et al.*, 1998; Claes and Heigele, 1999; Ament and Hofer, 2000).

One could argue whether the proposed framework, coupling the mechanics and biology of bone regeneration, is too complex. Compared to the mechanoregulatory models described in chapter 3 of this thesis, this model is certainly much more complex. Although these mechanoregulatory models use fairly simple mechanisms to predict the outcome of a regeneration process, they are capable of correctly simulating many aspects of various bone regeneration situations. However, in order to gain more insight into the governing processes of bone regeneration and in order to be able to make predictions on pathological healing and treatment strategies (especially those that rely on biology e.g. the administration of growth factors), more mechanistic models are required. Models only taking into account the influence of the mechanics

either assume that mechanics drives the biology completely or that biology acts as an unchanged background phenomenon. Both assumptions are wrong because in reality, biology may act independently of mechanics. Compared to the actual complexity of the bone regeneration process itself, this model only captures the tip of the iceberg. However, a model incorporating every detail of the biology would no longer be a practical tool. The complexity of the model should depend on its purpose. A model designed to investigate the influence of angiogenesis on the occurrence of nonunions, should contain a detailed description of angiogenesis, whereas the description of other processes (e.g. description of osteogenic and chondrogenic growth factors) could be kept relatively simple.

This mathematical framework requires the determination of many parameter values, which cannot all be corroborated by dedicated *in vivo* or *in vitro* experiments. Sensitivity analyses provide insight in the influence of the various parameter values on the simulation outcome. It is possible that, although the regulatory principles guiding the regeneration process are similar for various bone regeneration situations (fracture healing vs. implant osseointegration or bone regeneration in various species), the exact parameter values are not. Calibration of the model parameters for each regeneration situation should be carried out before simulating challenged regeneration processes and treatment strategies for that particular set-up. Additionally, special attention must be paid to the determination of the appropriate boundary conditions of each set-up, both for the biology as for the mechanics. In fact, it is also possible that one set of parameter values is valid for all experimental set-ups when the correct boundary conditions for each set-up are known.

To cite the science philosopher K. Popper once more, the refutation of a simple theory is a progressive step whereas the construction of a complex theory that is unrefutable is the opposite. This modelling framework is, although complex, far from unrefutable (Prendergast, 2001). Every aspect of the model is either based on experimental observations or based on experimentally testable assumptions. It is not a black box that predicts results based on a few input variables. It is a dynamic environment that can be altered and improved as knowledge increases. It can also contribute to this knowledge increase by performing theoretical experiments, simulating specific regeneration conditions or designing successful treatment strategies which afterwards, can be verified experimentally.

Experimental corroboration

Dedicated *in vitro* or *in vivo* experiments focussing on a specific aspect of the regeneration process, such as cell migration, growth factor produc-

tion, growth factor consumption etc. allow to verify the assumptions made in the development of the mathematical framework, as discussed in section 5.3. However, when using experimental data for corroboration, caution must be exerted in the transfer of results obtained with *in vitro* experiments conducted on specific cell lines in a highly controlled 2D environment, to events taking place in a highly variable and largely uncharacterised (*in vivo*) 3D environment. A clear example of this is, as discussed previously in this section, the difference between the global mechanical load exerted on the callus and the local mechanical stimulus experienced by the cells in that callus.

Results from tissue regeneration experiments, such as the *in vivo* bone chamber or the fracture healing set-ups discussed in the previous chapters, allow to test the overall performance of the mathematical framework. However, to be able to accurately assess the model's capabilities, a good knowledge of both the biological and mechanical conditions of the experimental set-up is important. For the *in vivo* bone chamber this would mean additional harvests at intermediate time points and a characterisation of the biology of the peri-implant regeneration processes (cell proliferation, growth factor expression, blood vessel formation). For the semi-stabilised fracture set-up this would constitute the quantification of the load exerted on the fracture limb and of the mechanical environment of the regenerating tissue. Recently, Leucht *et al.* (2007) developed a novel *in vivo* model of peri-implant bone regeneration. The mechanical situation in the peri-implant tissue, arising from highly controlled implant displacement which could be modelled accurately, was compared to biological data on vascularisation, cell proliferation, differentiation and bone remodelling. In short, a close coupling between theoretical work and experimental analysis is of paramount importance for the advancement of mathematical modelling of any biological process.

6.6 Conclusions

In summary, the work presented in this chapter shows the potential of combining mechanoregulatory and bioregulatory principles in the simulation of bone regeneration. A mathematical framework is presented in which parameters from the bioregulatory model, presented in chapter 5, depend on the magnitude of local mechanical stimuli. To illustrate the added value of such a model to the existing body of literature, parameters related to osteogenesis and angiogenesis were made dependent on the local fluid flow and this coupled model was applied to the *in* vivo bone chamber as well as the semi-stabilised fracture healing set-up, without preliminary sensitivity analysis or calibration of the model's parameters.
For the *in vivo* bone chamber, several implant displacement magnitudes as

well as intervals between consecutive loading events were tested. In general, moderate implant displacements allowed for osseointegration of the implant whereas excessive loading conditions led to fibrous encapsulation of the implant, comparable to the experimental observations in the bone chamber set-up and literature. However, for the non-loading case, no correspondence was observed between the simulation results and experimental observations.
Application of the coupled mechanobioregulatory model to the fracture healing set-up allowed to simulate non-loading, underloading and overloading situations. Simulation of these adverse mechanical circumstances predicted the formation of an avascular nonunion, which was corroborated by experimental observations reported in literature. Sufficient stabilisation of excessive motion of the fractured bone ends allowed for a recapitulation of a normal healing response with and without the administration of additional osteogenic growth factors.
Thorough sensitivity analyses need to be carried out to assess the impact of the simplifications and assumptions made in the course of this study. The influence of other mechanical parameters besides fluid flow will be added to the model. Finally, more biological variables need be made dependent on the local mechanical stimuli to enhance the understanding of the influence of both biological and mechanical signals on the bone regeneration process. The study presented in this chapter is a first illustration of the potential of such mathematical models.

Chapter 7

Conclusions and future perspectives

This chapter starts by concisely summarising the contents of this thesis. In section 7.2 the most important conclusions are repeated, followed by a discussion of the contribution of this work to the field of bone regeneration research. Finally, some topics for future research are indicated.

7.1 Summary

In the first chapter of this thesis, some basic notions on bone and bone regeneration have been explained. The need for further research in the field of bone regeneration for various application areas such as fracture healing and implant osseointegration has been identified. As the general hypothesis of this work is that mathematical models can contribute to bone regeneration research, chapters 3 to 6 describe the implementation and development of several existing and novel models for bone regeneration.
In chapters 3 and 4, the implementation of existing mechanoregulatory and bioregulatory models is described. These models have been applied to different experimental set-ups of implant osseointegration and fracture healing. The predictions made by these models have been compared to the experimental results, both in a qualitative and quantitative way. Thorough sensitivity analyses have been carried out on both types of models to asses the influence of the different model parameters on the predicted outcome. The bioregulatory models have furthermore been applied to simulate several pathological healing situations. Shortcomings of the models have been identified and suggestions for improvement have been made.
Chapter 5 describes the development of a novel bioregulatory model. This

new model is based on the existing models but adds several indispensable key features of the bone regeneration process such as angiogenesis and cell migration, thereby answering to some of the shortcomings that have been identified in chapter 4. Application of this model to the fracture healing set-ups has allowed for a quantitative corroboration of the model's predictions. Sensitivity analyses have been carried out, assessing the influence of the parameter values on the simulation outcome. Additionally, several cases of pathological healing and possible treatment strategies have been modelled.
The introduction to chapter 6 describes the State of the Art of the influence of mechanical loading on fracture healing and implant osseointegration in general and cellular behaviour in particular. The mechanoregulatory principles described in chapter 3 have been integrated in the novel bioregulatory model described in chapter 5. Simulation of bone regeneration, using this combined model, in both implant osseointegration and fracture healing has been carried out to demonstrate the functionality of the established modelling framework.

7.2 Conclusions

- Comparing the experimentally observed and numerically simulated tissue regeneration patterns in the bone chamber, no complete qualitative or quantitative correlation was obtained for the mechanoregulatory models under investigation (Carter *et al.*, 1998; Claes and Heigele, 1999; Prendergast *et al.*, 1997). However, certain aspects of the experimental observations could be captured by all models, such as the increased BIC incidence for screw-shaped implants compared to cylindrical implants and a higher BAF for the entire chamber compared to the 200 μm circular zone around the implant. Furthermore, depending on the mechanoregulatory model under investigation, the experimentally observed absence of difference in BAF between cylindrical and screw-shaped implants (models of Carter *et al.* (1998) and Claes and Heigele (1999)) and the spatial distribution of BAF throughout the chamber (model of Prendergast *et al.* (1997)) were predicted. Notably, a substantial influence of model parameters such as material properties and the boundary values of tissue phenotype transitions on the simulation outcome was demonstrated.

- After adaptation of a number of parameter values in the model of Bailón-Plaza and van der Meulen (2001), a good qualitative agreement was obtained between simulated results and experimental data for several important aspects of normal fracture healing, such as the global spatial and temporal evolution of cartilage and bone matrix density and the temporal evolution in the growth factor concentrations. Several

cases of pathological healing were simulated with variable success rates. For the experimental situation of delayed healing due to an increased fracture gap, successful healing was invariably predicted by the model if the analyses were continued long enough, indicating that the mechanisms responsible for the occurrence of the delay are not present in the model. The occurrence of a nonunion due to a lack of growth factor production and its treatment with an injectable carrier of osteogenic growth factors, showed a dose-dependent recapitulation of the healing process as described in literature. Finally, the simulation of atrophic nonunions (Brownlow *et al.*, 2001) and their treatment showed interesting results, but also emphasised the need for further extension of the mathematical model. Several essential regulators of the fracture healing process, such as angiogenesis and cell migration are lacking in this model. Furthermore, the combination of the fibrous and cartilaginous matrix in one mathematical variable and the phenomenological description of the endochondral ossification, prevent the quantitative comparison between simulation and experiments, which is indispensable in the design of clinical treatment strategies.

- A novel bioregulatory model, incorporating a number of bone regeneration key features, such as intramembranous and endochondral ossification, angiogenesis and cell migration, was established. Its results were successfully corroborated by comparison with experimental data on fracture healing, both on a qualitative and quantitative basis. Sensitivity analyses indicate the need for further experimental validation of the parameters involved in the description of fibrous tissue/fibroblasts and angiogenesis. Cases of pathological fracture healing due to impaired angiogenesis or the lack of mesenchymal stem cells (atrophic nonunion) were simulated, predicting results similar to the experimental observations. Additionally, several experimentally testable treatment strategies were implemented for the atrophic nonunion case, predicting a (dose-dependent) resumption of the healing response. Experimental validation of the latter simulations is currently underway (Keita Ito 2007, personal communication).

- A mathematical framework was presented, allowing for a direct coupling between the biological and mechanical regulatory aspects of bone regeneration. It is the first model of bone regeneration that directly links the local mechanical environment of the regenerating tissue to the angiogenic process, in a mechanistic manner. Several preliminary examples were given both for implant osseointegration as well as for fracture healing, to illustrate the potential of such coupled models. For each of the experimental set-ups, cases of pathological regeneration situations

due to insufficient or excessive loading were simulated. Furthermore, for the case of excessive motion induced fracture nonunion, stabilisation of the callus allowed for recapitulation of normal healing.

Are mathematical models capable of making a substantial contribution to the bone regeneration research, as was hypothesised at the beginning of this work? The research presented in this work strongly suggests the answer to this question should be affirmative. Mathematical models are able to make quantitative predictions on bone regeneration situations. Comparison of these predictions with experimental data allows for further optimisation of these models, as shown in this work and reported by others, e.g. Kitano (2002) (Figure 7.1). However, care must be taken that the predictions are interpreted in the appropriate context. Invariably, creating a mathematical model of biological phenomena constitutes a simplification of the processes under investigation. This simplification can be the omission of certain biological or mechanical factors involved, the restriction to a single time or length scale, the implementation of phenomenological descriptions of highly complex processes etc. Demarcation of the application area for each model is a necessary step in the assessment of its predictive powers.

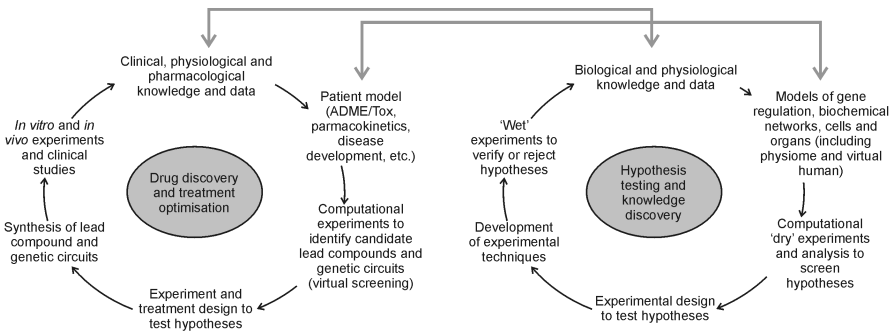


Figure 7.1: Computational systems biology with indication of the links between the basic systems biology research cycle and the drug discovery and treatment cycle (reproduced from Kitano (2002)).

Despite the aforementioned limitations, which in fact equally concern experimental studies, mathematical models can be engaged in the research into possible causes and treatment strategies of pathological healing. By performing theoretical experiments, mathematical models can help to identify interesting research questions, furthering the knowledge in this area.

This work has demonstrated the possibilities and limitations of a number of existing and newly developed mathematical models and has made recommendations for further improvement of these models. The most important contributions of this work to the existing body of literature are the development of a novel bioregulatory model of bone regeneration and the establishment of a mathematical framework in which the mechanobioregulatory aspects of the bone regeneration process can be assessed for different experimental set-ups. Figure 7.2 (page 168) provides an overview of these contributions.

Clearly, this work is not finished. The work presented in this thesis is merely a first, but indispensable, step towards an integrated modelling environment, capable of predicting the occurrence of pathological regeneration in patients and advising clinicians on the optimal treatment strategy.

7.3 Future research

The mathematical framework and the simulation methodology that was developed, was applied to simulate fracture healing and implant osseointegration in an *in vivo* bone chamber. Due to the generic nature of the modelling framework and simulation methodology, they can also be applied to simulate various bone regenerative situations or biological phenomena that were not treated in this thesis. At the division of Biomechanics and Engineering Design, various other cases of bone regeneration have been or are being treated. A model of an oral implant was created and its osseointegration was simulated by means of the mechanoregulatory models discussed in chapter 3 (Chaichanasiri, 2004) and the bioregulatory model discussed in chapter 4 (Amor *et al.*, 2006). The modelling framework established in this thesis also forms the basis for the development of a mechanobioregulatory model describing orthodontic tooth movement and the accompanying processes in the periodontal ligament. In the future, several aspects of the mathematical framework will be developed further, to enhance the model's mechanistic character and its predictive powers (as discussed below).

7.3.1 Modelling aspects

- As the coupled mechanobioregulatory model presented in chapter 6 is a simple first application demonstrating the potential of the coupling of mechanical and biological influences on the bone regeneration process, much work remains to be done. The influence of other mechanical parameters besides fluid flow will be added to the model. Furthermore, additional biological variables need to be made dependent on the local mechanical stimuli to enhance the understanding of the influence of both

biological and mechanical signals on the bone regeneration process. Finally, thorough sensitivity analyses need to be carried out to assess the impact of the simplifications and assumptions made in the development of the model.

- Several shortcomings of the existing mechano- and bioregulatory models were identified in chapters 3 and 4. An extended bioregulatory model was established in the framework of this thesis (chapter 5), in which a number of improvements with respect to these shortcomings was already implemented. However, several key-features of bone regeneration such as the influence of the inflammatory phase, hypoxia, matrix degradation and discrete cell maturation levels remain to be integrated in the mathematical model.

- The current PDE model (chapter 5) describes processes such as differentiation and migration by means of continuum expressions. The parameters used in those continuum expressions cannot be derived directly from information available in the literature. The design of detailed microscopic models, based on biochemical descriptions (kinetics) of the cell types and proteins involved (Levine *et al.*, 2001; Sherratt, 1993), will provide additional information on the correctness of the macroscopic descriptions. Through multi-scale analyses, a direct link can be made between the different length scales. This coupling is necessary in order to link the more mechanistic models at micro level to the macro model that is used to simulate pathological healing and possible treatment strategies.

7.3.2 Experimental aspects

Several assumptions and predictions made in the course of this work await experimental data for verification and corroboration. Experiments are underway (Keita Ito 2007, personal communication) looking into different treatment strategies for the atrophic nonunion model developed by Brownlow *et al.* (2001) and Makino *et al.* (2005).

The influence of mechanical loading on some aspects of the regeneration process has been (partially) quantified (section 6.1). However, many aspects of the influence of mechanics on bone regeneration still remain to be elucidated. Dedicated *in vivo* and *in vitro* experiments can be carried out to test both the assumptions made in developing the mathematical framework as well as the global predictive capacity of the model.

- Dedicated *in vitro* experiments can be designed to quantify aspects of cell migration, growth factor production and consumption and of the

synergy between different growth factors and between mechanical loading and growth factors. These *in vitro* experiments can help to improve certain aspects of the mathematical framework. *In vitro* experiments looking into the effect of mechanical loading on cells hardly ever test a whole range of stimulus magnitudes, however this information is indispensable in constructing mathematical models.

- In order to fully assess the global possibilities of the models developed in chapters 5 and 6, detailed information on both the biological and mechanical aspects of the experimental set-ups (*in vivo* models) is necessary. The repeated sampling bone chamber discussed in chapter 3 is an example of a highly controlled mechanical environment, but additional information on early time points in the osseointegration process, on the biological aspects of the peri-implant regeneratory process and on the mechanics of the tissue-implant interface is needed. As for the fracture healing models discussed in chapter 4, a quantification in terms of the mechanical properties of the fracture environment needs to be made.

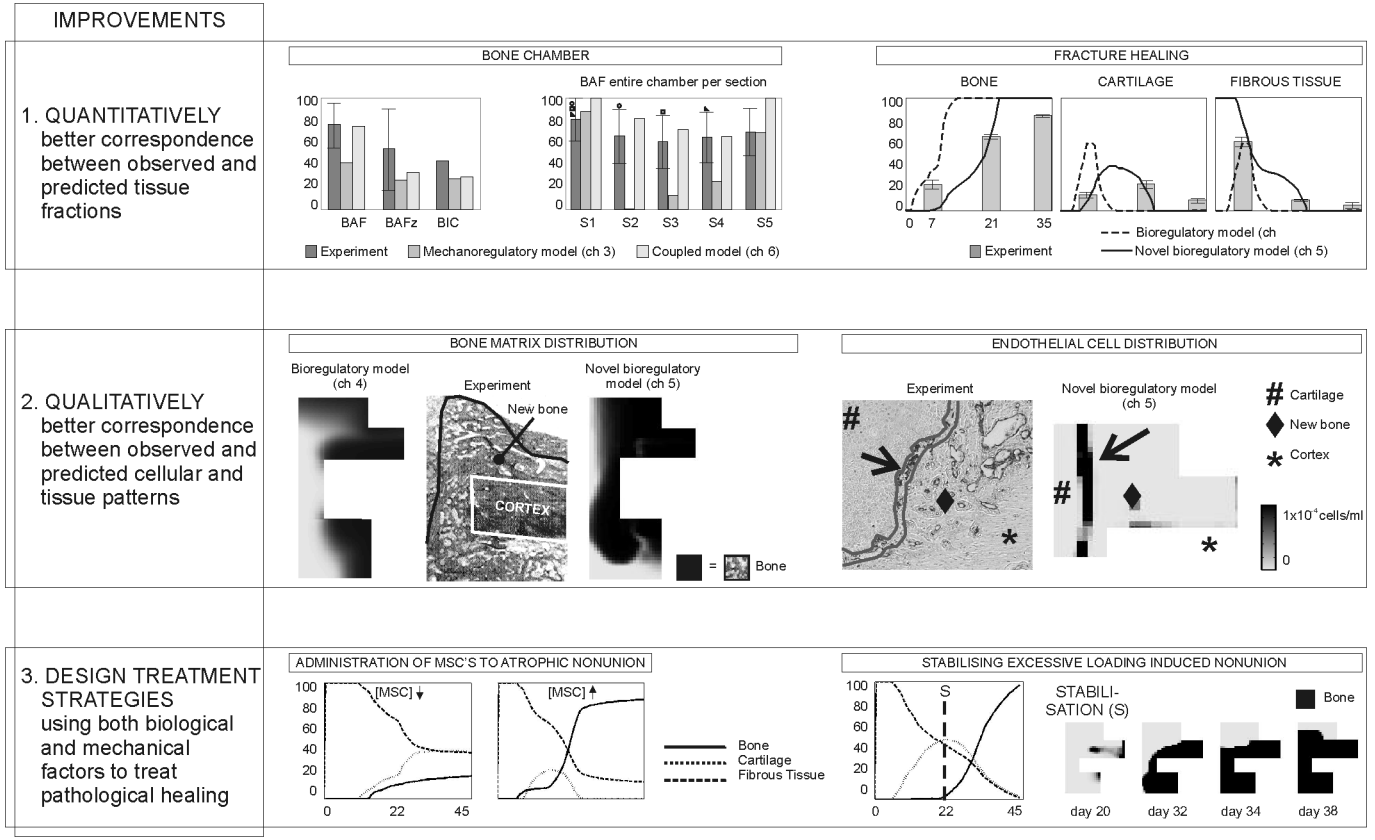


FIGURE 7.2: Overview figure showing the major contributions of this thesis.

Bibliography

Aaron, A.D., 1996. Bone Healing and Grafting. In: Kasser, J.R. (Ed.), Orthopaedic Knowledge Update 5. American Academy of Orthopaedic Surgeons, J.R. Rosemont, IL. 21-28.

Adam, J.A., 1999. A simplified model of wound healing (with particular reference to the critical size defect). Math. Comp. Mod. 30, 23-32.

Akagi, M., Nishimura, S., Yoshida, K., Kakinuma, T., Sawamura, T., Munakata, H., Hamanishi, C., 2006. Cyclic tensile stretch load and oxidized low density lipoprotein synergistically induce lectin-like oxidized ldl receptor-1 in cultured bovine chondrocytes, resulting in decreased cell viability and proteoglycan synthesis. J. Orthop. Res. 24(8), 1782-1790.

Ahrens, M., Ankenbauer, T., Schroder, D., Hollnagel, A., Mayer, H., Gross, G., 1993. Expression of human bone morphogenetic proteins-2 or -4 in murine mesenchymal progenitor C3H10T1/2 cells induces differentiation into distinct mesenchymal cell lineages. DNA Cell Biol. 12(10), 871-80.

Akagawa, Y., Ichikawa, Y., Nikai, H., Tsuru, H., 1993. Interface histology of unloaded and early loaded partially stabilized zirconia endosseous implant in initial bone healing. J. Prosthet. Dent. 69(6), 599-604.

Akimoto, K., Becker, W., Persson, R., Baker, D.A., Rohrer, M.D., O'Neal, R.B., 1999. Evaluation of titanium implants placed into simulated extraction sockets: a study in dogs. Int. J. Oral Max. Impl. 14, 351-360.

Alarcon, T., Byrne, H.M., Maini, P.K., 2005. A muliple scale model for tumor growth. Multiscale Mod. Sim. 3(2), 440-475.

Albrektsson, T., Sennerby, L., 1991. State of the art in oral implants. J. Clin. Periodontol. 18(6), 474-481.

Ambard, D., Swider, P., 2006. A predictive mechano-biological model of the bone-implant healing. Europ. J. Mech. - A/Solids 25(6), 927-937.

Ambrosi, D., Gamba, A., Serini, G., 2004. Cell directional and chemotaxis in vascular morphogenesis. Bull. Math. Biol. 66, 1851-1873.

Ament, C., Hofer, E.P., 2000. A fuzzy logic model of fracture healing. J. Biomech. 33(8), 961-968.

Amir, L.R., Becking, A.G., Jovanovic, A., Perdijk, F.B., Everts, V., Bronckers, A.L., 2006. Formation of new bone during vertical distraction osteogenesis of the human mandible is related to the presence of blood vessels. Clin. Oral Impl. Res. 17(4), 410-416.

Amor, N., Van Cleynenbreugel, T., Geris, L., Vander Sloten, J., Van Oosterwyck, H., 2006. Micro-macro mechanical modeling of bone-implant interface by means of the homogenization theory. In: Middleton, J., Jones, M.L., Shrive, N. (Eds.), Proceedings of the 7th international symposium on Computer Methods in Biomechanics and Biomedical Engineering, 22-25/3/2006, Antibes, France. CD-ROM-proceedings.

An, Y.H., Friedman, R.J., Draughn, R.A., 1999. Animal Models of Fracture or Osteotomy. In: An, Y.H., Friedman, R.J. (Eds.), Animal Models in Orthopaedic Research. CRC Press, Boca Raton, Fl. 197-218.

Anderson, A.R.A., Chaplain, M.A.J., 1998. Continuous and discrete mathematical models of tumor-induced angiogenesis. B. Math. Biol. 60, 857-900.

Anselme, K., 2000. Review: osteoblast adhesion on biomaterials. Biomat. 21, 667-681.

Aparicio, C., Rangert, B., Sennerby, L., 2003. Immediate/early loading of dental implants: a report from the Sociedad Espanola de Implantes World Congress consensus meeting in Barcelona, Spain, 2002. Clin. Implant Dent. Relat. Res. 5(1), 57-60.

Armstrong, C.G., Mow, V.C., 1982. Variations in the intrinsic mechanical properties of human articular cartilage with age, degeneration and water content. J. Bone Joint Surg. 64A, 88-94.

Arnold, J.S., Adam, J.A., 1999. A simplified model of wound healing II: The critical size defect in two dimensions. Math. Comput. Model. 30, 47-60.

Aspenberg, P., Goodman, S., Toksvig-Larsen, S., Ryd, L., Albrektsson, T., 1992. Intermittent micromotion inhibits bone ingrowth. Titanium implants in rabbits. Acta Orthop. Scand. 63(2), 141-145.

Athanasiou, K.A., Zhu, C.F., Lanctot, D.R., Agrawal, C.M., Wang, X., 2000. Fundamentals of biomechanics in tissue engineering of bone. Tis. Eng. 6(4), 361-81.

Attard, N.J., Zarb, G.A., 2005. Immediate and early implant loading protocols: a literature review of clinical studies. J. Prosthet. Dent. 94(3), 242-58.

Augat, P., Claes, L., 1997. Quantitative assessment of experimental fracture repair by peripheral computed tomography. Calc. Tis. Int. 60, 194-199.

Augat, P., Margevicius, K., Simon, J., Wolf, S., Suger, G., Claes, L., 1998. Local tissue properties in bone healing: influence of size and stability of the osteotomy gap. J. Orthop. Res 16(4), 475-481.

Augat, P., Burger, J., Schorlemmer, S., Henke, T., Peraus, M., Claes, L., 2003. Shear movement at the fracture site delays healing in a diaphyseal fracture model. J. Orthop. Res. 21, 1011-1017.

Bacabac, R.G., Smit, T.H., Mullender, M.G., Dijcks, S.J., Van Loon, J.J., Klein-Nulend, J., 2004. Nitric oxide production by bone cells is fluid shear stress rate dependent. Biochem. Biophys. Res. Commun. 315(4), 823-829.

Bailón-Plaza, A., van der Meulen, M.C.H., 2001. A mathematical framework to study the effects of growth factor influences on fracture healing. J. Theor. Biol. 212, 191-209.

Bailón-Plaza, A., van der Meulen, M.C.H., 2003. Beneficial effects of moderate, early loading and adverse effects of delayed or excessive loading on bone healing. J. Biomech. 36, 1069-1077.

Balshi, T.J., Wolfinger, G.J., 1997. Immediate loading of Branemark implants in edentulous mandibles: a preliminary report. Implant Dent. 6(2), 83-88.

Bancroft, G.N., Sikavitsas, V.I., van den Dolder, J., Sheffield, T.L., Ambrose, C.G., Jansen, J.A., Mikos, A.G., 2002. Fluid flow increases mineralized matrix deposition in 3D perfusion culture of marrow stromal osteoblasts in a dose-dependent manner. Proc. Natl Acad. Sci. 99(20), 12600-12605.

Barnes, G.L., Kostenuik, P.J., Gerstenfeld, L.C., Einhorn, T.A., 1999. Growth factor regulation of fracture repair. J. Bone Miner. Res. 14(11), 1805-1815.

Batra, N.N., Li, Y.L., Yellowley, C.E., You, L., Malone, A.M., Kim, C.H., Jacobs, C.R., 2005. Effects of short-term recovery periods on fluid-induced signaling in osteoblastic cells. J. Biomech. 38, 1909-1917.

Berglundh, T., Abrahamsson, I., Lang, N.P., Lindhe, J., 2003. De novo alveolar bone formation adjacent to endosseous implants. Clin. Oral Impl. Res. 14, 251-262.

Bland, Y.S., Critchlow, M.A., Ashhurst, D.E., 1999. The expression of the fibrillar collagen genes during fracture healing: heterogeneity of the matrices and differentiation of the osteoprogenitor cells. Histochem. J. 31, 797-809.

Bishop, N.E., Schneider, E., Ito, K., 2003. An experimental two degrees-of-freedom actuated external fixator for *in vivo* investigation of fracture healing. Med. Eng. Phys. 25(4), 335-40.

Bishop, N.E., van Rhijn, M., Tami, I., Corveleijn, R., Schneider, E., Ito, K., 2006. Shear Does Not Necessarily Inhibit Bone Healing. Clin. Orthop. Rel. Res. 443, 307-314.

Bolander, M.E., 1992. Regulation of fracture repair by growth factors. Proc. Soc. Exp. Biol. Med. 200, 165-170.

Bongrazio, M., Da Silva-Azevedo, L., Bergmann, E.C., Baum, O., Hinz, B., Pries, A.R., Zakrzewicz, A., 2006. Shear stress modulates the expression of thrombospondin-1 and CD36 in endothelial cells *in vitro* and during shear stress-induced angiogenesis *in vivo*. Int. J. Immunopathol. Pharmacol. 19(1), 35-48.

Botticelli, D., Berglundh, T., Buser, D., Lindhe, J., 2003a. Appositional bone formation in marginal defects at implants. Clin. Oral Impl. Res. 14, 1-9.

Botticelli, D., Berglundh, T., Buser, D., Lindhe, J., 2003b. The jumping distance revisited: An experimental study in the dog. Clin. Oral Impl. Res. 14, 35-42.

Botticelli, D., Berglundh, T., Lindhe, J., 2004. Hard-tissue alterations following immediate implant placement in extraction sites. J. Clin. Periodont. 31, 820-828.

Brooks, A.R., Lelkes, P.I., Rubanyi, G.M., 2002. Gene expression profiling of human aortic endothelial cells exposed to disturbed flow and steady laminar flow. Physiol. Genom. 9(1), 27-41.

Brownlow, H.C., Reed, A., Simpson, A.H.R.W., 2001. Growth factor expression during the development of atrophic non-union. Injury 32, 519-524.

Brownlow, H.C., Reed, A., Simpson, A.H.R.W., 2002. The vascularity of atrophic non-union. Injury 33, 145-150.

Bruder S.P. and Scaduto, T., 2005. Cell-based strategies for bone regeneration: from developmental biology to clinical therapy. In Bone Regeneration and Repair: Biology and Clinical Applications. Lieberman, J.R., Friedlaender, G.E. (Eds.). Humana Press Inc., Otowa NJ. 67-92.

Brunski, J.B., Moccia, A.F. Jr, Pollack, S.R., Korostoff, E., Trachtenberg, D.I., 1979. The influence of functional use of endosseous dental implants on the tissue-implant interface. II. Clinical aspects. J. Dent. Res. 58(10), 1970-1980.

Burger, E.H., Klein-Nulend, J., 1999. Mechanotransduction in bone–role of the lacuno-canalicular network. FASEB J. 13, S101-112.

Buser, D.A., Schroeder, A., Sutter, F., Lang, N.P., 1988. The new concept of ITI hollow-cylinder and hollow-screw implants: Part 2. Clinical aspects, indications, and early clinical results. Int. J. Oral Maxillofac. Implants 3(3), 173-181.

Buser, D., Schenk, R.K., Steinemann, S., Fiorellini, J.P., Fox, C.H., Stich, H., 1991. Influence of surface characteristics on bone integration of titanium implants. A histomorphometric study in miniature pigs. J. Biomed. Mater. Res. 25(7), 889-902.

Carano, R.A.D., Filvaroff, E.H., 2003. Angiogenesis and bone repair. Drugs Disc. Today 8(21), 980-989.

Carter, D.R., 1987. Mechanical loading history and skeletal biology, J. Biomech. 20, 1095-1109.

Carter, D.R., Blenman, P.R., Beaupré, G.S., 1988. Correlations between mechanical stress history and tissue differentiation in initial fracture healing. J. Orthop. Res. 6(5), 736-748.

Carter, D.R., Beaupré, G.S., Giori, N.J., Helms, J.A., 1998. Mechanobiology of skeletal regeneration. Clin. Orthop. Rel. Res. 355S, S41-S55.

Cañadell, J., Forriol, F. 1997. The external fixator in the treatment of infected pseudoarthrosis and bone defects. Osteosynthese Int. 5, 221-225.

Chai, B., Tang, X., Li, H., 1999. Osteogenic role played by fibroblasts in secondary healing of fracture. Chin. J. Traum. 2, 53-56.

Chaichanasiri, E., 2004. Simulation of bone healing in implant detistry. Master thesis, K.U.Leuven, Belgium.

Chao, E.Y.S., Inoue, N., Elias, J.J., Aro, H., 1998. Enhancement of fracture healing by mechanical and surgical intervention. Clin. Orthop. Rel. Res. 355S, 163-178.

Cheal, E.J., Mansmann, K.A., DiGioia III, A.M., Hayes, W.C., Perren, S.M., 1991. Role of interfragmentary strain in fracture healing: ovine model of a healing osteotomy. J. Orthop. Res. 9(1), 131-142.

Chen, B.P., Li, Y.S., Zhao, Y., Chen, K.D., Li, S., Lao, J., Yuan, S., Shyy, J.Y., Chien, S., 2001. DNA microarray analysis of gene expression in endothelial cells in response to 24-h shear stress. Physiol. Genom. 7(1), 55-63.

Chiapasco, M., Gatti, C., Rossi, E., Haefliger, W., Markwalder, T.H., 1997. Implant-retained mandibular overdentures with immediate loading. A retrospective multicenter study on 226 consecutive cases. Clin. Oral Implants Res. 8(1), 48-57.

Chien, S., Li, S., Shyy, Y.J., 1998. Effects of mechanical forces on signal transduction and gene expression in endothelial cells. Hypertension 31(1Pt2), 162-169.

Cho, T.-J., Gerstenfeld, L.C., Einhorn, T.A., 2002. Differential temporal expression of members of the transforming growth factor β superfamily during murine fracture healing. J. Bone Miner. Res. 17(3), 513-520.

Claes, L., Augat, P., Suger, G., Wilke, H.J., 1997. Influence of size and stability of the osteotomy gap on the success of fracture healing. J. Orthop. Res. 15(4), 577-584.

Claes, L.E., Heigele, C.A., Neidlinger-Wilke, C., Kaspar, D., Seidl, W., Margevicius, K.J., Augat, P., 1998. Effects of mechanical factors on the fracture healing process. Clin. Orthop. Rel. Res. 355S, S132-S147.

Claes, L.E., Heigele, C.A., 1999. Magnitudes of local stress and strain along bony surfaces predict the course and type of fracture healing. J. Biomech. 32(3), 255-266.

Claes, L., Eckert-Hübner, K., Augat, P., 2002. The effect of mechanical stabilizaty on local vascularization and tissue differentiation in callus healing. J. Orthop. Res. 20, 1099-1105.

Cochran, D.L., Morton, D., Weber, H.P., 2004. Consensus statements and recommended clinical procedures regarding loading protocols for endosseous dental implants. Int. J. Oral Maxillofac. Implants 19(Suppl), 109-113.

Coffey, R.J., Russell, W.E., Barnard, J.A., 1990. Pharmacokinetics of TGF beta with emphasis on effects in liver and gut. Ann. N.Y. Acad. Sci. 593, 285-291.

Colnot, C., Thompson, Z., Miclau, T., Werb, Z., Helms, J.A., 2003. Altered fracture repair in the absence of MMP9. Development 130, 4123-4133.

Colomina, L.E., 2001. Immediate loading of implant-fixed mandibular prostheses: a prospective 18-month follow-up clinical study–preliminary report. Implant Dent. 10(1), 23-29.

Corso, M., Sirota, C., Fiorellini, J., Rasool, F., Szmukler-Moncler, S., Weber, H.P., 1999. Clinical and radiographic evaluation of early loaded freestanding dental implants with various coatings in beagle dogs. J. Prosthet. Dent. 82(4), 428-435.

Coyle, C.H., Kader, K.N., 2007. Mechanisms of H2O2-induced oxidative stress in endothelial cells exposed to physiologic shear stress. ASAIO J. 53(1), 17-22.

Cramer, T., Schipani, E., Johnson, R.S., Swoboda, B., Pfander, D., 2004. Expression of VEGF isoforms by epiphyseal chondrocytes during low-oxygen tension is HIF-1alfa dependent. Osteoarthr. Cart. 12, 433-439.

Cruess, R.L., Dumont, J.R., 1985. Healing of Bone. In: Newton, C.D., Nunamaker, D.M. (Eds.), Textbook of small animal orthopaedics. International Veterinary Information Service, Ithaca, New York, USA.

Currey, J.D., 1995. The validation of algorithms used to explain adaptive remodelling in bone. In: Odgaard, A., Weinans, H. (Eds.), Bone structure and remodelling. World Scientific, Singapore, 9-13.

Dallon, J.C., Sherratt, J.A., Maini, P.K., 1999. Mathematical modelling of extracellular matrix dynamics using discrete cells: fiber orientation and tissue regeneration. J. Theor. Biol. 199, 449-471.

Dasch, J.R., Pace, D.R., Waegell, W., Inenaga, D., Ellingsworth, L., 1989. Monoclonal antibodies recognizing transforming growth factor-beta. Bioactivity neutralization and tansforming growth factor beta 2 affnity purification. J. Immunol. 142, 1536-1541.

Datta, N., Pham, Q.P., Sharma, U., Sikavitsas, V.I., Jansen, J.A., Mikos, A.G., 2006. *In vitro* generated extracellular matrix and fluid shear stress synergistically enhance 3D osteoblastic differentiation. Proc. Natl Acad. Sci. USA 103(8), 2488-2493.

Davies, P.F., Remuzzi, A., Gordon, E.J., Dewey, C.F. Jr, Gimbrone, M.A. Jr., 1986. Turbulent fluid shear stress induces vascular endothelial cell turnover *in vitro*. Proc. Natl Acad. Sci. USA 83(7), 2114-2117.

Davies, J.E., 2003. Understanding peri-implant endosseous healing. J. Dent. Educ. 67(8), 932-949.

Deckers, M.M., Karperien, M., van der Bent, C., Yamashita, T., Papapoulos, S.E., Lowik, C.W., 2000. Expression of vascular endothelial growth factors and their receptors during osteoblast differentiation. Endocrin. 141(5), 1667-1674.

De Smet, E., Jaecques, S.V., Wevers, M., Jansen, J.A., Jacobs, R., Sloten, J.V., Naert, I.E., 2006. Effect of controlled early implant loading on bone healing and bone mass in guinea pigs, as assessed by micro-CT and histology. Eur. J. Oral Sci. 114(3), 232-242.

De Smet, E., 2006. Mechanical determinants of bone (re)modelling around oral implants. PhD thesis, Katholieke Universiteit Leuven, Belgium.

Dickinson, R.B. and Tranquillo, R.T., 1993. A stochastic model for adhesion-mediated cell random motility and haptokinesis. J. Math. Biol. 31, 563-600.

Dimitriou R., Tsiridis, E., Giannoudis, P.V., 2005a. Current concepts of molecular aspects of bone healing. Injury 36(12), 1392-1404.

Dimitriou, R., Dahabreh, Z., Katsoulis, E., Matthews, S.J., Branfoot, T., Giannoudis, P.V., 2005b. Application of recombinant BMP-7 on persistent upper and lower limb non-unions. Injury 36(S4), S51-S59.

Dimmeler, S., Haendeler, J., Nehls, M., Zeiher, A.M., 1997. Suppression of apoptosis by nitric oxide via inhibition of interleukin-1beta-converting enzyme (ICE)-like and cysteine protease protein (CPP)-32-like proteases. J. Exp. Med. 185(4), 601-607.

Donahue, S.W., Donahue, H.J., Jacobs, C.R., 2003. Osteoblastic cells have refractory periods for fluid-flow-induced intracellular calcium oscillations for short bouts of flow and display multiple low-magnitude scillations during long-term flow. J. Biomech. 36, 35-43.

Donahue, T.L.H., Haut, T.R., Yellowley, C.E., Donahue, H.J., Jacobs, C.R., 2003. Mechanosensitivity of bone cells to oscilating fluid flow induced shear stress may be modulated by chemotransport. J. Biomech. 36, 1363-1371.

Duerrschmidt, N., Stielow, C., Muller, G., Pagano, P.J., Morawietz, H., 2006. JNO-mediated regulation of NAD(P)H oxidase by laminar shear stress in human endothelial cells. Physiol. 576(Pt 2), 557-567.

Duyck, J., De Cooman, M., Puers, R., Van Oosterwyck, H., Vander Sloten, J., Naert, I., 2004. A repeated sampling bone chamber methodology for the evaluation of tissue differentiation and bone adaptation around titanium implants under controlled mechanical conditions. J. Biomech. 37, 1819-1822.

Duyck, J., Vandamme, K., Geris, L., Van Oosterwyck, H., De Cooman, M., Vander Sloten, J., Puers, R., Naert, I., 2006. The influence of micro-motion on the tissue differentiation around immediately loaded cylindrical turned titanium implants. Arch. Oral Biol. 51, 1-9.

Edelman, E.R., Nugent, M.A., Karnovsky, M.J., 1993. Perivascular and intravenous administration of basic fibroblast growth factor: vascular and solid organ deposition. Proc. Natl Acad. Sci. USA. 90, 1513-1517.

Egginton, S., Zhou, A.L., Brown, M.D., Hudlicka, O., 2001. Unorthodox angiogenesis in skeletal muscle. Cardiovasc Res. 49(3), 634-646.

Einhorn, T.A., 1995. Enhancement of fracture healing. J. Bone Joint Surg. Am. 77, 940-956.

Einhorn, T.A., 1998. The cell and molecular biology of fracture healing. Clin. Orthop. Relat. Res. 355S, S7-S21.

Enomoto-Iwamoto, M., Iwamoto, M., Mukudai, Y., Kawakami, Y., Nohno, T., Higuchi, Y., Takemoto, S., Ohuchi, H., Noji, S., Kurisu, K., 1998. Bone morphogenetic protein signaling is required for maintenance of differentiatied phenotype, control of proliferation, and hypertrophy in chondrocytes. J. Cell Biol. 140, 409-418.

Evans, G.H., Mendez, A.J., Caudill, R.F., 1996. Loaded and nonloaded titanium versus hydroxyapatite-coated threaded implants in the canine mandible. Int. J. Oral. Maxillofac. Implants. 11(3), 360-371.

Fang, T.D., Salim, A., Xia, W., Nacamuli, R.P., Guccione, S., Song, H.M., Carano, R.A., Filvaroff, E.H., Bednarski, M.D., Giaccia, A.J., Longaker, M.T., 2005. Angiogenesis is required for successful bone induction during distraction osteogenesis. J. Bone Miner. Res. 20(7), 1114-1124.

Fedarko, N.S., D'Avis, P., Frazier, C.R., Burrill, M.J., Fergusson, V., Tayback, M., Sponseller, P.D., Shapiro, J.R., 1995. Cell proliferation of human fibroblasts and osteoblasts in osteogenesis imperfecta: influence of age. J. Bone Miner. Res. 10(11), 1705-1712.

Fiedler, J., Etzel, N., Brenner, R., 2004. To go or not to go: migration of human mesenchymal progenitor cells stimulated by isoforms of PDGF. J. Cell. Biochem. 93, 990-998.

Fiedler, J., Leucht, F., Waltenberger, J., Dehio, C., Brenner, R.E., 2005. VEGF-A and PlGF-1 stimulate chemotactic migration of human mesenchymal progenitor cells. Biochem. Biophys. Res. Comm. 334, 561-568.

Filion, R.J. and Popel, A.S., 2004. A Reaction-Diffusion Model of Basic Fibroblast Growth Factor Interactions with Cell Surface Receptors. Ann. Biomed. Eng. 32, 645-663.

Fiorelli, G., Orlando, C., Benvenuti, S., Franceschelli, F., Bianchi, S., Pioli, P., Tanini, A., Serio, M., Bartucci, F., Brandi, M.L. 1994. Characterization, regulation, and function of specific cell membrane receptors for insulin-like growth factor I on bone endothelial cells. J. Bone Miner. Res. 9, 329-337.

Folkman, J., Shing, Y., 1992. Angiogenesis. J. Biol. Chem. 267, 10931-10934.

Franchi, M., Orsini, E., Trire, A., Quaranta, M., Martini, D., Piccari, G.G., Ruggeri, A., Ottani, V., 2004. Osteogenesis and morphology of the peri-implant bone facing dental implants. Scient. World J. 14, 1083-1095.

Franchi, M., Fini, M., Martini, D., Orsini, E., Leonardi, L., Ruggeri, A., Giavaresi, G., Ottani, V., 2005. Biological fixation of endosseous implants. Micron 36, 665-671.

Frank, O., Heim, M., Jakob, M., Barbero, A., Schafer, D., Bendik, I., Dick, W., Heberer, M., Martin, I., 2002. Real-time quantitative RT-PCR analysis of human bone marrow stromal cells during osteogenic differentiation *in vitro*. J. Cell. Biochem. 85(4), 737-746.

Friedl, P., Zänker, K.S., Bröcker, E.B., 1998. Cell migration strategies in 3-d extracellular matrix: differences in mophology, cell matrix interactions, and integrin function. Micros. Res. Tech. 43, 369-378.

Friedlaender, G.E., Perry, C.R., Cole, J.D., Cook, S.D., Cierny, G., Muschler, G.F., Zych, G.A., Calhoun, J.H., LaForte, A.J., Yin, S., 2001. Osteogenic protein-1 (bone morphogenetic protein-7) in the treatment of tibial nonunions. J. Bone Joint Surg. Am. 83-A(S1(Pt2)), S151-S158.

Gaffney, E.A., Maini, P.K., Sherratt, J.A., Ruft, S., 1999. The mathematical modelling of cell kinetics in corneal epithelial wound healing. J. Theor. Biol. 197, 15-40.

Garcia-Cardena, G., Comander, J., Anderson, K.R., Blackman, B.R., Gimbrone, M.A. Jr., 2001. Biomechanical activation of vascular endothelium as a determinant of its functional phenotype. Proc. Natl Acad. Sci. USA 98(8), 4478-4485.

Gardner, M.J., van der Meulen, M.C., Demetrakopoulos, D., Wright, T.M., Myers, E.R., Bostrom, M.P., 2006. *in vivo* cyclic axial compression affects bone healing in the mouse tibia. J Orthop Res. 24(8), 1679-86.

Gapski, R., Wang, H.L., Mascarenhas, P., Lang, N.P., 2003. Critical review of immediate implant loading. Clin. Oral Impl. Res. 14, 515-527.

Gerber, H.-P., Vu, T.H., Ryan, A.M., Kowalski, J., Werb, Z., Ferrara, N., 1999. VEGF couples hypertrophic cartilage remodeling, ossification and angiogenesis during endochondral bone formation. Nat. Med. 5, 623-628.

Geris, L., Van Oosterwyck, H, Vander Sloten, J., Duyck, J., Naert, I., 2003. Assessment of Mechanobiological Models for the Numerical Simulation of Tissue Differentiation around Immediately Loaded Implants. Comp. Meth. Biomech. Biomed. Eng. 6, 277-288.

Geris, L., Andreykiv, A., Van Oosterwyck, H., Vander Sloten, J., van Keulen, F., Duyck, J., Naert, I., 2004. Numerical simulation of tissue differentiation around loaded titanium implants in a bone chamber. J. Biomech. 37, 763-769.

Geris, L., Gerisch, A., Maes, c., Carmeliet, G.,Weiner, R., Vander Sloten, J., Van Oosterwyck, H., 2006. Mathematical modeling of fracture healing in mice: Comparison between experimental data and numerical simulation results. Med. Biol. Eng. Comp. 44(4), 280-289.

Geris, L., Vandamme, K., Naert, I., Vander Sloten, J., Duyck, J., Van Oosterwyck, H., 2007. Application of mechanoregulatory models to simulate peri-implant tissue formation in an *in vivo* bone chamber. J. Biomech., Submitted for publication.

Gerisch, A., 2001. Numerical methods for the simulation of taxis-diffusion-reaction systems. PhD thesis, Martin-Luther-Universität Halle-Wittenberg, Germany.

Gerisch, A., Chaplain, M.A.J., 2005. Robust numerical methods for taxis-diffusion-reaction systems: applications to biomedical problems. Math. Comput. Model. 43, 49-75.

Gerisch A. and Geris L., 2007. A finite volume spatial discretisation for taxis-diffusion-reaction systems with axi-symmetry: application to fracture healing. In: Deutsch, A., Brusch, L., Byrne, H., de Vries, G., Herzel, H.-P. (Eds.), Advances in Mathematical Modeling of Biological Systems, Volume I, Birkhäuser, Boston, pp 303-316, ISBN 0-8176-4557-8.

Gerstenfeld, L.C., Cullinane, D.M., Barnes, G.L., Graves, D.T., Einhorn, T.A., 2003a. Fracture healing as a post-natal developmental process: molecular, spatial, and temporal aspects of its regulation. J. Cell. Biochem. 88, 873-884.

Gerstenfeld, L.C., Cho, T.-J., Kon, T., Aizawa, T., Tsay, A., Fitch, J., Barnes, G.L., Graves, D.T., Einhorn, T.A., 2003b. Impaired fracture healing in the absence of TNF-α signaling: the role of TNF-α in endochondral cartilage resorption. J. Bone Miner. Res. 18(9), 1584-1592.

Ghosh, K., Pan, Z., Guan, E., Ge, S., Liu, Y., Nakamura, T., Ren, X.D., Rafailovich, M., Clark, R.A., 2007. Cell adaptation to a physiologically relevant ECM mimic with different viscoelastic properties. Biomat 28(4), 671-679.

Giannoudis, P.V., Tzioupis, C., 2005. Clinical applications of BMP-7: the UK perspective. Injury 36(S3), S47-S50.

Glowacki, J., 1998. Angiogenesis in fracture repair. Clin. Orthop. Rel. Res. 355S, S82-S89.

Goodship, A.E., Kenwright, J., 1985. The influence of induced micromovement upon the healing of experimental tibial fractures. J. Bone Joint Surg. Br. 67B, 650-655.

Goodship, A.E., 1992. Mechanical stimulus to bone. Ann. Rheum. Dis. 51, 4-6.

Goodship, A.E., Cunningham, J.L., Kenwright, J., 1998. Strain rate and timing of stimulation in mechanical modulation of fracture healing. Clin. Orthop. Rel. Res. 355S, 105-115.

Gómez-Benito, M.J., García-Aznar, J.M., Kuiper, J.H., Doblaré, M., 2005. Influence of fracture gap size on the pattern of long bone healing: a computational study. J. Theor. Biol. 235, 105-119.

Grad, S., Lee, C.R., Wimmer, M.A., Alini, M., 2006. Chondrocyte gene expression under applied surface motion. Biorheol. 43(3-4), 259-269.

Gross, U.M., 1988. Biocompatibility: the interaction of biomaterials and host response. J. Dent. Educ. 52, 798- 803.

Gruler, H. and Bültmann, B.D., 1984. Analysis of cell movement. Blood cells 10, 61-77.

Guenther, H.L., Fleisch, H., Sorgente, N., 1986. Endothelial cells in culture secrete a potent bone cell active mitogen. Endocrin. 119, 193-201.

Hadjiargyrou, M., Lombardo, F., Zhao, S., Ahrens, W., Joo, J., Ahn, H., Jurman, M., White, D.W., Rubin, C.T., 2002. Transcriptional profiling of bone regeneration. J. Biol. Chem. 277(33), 30177-30182.

Hall, A.C., Urban, J.P., Gehl, K.A., 1991. The effects of hydrostatic pressure on matrix synthesis in articular cartilage. J. Orthop. Res. 9, 1-10.

Hansen, U., Schunke, M., Domm, C., Ioannidis, N., Hassenpflug, J., Gehrke, T., Kurz, B., 2001. Combination of reduced oxygen tension and intermittent hydrostatic pressure: a useful tool in articular cartilage tissue engineering. J. Biomech. 34, 941-949.

Hansson, H.A., Albrektsson, T., Brånemark, P.I., 1983. Structural aspects of the interface between tissue and titanium implants. J. Prosthet. Dent. 50(1), 108-113.

Harrison, L.J., Cunningham, J.L., Strömberg, L., Goodship, A.E., 2003. Controlled induction of a pseudarthrosis: a sudy using a rodent model. J. Orthop. Trauma 17, 11-21.

Hart, R.T. (2001), Bone Modeling and remodeling: theories and computation. In Cowin, S.C. (Ed.), Bone mechanics handbook, CRC Press LCC, Boca Raton, Florida, 31.1-31.42.

Hashimoto, M., Akagawa, Y., Nikai, H., Tsuru, H., 1988. Single-crystal sapphire endosseous dental implant loaded with functional stress–clinical and histological evaluation of peri-implant tissues. J. Oral Rehabil. 15(1), 65-76.

Helm, C.E., Fleury, M.E., Zisch, A.H., Boschetti, F., Swartz, M.A., 2005. Synergy between interstitial flow and VEGF directs capillary morphogenesis *in vitro* through a gradient amplification mechanism. P. Natl Acad. Sci. USA 102, 15779-15784.

Henle, P., Zimmermann, G., Weiss, S., 2005. Matrix metalloproteinases and failed fracture healing. Bone 37, 791-798.

Henté, R., Füchtmeier, B., Schlegel, U., ErnstBerger, A., Perren, S.M., 2004. The influence of cyclic compression and distraction on the healing of experimental tibial fractures. J. Orthop. Res. 22, 709-715.

Hermann, C., Zeiher, A.M., Dimmeler, S., 1997. Shear stress inhibits H2O2-induced apoptosis of human endothelial cells by modulation of the glutathione redox cycle and nitric oxide synthase. Arterioscler. Thromb. Vasc. Biol. 17(12), 3588-3592.

Hobkirk, J.A., Wiskott, H.W. On behalf of Working Group 1, 2006. Biomechanical aspects of oral implants. Clin Oral Implants Res. 17(Suppl 2), 52-54.

Holtorf, H.L., Jansen, J.A., Mikos, A.G., 2005. Flow perfusion culture induces the osteoblastic differentiation of marrow stroma cell-scaffold constructs in the absence of dexamethasone. J. Biomed. Mater. Res. A. 72(3), 326-334.

Honda, K., Ohno, S., Tanimoto, K., Ijuin, C., Tanaka, N., Doi, T., Kato, Y., Tanne, K., 2000. The effects of high magnitude cyclic tensile load on cartilage matrix metabolism in cultured chondrocytes. Eur. J. Cell Biol. 79(9), 601-309.

Hori, R.Y., Lewis, J.L., 1982. Mechanical properties of the fibrous tissue found at the bone-cement interface following total joint replacement. J. Biomed. Mater. Res. 16, 911-927.

Huiskes, R., Van Driel, W.D., Prendergast, P.J., Søballe, K., 1997. A biomechanical regulatory model for periprosthetic fibrous-tissue differentiation. J. Mater. Sci.: Mat. Med. 8, 785-788.

Hulth, A., 1989. Current concepts of fracture healing. Clin. Orthop. 249, 265-284.

Hundsdorfer, W., Verwer, J.G., 2003. Numerical Solution of Time-Dependent Advection-Diffusion-Reaction Equations. Springer Series in Computational Mathematics 33, Springer Verlag.

Hunter, C.J., Imler, S.M., Malaviya, P., Nerem, R.M., Levenston, M.E., 2002. Mechanical compression alters gene expression and extracellular matrix synthesis by chondrocytes cultured in collagen I gels. Biomat. 23(4), 1249-1259.

Idelsohn, S., Planell, J.A., Gil, F.J., Lacroix, D., 2006. Development of a dynamic mechano-regulation model based on shear strain and fluid flow to optimize distraction osteogenesis. J. Biomech. 39 S1, S9-S10.

Ignatius, A., Blessing, H., Liedert, A., Schmidt, C., Neidlinger-Wilke, C., Kaspar, D., Friemert, B., Claes L., 2005. Tissue engineering of bone: effects of mechanical strain on osteoblastic cells in type I collagen matrices. Biomat. 26, 311-318.

Isaksson, H., Wilson, W., van Donkelaar, C., Huiskes, R., Ito, K., 2006a. Comparison of biophysical stimuli for mechano-regulation of tissue differentiation during fracture healing. J. Biomech. 39, 1507-1516.

Isaksson, H., van Donkelaar, C., Huiskes, R., Ito, K., 2006b. Corroboration of mechanoregulatory algorithms for tissue differentiation during fracture healing: comparison with *in vivo* results. J. Orthop. Res. 24, 898-907.

Isaksson, H., Comas, O., van Donkelaar, C., Mediavilla, J., Wilson, W., Huiskes, R., Ito, K., 2006c. Bone regeneration during distraction osteogenesis: Mechano-regulation by shear strain and fluid velocity. J. Biomech., available online.

Jacobs,C.R., Yellowley, C.E., Davis, B.R., Zhou, Z., Cimbala, J.M., Donahue, H.J., 1998. Differential effect of steady versus oscillating flow on bone cells. J. Biomech 31, 969-976.

Jaffin, R.A., Kumar, A., Berman, C.L., 2000. Immediate loading of implants in partially and fully edentulous jaws: a series of 27 case reports. J. Periodontol. 71(5), 833-838.

Jagodzinski, M., Drescher, M., Zeichen, J., Hankemeier, S., Krettek, C., Bosch, U., van Griensven, 2004. Effects of cyclic longitudinal mechanical strain and dexamthasone on osteogenic differentiation of human bone marrow stromal cells. Europ. Cells Mat. 7, 35-41.

Jaiswal, N., Haynesworth, S.E., Caplan, A.I., Bruder, S.P., 1997. Osteogenic differentiation of purified, culture-expanded human mesenchymal stem cells *in vitro*. J. Cell. Biochem. 64(2), 295-312.

Jin, X., Mitsumata, M., Yamane, T., Yoshida, Y., 2001. Induction of human inhibitor of apoptosis protein-2 by shear stress in endothelial cells. FEBS Lett. 529(2-3), 286-292.

Johnson, E.E., Urist, M.R., 1998. One-stage lengthening of femoral nonunion augmented with human bone morphogenetic protein. Clin. Orthop. Relat. Res. 347, 105-116.

Joyce, M.E., Terek, R.M., Jingushi, S., Bolander, M.E., 1990. Role of transforming growth factor-b in fracture repair. Ann. N. Y. Acad. Sci. 593, 107-123.

Jurvelin, J.S., Buschmann, M.D., Hunziker, E.B., 1997. Optical and mechanical determination of poisson's ratio of adult bovine humeral articular cartilage. J. Biomech. 30, 235-241.

Kadohama, T., Akasaka, N., Nishimura, K., Hoshino, Y., Sasajima, T., Sumpio, B.E., 2006. p38 Mitogen-activated protein kinase activation in endothelial cell is implicated in cell alignment and elongation induced by fluid shear stress. Endothelium 13(1), 43-50.

Kamioka, H., Sugawara, Y., Murshid, S.A., Ishihara, Y., Honjo, T., Takano-Yamamoto, T.J., 2006. Fluid shear stress induces less calcium response in a single primary osteocyte than in a single osteoblast: implication of different focal adhesion formation. Bone Miner. Res. 21(7), 1012-1021.

Kaspar, D., Seidl, W., Neidlinger-Wilke, C., Ignatius, A., Claes, L., 2000. Dynamic cell stretching increases human osteoblast proliferation and CICP synthesis but decreases osteocalcin synthesis and alkaline phosphatase activity. J. Biomech. 33, 45-51

Kasperk, C.H., Börcsök, I., Schairer, H.U., Schneider, U., Nawroth, P.P., Niethard, F.U., Ziegler, R., 1997. Endothelin-1 is a potent regulator of human bone cell metabolism *in vitro*. Calcif. Tissue Int. 60, 368-374.

Kearney, E.M., Prendergast, P.J., Campbell, V.A., 2006. The influence of mechanical strain on the proliferation of adult marrow stromal cells. Presented at the Scientific Advisory Board Review, Trinity College Dublin, 2006.

Keaveny, T.M., Wachtel, E.F., Ford, C.M., Hayes, W.C., 1994. Differences between the tensile and compressive strengths of bovine tibial trabecular bone depend on modulus. J. Biomech. 27(9), 1137-46.

Kelly, D.J., Prendergast, P.J., 2005. Mechano-regulation of stem cell differentiation and tissue regeneration in osteochondral defects. J. Biomech. 38, 1413-1422.

Kenwright, J., Richardson, J.B., Cunningham, J.L., White, S.H., Goodship, A.E., Adams, M.A., Magnussen, P.A., Newman, J.H., 1991. Axial movement and tibial fractures. A controlled randomised trial of treatment. J. Bone Joint Surg. Br. 73B, 654-659.

Kenwright, J., Gardner, T. 1998. Mechanical influences on tibial fracture healing. Clin. Orthop. Rel. Res. 355S, 179-190.

Kirchen, M.E., O'Connor, K.M., Gruber, H.E., Sweeney, J.R., Fras, I.A., Stover, S.J., Sarmiento, A., Marshall, G.J., 1995. Effects of microgravity on bone healing in a rat fibular osteotomy model. Clin. Orthop. Relat. Res. 318, 231-242.

Kirsch, A., Donath, K., 1984. Tierexperimentelle untersuchungen zur bedeutung der mikromorphologie von titanimplantatoberflächen. Fortschr. Zahnärztl. Implantol. 1, 35-40.

Kitano, H., 2002. Computational systems biology. Nature 420, 206-210.

Klein, P., Schell, H., Streitparth, F., Heller, M., Kassi, J.P., Kandziora, F., Bragulla, H., Haas, N.P., Duda, G.N., 2003. The initial phase of fracture healing is specifically sensitive to mechanical conditions. J. Orthop. Res. 21, 662-669.

Knippenberg, M., Helder, M.N., Doulabi, B.Z., Semeins, C.M., Wuisman, P.I., Klein-Nulend, J., 2005. Adipose tissue-derived mesenchymal stem cells acquire bone cell-like responsiveness to fluid shear stress on osteogenic stimulation. Tissue Eng. 11(11-12), 1780-1788.

Knoll, B.I., McCarthy, T.L., Centrella, M., Shin, J., 2005. Strain-dependent control of transforming growth factor-beta function in osteoblasts in an *in vitro* model: biochemical events associated with distraction osteogenesis. Plast. Reconstr. Surg. 116(1), 224-33.

Kokubu, T., Hak, D.J., Hazelwood, S.J., Reddi, A.H., 2003. Development of an atrophic nonunion model and comparison to a closed healing fracture in rat femur. J. Orthop. Res. 21, 503-510.

Kreke, M.R., Huckle, W.R., Goldstein, A.S., 2005. Fluid flow stimulates expression of osteopontin and bone sialoprotein by bone marrow stromal cells in a temporally dependent manner. Bone 36(6), 1047-1055.

Kuiper, J.H., Ashton, B.A., Richardson, J.B., 2000. Computer simulation of fracture callus formation and stiffness restoration. In: Proceedings of the 12th conference of the ESB. European Society of Biomechanics, Dublin.

Kuntz, R.M., Saltzman, W.M., 1997. Neutrophil motility in extra-cellular matrix gels: mesh size and adhesion affect speed of migration. Biophys. J. 72(3), 1472-1480.

Kurpinski, K., Chu, J., Hashi, C., Li, S., 2006. Anisotropic mechanosensing by mesenchymal stem cells. Proc. Natl Acad. Sci. USA 103(44), 16095-16100.

Lacroix, D., 2000. Simulation of tissue differentiation during fracture healing. PhD thesis, Trinity College Dublin, Ireland.

Lacroix, D., Prendergast, P.J., 2002. A mechano-regulation model for tissue differentiation during fracture healing: analysis of gap size and loading. J. Biomech. 35, 1163-1171.

Lacroix, D., Prendergast, P.J., Li, G., Marsh, D., 2002b. Biomechanical model to simulate tissue differentiation and bone regeneration: application to fracture healing. Med. Biol. Eng. Comp. 40, 14-21.

Lahiji, K., Polotsky, A., Hungerford, D.S., Frondoza, C.G., 2004. Cyclic strain stimulates proliferative capacity, alpha2 and alpha5 integrin, gene marker expression by human articular chondrocytes propagated on flexible silicone membranes. *in vitro* Cell. Dev. Biol. Anim. 40(5-6), 138-142.

Lammi, M.J., Inkinen, R., Parkkinen, J.J., Häkkinen, T., Jortikka, M., Nelimarkka, L.O., Järveläinen, H.T., Tammi, M.I., 1994. Expression of reduced amounts of structurally altered aggrecan in articular cartilage chondrocytes exposed to high hydrostatic pressure. Biochem. J. 304, 723-730.

Landry, P.S., 2000. Effect of soft-tissue trauma on the early periosteal response of bone to injury. J. Trauma 48, 479-483.

Laplantine, E., Rossi, F., Sahni, M., Basilico, C., Cobrinik, D., 2002. FGF signaling targets the pRb-related p107 and p130 proteins to induce chondrocyte growth arrest. J. Cell Biol. 158, 741-750.

Le, A.X., Miclau, T., Hu, D., Helms, J.A., 2001. Molecular aspects of healing in stabilized and non-stabilized fractures. J. Orthop. Res. 19(1), 78-84.

Lee, T.-Y.J., Gotlieb, A.I., 1999. Early stages of endothelial wound repair: conversion of quiescent to migrating endothelial cells involves tyrosine phosphorylation and actin microfilament reorganization. Cell Tissue Res. 297, 435-450.

Lee, M.S., Trindade, M.C., Ikenoue, T., Schurman, D.J., Goodman, S.B., Smith, R.L., 2002. Effects of shear stress on nitric oxide and matrix protein gene expression in human osteoarthritic chondrocytes *in vitro*. J. Orthop. Res. 20(3), 556-561.

Lee, M.S., Trindade, M.C., Ikenoue, T., Schurman, D.J., Goodman, S.B., Smith, R.L., 2003. Intermittent hydrostatic pressure inhibits shear stress-induced nitric oxide release in human osteoarthritic chondrocytes *in vitro*. J. Rheumatol. 30(2), 326-328.

Lefkove, M.D., Beals, R.P., 1990. Immediate loading of cylinder implants with overdentures in the mandibular symphysis: the titanium plasma-sprayed screw technique. J. Oral Implantol. 16(4), 265-271.

Leucht, P., Kim, J.B., Wazen, R., Currey, J.A., Nanci, A., Brunski, J.B., Helms, J.A., 2007. Effect of mechanical stimuli on skeletal regeneration around implants. Bone, In press.

Levesque, M.J., Nerem, R.M., Sprague, E.A., 1990. Vascular endothelial cell proliferation in culture and the influence of flow. Biomat. 11(9), 702-707.

Levine, H.A., Pamuk, S., Sleeman, B.D., Nilsen-Hamilton, M., 2001. Mathematical modelling of capillary formation and development in tumor angiogenesis: penetration into the stroma. B. Math. Biol. 63, 801-863.

Li, Y.J., Batra, N.N., You, L., Meier, S.C., Coe, I.A., Yellowley, C.E., Jacobs, C.R., 2004. Oscillatory fluid flow affects human marrow stromal cell proliferation and differentiation. J. Orthop. Res. 22, 1283-1289.

Li, G., Cui, Y., McIlmurray, L., Allen, W.A., Wang, H., 2005a. rhBMP-2, rhVEGF165, rhPTN and thrombin-related peptide, TP508 induce chemotaxis of human osteoblasts and microvascular endothelial cells. J. Orthop. Res. 23, 680-685.

Li, Y.S., Haga, J.H., Chien, S., 2005b. Molecular basis of the effects of shear stress on vascular endothelial cells. J. Biomech. 38(10), 1949-1971.

Lieberman, J.R., Dluiski, A., Einhor, T.A., 2002. The role of growth factors in the repair of bone: biology an clinical applications. J. Bone Joint Surg. 84A(6), 1032-1044.

Lienau, J., Schell, H., Duda, G.N., Seebeck, P., Muchow, S., Bail, H.J., 2005. Initial vascularization and tissue differentiation are influenced by fixation stability. J Orthop Res. 23(3), 639-645.

Lienau, J., Schell, H., Epari, D.R., Schutze, N., Jakob, F., Duda, G.N., Bail, H.J, 2006. CYR61 (CCN1) protein expression during fracture healing in an ovine tibial model and its relation to the mechanical fixation stability. J. Orthop. Res. 24(2), 254-262.

Lind, M., Eriksen, E.F., Bü, C., 1996. Bone Morphogenetic protein-2 but not bone morphogenetic protein-4 and -6 stimulates chemotactic migration of human osteoblasts, human marrow osteoblasts, and U2-OS cells. Bone 18, 53-57.

Lippiello, L., Kaye, C., Neumata, T., Mankin, H.J., 1985. *In vitro* metabolic response of articular cartilage segments to low levels of hydrostatic pressure. Connect. Tissue Res. 13, 99-107.

Loboa, E.G., Beaupré, G.S., Carter, D.R., 2001. Mechanobiology of initial pseudarthrosis formation with oblique fractures. J Orthop Res. 19, 1067-1072.

Lu, C., Miclau, T., Hu, D., Marcucio, R.S., 2007. Ischemia leads to delayed union during fracture healing: a mouse model. J. Orthop. Res. 25(1),51-61.

Luo, Q., Kang, Q., Si, W., Jiang, W., Park, J.K., Peng, Y., Li, X., Luu, H.H., Luo, J., Montag, A.G., Haydon, R.C., He, T.C., 2004. Connective tissue growth factor (CTGF) is regulated by Wnt and bone morphogenetic proteins signaling in osteoblast differentiation of mesenchymal stem cells. J. Biol. Chem. 279(53), 55958-55968.

Lutolf, M.P., Lauer-Fields, J.L., Schmoekel, H.G., Metters, A.T., Weber, F.E., Fields, G.B., Hubbell, J.A., 2003. Synthetic matrix metalloproteinase-sensitive hydrogels for the conduction of tissue regeneration: engineering cell-invasion characteristics. Proc. Natl Acad. Sci. 100(9), 5413-5418.

Luu, H.H., Song, W.X., Luo, X., Manning, D., Luo, J., Deng, Z.L., Sharff, K.A., Montag, A.G., Haydon, R.C., He, T.C., 2007. Distinct roles of bone morphogenetic proteins in osteogenic differentiation of mesenchymal stem cells. J. Orthop. Res., available online.

Maeda, S., Nishida, J., Sato, T., Inomata, Y., Shimamura, T., Horiuchi, S., 2005. Changes in microstructure and gene expression of articular chondrocytes cultured in a tube under mechanical stress. Osteoarthr. Cart. 13(2), 154-161.

Maes, C., Carmeliet, P., Moermans, K., Stockmans, I., Smets, N., Collen, D., Bouillon, R., Carmeliet, G., 2002. Impaired angiogenesis and endochondral bone formation in mice lacking the vascular endothelial growth factor isoforms VEGF164 and VEGF188. Mech. Dev. 111, 61-73.

Maes, C., 2004. Angionensis and bone: the role of the vascular endothelial growth factor family in bone development and repair. PhD thesis (Acta Biomedica Lovaniensia 310), Leuven University Press, Leuven, Belgium.

Maes, C., Coenegrachts, L., Stockmans, I., Daci, E., Luttun, A., Petryk, A., Gopalakrishnan, R., Moermans, K., Smets, N., Verfaillie, C.M., Carmeliet, P., Bouillon, R., Carmeliet, G., 2006. Placental growth factor mediates mesenchymal cell development, cartilage turnover, and bone remodeling during fracture repair. J. Clin. Invest. 116, 1230-1242.

Maheshwari, G., Lauffenburger, D.A., 1998. Deconstructing (and reconstructing) cell migration, Micr. Res. Tech. 43, 358-368.

Maheswari, G., Wells, A., Griffith, L.G., Lauffenburger, D.A., 1999. Biophysical integration of effects of epidermal growth factor and fibronectin on fibroblast migration. Biophys. J. 76, 2814-2823.

Makino, T., Hak, D.J., Hazelwood, S.J., Curtiss, S., Reddi, H.A., 2005. Prevention of atrophic nonunion development by recombinant human bone morphogenetic protein-7. J. Orthop. Res. 23, 632-638.

Malek, A.M., Izumo, S., 1995. Control of endothelial cell gene expression by flow. J. Biomech. 28(12), 1515-1528.

Malizos, K.N., Papatheodorou, L.K., 2005. The healing potential of the periosteum, molecular aspects. Injury 36S, S13-S19.

Marsh, D., Buckwalter, J.A., McCollister-Evarts, C., 1994. Delayed union, nonunion, malunion and avascular necrosis. In Epps, C.H. (Eds.), Complications in Orthopaedic Surgery. JB Lippinscott, Philadelphia, 183-211.

Marsh, D., 1998. Concepts of fracture union, delayed union, and nonunion. Clin. Orthop. S355, S22-S30.

Martin, R.B., Burr, D.B., Sharkey, N.A., 1998. Skeletal tissue mechanics. Springer-Verlag, NY.

Mayer, H., Bertram, H., Lindenmaier, W., Korff, T., Weber, H., Weich, H., 2005. Vascular endothelial growth factor (VEGF-A) expression in human mesenchymal stem cells: autocrine and paracrine role on osteoblastic and endothelial differentiation. J. Cell. Biochem. 95, 827-839.

Mayr-Wohlfart, U., Waltenberger, J., Hausser, H., Kessler, S., Günther, K.-P., Dehio, C., Puhl, W., Brenner, R.E., 2002. Vascular endothelial growth factor stimulates chemotactic migration of primary human osteoblasts. Bone 30, 472-477.

McCormick, S.M., Eskin, S.G., McIntire, L.V., Teng, C.L., Lu, C.M., Russell, C.G., Chittur, K.K., 2001. DNA microarray reveals changes in gene expression of shear stressed human umbilical vein endothelial cells. Proc. Natl Acad. Sci. USA 98(16), 8955-8960.

McDougall, S.R., Anderson, A.R.A., Chaplain, M.A.J., Sherratt, J.A., 2002. Mathematical modelling of flow through vascular networks: implications for tumour-induced angiogenesis and chemotherapy strategies. B. Math. Biol. 64, 673-702.

McKibbin, B., 1978. The biology of fracture healing in long bones. J. Bone Joint Surg. Br. 60-B, 150-162.

McMahon, L.A., Reid, A.J., Campbell, Prendergast, P.J., 2006. Investigation into the effect of growth factors and mechanical strain on the chondrogenesis of marrow stromal cells. Presented at the Scientific Advisory Board Review, Trinity College Dublin, 2006.

Metheny-Barlow, L.J., Tian, S., Hayes, A.J., Li, L.Y., 2004. Direct chemotactic action of angiopoietin-1 on mesenchymal cells in th epresence of VEGF. Microvasc. Res. 68, 221-230.

Meyer, U., Joos, U., Mythili, J., Stamm, T., Hohoff, A., Fillies, T., Stratmann, U., Wiesmann, H.P., 2004. Ultrastructural characterization of the implant/bone interface of immediately loaded dental implants. Biomat. 25, 1959-1967.

Michaeli, Y., Shamir, D., Weinreb, M., Steigman, S., 1994. Effect of loading on the migration of periodontal fibroblasts in the rat incisor. J Periodontal Res. 29(1), 25-34.

Miclau, T., Thompson, Z., Colnot, C., 2000. The effect of fracture stability on the expression of angiogenic factors during fracture repair. Orthop. Trauma Ass., San Antonio 2000, 16, 1210.

Miclau, T., Thompson, Z., Colnot, C., Huang, S., Werb, Z., Helms, J.A., 2002. The effect of early stability on fracture repair. Trans. Orthop. Res. Soc. 27, 0709.

Miclau, T., Lu, C., Thompson, Z., Choi, P., Colnot, C., Werb, Z., Helms, J.A., 2004. The effect of varying time to stabilization on fracture repair. Trans. Orthop. Res. Soc. 29, 0483.

Midy, V., Plouet, J., 1994. Vasculotropin/vascular endothelial growth factor induces differenatiation in cultured osteoblasts. Biochem. Biophys. Res. Comm. 199, 380-386.

Misch, C.E., 1999. Implant design considerations for the posterior regions of the mouth. Implant Dent. 8(4), 376-386.

Misch, C.E., Hahn, J., Judy, K.W., Lemons, J.E., Linkow, L.I., Lozada, J.L., Mills, E., Misch, C.M., Salama, H., Sharawy, M., Testori, T., Wang, H.L., 2004. Immediate Function Consensus Conference. Workshop guidelines on immediate loading in implant dentistry. November 7, 2003. J. Oral Implantol. 30(5), 283-288.

Mitsumata, M., Nerem, R.M., Alexander, R.W., Berk, B., 1997. Shear stress inhibits endothelial cell proliferation by growth arrest in the G0/G1 phase of the cell cycle, FASEB J. 5, A527.

Mizuno, M., Kuboki, Y., 2001. Osteoblast-related gene expression of bone marrow cells during the osteoblastic differentiation induced by type I collagen. J. Biochem. (Tokyo). 129(1), 133-138.

Moalli, M.R., Caldwell, N.J., Patil, P.V., Goldstein, S.A., 2000. An *in vivo* Model for Investigations of Mechanical Signal Transduction in Trabecular Bone. J. Bone Miner. Res. 15, 1346-1353.

Moreira, J., Deutsch, A., 2002. Cellular automaton models of tymour development: a critical review. Adv. Compl. Syst. 5, 247-267.

Mow, V.C., Kuei, S.C., Lai, W.M., Armstrong, C.G., 1980. Biphasic creep and stress relaxation of articular cartilage in compression: theory and experiments. J. Biomech. Eng. 102, 73-84.

Mullender, M.G., Huiskes, R., 1997. Osteocytes and bone lining cells: which are the best candidates for mechano-sensors in cancellous bone? Bone 20(6),527-532.

Mullender, M.G., Dijcks, S.J., Bacabac, R.G., Semeins, C.M., Van Loon, J.J., Klein-Nulend, J., 2006. Release of nitric oxide, but not prostaglandin E2, by bone cells depends on fluid flow frequency. J. Orthop. Res. 24(6), 1170-1177.

Murray, J.D., 2002. Mathematical Biology: I. An introduction (3rd edition). Springer, New York, USA.

Nagy, J.A., Senger, D.R., 2006. VEGF-A, cytoskeletal dynamics, and the pathological vascular phenotype. Exp. Cell Res. 312, 538-548.

Niikura, T., Hak, D.J., Redi, A.H., 2006. Global gene profiling reveals a down-regulation of BMP gene expression in experimental atrophic nonunions compared to standart healing fractures. J. Orthop. Res. 24, 1463-1471.

Nikellis, I., Levi, A., Nicolopoulos, C., 2004. Immediate loading of 190 endosseous dental implants: a prospective observational study of 40 patient treatments with up to 2-year data. Int. J. Oral Maxillofac. Implants 19(1), 116-123.

Nkenke, E., Fenner, M., 2006. Indications for immediate loading of implants and implant success. Clin. Oral Implants Res. 17(Suppl 2), 19-34.

Nogami, H., Oohira, A., 1984. Postnatal new bone formation. Clin. Orthop. Relat. Res. 184, 106-113.

Nordin, M., Frankel, V.H., (Eds.), 1989. Basic biomechanics of the musculoskeletal system. Lea and Febiger, Philadelphia.

Olsen, L., Sherratt, J., Maini, P., 1995. A mechanochemical model for adult dermal wound contraction and the permanence of the contracted tissue diplacement profile. J. Theor. Biol 177, 113-128.

Ochoa, J.A., Hillberry, B.M., 1992. Permeability of bovine cancellous bone. Trans. 38th Orthop. Res. Soc., 162.

O'Connor, J.A., Lanyon, L.E., 1982. The influence of strain rate on adaptive bone remodelling. J. Biomech. 15, 175-196.

Ohno, S., Tanaka, N., Ueki, M., Honda, K., Tanimoto, K., Yoneno, K., Ohno-Nakahara, M., Fujimoto, K., Kato, Y., Tanne, K., 2005. Mechanical regulation of terminal chondrocyte differentiation via RGD-CAP/beta ig-h3 induced by TGF-beta. Connect. Tissue Res. 46(4-5), 227-234.

Olsen, L., Sherratt, J., Maini, P., Arnold, F., 1997. A mathematical model for the capillary endothelial cell-extracellular matrix interactions in wound-healing angiogenesis. IMA J. Math. Appl. Med. Biol. 14, 261-281.

Oni, O.O., Stafford, H., Gregg, P.J., 1989. An experimental study of the patterns of periosteal and endosteal damage in tibial shaft fractures using a rabbit trauma model. J. Orthop. Trauma 3, 142-147.

Orr, A.W., Ginsberg, M.H., Shattil, S.J., Deckmyn, H., Schwartz, M.A.,2006. Matrix-specific suppression of integrin activation in shear stress signaling. Mol. Biol. Cell. 17(11), 4686-4697.

Ortega, N., Behonick, D.J., Werb, Z., 2004. Matrix remodeling during endochondral ossification. Trends Cell Biol. 14(2), 86-93.

Overgaard, S., 2000. Calcium phosphate coatings for fixation of bone implants. Evaluated mechanically and histologically by stereological methods. J. Orthop. Res. 71(S297).

Owan, I., Burr, D.B., Turner, C.H., Qiu, J., Tu, Y., Onyia, J.E., Duncan, R.L., 1997. Mechanotransduction in bone: osteoblasts are more responsive to fluid force than mechanical strain. Am. J Phys. 273, C810-815.

Park, S.H., O'Connor, K., McKellop, H., Sarmiento, A., 1998. The influence of active shear or compressive motion on fracture-healing. J. Bone Joint Surg. 80, 868-878.

Park, S.H., O'Connor, K., Sung, R., McKellop, H., Sarmiento, A., 1999. Comparison of healing process in open osteotomy model and closed fracture model. J Orthop Trauma 13, 114-20.

Parkkinen, J.J., Ikonen, J., Lammi, M.J., Laakkonen, J., Tammi, M., Helminen, H.J., 1993. Effects of cyclic hydrostatic pressure on proteoglycan synthesis in cultured chondrocytes and articular cartilage explants. Arch. Biochem. Biophys. 300, 458-465.

Pauwels, F., 1960. Eine neue Theorie über den Einfluβmechanischer Reize auf die Differenzierung der Stützgewebe. Z. Anat. Entwicklungsgeschichte. 121, 478-515.

Peng, H., Wright, V., Usas, A., Gearhart, B., Shen, H.C., Cummins, J., Huard, J., 2002. Synergistic enhancement of bone formation and healing by stem cell-expressed VEGF and bone morphogenetic protein-4. J. Clin. Invest. 110(6), 751-759.

Peng, Y., Kang, Q., Luo, Q., Jiang, W., Si, W., Liu, B.A., Luu, H.H., Park, J.K., Li, X., Luo, J., Montag, A.G., Haydon, R.C., He, T.C., 2004. Inhibitor of DNA Binding/Differentiation Helix-Loop-Helix Proteins Mediate Bone Morphogenetic Protein-induced Osteoblast Differentiation of Mesenchymal Stem Cells. Biol. Chem. 279(31), 32941-32949.

Perren, S.M., 1979. Physical and biological aspects of fracture healing with special reference to internal fixation. Clin. Orthop. Rel. Res. 138, 175-195.

Perren, S.M., Cordey, J., 1980. Concepts of interfragmentary strain. In: Uhthoff, H.K. (Ed.) Current concepts of internal fixation of fractures. Springer-Verlag, New York, 63-77.

Pettet, G.J., Byrne, H.M., McElwain, D.L.S., Norburry, J., 1996. A model of wound-healing angiogenesis in soft tissue. Math. Biosci. 136, 35-63.

Piattelli, A., Ruggeri, A., Franchi, M., Romasco, N., Trisi, P., 1993. A histologic and histomorphometric study of bone reactions to unloaded and loaded non-submerged single implants in monkeys: a pilot study. J. Oral Implant. 19, 314-320.

Pilliar, R.M., Lee, J.M., Maniatopoulos, C., 1986. Observations of the effect of movement on bone ingrowth into porous-surfaces implants. Clin. Orthop. Relat. Res. 208, 108-113.

Pittenger, M.F., Mackay, A.M., Beck, S.C., Jaiswal, R.K., Douglas, R., Mosca, J.D., Moorman, M.A., Simonetti, D.W., Craig, S., Marshak, D.R., 1999. Multilineage potential of adult human mesenchymal stem cells. Science 284(5411), 143-147.

Plank, M.J., Sleeman, B.D., Jones, P.F., 2004. A mathematical model of tumour angiogenesis, regulated by vascular endothelial growth factor and the angiopoietins. J. Theor. Biol. 229, 435-454.

Plant, A., Tobias, J.H., 2001. Characterisation of the temporal sequence of osteoblast gene expression during estrogen-induced osteogenesis in female mice. J. Cell. Biochem. 82(4), 683-691.

Plenk, H. Jr., Zitter, H. (1996). Material considerations. In: Watzek, G. (Ed.), Endosseous implants: scientific and clinical aspects. Quintessence Publishing Co., Chicago. 63-99.

Ponik, S.M., Triplett, J.W., Pavalko, F.M., 2007. Osteoblasts and osteocytes respond differently to oscillatory and unidirectional fluid flow profiles. J. Cell. Biochem. 100(3), 794-807.

Postlethwaite, A.E., Keski-Oja, J., Moses, H.L., Kang, A.H., 1987. Simulation of the chemotactic migration of human fibroblasts by transforming growth factor β. J. Exp. Med. 165, 251-256.

Pountos, I., Giannoudis, P.V., 2005. Biology of mesenchymal stem cells. Injury 36S, S8-S12.

Prendergast, P.J., Van Driel, W.D., Kuiper, J.-H., 1996. A comparison of finite element codes for the solution of biphasic poroelastic problems. In: Proc. Inst. Mech. Eng., Part H: J. Eng. Med. 210, 131-136.

Prendergast, P.J., Huiskes, R., Søballe, K., 1997. Biophysical stimuli on cells during tissue differentiation at implant interfaces. J. Biomech. 30(6), 539-548.

Prendergast, P.J., 2001. An analysis of theories in biomechanics. Eng. Trans. (Rozprawy Inżynierskie) 49, 117-133.

Prendergast, P.J., 2004. Mechanobiology: experiment and computation. In: Prendergast, P.J., McHugh, P.E., (Eds.), Topics in bio-mechanical engineering. ColourBooks Ltd., Dublin, 41-57.

Preziosi, L., (Ed.), 2003. Cancer Modelling and Simulation. CRC Press, Boca Raton, FL.

Pufe, T., Petersen, W., Kurz, B., 2003. Mechanical factors influence the expression of endostatin - an inhibitor of angiogenesis - in tendons. J. Orthop. Res. 21, 610-616.

Pufe, T., Kurz, B., Petersen, W., Varoga, D., Mentlein, R., Kulow, S., Lemke, A., Tillmann, B., 2005. The influence of biomechanical parameters on the expression of VEGF and endostatin in the bone and joint system. Ann Anat. 187(5-6), 461-472.

Randow, K., Ericsson, I., Nilner, K., Petersson, A., Glantz, P.O., 1999. Immediate functional loading of Branemark dental implants. An 18-month clinical follow-up study. Clin. Oral Implants Res. 10(1), 8-15.

Reed, A., Joyner, C.J., Brownlow, H.C., Simpson, A.H.R.W., 2002. Human atrophic fracture non-unions are not avascular. J. Orthop. Res. 20, 593-599.

Reed, A., Joyner, C.J., Isefuku, S., Brownlow, H.C., Simpson, A.H.R.W., 2003. The vascularity in a new model of atrophic non-union. J. Bone Joint Surg. Br. 85, 604-610.

Rhinelander, F.W., 1974. Tibial blood supply in relation to fracture healing. Clin. Orthop. Rel. Res. 80, 155-160.

Rickard, D.J., Sullivan, T.A., Shenker, B.J., Leboy, P.S., Kazhdan, I., 1994. Induction of rapid osteoblast differentiation in rat bone marrow stromal cell cultures by dexamethasone and BMP-2. Dev. Biol. 161(1), 218-28.

Rimondini, L., Bruschi, G.B., Scipioni, A., Carrassi, A., Nicoli-Aldini, N., Giavaresi, G., Fini, M., Mortellaro, C., Giardino, R., 2005. Tissue healing in implants immediately placed into postextraction sockets: a pilot study in a mini-pig model. Oral Surg. Oral Med. Oral Pathol. Oral Radiol. Endod. 100(3), e43-e50.

Rivilis, I., Milkiewicz, M., Boyd, P., Goldstein, J., Brown, M.D., Egginton, S., Hansen, F.M., Hudlicka, O., Haas, T.L., 2002. Differential involvement of MMP-2 and VEGF during muscle stretch- versus shear stress-induced angiogenesis. Am. J. Physiol. Heart Circ. Physiol. 283(4), H1430-438.

Roberts, W.E., 1993. Fundamental principles of bone physiology, metabolism and loading. In: Naert, I., van Steenberghe, D., Worthington, P. (Eds.), Osseointegration and oral rehabilitation. An Introductory textbook. Quintessence, London. 175-190.

Rodriguez-Merchan, E.C., Forriol, F., 2004. Nonunion: general principles and experimental data. Clin. Orthop. Rel. Res. 419, 4-12.

Ronga, M., Baldo, F., Zappala, G., Cherubino, P., 2006. Recombinant human bone morphogenetic protein-7 for treatment of long bone non-union: An observational, retrospective, non-randomized study of 105 patients. Injury 37(S3), S51-S56.

Rossi, F., MacLean, H.E., Yuan, W., Francis, R.O., Semenova, E., Lin, C.S., Kronenberg, H.M., Cobrinik, D., 2002. p107 and p130 coordinately regulate proliferation, Cbfa1 expression, and hypertrophic differentiation during endochondral bone development. Dev. Biol. 247, 271-285.

Rupnick, M.A., Stokes, C.L., Williams, S.K., Lauffenburger, D.A., 1988. Quantitative analysis of human microvessel endothelial cells using a linear under-agarose assay. Lab. Invest. 59, 363-372.

Sagara, M., Akagawa, Y., Nikai, H., Tsuru, H., 1993. The effects of early occlusal loading on one-stage titanium alloy implants in beagle dogs: a pilot study. J. Prosthet. Dent. 69(3), 281-288.

Sakai, K., Mohtai, M., Iwamoto, Y., 1998. Fluid shear stress increases transforming growth factor beta 1 expression in human osteoblast-like cells: modulation by cation channel blockades. Calcif. Tissue Int. 63(6), 515-20.

Sarmiento, A., Schaeffer, J.F., Beckerman, L., Latta, L.L., Enis, J.E., 1977. Fracture healing in rat femora as affected by functional weight-bearing. J. Bone Joint Surg. Am. 59(3), 369-375.

Sato, Y., Rifkin, D.B., 1988. Autocrine activities of basic FGF: regulation of cell movement, plasminogen activator synthesis and DNA synthesis. J. Cell. Biol. 107, 1199-1205.

Schell, H., Epari, D.R., Kassi, J.P., Bragulla, H., Bail, H.J., Duda, G.N.,2005. The course of bone healing is influenced by the initial shear fixation. J. Orthop. Res. 23, 1022-1028.

Schenk, R.K., Herrmann, R.W., 1984. Histologic studies on the incorporation of uncemented implants. In: Morscher, E. (Ed.), The cementless fixation of hip endoprostheses. Springer-Verlag Berlin, 52-58.

Schnitman, P.A., Wohrle, P.S., Rubenstein, J.E., DaSilva, J.D., Wang, N.H., 1997. Ten-year results for Branemark implants immediately loaded with fixed prostheses at implant placement. Int. J. Oral Maxillofac. Implants 12(4), 495-503.

Schroeder, A., van der Zypen, E., Stich, H., Sutter, F., 1981. The reactions of bone, connective tissue, and epithelium to endosteal implants with titanium-sprayed surfaces. J. Maxillofac. Surg. 9(1), 15-25.

Schwartz, Z., Kieswetter, K., Dean, D.D., Boyan, B.D., 1997. Underlying mechanisms at the bone-surface interface during regeneration. J. Periodont. Res. 32, 166-171.

Seeherman, H., Li, R., Wozney, J., 2003. A review of preclinical program development for evaluating injectable carriers for osteogenic factors. J. Bone Joint Surg. Am. 85, 96-108.

Seppä, H., Grotendorst, G., Seppä, S., Schiffmann, E., Martin, G.R., 1982. Platelet-derived growth factor is chemotactic for fibroblasts. J. Cell Biol. 92, 584-588.

Shefelbine, S.J., Augat, P., Claes, L., Simon, U., 2005. Trabecular bone fracture healing simulation with finite element analysis and fuzzy logic. J Biomech. 38(12), 2440-2450.

Sherratt, J.A., Murray, J.D., 1990. Models of epidermal wound healing. P. Roy. Soc. Lond. B Biol. 241, 29-36.

Sherratt, J.A., Sage, E.H., Murray, D., 1993. Chemical control of eukaryotic cell movement: a new model. J. Theor. Biol. 162, 23-40.

Sherratt, J., 1994. Chemotaxis and chemokinesis in eukaryotic cells: the keller-segel equations as an approximation to a detailed model. Bull. Math. Biol. 56, 129-146.

Shima, D.T., Deutsch, U., D'Amore, P.A., 1995. Hypoxic induction of vascular endothelial growth factor (VEGF) in human epithelial cells is mediated by increases in mRNA stability. FEBS Lett. 370, 203-208.

Shukla, A., Dunn, A.R., Moses, M.A., Van Vliet, K.J., 2004. Endothelial cells as mechanical transducers: enzymatic activity and network formation under cyclic strain. Mech. Chem. Biosyst. 1(4), 279-290.

Simmons, C.A., Valiquette, N., Pilliar, R.M., 1999. Osseointegration of sintered porous-surfaced and plasma spray-coated implants: An animal model study of early postimplantation healing response and mechanical stability. J. Biomed. Mater. Res. 47, 127-138.

Simmons, C.A., Meguid, S.A., Pilliar, R.M., 2001. Mechanical regulation of localized and appositional bone formation around bone-interfacing implants. J. Biomed. Mat. Res. 55, 63-71.

Simon, U., Augat, P., Claes, L., 2004. 3d fracture healing model can help to explain delayed healing with interfragmentary shear movement compared to axial movement. In: Middleton, J., Jones, M.L., Shrive, N. (Eds.), Proceedings of the 6th international symposium on Computer Methods in Biomechanics and Biomedical Engineering, 2004, Madrid, Spain. CD-ROM-proceedings.

Sironen, R.K., Karjalainen, H.M., Elo, M.A., Kaarniranta, K., Torronen, K., Takigawa, M., Helminen, H.J., Lammi, M.J., 2002. cDNA array reveals mechanosensitive genes in chondrocytic cells under hydrostatic pressure. Biochim. Biophys. Acta. 1591(1-3), 45-54.

Skalak, R., 1985. Aspects of biomechanical considerations. In: Brånemark, P.I., Zarb, G. Albrektsson, T. (Eds.), Tissue-integrated prosthesis: osseointegration in clinical dentistry. Quintessence, Chicago. 117-128.

Smalt, R., Mitchell, F.T., Howard, R.L., Chambers, T.J., 1997. Induction of no and prostaglandin e2 in osteoblasts by wall-shear stress but not mechanical strain. Am. J. Phys. 273, E751-E758.

Smith, E.L., Gilligan, C., McAdam, M., 1989. Deterring bone loss by exercise intervention in premenopausal and postmenopausal woman. Calc. Tissue Int. 44, 312-321.

Smith, R.L., Rusk, S.F., Ellison, B.E., Wessells, P., Tsuchiya, K., Carter, D.R., Caler, W.E., Sandell, L.J., Schurman, D.J., 1996. *In vitro* stimulation of articular chondrocyte mRNA and extracellular matrix synthesis by hydrostatic pressure. J. Orthop. Res. 14, 53-60.

Smith, R.L., Lin, J., Trindade, M.C., Shida, J., Kajiyama, G., Vu, T., Hoffman, A.R., van der Meulen, M.C., Goodman, S.B., Schurman, D.J., Carter, D.R., 2000. Time-dependent effects of intermittent hydrostatic pressure on articular chondrocyte type II collagen and aggrecan mRNA expression. J. Rehabil. Res. Dev. 37, 153-161.

Smith-Adaline, E.A., Volkman, S.K., Ignelzi Jr., M.A., Slade, J., Platte, S., Goldstein, S.A., 2004. Mechanical environment alters tissue formation patters during fracture repair. J. Orthop. Res. 22, 1079-1085.

Søballe, K., Rasmussen, H.B., Hansen, E.S., Bünger, C., 1992a. Hydroxyapatite coating modifies implant membrane formation (controlled micromotion in dogs). Acta Orthop. Scan. 63(2), 128-140.

Søballe, K., Hansen, E.S., Rasmussen, H.B., Jorgensen, P.H., Bünger, C., 1992b. Tissue Ingrowth into Titanium and Hydroxyapatite-Coated Implants During Stable and Unstable Mechanical Conditions. J. Orthop. Res. 10(2), 285-299.

Søballe, K., 1993. Hydroxyapatite ceramic coating for bone implant fixation. Acta Orthop. Scan. 64(S255), 1-48.

Sommerfeldt, D.W., Rubin, C.T., 2001. Biology of bone and how it orchestrates the form and function of the skeleton. Europ. Spine J. 10, S86-S95.

Southwood, L.L., Frisbie, D.D., Kawcak, C.E., McIlwraith, C.W., 2004. Delivery of growth factors using gene therapy to enhance bone healing. Vet. Surg. 33, 565-578.

Spector, M., 1988. Non-cemented total hip arthroplasty. In: Fitzgerald Jr, R.H. (Ed.), Current concepts of bony ingrowth and remodeling. Raven Press, NY. 69-86.

Sprague, E.A., Luo, J., Palmaz, J.C., 1997. Human aortic endothelial cell migration onto stent surfaces under static and flow conditions. J. Vasc. Interv. Radiol. 8(1Pt1), 83-92.

Steflik, D.E., Corpe, R.S., Lake, F.T., Young, T.R., Sisk, A.L., Parr, G.R., Hanes, P.J., Berkery, D.J., 1998. Ultrastructural analyses of the attachment (bonding) zone between bone and implanted biomaterials. J. Biomed. Mater. Res. 39, 611-620.

Stokes, C.L., Rupnick, M.A., Williams, S.K., Lauffenburger, D.A., 1990. Chemotaxis of human microvessel endothelial cells in response to acidic fibroblast growth factor. Lab. Invest. 63, 657-668.

Street, J., Winter, D., Wang, J.H., Wakai, A., McGuinness, A., Redmond, H.P., 2000. Is human fracture hematoma inherently angiogenic? Clin. Orthop. Rel. Res 378, 224-237.

Street, J., Bao, M., deGuzman, L., Bunting, S., Peale Jr., F.V., Ferrara, N., Steinmetz, H., Hoeffel, J., Cleland, J.L., Daugherty, A., van Bruggen, N., Redmond, H.P., Carano, R.A.D., Filvaroff, E.H., 2002. Vascular endothelial growth factor stimulates bone repair by promoting angiogenesis and bone turnover. P. Natl Acad. Sci. USA 99(15), 9656-9661.

Sun, S., Wheeler, M.F., Obeyesekere, M., Patrick, C., 2005. Multiscale angiogenesis modeling using mixed finite element methods. Multiscale Mod. Sim. 4(4), 1137-1167.

Sun, H.W., Li, C.J., Chen, H.Q., Lin, H.L., Lu, H.X., Zhang, Y., Zhang, M., 2007. Involvement of integrins, MAPK, and NF-kappaB in regulation of the shear stress-induced MMP-9 expression in endothelial cells. Biochem. Biophys. Res. Commun. 353(1), 152-158.

Sundaramurthy, S., Mao, J.J., 2006. Modulation of endochondral development of the distal femoral condyle by mechanical loading. J. Orthop. Res. 24(2), 229-41.

Szmukler-Moncler, S., Reingewirtz, Y., Weber, H.P., 1996. Bone response to early loading: the effect of surface state. In: Davidovitch, Z., Norton, L.A. (Eds.), Biological mechanisms of tooth movement and craniofacial adaptation. Harvard Soc. Adv. Orthodont., Boston. 611-616.

Szmukler-Moncler, S., Salama, H., Reingewirtz, Y., Dubruille, J.H., 1998. Timing of loading and effect of micromotion on bone-dental implant interface: review of experimental literature. J. Biomed. Mat. Res. 43, 192-203.

Szmukler-Moncler, S., Piatelli, S., Favero, G., Dubruille, J.H., 2000. Considerations preliminary to the application of early and immediate loading protocols in dental implantology. Clin. Oral Impl. Res. 11, 12-25.

Taba, Y., Miyagi, M., Miwa, Y., Inoue, H., Takahashi-Yanaga, F., Morimoto, S., Sasaguri, T., 2003. 15-deoxy-delta 12,14-prostaglandin J2 and laminar fluid shear stress stabilize c-IAP1 in vascular endothelial cells. Am. J. Physiol. Heart Circ. Physiol. 285(1), H38-46.

Tagil, M., Aspenberg, P., 1999. Cartilage induction by controlled mechanical stimulation *in vivo*. J. Orthop. Res., 17(2), 200-204.

Taguchi, K., Ogawa, R., Migita, M., Hanawa, H., Ito, H., Orimo, H., 2005. The role of bone marrow-derived cells in bone fracture repair in a green fluorescent protein chimeric mouse model. Biochem. Biophys. Res. Comm. 331, 31-36.

Takano-Yamamoto, T., Soma, S., Nakagawa, K., Kobayashi, Y., Kawakami, M., Sakuda, M., 1991. Comparison of the effects of hydrostatic compressive force on glycosaminoglycan synthesis and proliferation in rabbit chondrocytes from mandibular condylar cartilage, nasal septum, and sphenooccipital synchondrosis *in vitro*. Am. J. Orthod. Dentofac. Orthop. 99, 448-455.

Tanaka, S.M., Sun, H.B., Roeder, R.K., Burr, D.B., Turner, C.H., Yokota, H., 2005. Osteoblast responses one hour after load-induced fluid flow in a three-dimensional porous matrix. Calcif. Tissue Int. 76(4), 261-271.

Tao, J., Yang, Z., Wang, J.M., Tu, C., Pan, S.R., 2006. Effects of fluid shear stress on eNOS mRNA expression and NO production in human endothelial progenitor cells. Cardiology 106(2), 82-88.

Tarbell, J.M., Pahakis, M.Y., 2006. Mechanotransduction and the glycocalyx. J. Intern Med. 259(4), 339-350.

Terranova, V.P., Diflorio, R., Lyall, R.M., Hic, S., Friesel, R., Maciag, T., 1985. Human endothelial cells are chemotactic to endothelial cell growth factor and heparin. J. Cell Biol. 101, 2330-2334.

Thies, R.S., Bauduy, M., Ashton, B.A., Kurtzberg, L., Wozney, J.M., Rosen, V., 1992. Recombinant human bone morphogenetic protein-2 induces osteoblastic differentiation in W-20-17 stromal cells. Endocrin. 130(3), 1318-1324.

Thompson, Z., Miclau, T., Hu, D., Helms, J.A., 2002. A model for intramembranous ossification during fracture healing. J. Orthop. Res. 20, 1091-1098.

Thorne, R.G., Hrabetova, S., Nicholson, C., 2004. Diffusion of epidermal growth factor in rat brain extracellular space measured by integrative optical imaging. J. Neurophysiol. 92, 3471-81.

Tranquillo, R.T., Murray, J.D., 1992. Continuum model of fibroblast-driven wound contraction-inflammation mediation. J. Theor. Biol. 158, 135-172.

Turner, N.D., Knapp, J.R., Byers, F.M., Kopchick, J.J., 2001. Physical and mechanical characteristics of tibias from transgenic mice expressing mutant bovine growth hormone genes. Exp. Biol. Med. 226, 133-139.

Turner, S., Sherratt, J.A., 2002. Intercellular adhesion and cancer invasion: a discrete simulation using the extended Potts model. J. Theor. Biol., 216, 85-100.

Uchida, S., Sakai, A., Kudo, H., Otomo, H., Watanuki, M., Tanaka, M., Nagashima, M., Nakamura, T., 2003. Vascular endothelial growth factor is expressed along with its receptors during the healing process of bone and bone marrow after drill-hole injury in rats. Bone 32, 491-501.

Ulm, C.W., Kneissel, M., Hahn, M. Solar, P., Matejka, M., Donath, K., 1997. Characteristics of the cancellous bone of edentulous mandibles. Clin. Oral Impl. Res. 8, 125-130.

Vandamme, K., Naert, I., Geris, L., Vander Sloten, J., Puers, R., Duyck, J., 2006a. Histodynamics of bone tissue formation around immediately loaded cylindrical implants in the rabbit. Clin. Oral Impl. Res., accepted for publication.

Vandamme, K., Naert, I., Geris, L., Vander Sloten, J., Puers, R., Duyck, J., 2007. The influence of controlled immediate loading and implant design on peri-implant bone formation. J. Clin. Periodont., 34, 172-181.

Vandamme, K., Naert, I., Vander Sloten, J., Puers, R., Duyck, J., 2006c. Effect of implant surface roughness and loading on peri-implant bone formation. J. Periodont., accepted for publication.

Vandamme, K., Naert, I., Geris, L., Vander Sloten, J., Puers, R., Duyck, J., 2007. The effect of micromotion on the tissue response around immediately loaded roughened titanium implants in the rabbit. Europ. J. Oral Sci., 115, 21-29.

Vander, A., Sherman, J., Luciano, D., 1998. Human Physiology: the Mechanisms of Body Function. WCB McGraw-Hill, Boston, MA.

van der Meulen, M.C.H., Huiskes, R., 2002. Why mechanobiology? J. Biomech. 35, 401-414.

van Kampen, G.P., Veldhuijzen, J.P., Kuijer, R., van de Stadt, R.J., Schipper, C.A., 1985. Cartilage response to mechanical force in high-density chondrocyte cultures. Arthritis Rheum. 28, 419-424.

Van Oosterwyck, H., 2000. Study of biomechanical determinants of bone adaptation around functionally loaded oral implants. PhD thesis, K.U.Leuven, Belgium.

van Steenberghe, D., Molly, L., Jacobs, R., Vandekerckhove, B., Quirynen, M., Naert, I., 2004. The immediate rehabilitation by means of a ready-made final fixed prosthesis in the edentulous mandible: a 1-year follow-up study on 50 consecutive patients. Clin. Oral Implants Res. 15(3), 360-365.

Vara, D.S., Punshon, G., Sales, K.M., Hamilton, G., Seifalian, A.M., 2006. The effect of shear stress on human endothelial cells seeded on cylindrical viscoelastic conduits: an investigation of gene expression. Biotechnol. Appl. Biochem. 45(Pt 3), 119-130.

Vezeridis, P.S., Semeins, C.M., Chen, Q., Klein-Nulend, J., 2006. Osteocytes subjected to pulsating fluid flow regulate osteoblast proliferation and differentiation. Biochem. Biophys. Res. Commun. 348(3), 1082-1088.

Villenueva, J.E., Nimni, M.E., 1997. Promotion of calvarial cell osteogenesis by endothelial cells. J. Bone Miner. Res. 5, 733-739.

Walboomers, X.F., Habraken, W.J.E.M., Feddes, B., Winter, L.C., Bumgardner, J.D., Jansen, J.A., 2004. Stretch-mediated responses of osteoblast-like

cells cultured on titanium-coated substrates *in vitro*. J. Biomed. Mater. Res. 69A, 131-139.

Wallace, A.L., Draper, E.R., Strachan, R.K., McCarthy, I.D., Hughes, S.P., 1994. The vascular response to fracture micromovement. Clin. Orthop. Rel. Res. 301, 281-290.

Wang, D.S., Miura, M., Demura, H., Sato, K., 1997. Anabolic effects of 1,25-dihydroxyvitamin D3 on osteoblasts are enhanced by vascular endothelial growth factor produced by osteoblasts and by growth factors produced by endothelial cells. Endocrin. 138, 2953-2962.

Wasserman, S.M., Mehraban, F., Komuves, L.G., Yang, R.B., Tomlinson, J.E., Zhang, Y., Spriggs, F., Topper, J.N., 2002. Gene expression profile of human endothelial cells exposed to sustained fluid shear stress. Physiol. Genom. 12(1), 13-23.

Weinberg, C.B., Bell, E., 1985. Regulation of proliferation of bovine aortic endothelial cells, smooth muscle cells and adventitial fibroblasts in collagen lattices. J. Cell. Physiol. 122, 410-414.

Weiner, R., Schmitt, B.A., Podhaisky, H., 1997. ROWMAP - a ROW-code with Krylov techniques for large stiff ODEs. Appl. Numer. Math. 25, 303-319.

Wessells, H., Teal, T.H., Engel, K., Sullivan, C.J., Gallis, B., Tran, K.B., Chitaley, K., 2006. Fluid shear stress-induced nitric oxide production in human cavernosal endothelial cells: inhibition by hyperglycaemia. BJU Int. 97(5), 1047-1052.

Wheeler, S.L., 1996. Eight-year clinical retrospective study of titanium plasma-sprayed and hydroxyapatite-coated cylinder implants. Int. J. Oral Maxillofac. Implants. 11(3), 340-350.

Whiteside, L.A., 1978. The effects of extraperiosteal and subperiosteal dissection. II. On fracture healing. J. Bone Joint Surg. Am. 60, 26-30.

Wolf, S., Janousek, A., Pfeil, J., Veith, W., Haas, F., Duda, G., Claes, L., 1998. The effects of external mechanical stimulation on the healing of diaphyseal osteotomies fixed by flexible external fixation. Clin. Biomech. 13, 359-364.

Wolfe, L.A., Hobkirk, J.A., 1989. Bone response to a matched modulus endosseous implant material. Int. J. Oral Maxillofac. Implants 4(4), 311-320.

Wong, M., Siegrist, M., Goodwin, K., 2003. Cylic tensile strain and cyclic hydrostatic pressure differentially regulate expression of hypertrophic markers in primary chondrocytes. Bone 33, 685-693.

Wu, M.H., Kouchi, Y., Onuki, Y., Shi, Q., Yoshida, H., Kaplan, S., Viggers, R.F., Ghali, R., Sauvage, L.R., 1995. Effect of differential shear stress on platelet aggregation, surface thrombosis, and endothelialization of bilateral carotid-femoral grafts in the dog. J. Vasc. Surg. 22(4), 382-392.

Yang, X., Karsenty, G., 2002. Transcription factors in bone: developmental and pathological aspects. Trends Mol. Med. 8(7), 340-345.

Yokota, H., Goldring, M.B., Sun, H.B0, 2003. CITED2-mediated regulation of MMP-1 and MMP-13 in human chondrocytes under flow shear. J. Biol. Chem. 278(47), 47275-47280.

Yoshizato, K., Taira, T., Yamamoto, N., 1985. Growth inhibition of human fibroblasts by reconstituted collagen fibrils. Biomed. Res. 6, 61-71.

You, J., Yellowley, C.E., Donahue, H.J., Zhang, Y., Chen, Q., Jacobs, C.R., 2000. Substrate deformation levels associated with routine physical activity are less stimulatory to bone cells relative to loading-induced oscillatory fluid flow. J. Biomech. 122(4), 387-393.

You, L., Cowin, S.C., Schaffler, M.B., Weinbaum, S., 2001. A model for strain amplification in the actin cytoskeleton of osteocytes due to fluid drag on pericellular matrix. J. Biomech. 34, 1375-1386.

Zaman, M.H., Trapani, L.M., Sieminski, A.L., MacKellar, D., Gong, H., Kamm, R.D., Wells, A., Lauffenburger, D.A., Matsudaira, P., 2006. Migration of tumor cells in 3D matrices is governed by matrix stiffness along with cell-matrix adhesion and proteolysis. Proc. Natl Acad. Sc. 103(29), 10889-10894.

Zhang, R., Supowit, S.C., Klein, G.L., Lu, Z., Christensen, M.D., Lozano, R., Simmons, D.J., 1995. Rat tail suspension reduces messenger RNA level for growth factors and osteopontin and decreases the osteoblastic differentiation of bone marrow stromal cells. J. Bone Miner. Res. 10(3), 415-423.

Zhang, X., Sui, S., Bao, K., Zeng, B., 2001. Osteoporosis influence the fracture healing in ovariectomized rat: ultrastructure study. Chin. Med. J. 114, 15-21.

Zhang, Y., Lee, T.S., Kolb, E.M., Sun, K., Lu, X., Sladek, F.M., Kassab, G.S., Garland, T. Jr., Shyy, J.Y., 2006. AMP-activated protein kinase is involved in endothelial NO synthase activation in response to shear stress. Arterioscler. Thromb. Vasc. Biol. 26(6), 1281-1287.

Zhou, A.L., Egginton, S., Brown, M.D., Hudlicka, O., 1998. Capillary growth in overloaded, hypertrophic adult rat skeletal muscle: an ultrastructural study. Anat Rec. 252(1), 49-63.

Zimmermann, G., Moghaddam, A., Wagner, C., Vock, B., Wentzensen, A., 2006. Clinical experience with bone morphogenetic protein 7 (BMP 7) in nonunions of long bones. Unfallchirurg 109(7), 528-537.

Curriculum Vitae

Personal data

Name: Liesbet Laura Jo GERIS
Date of birth: 4th June 1979
Place of birth: Hasselt, Belgium

Work address:
Division of Biomechanics and Engineering Design
Department of Mechanical Engineering, Katholieke Universiteit Leuven
Celestijnenlaan 300C, B-3001 Leuven, Belgium
Tel: (+32) 16 32 89 97, Fax: (+32) 16 32 79 94

Email: Liesbet.Geris@mech.kuleuven.be

Education

- 1991-1997: Sciences - Mathematics (8h math program) at Humaniora Virga Jesse, Hasselt

- 1997-2002: Bachelor & Master of Science in Mechanical Engineering (Burgerlijk Ingenieur), option Mechatronics and Product Development at the Department of Mechanical Engineering of the Katholieke Universiteit Leuven. Title Master's thesis: Study of modeling techniques for designing scaffolds for trabecular bone tissue engineering. Graduated summa cum laude (86%)

- 2002-2007: Graduate student at the Division of Biomechanics and Engineering Design, Department of Mechanical Engineering, Katholieke Universiteit Leuven

- 2003-2007: Research Assistant of the Research Foundation - Flanders (FWO - Vlaanderen)

Scientific Honours and Awards

- Recipient of the ESB (European Society of Biomechanics) student award (1st prize) 2006, 5th World Congress of Biomechanics, Munich, Germany
- European Commission young researcher travel award to attend the Euroconference "Which Mathematics for Biology?" Crete, 2006.
- Recipient of the award for the best oral student presentation 2006, 7th International Symposium on Computer Methods in Biomechanics and Biomedical Engineering, Antibes, France
- Recipient of the award for the best poster 2005, European Conference on Mathematical and Theoretical Biology, Dresden, Germany
- ESMTB scholarship to attend the 5th European Conference on Mathematical and Theoretical Biology, Dresden, Germany
- Recipient of the award for the best oral student presentation 2004, 6th International Symposium on Computer Methods in Biomechanics and Biomedical Engineering, Madrid, Spain
- Recipient of the award for the best oral student presentation 2003, European Cells and Materials Conference IV, Davos, Switzerland
- Laureate student awards 2003 of the Royal Flemish Engineering Society KVIV, recipient of the Silver Engineering Award
- Laureate 2002 of the Biomedical Society (Society for Biomedical Technology and Health Care, Technological Institute of the Royal Flemish Engineering Society KVIV)

List of publications

International peer reviewed journal articles

1. **Geris, L.**, Vander Sloten, J., Van Oosterwyck, H., 2007. Angiogenesis in Bone Fracture Healing: a Bioregulatory Model. J. Theor. Biol., In preparation.

2. **Geris, L.**,Vandamme, K., Naert, I., Vander Sloten, J., Duyck, J., Van Oosterwyck, H., 2007. Application of mechanoregulatory models to simulate peri-implant tissue formation in an *in vivo* bone chamber, J. Biomech., Submitted for publication (SCI: 2.364).

3. Vandamme, K., Naert, I., **Geris, L.**, Vander Sloten, J., Puers, R., Duyck, J., 2007. Histodynamics of bone tissue formation around immediately loaded cylindrical implants in the rabbit. Clin. Oral Implants Res. Accepted for publication. (SCI: 2.139)

4. Vandamme, K., Naert, I., **Geris, L.**, Vander Sloten, J., Puers, R., Duyck, J., 2007. The effect of micromotion on the tissue response around immediately loaded moderately roughened titanium implants in the rabbit. Eur. J. Oral Sci. 115, 21-29. (SCI: 1.784)

5. Vandamme, K., Naert, I., **Geris, L.**, Van Oosterwyck, H., Vander Sloten, J., Puers, R., Duyck, J., 2007. The influence of controlled immediate loading and implant design on peri-implant bone formation. J. Clin. Periodont. 34, 172-181. (SCI: 2.225)

6. **Geris, L.**, Gerisch, A., Maes, C., Carmeliet, G., Weiner, R., Vander Sloten, J., Van Oosterwyck, H., 2006. Mathematical modeling of fracture healing in mice: Comparison between experimental data and numerical simulation results. Med. Biol. Eng. Comp. 44(4), 280-289. (SCI: 1.09)

7. Duyck, J., Vandamme, K., **Geris, L.**, Van Oosterwyck, H., De Cooman, M., Vander Sloten, J., Puers, R., Naert, I., 2006. The influence of

micro-motion on the tissue differentiation around immediately loaded cylindrical turned titanium implants. Arch. Oral Biol. 51(1), 1-7. (SCI: 1,098, number of citations: 3)

8. **Geris, L.**, Andreykiv, A., Van Oosterwyck, H., Vander Sloten, J., van Keulen, F., Duyck, J., Naert, I., 2004. Numerical simulation of tissue differentiation around loaded titanium implants in a bone chamber. J. Biomech. 37(5), 763-769. (SCI: 2.005, number of citations: 3)

9. **Geris, L.**, Van Oosterwyck, H., Vander Sloten, J., Duyck, J., Naert, I., 2003. Assessment of mechanobiological models for the numerical simulation of tissue differentiation around immediately loaded implants. Comp. Meth. Biomech. Biomed. Eng. 6(5-6), 277-288. (number of citations: 2)

Chapters in books

1. Gerisch, A., **Geris, L.**, 2007. A finite volume spatial discretisation for taxis-diffusion-reaction systems with axi-symmetry: application to fracture healing. In: Deutsch, A., Brusch, L., Byrne, H., de Vries, G., Herzel, H.-P. (Eds.), Advances in Mathematical Modeling of Biological Systems, Volume I. Birkhäuser, Boston. 303-316.

2. Duyck, J., **Geris, L.**, Van Oosterwyck, H., Vander Sloten, J., Naert, I., 2005. Kanttekeningen bij immediate belasting van orale implantaten. In: de Baat, C., Aps, J.K.N., Brands, W.G., Carels, C.E.L., Jacobs, R., Koole, R., van Welsenes, W. (Eds.), Het Tandheelkundig jaar 2006. Bohn Stafleu van Loghum, The Netherlands. 132-145. (ISBN 90-313-4546-6)

3. **Geris, L.**, Van Oosterwyck, H., Duyck, J., Naert, I., Vander Sloten, J., 2005. Mechanobiology of bone regeneration and bone adaptation to achieve stable long-term fixation of endosseous implants. In: Zeman, M.E., Cerrolaza, M. (Eds.) Computational Modeling of Tissue Surgery (Series: Advances in Bioengineering, Vol. 1). WITPress, Southampton, UK. 2-37. (ISBN 1-85312-749-3)

4. Gerisch, A., **Geris, L.**, Van Oosterwyck, H., Vander Sloten, J., Weiner, R., 2005. Reliable and efficient numerical simulation of a model of tissue differentiation in a bone chamber model. In: Bischoff, G. (Ed.) Micro- and Nanostructures of Biological Systems. 60-76. (ISBN 3-8322-3868-9)

Proceedings of international conferences

Full paper in proceedings

1. **Geris, L.**, Vander Sloten, J., Van Oosterwyck, H., 2007. A novel mathematical model to simulate and predict tissue regeneration. In: Middleton, J., Jones, M.L., Shrive, N. (Eds.) Proceedings of the 7th international symposium on Computer Methods in Biomechanics and Biomedical Engineering, 22-25/3/2006, Antibes, France, CD-ROM-proceedings, 6pp.

2. Amor, N., Van Cleynenbreugel, T., **Geris, L.**, Vander Sloten, J., Van Oosterwyck, H., 2007. Micro-macro mechanical modeling of bone-implant interface by means of the homogenization theory. In: Middleton, J., Jones, M.L., Shrive, N. (Eds.) Proceedings of the 7th international symposium on Computer Methods in Biomechanics and Biomedical Engineering, 22-25/3/2006, Antibes, France, CD-ROM-proceedings, 6pp.

3. Duyck, J., Vandamme, K., **Geris, L.**, Van Oosterwyck, H., De Cooman, M., Vander Sloten, J., Puers, R., Naert, I., 2005. The influence of micro-motion on the tissue differentiation around immediately loaded cylincrical turned titanium implants. Comp. Meth. Biomech. Biomed. Eng. 8(S1), 93-94.

4. Vandamme, K., Duyck, J., **Geris, L.**, Van Oosterwyck, H., De Cooman, M., Vander Sloten, J., Puers, R., Naert, I., 2005. The influence of mechanical parameters on tissue differentiation and bone formation around immediately loaded implants in the bone chamber model. Comp. Meth. Biomech. Biomed. Eng. 8(S1), 275-276.

5. **Geris, L.**, Gerisch, A., Maes, C., Carmeliet, G., Weiner, R., Vander Sloten, J., Van Oosterwyck, H., 2005. Tissue differentiation during fracture healing in mice: comparison of an experimental and numerical study. In: Proceedings of the first thematic workshop of the European Society of Biomechanics on Mechanobiology of Cells and Tissue Engineering, 28-30/8/2005, Leuven. 35-36.

6. Vandamme, K., **Geris, L.**, Duyck, J., Van Oosterwyck, H., De Cooman, M., Puers, R., Vander Sloten, J., Naert, I., 2005. The influence of mechanical parameters on tissue differentiation and bone formation around immediately loaded implants in the bone chamber model. In: Proceedings of the first thematic workshop of the European Society of Biomechanics on Mechanobiology of Cells and Tissue Engineering, 28-30/8/2005, Leuven. 23-24.

7. **Geris, L.**, Gerisch, A., Maes, C., Carmeliet, G., Weiner, R., Van Oosterwyck, H., Vander Sloten, J., 2005. Experimental and numerical study of fracture healing in a murine fracture model In: Proceedings of the Summer Bioengineering Conference, 22-26/6/2005, Vail, CO (USA). CD-ROM Proceedings (ISBN 0-9742492-1-1), 2 pp.
8. **Geris, L.**, Van Oosterwyck, H., Vander Sloten, J., Duyck, J., Naert, I., 2004. Different mechanoregulatory models predict different patterns of tissue differentiation. In: Middleton, J., Jones, M.L., Shrive, N. (Eds.) Proceedings of the 7th international symposium on Computer Methods in Biomechanics and Biomedical Engineering. CD-ROM-proceedings, 6 pp.
9. **Geris, L.**, Van Oosterwyck, H., Andreykiv, A., Vander Sloten, J., van Keulen, F., Duyck, J., Naert, I., 2003. Numerical simulation of peri-implant tissue differentiation in a bone chamber. Eur. Cells Mat. 5(S2), 16-17.
10. Vandamme, K., **Geris, L.**, Duyck, J., Van Oosterwyck, H., Vander Sloten, J., De Cooman, M., Puers, R., Naert, I., 2003. Quantification of the role of mechanical parameters on the bone response around loaded titanium implants. Eur. Cells Mat. 5(S2), 96-97.

Abstract in proceedings

1. **Geris, L.**, Vander Sloten, J., Van Oosterwyck, H., 2006. Mathematical modeling of bone regeneration including the angiogenic process. In: Proceedings of the fifth World Congress of Biomechanics, 29/7-4/8/2006, Munich, Germany. CD-ROM proceedings.
2. Vandamme, K., Naert, I., **Geris, L.**, Van Oosterwyck, H., Vander Sloten, J., Puers, R., Duyck, J., 2006. Bone Formation around Immediately Loaded Implants: a Bone Chamber Model (2006). In: Proceedings of the 84th General Session & Exhibition of the IADR, 28/6-1/7/2006, Brisbane, Australia.
3. **Geris, L.**, Gerisch, A., Maes, C., Carmeliet, G., Weiner, R., Van Oosterwyck, H., Vander Sloten, J., 2005. Numerical simulation and experimental validation of murine fracture healing. In: Proceedings of the fifth national day on biomedical engineering, Belgian Society Medical and Biological Engineering and Computing & National Committee Biomedical Engineering, 28/10/2005, Brussels.
4. **Geris, L.**, Gerisch, A., Maes, C., Carmeliet, G., Weiner, R., Van Oosterwyck, H., Vander Sloten, J., 2005. Numerical simulation and experimental validation of murine fracture healing. In: Proceedings of

the European Conference on Mathematical and Theoretical Biology, 17-22/7/2005, Dresden, Germany.

5. Vandamme, K., Duyck, J., Van Oosterwyck, H., **Geris, L.**, Vander Sloten, J., De Cooman, M., Puers, R., Naert, I., 2005. De invloed van mechanische parameters op de weefselrespons bij immediaat belaste titanium implantaten: een botkamermodel. In: Proceedings van het Congres Verbond der Vlaamse Tandartsen, 26-28/05/2005, Ostend, Belgium.

6. Van Oosterwyck, H., **Geris, L.**, Gerisch, A., Vandamme, K., Duyck, J., De Cooman, M., Weiner, R., Puers, R., Naert, I., Vander Sloten, J., 2004. Application of different mathematical models for the prediction of bone regeneration in an *in vivo* bone chamber. In: Lecture notes of workshop Numerical models of bone adaptation and repair, Germany.

7. **Geris, L.**, Van Oosterwyck, H., Duyck, J., De Cooman, M., Puers, R., Naert, I., Vander Sloten, J., 2004. The mechanobiology of tissue differentiation around immediately loaded implants: a bone chamber experiment. In: Proceedings of the 14th conference of the European Society of Biomechanics, 's Hertogenbosch, The Netherlands.

8. Vandamme, K., Duyck, J., Van Oosterwyck, H., **Geris, L.**, Vander Sloten, J., De Cooman, M., Puers, R., Naert, I., 2004. Tissue response around loaded titanium implants in the bone chamber model. In: Proceedings of the 14th conference of the European Society of Biomechanics, 's Hertogenbosch, The Netherlands.

9. **Geris, L.**, Van Oosterwyck, H., Gerisch, A., Vandamme, K., Duyck, J., De Cooman, M., Weiner, R., Puers, R., Naert, I., Vander Sloten, J., 2004. Prediction of bone regeneration in an *in vivo* bone chamber: application of different mathematical models. In: Lecture notes of Advanced course on tissue remodelling ACTR04, Warsaw, Poland.

10. **Geris, L.**, Van Oosterwyck, H., Vander Sloten, J., Duyck, J., Naert, I., 2003. Simulation of tissue ingrowth and differentiation around a loaded titanium implant in a bone chamber. In: Veraart, C., Verdonck, P. (Eds.), Proceedings of the third national day on biomedical engineering. Belgian Society Medical and Biological Engineering and Computing & National Committee Biomedical Engineering, Brussels, 50.

11. Van Oosterwyck, H., **Geris, L.**, Duyck, J., De Cooman, M., Andreykiv, A., van Keulen, F., Puers, R., Naert, I., Vander Sloten, J., 2003. Experimental and numerical study on mechanoregulation of tissue differentiation around a loaded implant in a bone chamber. In: Bischoff, G., Hein,

H.-J. (Eds.), Proceedings of the seventh conference of ESEM. European society for engineering and medicine, Halle, Germany.

12. Van Oosterwyck, H., **Geris, L.**, Vander Sloten, J., Andreykiv, A., van Keulen, F., Duyck, J., Naert, I., 2003. Numerical simulations of tissue ingrowth and differentiation around a loaded titanium implant in a bone chamber. In: Proceedings of the symposium on integrated systems in dental healthcare. Medical engineering and technology research network, Milan.

13. **Geris, L.**, De Gersem, H., Van Cleynenbreugel, T., Van Oosterwyck, H., Vander Sloten, J., Van der Perre, G., 2002. Computer modelling techniques for trabecular bone tissue engineering scaffold design, In: Proceedings of the second national day on biomedical engineering. Belgian Society Medical and Biological Engineering and Computing & National Committee Biomedical Engineering, Brussels.

Other publications

1. De Gersem, H., **Geris, L.**, 2003. Zoektocht naar een levende prothese. Het Ingenieursblad 72(8-9), 54-60.

Nederlandse samenvatting
Summary in Dutch

Wiskundige modellering van botregeneratie tijdens breukheling en implantaat osseointegratie

Hoofdstuk 1 Algemene inleiding

1.1 Bot en botweefsel

Bot is een fascinerend weefsel, uniek in zijn vermogen om te helen zonder litteken. Het is ook een intelligent materiaal aangezien het in staat is zichzelf aan te passen aan de veranderende mechanische en biologische omgeving waarin het zich bevindt.

Botweefsel bestaat uit een organische fase, een inorganische fase (mineraal) en water. Collageen is de belangrijkste bouwsteen van de organische fase terwijl de inorganische fase voornamelijk bestaat uit hydroxyappatiet kristallen. Een klein deel van het botvolume wordt ingenomen door de botcellen die zorgen voor de productie, resorptie en onderhoud van de matrix, nl. osteoblasten, osteocyten, botrandcellen en osteoclasten. Osteoblasten zijn de botvormende cellen, zij zorgen voor de productie van de botmatrix. In een later stadium van differentiatie, wanneer zij volledig omgeven zijn door botmatrix, veranderen ze in osteocyten. Osteocyten worden geacht een belangrijke rol te spelen in het waarnemen van mechanische belasting door botweefsel. Botrandcellen zijn ook vroegere osteoblasten maar bevinden zich aan de rand van de botmatrix. Deze cellen zijn inactief maar worden gereactiveerd bij een hervatting van de botmatrix productie. Osteoclasten tot slot, zijn meerkernige cellen die botmatrix resorberen.

Op macroscopische schaal kan bot worden onderverdeeld in twee categorieën. Compact bot of corticaal bot enerzijds, dat zich aan de buitenzijde van de beenderen bevindt, en trabeculair of spongieus bot anderzijds, voornamelijk aanwezig in de uiteinden van lange beenderen. Op microscopisch niveau kan bot opnieuw in twee categorieën worden opgedeeld, aan de éne kant het traag gevormde maar goed georganiseerde lamellaire bot en aan de andere kant het snel gevormde, slecht georganiseerde geweven bot waarin collageen vezels en mineraal kristallen min of meer willekeurig verdeeld zijn.

1.2 Botvorming en bot(her)modellering

Botvorming gebeurt in twee stappen. De eerste stap omvat de afzetting van botmatrix door de osteoblasten. Afhankelijk van het substraat waarop dit gebeurt, krijgt het proces een andere naam: bij intramembraneuze botvorming vormt bindweefsel het substraat, bij endochondrale ossificatie is dit kraakbeen en bij appositionele botvorming is dit eerder gevormd bot. De tweede stap is de mineralisatie van de gevormde botmatrix.

Twee processen spelen een belangrijke rol in de ontwikkeling en het onderhoud van een gezond en flexibel skelet: botmodellering en -hermodellering. In het eerste geval gaat het om een onafhankelijke actie van osteoclasten en osteoblasten. Bot modellering kan zowel formatief als resorptief zijn en kent een drastische afname bij het bereiken van skeletale maturiteit. Bothermodellering met zijn koppeling tussen de acties van osteoclasten en osteoblasten, is een proces dat gewoonlijk geen invloed heeft op de geometrie van het bot. Dit proces herstelt microscopische schade, voorkomt de opstapeling van vermoeiingsschade en zorgt voor de fijnregeling om een optimale mechanische efficiëntie te bekomen.

1.3 Botregeneratie

Botregeneratie is een complex fysiologisch proces dat bestaat uit de acties en interacties van vele cellen en weefsels, geregeld door een myriade van biochemische en mechanische factoren. De principes van peri-implantaat heling zijn vergelijkbaar met deze van breukheling. De regeneratie respons kan onderverdeeld worden in primaire en secundaire heling. Primaire heling treedt op onder ideale mechanische omstandigheden, zijnde mechanische stabiliteit en de afwezigheid van openingen tussen de bothelften in het geval van breukheling en tussen het omliggende bot en het implantaat in het geval van implantaat osseointegratie. In dergelijke gevallen zal een bothermodelleringsproces optreden en vindt heling plaats zonder de vorming van een callus. In de afwezigheid van zulke ideale mechanische omstandigheden, treedt secundaire botvorming op (het meest voorkomende geval van botregeneratie).

Regeneratie verloopt dan in drie fases: een inflammatiefase, een reparatiefase en een hermodelleringsfase. Onmiddellijk na het optreden van bottrauma (zij het door breukheling of implantaat installatie) vormt zich een bloedklonter op de plaats van het trauma. In deze klonter bevinden zich allerhande groeifactoren die een belangrijke rol spelen bij het verdere verloop van het regeneratie proces. Dit is het begin van de inflammatiefase. Allerhande cellen en (nog meer) groeifactoren komen vanuit de omliggende weefsel naar de regeneratie plaats. De initieel gevormde granulatie weefsel matrix wordt geleidelijk aan vervangen door een fibreuze weefsel matrix. In deze zachte weefsel matrix, zullen mesenchymale stamcellen differentiëren naar verschillende celtypes, beïnvloed door allerhande biologische en mechanische signalen in hun micro-omgeving. Dit is de start van de reparatiefase en deze verschilt lichtjes tussen breukheling en implantaat inheling.
Bij implantaat inheling zijn er twee fenomenen belangrijk voor een succesvolle osseointegratie, nl. contact osteogenese en afstand osteogenese. Contact osteogenese omvat de migratie van potentieel osteogene cellen naar het implantaatoppervlak, de differentiatie van deze cellen naar osteoblasten (osteoconductie) en de synthese van botweefsel op het implantaatoppervlak (*de novo* botvorming). Afstand osteogenese of appositionele botvorming omvat de vorming van nieuw botweefsel op het oppervlak van het bestaande bot.
Bij breukheling wordt de reparatiefase gekenmerkt door intramembraneuze botvorming enerzijds en kraakbeen productie gevolgd door endochondrale botvorming anderzijds. Op basis van de mechanische en biologische stimuli die de mesenchymale stamcellen in de zachte weefsel matrix ondervinden differentiëren zij naar chondrocyten (kraakbeen vormende cellen - voornamelijk in het centrale gedeelte van de breuk) of osteoblasten (naast de cortex). Wanneer de breukzone voldoende gestabiliseerd is, mineraliseert de gevormde kraakbeen matrix en dringen bloedvaten, gevolgd door osteoblasten, deze matrix binnen (endochondrale ossificatie). Reeds tijdens de reparatieve fase begint de laatste hermodelleringsfase waarin het herstellende bot in de regeneratie zone terugkeert naar zijn oorspronkelijke staat.

In de klinische praktijk werden tot voor enkele jaren implantaten na plaatsing terug afgedekt om gedurende 6 maanden onbelast te kunnen inhelen, alvorens ze belast mochten worden door de patiënt. Omwille van allerlei fysiologische, psychologische en sociologische redenen wordt er tegenwoordig steeds vaker overgestapt naar een helingsprotocol waarbij de patiënt onmiddellijk zijn vaste prothese krijgt en de implantaten bijgevolg immediaat belast worden. In de literatuur zijn studies terug te vinden rond immediate belasting die zowel positieve als negatieve resultaten rapporteren. Desalniettemin bestaat er consensus rond het feit dat een beperkte hoeveelheid mechanische belasting niet schadelijk is voor het goede verloop van de implantaat osseoin-

tegratie, daar waar overbelasting leidt tot een falen van het implantaat. Er bestaan echter weinig goed gekarakteriseerde studies die het effect van mechanische belasting op peri-implantaat weefseldifferentiatie onderzoeken *in vivo*. Bij breukheling spreekt men van een vertraagde heling wanneer er nog geen unie tussen de bothelften zichtbaar is op het moment dat uit klinische praktijk geweten is dat dit wel zo moet zijn. Niet-unie is het geval waarbij dat zelfs na een zeer lange periode geen breukheling optreedt. Deze pathologische gevallen van vertraagde en niet-unie kennen verscheidene mechanische en biologische oorzaken. Verschillende behandelingsmethodes, inspelende op de biologische zowel als de mechanische aspecten van het helingsproces, zijn reeds aanwezig. Desalniettemin is er bijkomend onderzoek nodig om de precieze mechanismen van niet-heling en de bijhorende optimale behandelingsstrategieën te bepalen.

Hoofdstuk 2 Hypothese en doelstellingen

2.1 Hypothese en doelstellingen

Uit de inleiding blijkt dat er nood is aan verder onderzoek naar de oorzaken en de behandelingsmethoden van falende botregeneratie. Tot hier toe was het grootste gedeelte van dit onderzoek van experimentele aard. **De hypothese die aan de basis ligt van dit werk, stelt dat wiskundige modellen een substantiële bijdrage kunnen leveren aan het onderzoeksdomein van de botregeneratie.** Modellen zijn immers in staat zowel normale als pathologische botregeneratie te simuleren en kunnen een rol spelen in het ontwerpen van behandelingsstrategieën voor deze laatste. Bovendien kunnen modellen toegepast worden in het ontwerp, de begeleiding en de ondersteuning van (nieuwe) experimenten. Tot slot kunnen resultaten van theoretische experimenten interessante onderzoeksvragen oproepen en een nieuwe (meer kwantitatieve) kijk op de biologie van de botregeneratie opwekken.

Specifieke doestellingen werden opgesteld om de bovenstaande hypothese te onderzoeken. In de hierna volgende hoofdstukken komt telkens één van deze doelstellingen aan bod.

- *Implementatie van bestaande mechanoregulatorische en bioregulatorische modellen*
  Bestaande mechano- en bioregulatorische modellen werden toegepast op verschillende experimentele opstellingen van implantaat osseointegratie en breukheling. De experimentele en numerieke resultaten werden met elkaar vergeleken op een kwalitatieve en kwantitatieve basis. Grondige sensitiviteitsanalyses werden uitgevoerd om de invloed van de verschillende modelparameters op het simulatie resultaat te onderzoeken. Tekortkomingen van de modellen werden geïdentificeerd en suggesties voor

verbeteringen werden gemaakt. De resultaten zijn beschreven in hoofdstukken 3 en 4.

- *Ontwikkeling van een nieuw bioregulatorisch model*
  Een nieuw wiskundig bioregulatorisch model werd ontwikkeld, gebaseerd op de bestaande modellen, met toevoeging van verschillende essentiële onderdelen van het botregeneratie proces. Dit model komt tegemoet aan verscheidene van de in hoofdstuk 4 geïdentificeerde tekortkomingen. Toepassing van dit model op een experimenteel breukhelingsmodel liet, naast een kwalitatieve, ook een kwantitatieve corroboratie van het nieuwe bioregulatorische model toe (hoofdstuk 5).

- *Ontwikkeling van een nieuw mechanoregulatorisch model*
  Het concept van de mechanoregulatie van biologische processen werd geïntegreerd in het nieuwe bioregulatorische model beschreven in hoofdstuk 5. Hoofdstuk 6 beschrijft het opstellen van een wiskundig kader dat het onderzoek naar de rol van mechanische en biologische stimuli op het regeneratie proces faciliteert. Ter illustratie van het potentieel van het ontwikkelde wiskundige kader, werd een eenvoudig mechanobioregulatorisch model voorgesteld en werden toepassingen in zowel breukheling als implantaat osseointegratie ontwikkeld.

2.2 Methodologie

Deze thesis omvat experimentele resultaten van verschillende dierstudies. Een *in vivo* botkamer, ontwikkeld door de BIOMAT onderzoeksgroep (Prothetische Tandheelkunde, K.U.Leuven, België), in samenwerking met de MICAS groep (ESAT, K.U.Leuven, België), vormt een unieke omgeving voor de studie van peri-implant regeneratie. Resultaten van een semi-gestabiliseerd muizen breukmodel met inbegrip van uitgebreide biologische data omtrent het angiogenese aspect van breukheling werden ter beschikking gesteld door het Laboratorium van Experimentele Geneeskunde en Endocrinologie (K.U.Leuven, België (Maes *et al.*, 2006)). Tenslotte werd gebruik gemaakt van de resultaten van het gestandaardiseerde ratten femorale breukmodel (Royal Veterinary College, Londen, UK (Harrison *et al.*, 2003)) dat door het kwantitatieve karakter van de experimentele data (opgemeten in gestandaardiseerde regeneratie zones) een goede kwantitatieve vergelijking tussen experimentele en numerieke data mogelijk maakt.

In het kader van deze thesis werden bijdragen geleverd aan de ontwikkeling van de nieuwe experimentele botkamer opstelling. Bovendien werd de software ontwikkeld voor de implementatie van de mechanoregulatorische en gekoppelde mechanobioregulatorische modellen. De belangrijkste bijdrage en

het innovatieve aspect van dit werk situeren zich echter in de grondige studie van de bestaande mechano- en bioregulatorische modellen en de ontwikkeling van een nieuw bioregulatorisch model en wiskundig kader voor gekoppelde mechanobioregulatorische modellen. Toepassingen van deze modellen in de simulatie van pathologische regeneratie demonstreren het potentieel van wiskundige modellen in het assisteren, verfijnen, induceren en ontwikkelen van experimenten. Dit alles leidt tot een vergroting van de kennis omtrent botregeneratie.

De numerieke implementatie van de mechanobioregulatische modellen werd door de auteur ontwikkeld in het kader van deze thesis, gebruik makende van een koppeling van Matlab (The Mathworks, Inc.) met het eindige elementen programma MSC.Marc, door middel van de gebruikerssubroutines van deze laatste (hoofdstuk 3). De simulaties van de bioregulatorische modellen (hoofdstukken 4 en 5) werden uitgevoerd in een speciaal voor biologische problemen ontwikkelde eindige volumes code (met dank aan Dr. Gerisch, Martin-Lüther Universität Halle-Wittenberg). Voorgaande implementaties werden gecombineerd in een nieuw software-kader (in de Matlab omgeving) om onderzoek naar gekoppelde mechanobioregulatorische problemen mogelijk te maken (hoofdstuk 6).

Hoofdstuk 3 Mechanoregulatorische modellen voor botregeneratie

3.1 Introductie en hypothese

De eerste theoretische modellen die de mechanoregulatie van breukheling beschrijven dateren reeds van 1960. Tijdens het laatste decennium hebben een aantal onderzoeksgroepen mechanoregulatorische modellen van breukheling naar voor geschoven waarin weefseldifferentiatie wordt gemodelleerd op basis van de lokale mechanische stimuli in het regenererende weefsel (Prendergast *et al.* (1997), Carter *et al.* (1998) and Claes and Heigele (1999)). Deze modellen gebruiken allemaal een combinatie van hydrostatische en distortionele mechanische stimuli en werden tot hier toe met wisselend succes toegepast op verschillende regeneratie gevallen zoals breukheling, distractie osteogenese en de heling van osteochondrale defecten. De hypothese van dit hoofdstuk stelt dat de hoger vermelde mechanoregulatorische modellen in staat zijn om peri-implantaat botvorming in een *in vivo* botkamer te voorspellen.

3.2 Botkamer experimenten

Verschillende botkamer studies werden uitgevoerd in de loop van dit onderzoek waarbij de invloed werd nagegaan van de helingsperiode, de magnitude van de implantaatverplaatsing, de implantaat geometrie en de oppervlakteruwheid van het implantaat op het regeneratieproces. De experimentele resultaten toonden aan dat mechanische belasting een positieve invloed had op de weefseldifferentiatie en botvorming rond cilindervormige implantaten en op de mineralisatie van het weefsel aan het implantaatoppervlak. Schroefvormige implantaten ondervonden een gelijkaardige invloed van mechanische belasting, maar bevorderden de mineralisatie van het weefsel aan het implantaatoppervlak in vergelijking met cilindervormige implantaten. Een opruwing van het (schroefvormig) implantaatoppervlak had enkel invloed op de implantaat osseointegratie in het geval van niet-belasting van het implantaat. Bij verschillende magnitudes van een cilindervormig implantaat verplaatsing werd een stijging waargenomen in botdensiteit bij stijgende implantaatverplaatsing terwijl de kans op bot-implantaat-contact daalde in het geval van belasting. Voor opgeruwde schroefvormige implantaten werd een verbeterde botreactie waargenomen in de omgeving en aan het oppervlak van het implantaat, voor stijgende implantaatverplaatsingen.

3.3 Implementatie en numerieke simulaties

Zowel 2D als 3D eindige elementen modellen werden opgesteld van het weefsel in de botkamer. De botkamer en het omgevende weefsel werden vervangen door gepaste randvoorwaarden. Weefseldifferentiatie voor beide implantaatgeometrieën (cilinder en schroefvormig) en de verschillende implantaatverplaatsingen die in de experimenten aan bod kwamen, werden gesimuleerd met verschillende mechanoregulatorische modellen. De eindige elementen analyses werden uitgevoerd met behulp van MSC.Marc, de interpretatie van de lokale mechanische stimuli en de aanpassing van de materiaaleigenschappen overeenkomstig de voorspelde differentiatie van het weefsel gebeurde in Matlab. Voor geen enkel van de onderzochte mechanoregulatorische modellen kon er een duidelijke kwalitatieve of kwantitatieve correlatie gevonden worden tussen de volledige set van experimenteel geobserveerde en numeriek gesimuleerde weefsels en weefsel distributie patronen. Desalniettemin, afhankelijk van het gebruikte model, werden sommige aspecten van de experimentele observaties door sommige modellen gevat:

- Een toename in de kans op bot-implantaat-contact voor de schroefvormige implantaten vergeleken met de cilindervormige implantaten werd voorspeld door alle modellen en waargenomen in de experimenten.
- Een grotere hoeveelheid bot in hele kamer in vergelijking met een 200 μm

cirkelvormige zone rond het implantaat was voorspeld door alle modellen evenals experimenteel waargenomen.

- Een substantieel verschil tussen de hoeveelheden bot voor cilindervormige en schroefvormige implantaten was noch voorspeld door de modellen van Carter *et al.* (1998) en Claes and Heigele (1999), noch experimenteel opgemeten.
- Gebruik makende van 3D simulaties met het model van Prendergast *et al.* (1997), werd de experimenteel geobserveerde spatiale verdeling van de hoeveelheid bot in de kamer voorspeld.

Uitgebreide sensitiviteitsanalyses wezen echter ook op de substantiële invloed van modelparameters zoals materiaaleigenschappen en weefsel fenotype grenswaarden op de simulatieresultaten.

3.4 Conclusie

Het voorgaande maakt dat de aan het begin van dit hoofdstuk vooropgestelde hypothese, dat de mechanoregulatorische modellen van Prendergast *et al.* (1997), Carter *et al.* (1998) en Claes and Heigele (1999) in staat zijn de histodynamica van de vorming van botweefsel in de botkamer te voorspellen, niet volledig kon bevestigd worden. Een betere karakterisatie van de experimentele opstellingen en de introductie van biologische factoren in de mechanoregulatorische modellen zou kunnen leiden tot een betere overeenkomst tussen de experimentele waarnemingen en de simulatie resultaten. De volgende twee hoofdstukken zullen een bestaand (hoofdstuk 4) en een nieuw (hoofdstuk 5) bioregulatorisch model voor botregeneratie bespreken. De koppeling tussen de mechanica en de biologie zal aan bod komen in hoofdstuk 6.

Hoofdstuk 4 Een bioregulatorisch model voor botregeneratie

4.1 Introductie en hypothese

In tegenstelling tot de domeinen van de zachte weefsels en de tumoren, zijn in het domein van botregeneratie slechts zeer weinig wiskundige modellen beschikbaar die de regulerende invloed van biochemische factoren expliciet in rekening brengen. Bailón-Plaza and van der Meulen (2001) ontwikkelden een model waarin onder andere celdifferentiatie, matrix productie en matrix degradatie geregeld werden door de aanwezige osteogene en chondrogene groeifactoren. De onderliggende onderzoekshypothese voor dit hoofdstuk is dat het

model van Bailón-Plaza and van der Meulen (2001) in staat is de belangrijkste aspecten van breukheling te vatten, zodat onderzoek naar mogelijke oorzaken van pathologische heling mogelijk wordt.

4.2 Implementatie

De implementatie van dit model is een eerste stap in het opzetten van een gecombineerd experimenteel en theoretisch kader voor de verdere studie van pathologische breukheling en breukheling in genetisch gemodificeerde muizen. Het wiskundig model werd toegepast op een semi-gestabiliseerd muizen breukmodel (Maes *et al.*, 2006) evenals op een gestandaardiseerd ratten breukmodel (Harrison *et al.*, 2003). De implementatie gebeurde in een specifiek voor biologische problemen ontwikkelde eindige volumes code (Gerisch, 2001), waarin speciale aandacht werd geschonken aan de vereisten van massabehoud en niet-negativiteit van de variabelen.

4.3 Numerieke simulaties

Met een licht aangepaste set parameterwaardes, werd een goede kwalitatieve overeenkomst bekomen tussen de simulatieresultaten en de experimentele data voor verschillende belangrijke aspecten van het normale breukhelingsproces, zoals de globale spatiale en temporele evolutie van de bot- en kraakbeenmatrix en de temporele evolutie van de groeifactorconcentraties. Deze kwalitatieve overeenkomst werd verder gecorroboreerd door experimentele resultaten uit de literatuur. Een kwantitatieve vergelijking tussen simulatieresultaten en experimentele data, waarbij een redelijke overeenkomst aanwezig was voor de botmatrix, werd bemoeilijkt door combinatie van kraakbeen en fibreus weefsel in één en dezelfde wiskundige variabele.

Sensitiviteitsanalyses werden uitgevoerd waarin de invloed van alle parameterwaardes op het simulatieresultaat werd nagegaan. Een aantal parameters gebruikt in de beschrijving van de synthese en degradatie van zowel de zachte als de harde weefsel matrix, de productie en afbraak van groeifactoren en de initiële concentratie mesenchymale stamcellen bleken een substantiële invloed te hebben op het simulatieresultaat. Verschillende gevallen van pathologische heling werden getest. In het gestandaardiseerde breukmodel, zorgde een verzesvoudiging van de afstand tussen beide breukhelften voor het optreden van een niet-unie, in tegenstelling tot de simulaties waar heling steeds - zij het sterk vertraagd - optrad. Een model van niet-unie door een afwijking in de osteogene groeifactor productie en een model van atrofe niet-unie werden succesvol gemodelleerd. Eveneens werden enkele mogelijke behandelingsstrategieën uitgetest. Zoals hoger vermeld, was een grondige kwantitatieve vergelijking met experimentele resultaten ook hier niet mogelijk. Bovendien was het

model beperkt in zijn mogelijkheden om pathologische gevallen en bijhorende therapieën te simuleren en te onderzoeken door het ontbreken van enkele essentiële regeneratieaspecten zoals angiogenese, (een uitgebreide beschrijving van) celmigratie en mechanische belasting.

4.4 Conclusie

Het wiskundige model van Bailón-Plaza and van der Meulen (2001) werd toegepast op verschillende experimentele breukhelingsmodellen. Een goede kwalitatieve overeenkomst werd gevonden tussen experimentele data en simulatieresultaten. Het ontbreken van een aantal essentiële regulerende mechanismen van het breukhelingsproces en van een afzonderlijke beschrijving van fibreus weefsel en kraakbeen, verhinderden een goede kwantitatieve vergelijking tussen experimentele en simulatie data, nodig voor het maken van klinisch relevante voorspellingen omtrent pathologische heling en de behandeling ervan.

Deze tekortkomingen en de bijhorende uitbreidingen van het model zullen in de volgende hoofdstukken behandeld worden. De structuur van de eindige volumes code is zodanig dat zij op eenvoudige wijze de incorporatie toelaat van bijkomende cellen en weefseltypes, zoals fibroblasten en endotheel cellen (hoofdstuk 5) en bijkomende regulerende mechanismen zoals mechanische belasting (hoofdstuk 6), angiogenese (hoofdstuk 5) of additionele groeifactoren (hoofdstuk 5).

Hoofdstuk 5 Een bioregulatorisch model met inbegrip van angiogenese

5.1 Introductie en hypothese

Angiogenese is een essentieel onderdeel van het regeneratieproces. Steeds meer bewijs is voorhanden dat de angiogene groeifactoren de belangrijkste koppeling vormen tussen angiogenese en osteogenese tijdens botregeneratie. Vele gevallen van pathologische heling zijn dan ook terug te brengen tot problemen met de totstandkoming van een goede vascularisatie in het regenererende weefsel. Bestaande wiskundige modellen voor botregeneratie verwaarlozen deze belangrijke regulerende invloed van angiogenese. De hoofddoelstellingen voor dit hoofdstuk waren (1) de ontwikkeling van een uitgebreid bioregulatorisch model en (2) het onderzoek naar mogelijke oorzaken en behandelingsstrategieën van pathologische breukheling.

5.2 Opstellen van het wiskundig model

Een uitgebreid bioregulatorisch model werd opgesteld waarin een aantal essentiële breukhelingsprocessen zoals intramembraneuze en endochondrale botvorming, angiogenese en celmigratie aan bod komen. De beschrijving van deze fenomenen werd opgesteld op basis van bestaande modellen van onder meer tumorangiogenese of werden gebaseerd op experimentele waarnemingen. De parameter waardes werden afgeleid van experimentele resultaten gerapporteerd in de literatuur of geschat indien geen relevante data voorhanden was. Dit model werd toegepast op het gestandaardiseerde ratten breukmodel. Implementatie gebeurde in de hoger beschreven code, specifiek ontwikkeld voor biologische problemen en uitgebreid met een speciale beschrijving voor axisymmetrische domeinen (Gerisch and Geris, 2007).

5.3 Numerieke simulaties

Een goede kwalitatieve overeenkomst tussen de experimenteel waargenomen en numeriek voorspelde resultaten kon aangetoond worden, samen met een verbeterde kwantitatieve overeenkomst in vergelijking met het eerder gebruikte wiskundige model, besproken in hoofdstuk 4. Ook werd een verhoogd potentieel van het ontwikkelde model aangetoond voor het onderzoeken van pathologische regeneratie dankzij de aanwezigheid van angiogenese.

De sensitiviteitsanalyse toonde de relatieve robuustheid aan van de voorspellingen van het model voor kleine wijzigingen (< 1000 % en > 10 %) in de parameterwaardes gebruikt in de beschrijving van fibroblasten/fibreus weefsel, angiogenese en celmigratie. Dit toont de nood aan voor bijkomende experimentele data om deze parameters te evalueren en wijst tegelijkertijd op mogelijke pathologieën. Gevallen van pathologische heling veroorzaakt door inadequate angiogenese werden gesimuleerd, overeenkomstig met experimentele studies gerapporteerd in de literatuur. De voorspelde resultaten waren gelijkaardig aan de experimentele observaties. Bovendien werd de therapeutische waarde van het model getest op een model van atrofe niet-unie. Verscheidene, experimenteel testbare, behandelingsstrategieën werden gesimuleerd zoals toevoeging van mesenchymale stamcellen en/of groeifactoren op verschillende tijdstippen in het helingsproces. Een (dosis afhankelijke) recapitulatie van het helingsproces werd voorspeld. Experimenten zijn in uitvoering om deze voorspellingen te onderzoeken.

5.4 Conclusie

De aan het begin van dit hoofsdtuk gestelde doelen, zijnde de ontwikkeling van een uitgebreid bioregulatorisch model en het gebruik ervan in het

onderzoek naar mogelijke oorzaken en therapieën van pathologische regeneratie, werden bereikt. In de loop van de studie voorgesteld in dit hoofdstuk werden een aantal mogelijke aanpassingen aan het model geïdentificeerd die een verdere verhoging zouden kunnen betekenen van de mogelijkheden van dit model in de simulatie van pathologische heling en de behandeling ervan. Eén van deze verbeteringen, de toevoeging van de reguleren invloed van mechanische belasting op het helingsproces, wordt besproken in het volgende hoofdstuk.

Hoofdstuk 6 Combinatie van mechanoregulatorische en bioregulatorische modellen

6.1 Introductie en hypothese

In de literatuur is er reeds zeer veel experimentele data voorhanden die de invloed beschrijft van mechanische belasting op het globale proces van breukheling en implantaat osseointegratie enerzijds en op verschillende cellulaire deelprocessen anderzijds. Bij het onderzoeken van de globale processen valt op dat de invloed van de mechanische belasting, door clinici uitgedrukt in termen van stabiliteit, beweging van de breukhelften, fixatie, implantaatontwerp en dergelijke, terug te brengen is op een verandering van lokale mechanische omgeving waargenomen door de cellen. Onderzoek naar de invloed van mechanische belasting op het gedrag van de cellen zelf toont aan dat de verschillende belastingsmodi een verschillend effect hebben in termen van signalisatie en genexpressie. Hoewel reeds veel geweten is, blijven vele vragen tot op heden onbeantwoord. Daarenboven is de relatie tussen de mechanische stimulus waargenomen door de cellen (micro) en de belasting uitgeoefend op het regenererende weefsel (macro) onbekend. Tenslotte worden vaak ogenschijnlijk tegenstrijdige resultaten gerapporteerd. Een gedetailleerde vergelijking van alle aspecten van de experimentele opstellingen zou hier waarschijnlijk een uitleg voor kunnen vinden. Samengevat, de meeste processen lijken (zijnde het direct of indirect) afhankelijk van mechanische belasting, maar uit de in de literatuur beschikbare data komen geen duidelijke antwoorden naar voor op de vraag volgens welke mechanismen dit precies gebeurt.

Een wiskundig model kan gebruikt worden om na te gaan hoe de invloed van mechanisch belasting op verscheidene cellulaire processen (proliferatie, differentiatie, groeifactorproductie) het globale regeneratieproces verandert. Bovendien kan het nieuwe inzichten verschaffen in de regeneratieprocessen in het algemeen en de koppeling tussen mechanica en biologie in het bijzonder, bv. door de identificatie van het dominante stimulustype aanwezig in het

regenererende weefsel of de belangrijkste koppelingsmechanismen tussen mechanica en biologie. Het werk gepresenteerd in dit hoofdstuk heeft niet als doel om bovenstaande vragen te beantwoorden of een 'volledig' mechanobioregulatorisch model naar voor te schuiven. Het zoekt daarentegen de ontwikkeling van een wiskundig kader waarin de rol van zowel mechanische als biologische stimuli in het regeneratieproces kunnen onderzocht worden.

6.2 Implementatie

Een wiskundig kader werd ontwikkelend waarin de parameters van het bioregulatorische model, voorgesteld in het vorige hoofdstuk, afhankelijk zijn van de grootte van mechanische stimuli. Ter illustratie van de toegevoegde waarde van een dergelijk model bovenop de bestaande literatuur, werden de parameters gerelateerd aan osteogenese en angiogenese afhankelijk gemaakt van de locale vloeistofstroming. Dit gekoppelde model werd toegepast op zowel de *in vivo* botkamer als op het semi-gestabiliseerde muizen breukmodel, zonder voorafgaande sensitiviteitsanalyses of calibratie van de modelparameters. Voor de implementatie van deze gekoppelde modellen werd gebruik gemaakt van een koppeling van de specifieke code voor biologische problemen in Matlab (hoofdstuk 5) met het eindige elementen programma MSC.Marc, door middel van de gebruikerssubroutines van deze laatste.

6.3 Numerieke simulaties

Voor de *in vivo* botkamer werden verschillende implantaat verplaatsingsmagnitudes alsook verschillende tijdsintervallen tussen opeenvolgende belastingen getest. Een beperkte implantaatverplaatsing (< 150 μm) liet implantaat osseointegratie toe terwijl excessieve belastingscondities leidden tot een fibreuze inkapseling van het implantaat. Deze resultaten corresponderen met de experimentele observaties in de botkamer en in de literatuur. Daarentegen, voor het niet belaste geval, was er geen overeenkomst waarneembaar tussen de numerieke simulaties (geen bot-implantaat-contact en quasi geen botingroei) en de experimentele observaties.

Toepassing van het gekoppelde mechanobioregulatorische model op de hoger vernoemde breukhelingsopstelling liet de simulatie toe van niet-belaste, onderbelaste en overbelaste breuken. Simulaties van deze ongunstige belastingscondities voorspelde de vorming van een avasculaire niet-unie, hetgeen gecorroboreerd werd door experimentele observaties gerapporteerd in de literatuur. Voldoende stabilisatie van de overmatige beweging van de breukuiteinden zorgde voor een recapitulatie van een normale helingsrespons, met en zonder de toediening van bijkomende osteogene groeifactoren.

6.4 Conclusie

Een degelijke sensitiviteitsanalyse moet nog uitgevoerd worden om de impact van de verschillende, in de loop van de studie gemaakte, vereenvoudigingen en aannames op het simulatieresultaat te testen. De invloed van andere mechanische parameters (naast vloeistofstroming) zal eveneens toegevoegd worden. Tenslotte dienen meer biologische parameters afhankelijk gemaakt te worden van de locale mechanische stimuli om het inzicht in de invloed van zowel biologische als mechanische signalen op het regeneratieproces te vergroten. De studie voorgesteld in dit hoofdstuk is een eerste illustratie van het potentieel van zulke wiskundige modellen.

Hoofdstuk 7 Conclusies en toekomstperspectieven

7.1 Samenvatting

Het eerste deel van dit werk beschrijft de implementatie van bestaande mechano- en bioregulatorische modellen en de toepassing ervan op zowel implantaat osseointegratie als breukhelingssituaties. Een kwantitatieve vergelijking met de experimentele resultaten is uitgevoerd, evenals grondige sensitiviteitsanalyses ter bepaling van de invloed van verschillende modelleringsaspecten op het simulatieresultaat. Tekortkomingen van deze modellen zijn geïdentificeerd en suggesties voor verbeteringen geformuleerd.
In het tweede deel van dit werk is een nieuw bioregulatorisch model voor botregeneratie ontwikkeld, dat aan verschillende van de hoger gedefinieerde tekortkomingen tegemoet komt. Dit model omvat verscheidene kernaspecten van het regeneratie proces zoals intramembraneuze en endochondrale botvorming, angiogenese en gerichte celmigratie. De simulatieresultaten zijn zowel op kwalitatief als kwantitatief niveau gecorroboreerd door vergelijking met experimentele data voor normale breukheling. Gevallen van pathologische breukheling zijn gesimuleerd en experimenteel testbare behandelingsstrategieën geïmplementeerd.
Het laatste deel van dit werk beschrijft de ontwikkeling van een wiskundig kader, gebaseerd op het eerder ontworpen bioregulatorisch model, dat de regulerende invloed van zowel biologische als mechanische factoren combineert. Dit is het eerste model van botregeneratie dat de koppeling tussen mechanische belasting en angiogenese maakt op een expliciete en mechanistische wijze. Verschillende voorbeelden illustreren de toegevoegde waarde van deze aanpak in de simulatie van normale en pathologische botregeneratie.

7.2 Conclusies

- Bij de vergelijking van experimenteel waargenomen en numeriek gesimuleerde weefsel regeneratie patronen in de botkamer, werd geen volledige kwalitatieve of kwantitatieve overeenkomst gevonden voor de onderzochte mechanorgulatorische modellen. Desalniettemin konden een aantal van de experimentele waarnemingen gesimuleerd worden door alle modellen, zoals de verhoogde kans op bot-implantaat-contact voor schroefvormige implantaten in vergelijking met cilindervormige implantaten en de hogere hoeveelheid bot aanwezig in de hele kamer in vergelijking met de 200 μm peri-implantaat zone. Bovendien konden, afhankelijk van het gebruikte model, het experimenteel waargenomen verschil in bothoeveelheid tussen cilinder en schroefvormige implantaten (modellen van Carter *et al.* (1998) en Claes and Heigele (1999)) en de spatiale verdeling van het botweefsel doorheen de kamer (model van Prendergast *et al.* (1997)) voorspeld worden. Hierbij dient opgemerkt te worden dat sensitiviteitsanalyses een grote invloed aantoonden van modelparameters zoals materiaaleigenschappen en fenotype grenswaardes op de simulatieresultaten.

- Na aanpassing van een aantal parameterwaardes in het model van Bailón-Plaza and van der Meulen (2001), werd een goede kwalitatieve overeenkomst bekomen tussen de simulatieresultaten en de experimentele data voor een aantal belangrijke aspecten van normale breukheling, zoals globale spatiale en temporele evolutie van kraakbeen en botmatrix densiteit en de temporele evolutie in de groeifactor concentraties. Verschillende pathologische gevallen werden gesimuleerd met wisselend succes. Simulatie van het experimentele model voor niet-unie veroorzaakt door een grote afstand tussen de breukhelften, leidde onveranderlijk tot succesvolle heling bij een voldoende lange simulatietijd. Dit wijst erop dat de mechanismen verantwoordelijk voor het optreden van de niet-unie niet aanwezig zijn in het model. Het voorkomen van een niet-unie omwille van een gebrek aan groeifactorproductie en zijn behandeling door middel van injectie van extra groeifactoren, toonde een dosisafhankelijke recapitulatie van het helingsproces aan, zoals waargenomen in de literatuur. Tenslotte, de simulatie van atrofe niet-unies en hun behandeling gaf aanleiding tot interessante resultaten, maar benadrukte ook de nood voor verder uitbreiding van het wiskundige model. Verschillende essentiële regulatoren van het regeneratie proces, zoals angiogenese en gerichte celmigratie ontbreken in het wiskundige model. Bovendien verhindert de combinatie van de fibreuze en kraakbeen matrix in één variabele een kwantitatieve vergelijking tussen simulatie en experimenten, hetgeen onontbeerlijk is bij het ontwerpen van klinische

behandelingsstrategieën.

- Een nieuw bioregulatorisch model werd opgesteld, met inbegrip van een aantal sleutelprocessen van het botregeneratie proces, zoals intramembraneuze en endochondrale botvorming, angiogenese en gerichte celmigratie. De resultaten ervan werden succesvol gecorroboreerd door vergelijking met experimentele breukhelingsdata, zowel op kwalitatief als kwantitatief niveau. Sensitiviteitsanalyses toonden de nood aan voor verdere experimentele validatie van de parameters betrokken bij de beschrijving van fibreus weefsel/fibroblasten en angiogenese. Simulaties van gevallen van pathologische breukheling veroorzaakt door inadequate angiogenese of het gebrek aan mesenchymale stamcellen (atrofe niet-unie) voorspelden resultaten die vergelijkbaar waren met de experimentele observaties. Daarenboven werden verscheidene, experimenteel testbare, behandelingsstrategieën geïmplementeerd voor dit niet-unie geval, waarbij een (dosis-afhankelijke) recapitulatie van het helingsproces voorspeld werd. Experimentele validatie van deze simulaties is onderweg.

- Een wiskundig kader werd voorgesteld waarin een directe koppeling tussen de biologische en mechanische regulatorische aspecten van botregeneratie mogelijk is. Het is het eerste botregeneratie model dat een directe koppeling tussen de locale mechanische omgeving van het regenererende weefsel en het angiogenese proces voorziet op een mechanistische manier. Verscheidene preliminaire voorbeelden werden uitgewerkt voor zowel implantaat osseointegratie als breukheling, ter illustratie van het potentieel van zulke gekoppelde modellen. Voor elk van de experimentele opstellingen werden gevallen van pathologische regeneratie omwille van onvoldoende of overmatige belasting gesimuleerd. Bovendien werd aangetoond dat, voor het geval van niet-unie veroorzaakt door overmatige belasting van de breukzone, stabilisatie leidt tot herneming van het normale helingsproces.

Dit werk heeft de mogelijkheden en beperkingen van een aantal bestaande en nieuwe wiskundige modellen aangetoond en heeft raadgevingen gedaan voor verdere verbeteringen van deze modellen. De belangrijkste bijdragen van dit werk aan de bestaande literatuur zijn de ontwikkeling van het nieuwe bioregulatorische model voor botregeneratie en het opstellen van een wiskundig kader waarin de mechanobioregulatorische aspecten van het botregeneratie proces kunnen onderzocht worden voor verscheidene experimentele opstellingen.
Dit werk is duidelijk niet voltooid. Het werk gepresenteerd in deze thesis is slechts een eerste, evenwel onontbeerlijke, stap in de richting van een geïntegreerde modelleeromgeving die in staat is om het voorkomen van pathologische regeneratie bij patiënten te voorspellen en de clinici te adviseren

omtrent de optimale behandelingsstrategie.

7.3 Toekomstperspectieven

Door het generische karakter van het ontwikkelde modelleringskader en simulatie methodologie, kunnen deze toegepast worden in de simulatie van andere biologische fenomenen. Aan de afdeling Biomechanica en Grafisch Ontwerpen (K.U.Leuven) werd de osseointegratie van orale implantaten gesimuleerd met de in dit werk beschreven modellen. Deze modellen dienen ook als basis voor het ontwikkelen van mechanobioregulatorische modellen van orthodontische tandmigratie en de bijhorende processen in het periodontaal ligament.

In de toekomst zullen verschillende theoretische en experimentele aspecten van het beschreven wiskundige kader verder uitgewerkt worden.

- Voor het mechanobioregulatorische model beschreven in hoofdstuk 6 zal de afhankelijkheid van bijkomende biologische parameters van mechanische belasting en de invloed van bijkomende mechanische parameters onderzocht worden. Uitgebreide sensitiviteitsanalyses zullen uitgevoerd worden ter bepaling van de invloed van de simplificaties en aannames op het simulatieresultaat.

- Een aantal belangrijke aspecten van het regeneratie proces zoals de invloed van de inflammatiefase, hypoxie, matrix degradatie en discrete niveaus van celmaturatie dienen nog geïntegreerd te worden in het bioregulatorische model

- Multi-schaal analyses laten een directe koppeling toe tussen de verschillende lengteschalen in het regeneratieproces. Een dergelijke koppeling is nodig om de meer mechanistische modellen op micro niveau (gebaseerd op kinetica) te koppelen aan het macro niveau, zijnde het niveau waarop pathologische heling en de behandeling ervan gesimuleerd wordt.

- Specifieke *in vitro* experimenten kunnen ontwikkeld worden ter kwantificatie van bepaalde aspecten van celmigratie, groeifactor productie en consumptie en van de synergie tussen verschillende groeifactoren en tussen mechanische belasting en groeifactoren, zoals deze in de ontwikkelde modellen van hoofdstukken 5 en 6 voorkomen.

- Teneinde de mogelijkheden van de modellen ontwikkeld in hoofdstukken 5 en 6 volledig te waarderen is bijkomende informatie nodig over zowel de biologische als de mechanische aspecten van de gebruikte experimentele opstellingen. Voor de *in vivo* botkamer betekent dit bijkomende

informatie over vroegere tijdstippen in het regeneratieproces, de bepaling van bijkomende biologische parameters (bv. vascularisatie) en van de mechanische aspecten van de weefsel-implantaat interface. Voor de breukhelingsmodellen betekent dit een kwantificatie van de breukhelingsomgeving in termen van mechanische eigenschappen.

Appendix

Details of the bioregulatory model (chapter 4)

This appendix contains the non-dimensionalized equations and parameters of the mathematical model presented by Bailón-Plaza and van der Meulen (2001), the temporal and spatial parameters of the model, the scaling values for the seven dependent variables and the values of boundary and initial conditions. The seven dependent variables are the concentration of mesenchymal stem cells (c_m), chondrocytes (c_c) and osteoblasts (c_b), the density of the fibrous/cartilaginous (m_c) and bone (m_b) ECM (total matrix density $m = m_c + m_b$) and the concentration of a chondrogenic (g_c) and an osteogenic (g_b) growth factor. The meaning of the model parameters is explained in Bailón-Plaza and van der Meulen (2001). Most of the parameter values were derived from experimental results reported in literature but a few of them were estimated. Some of these estimated parameter values were altered (boldface) in this study, in order to obtain a better correspondence between simulation results and experimental data.

- Equations:

$$\begin{aligned}
\frac{\partial c_m}{\partial t} &= \nabla\left[D_{cm}\nabla c_m - C c_m \nabla m\right] + A_m c_m\left[1-\alpha_m c_m\right] - F_1 c_m - F_2 c_m \\
\frac{\partial c_c}{\partial t} &= A_c c_c\left[1-\alpha_c c_c\right] + F_2 c_m - F_3 c_c \\
\frac{\partial c_b}{\partial t} &= A_b c_b\left[1-\alpha_b c_b\right] + F_1 c_m + F_3 c_c - d_b c_b \\
\frac{\partial m_c}{\partial t} &= P_{cs}\left(1-\kappa_c m_c\right)\times\left(c_m + c_c\right) - Q_{cd2} m_c c_b \\
\frac{\partial m_b}{\partial t} &= P_{bs}\left(1-\kappa_b m_b\right) c_b \\
\frac{\partial g_c}{\partial t} &= \nabla\left[D_{gc}\nabla g_c\right] + E_{gc} c_c - d_{gc} g_c \\
\frac{\partial g_b}{\partial t} &= \nabla\left[D_{gb}\nabla g_b\right] + E_{gb} c_b - d_{gb} g_b
\end{aligned}$$

- Functional forms:

$$\begin{aligned}
D_{cm} &= \frac{D_h}{\left(K_h^2 + m^2\right)} m & F_1 &= \frac{Y_1}{\left(H_1 + g_b\right)} g_b \\
C &= \frac{C_k}{\left(K_k + m\right)^2} & F_2 &= \frac{Y_2}{\left(H_2 + g_c\right)} g_c \\
A_m &= \frac{A_{mo}}{\left(K_m^2 + m^2\right)} m & F_3 &= \frac{m_c^6}{\left(B_{ec}^6 + m_c^6\right)} \times \frac{Y_3}{\left(H_3 + g_b\right)} g_b \\
A_c &= \frac{A_{co}}{\left(K_c^2 + m^2\right)} m & E_{gc} &= \frac{G_{gc} g_c}{\left(H_{gc} + g_c\right)} \times \frac{m}{\left(K_{gc}^3 + m^3\right)} \\
A_b &= \frac{A_{bo}}{\left(K_b^2 + m^2\right)} m & E_{gb} &= \frac{G_{gb} g_b}{\left(H_{gb} + g_b\right)}
\end{aligned}$$

- Scaling parameters:

$$\begin{aligned}
\tilde{t} &= \frac{t}{T}, \quad \tilde{x} = \frac{x}{L}, \quad \tilde{y} = \frac{y}{L}, \quad \tilde{c_m} = \frac{c_m}{c_0}, \quad \tilde{c_c} = \frac{c_c}{c_0}, \\
\tilde{c_b} &= \frac{c_b}{c_0}, \quad \tilde{m_c} = \frac{m_c}{m_0}, \quad \tilde{m_b} = \frac{m_b}{m_0}, \quad \tilde{g_c} = \frac{g_c}{g_0}, \quad \tilde{g_b} = \frac{g_b}{g_0}
\end{aligned}$$

  $T = 1$ day, $L = 3.5$ mm, $c_0 = 10^6$ cells ml^{-1}, $m_0 = 0.1$ g ml^{-1} [6], $g_0 = 100$ ng ml^{-1} [7].

- Non-dimensionalised parameter values:
  $\tilde{D}_h = 0.014$ [1], $\tilde{K}_h = 0.25$ [1], $\tilde{C}_k = 0.0034$ [1], $\tilde{K}_k = 0.5$ [1], $\tilde{A}_{mo} = 1.01$, $\tilde{K}_m = 0.1$, $\tilde{\alpha}_m = 1$, $\tilde{\mathbf{A}}_{\mathbf{co}} = \mathbf{0.101}$, $\tilde{K}_c = 0.1$,

$\tilde{\alpha}_c = 1$, $\tilde{A}_{bo} = 0.202$ [2], $\tilde{K}_b = 0.1$, $\tilde{\alpha}_b = 1$, $\tilde{Y}_1 = 10$, $\tilde{H}_1 = 0.1$, $\tilde{Y}_2 = 50$, $\tilde{H}_2 = 0.1$, $\mathbf{\tilde{Y}_3} = \mathbf{500}$, $\tilde{B}_{ec} = 1.5$, $\tilde{H}_3 = 0.1$, $\tilde{d}_b = 0.1$, $\tilde{P}_{cs} = 0.2$ [3], $\tilde{\kappa}_c = 1$ [3], $\mathbf{\tilde{Q}_{cd2}} = \mathbf{1.5}$, $\tilde{P}_{bs} = 2$, $\tilde{\kappa}_b = 1$, $\tilde{D}_{gc} = 0.005$ [4], $\tilde{D}_{gb} = 0.005$ [4], $\tilde{G}_{gc} = 50$, $\tilde{H}_{gc} = 1$, $\tilde{K}_{gc} = 0.1$, $\mathbf{\tilde{G}_{gb}} = \mathbf{350}$, $\tilde{H}_{gb} = 1$, $\tilde{d}_{gc} = 100$ [5], $\tilde{d}_{gb} = 100$ [5].

- Initial and boundary conditions: $\tilde{m}_{c_ini} = 0.1, \mathbf{\tilde{c}_{m_bc}} = \mathbf{0.02}$ (during the first 3 days), $\tilde{g}_{c_bc} = \tilde{g}_{b_bc} = 2$ (during 20 days).

[1] Gruler and Bültmann (1984)
[2] Fedarko *et al.* (1995)
[3] Olsen *et al.* (1997)
[4] Joyce *et al.* (1990), Vander *et al.* (1998)
[5] Coffey *et al.* (1990), Dasch *et al.* (1989), Edelman *et al.* (1993)
[6] Olsen *et al.* (1995)
[7] Joyce *et al.* (1990)